Developments on Computer Simulation of Injection Moulding

— Modelling with Boundary Element and Finite Element Methods

by

Xiaoshi Jin

This thesis is submitted for the degree of
Doctor of Philosophy in
the University of Glasgow

April, 1992

Abstract

Several mathematical models which are based mainly on the boundary integral equations are developed for computer simulation of injection moulding. The models are then implemented for the viscous flows in the filling stage, and the temperature field during the cooling stage of the process. Starting with the modelling of nonisothermal laminar flow in ducts, the dependence of viscosity on the pressure, temperature and shear rate is taken into account, and the velocity and temperature solutions to fully developed flow are developed. The solutions are used to obtain the approximate axial solutions and possibility of choking is discussed. The solutions are further extended to the cases of a slightly tapered circular pipe, and of cross sections of any shape the latter of which uses a boundary element model.

Boundary element methods are chosen for the computer simulation because of their efficiency and accuracy resulting from one dimension reduction in the modelling and continuous solution in the domain. The melt flow in the filling stage is characterised by a moving front. It is suggested that a Lagrangian description for the modelling is better than the traditional Eulerian description for fluid mechanics. A boundary element method based on the Lagrangian description has the apparent advantage avoiding the mesh tangling problems which have troubled the models based on the domain grid system for many years. Also when a part geometry is very complicated from a modelling point of view, a boundary element approach can certainly reduce the effort in its cooling analysis. On the basis of these ideas, a previously developed boundary element model for the filling process of thin cavities is firstly reviewed and discussed before a new and better model derived. The model is implemented for flow pattern analysis, and two examples are given for showing the efficiency and accuracy. The multi-medium transient heat conduction problem is modelled by the boundary element method based on the time-dependent fundamental solution, and two cooling examples are calculated. Discussion then follows on the simplifications of the model without interfacial elements or division into convex sub-domains.

Boundary element studies were also carried out for particle and fibre orientations caused by the fountain flow effects during the filling stage, and the particle-in-domain idea is introduced for the simulations. The result of the particle orientation explains the phenomena of "V" mark, and it agrees

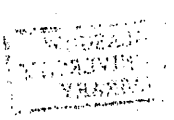

with the experimental results given by Dr. Schmidt*. The fibre orientation is based on Jeffery's formulation. A further development of the boundary integral equation method is presented for modelling unsteady viscous flow with a free surface. The formulations are based on the Lagrangian description and the Oseenlet solutions. Two examples are given on compression moulding.

Several practical mouldings of plastics components are simulated by using a finite element package called MOLDFLOW, and a principle for balancing a feed system for a family set of moulds is suggested. Detailed analyses on materials, moulding conditions and shapes of geometry are given.

A computer package named CASIM is the result of the author's work in modelling injection moulding. The kernel of the package is the BEM modules which have been developed, and a graphically enhanced pre- and post-processor is designed to assist the simulation.

---

*Schmidt, L.R., "Interrelationship of Flow, Structure, and Properties in Injection Molding", *the Proceedings of the 2nd World Congress of Chemical Engineering*, Montreal, Canada, Vol.VI, p516-518, Oct., 1981.

To my wife, my parents
and my motherland.

Acknowledgements

The financial supports from Glasgow City Council and the ORS Scheme of the CVCP (Committee of Vice-Chancellors and Principals) during the three-year-course of study are gratefully acknowledged. The QET award from IMechE for the author's attending the International Conference of BEM13 in USA is also very much appreciated. The author would like to express his gratitude to Dr. C.A. Brebbia and his colleagues for encouraging the author's BEM developments and applications. Thanks are also given to Dr. L.R. Schmidt and the Research and Development Centre of General Electric Company for the pictures and the permission to put them in Chapter Five. The author is very grateful to Mr. Alan Crombie and IBM(UK) in Greenock for supplying the drawings and samples for the simulations using MOLDFLOW which are shown in Chapter Seven.

Acknowledgements are due to the University of Glasgow in which the author has used its resources for three years during his study, and especially to the staff of the Computer Service Centre for supporting his endeavours in using MOLDFLOW and developing CASIM. The author thanks Professor B.F. Scott and Dr. R.D. Thomson for their assistance, and other members of staff in Department of Mechanical Engineering for their help during his research.

The author is especially indebted to Dr. David K. Brown for his deliberate and patient guidance, without whom he couldn't have completed his work. Finally, the author would like to acknowledge his wife, Shuqing Ji, who has always supported him in his professional pursuits.

Declaration

I declare that the whole work of the thesis is solely done by myself.

CONTENTS

Chapter One

Overview

1.1 Injection Moulding Technology

Plastic material is one of the most widely used materials and its industry is one of the fastest growing industries in the world. Injection moulding is one of the major methods by which plastics are fabricated. The importance of injection moulding to the plastic industry is indicated by the great amount of material fabricated by the process, approximately one third by weight of all plastics processed goes through injection moulding machines[1].

Historically, injection moulding was similar to the centuries-old process of metal die-casting, in which melted metal was poured into a closed mould made of sand or plaster. Most metal parts are still made by the die-casting process, in thousands of metal foundries all over the world. By 1872 the Hyatt Brothers (John and Isaiah) in the United States had patented the first plastics injection moulding machine, which was used to mould cellulose nitrate (Celluloid), the first man-made plastic, invented by John Hyatt a few years earlier. However, the process was not widely used until the 1920's when the first to be produced in series was a plunger-type machine, manufactured in 1926[2,3]. The real impetus for the widespread use of injection moulding came in the 1930's with the introduction of polymethyl methacrylate and polystyrene moulding materials. These could not be fully exploited using the then widely practised art of compression moulding which had blossomed following the invention of phenol-formaldehyde resins (Bakelite resins) in 1909.

The next major development occurred in 1951 when William H. Wilert developed the reciprocating screw plasticizer for injection moulding machines[4] which can be found on most injection moulding machines built and used today. They are replacing the earlier plunger injection units which have a disadvantage of high pressure loss (about 80 per cent of the total ram pressure) in the cylinder, with correspondingly longer injection time. The most recent development concerns process controls that permit controlling the plastic melt.

The advantage of injection moulding is that moulded parts can be manufactured economically in unlimited quantities with little or practically no finishing operations. Principally, it is a mass-production method, and because of the high capital investment in machines, moulds, and auxiliary equipments, it operates most economically only as such. The surface of the injection mouldings is as smooth and bright or as grained and engraved as the surfaces of the mould cavity in which they were prepared. There are many developments and potentials, such as reinforced reaction injection moulding (RRIM), foam moulding, and blow moulding, etc. New plastic materials continue to be born, which may require better technology, tougher conditions, or on the contrary, have wider working range of processing.

Because of ever-growing requirements, injection moulding plants continue to expand, to modernise or to be built up. These plants are aiming at production of quality injection moulded parts to meet the customers' performance requirements to get economic success. Although this success depends on some other factors, one of the essential factors is how to produce parts as good as possible. Only with the beginning of deeper understanding of the process mechanism and their underlying physical laws has plastic processing technology and machinery design made any real progress.

Although the complete operation of injection moulding is a much more complicated process than the term "injection moulding" can describe, a block diagram shown in Fig. 1.1.1 outlines the major technical operations:

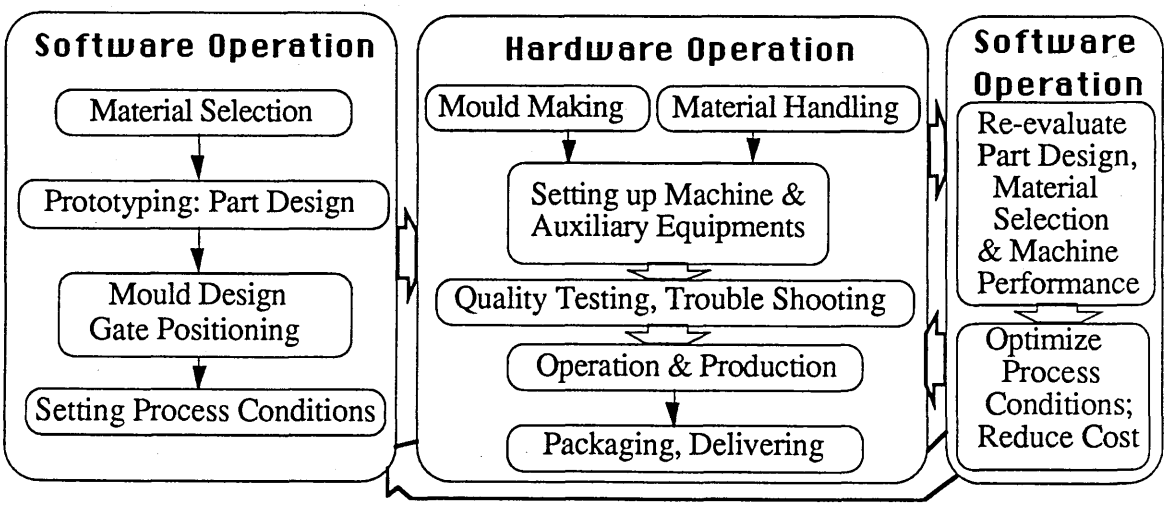

Figure 1.1.1 Injection Moulding Technical Operations

The software operations have their significant importance. Part design requires basically the information of the properties of plastics, structure re-

sponses, performance characteristics, process variables, part shape, and economics, whereas mould design is mainly based on the past experiences. Even for recognised experts the complexity of a viscoelastic polymer material, an irregular mould geometry, steep temperature gradients and other criteria such as appearance and dimensional tolerances make mould design a difficult task. Prototyping is one of the steps by which the engineering and feasibility studies can be converted into a product. Numerous iterations in prototyping a plastics part prior to satisfactory moulding are costly in terms of engineering resources. Misuse and misapplication often result in higher cost paid. Successful designs and control settings can lead to a great deal of gain by material saving and high productivity. This success must be strongly based on engineering and processing analysis along with practical troubleshooting. One may associate the software operations with computers. In fact, computers, which have been developing in parallel to the evolution of the plastic industry, are really manifesting themselves as the key roles. Even in hardware operation, CAD/CAM in mould-making, digital-computers in machine-controlling, and on-line operation robot handling are very common nowadays. To analyse the processing of injection moulding, one has to understand the characteristics of the polymer materials and the basic processing principles in the injection moulding machine. Fig. 1.1.2 shows the main parts of an injection moulding machine.

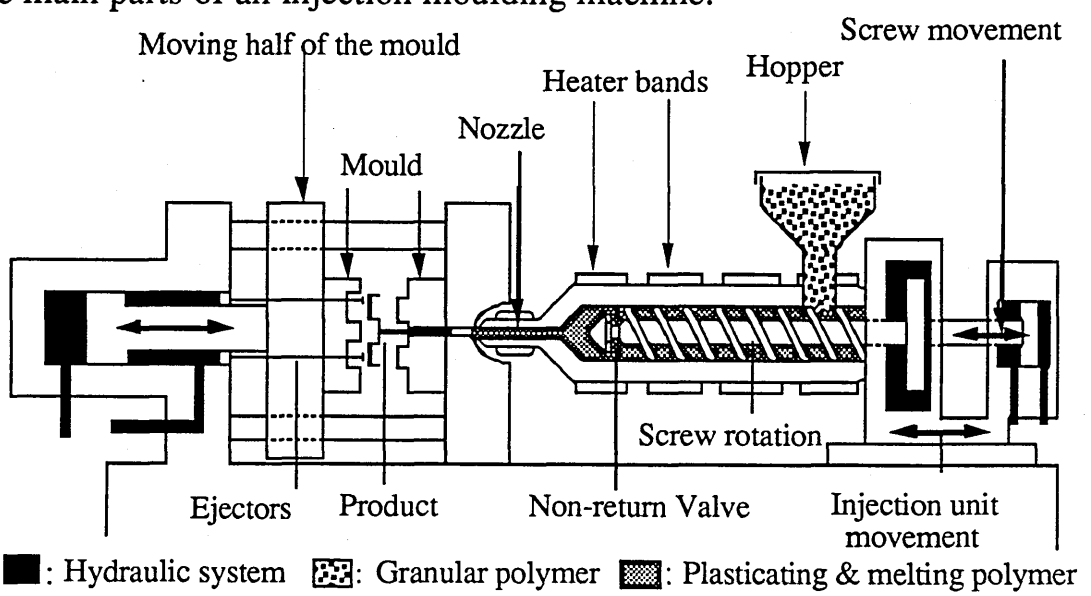

Figure 1.1.2. Main parts of an injection moulding machine

In a typical cycle action as shown in Fig. 1.1.3, the mould is first closed and the plastic material comes from a hopper whose tapered portion is connected to the throat, where the rotating screw is exposed to the material for

pickup. The rotation causes the material to move forward, be compressed and sheared while heaters around the cylinder chamber heat it up until it is fully and homogeneously plasticised into a melted state, at the same time forcing the already prepared and metered melted material into the clamped mould. The mould may consist of a single cavity or a number of similar or

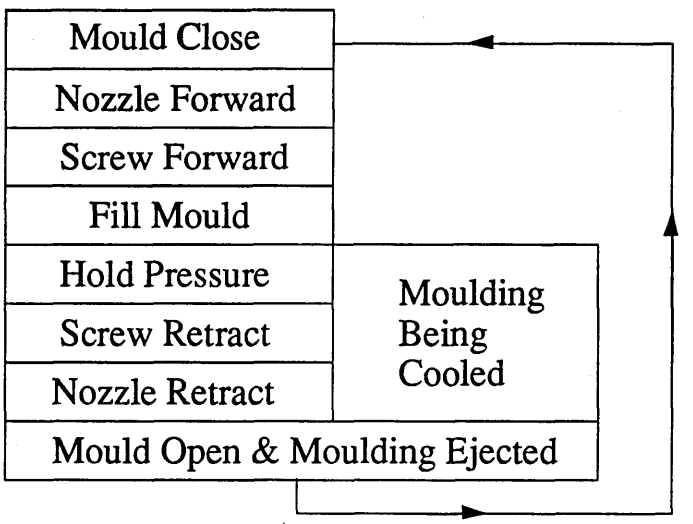

Figure 1.1.3 A typical moulding cycle

dissimilar cavities, each connected to flow runners that direct the flow of the melted plastic to the individual cavities. Adequate pressure is then maintained for some time after the mould was filled to permit the plastic in the mould to solidify, and cooling water is circulated through channels in the mould so as to keep the mould cavity walls at a temperature usually between room temperature and the softening temperature of the polymer. Thus, the hot polymer begins to cool as it enters the mould. When it is cooled to a sufficiently rigid state, the mould is opened and the piece is ejected out by pin ejectors.

1.2 Characteristics of the injection moulding

From the general description in section 1.1 one can see a few of basic but important features about the process. The significant complicating features are the nonisothermal, compressible and visco-elastic characters. It should have become evident that the injection moulding can not be done without controlling those features by a number of process parameters. Before more detailed research is presented about these features a few major variables are introduced hereafter.

1.2.1 Temperature

One fundamental principle of injection moulding is that hot material enters the mould, where it cools rapidly to a temperature at which it solidifies sufficiently to retain the shape of the impression. The temperatures of the mould and the melt are therefore important as they govern a portion of the overall moulding cycle. The hot melt flows more freely in a hot mould, yet a greater cooling period is required before the solidified moulding can be ejected. Alternatively, while the melt solidifies quickly in a cold mould it may not reach the extremities of the impression. A compromise between the two extremes must therefore be accepted to obtain the optimum moulding cycle. The main parameters for controlling the thermal feature are then the melt temperature and mould temperature. The more detail and more practical discussion of these two parameters will be given in chapter seven.

There are three thermal phenomena which complicate the process. In the first place the mould surfaces, which are the flow boundaries, are not usually at the same temperature as the melt. This follows principally from the difficulty of uniform control of temperature throughout the mould block. In addition to spatial variations of temperature, the cyclic nature of the process involves time-varying temperature within the mould block. Thus the dynamics of heat transfer in the mould block contributes an unsteady nonisothermal character to the mould-filling process. A consequence of the nonisothermal boundaries is the freezing of the polymer at the flow boundaries if they are sufficiently cold. The principal effect of boundary solidification is the constriction of the flow path, which leads to large pressure increases. This can be noticed especially in the filling stage of a thin cavity. A third nonisothermal feature is due to viscous heating. Under some conditions the combination of high viscosity and small flow channels can lead to significant temperature rises of the melt as it proceeds toward the cavity. With some polymers this creates the possibility of thermal degradation. In any event significant temperature rises will strongly affect the relationship between the pressure drop and the flow rate. Because injection moulding can involve pressure as high as several thousand atmospheres, it is necessary to keep in mind that the viscosity of melted polymer is known to depend on pressure.

1.2.2 Pressure

Pressure in injection moulding process varies according to location and time of the action. It would be confusing if the term "injection pressure" were used for analysis or operation because it could be hydraulic pressure supplied by the drive unit of the machine, or cavity pressure inside the cavity, or the holding pressure specially for a secondary pressure stage. The hydraulic pressure can not be set at the machine because it depends on the flow resistance of the runner system, gate, and mould cavity. It is a reflection of many factors like screw speed, melt temperature, mould temperature, material viscosity, shape of the geometry, and switch-over time, etc. The readings of the hydraulic pressure provide no basis for conclusions regarding the holding pressure stage and the pressure inside the cavity[5]. For analysing or controlling the flow process, the cavity pressure plays a central role.

The information obtainable from a cavity pressure curve is illustrated in Fig. 1.2.1 by a characteristic curve with technical parts.

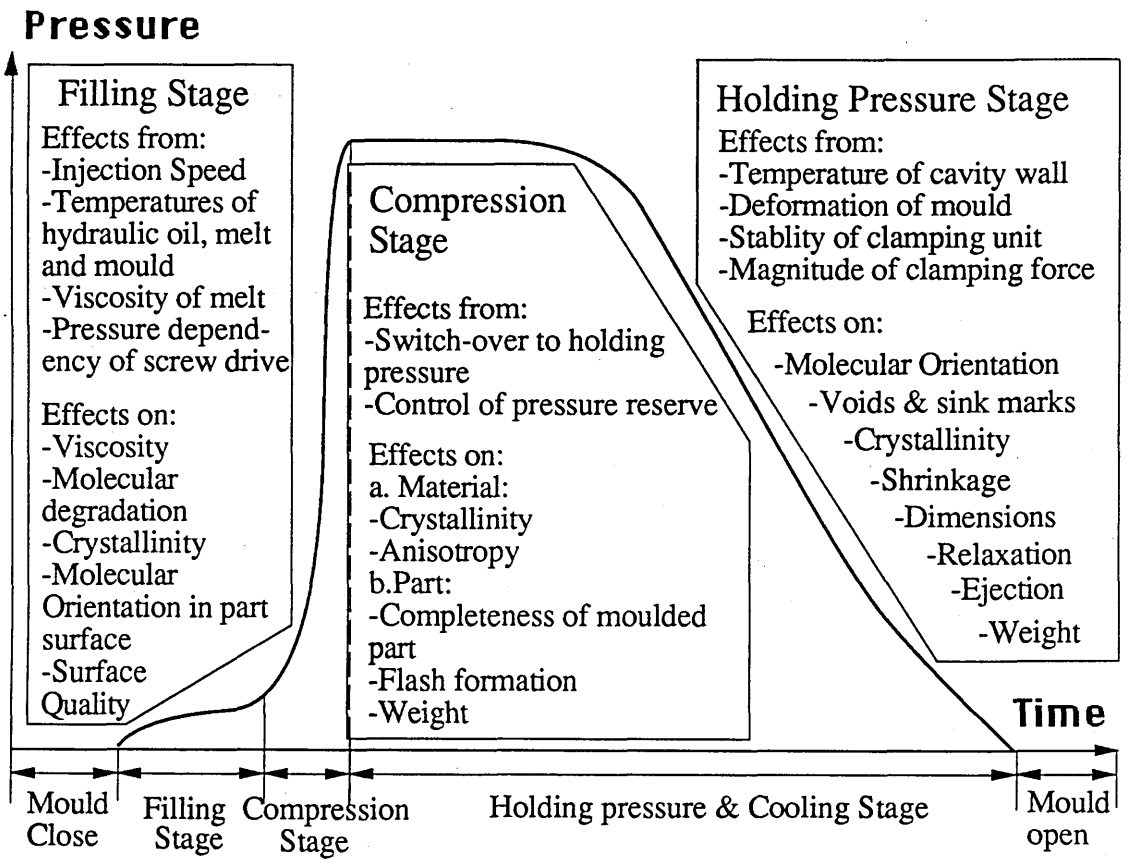

Figure 1.2.1. A characteristic curve of pressure with technical explanations.

From the graph, it is possible to classify it into three fundamental stages: filling stage (or called injection stage in some sources), compression stage, and holding pressure stage (or called cooling stage). (The stage classification can also be done in terms of times, which are "boost time" for filling and compression stages, "dwell time" for the rest; or in terms of volume, which are filling phase for the period until the mould is just filled, pressurisation phase for extra 15% of the material and compensation phase for compensating 25% volumetric change from the melt to the solid[6], etc.). These three stages can be related to certain effects as well as to quality criteria. The filling stage primarily affects the cosmetics of the moulded part, while the holding pressure controls, above all, the dimensions. The graph illustrates the relative importance of the cavity pressure very well. The first section of the curve shows the function of overcoming the flow resistance from the nozzle to the cavity, which keeps going up almost linearly. If there was any pressure drop in this section, it would either be back flow or render the computer analysis unsuitable. The back flow gives bad orientation of the material, and cause flaws. The second section (compression stage) of the curve provides information about typical mistakes in the process technique. A high pressure peak in the compression stage may cause serious difficulty. It results from an incorrectly set or unreliably functioning switch-over to lower holding pressure and produces flash or even worse, a packed mould. Fig.1.2.2 shows four basic possibilities of switch-over:

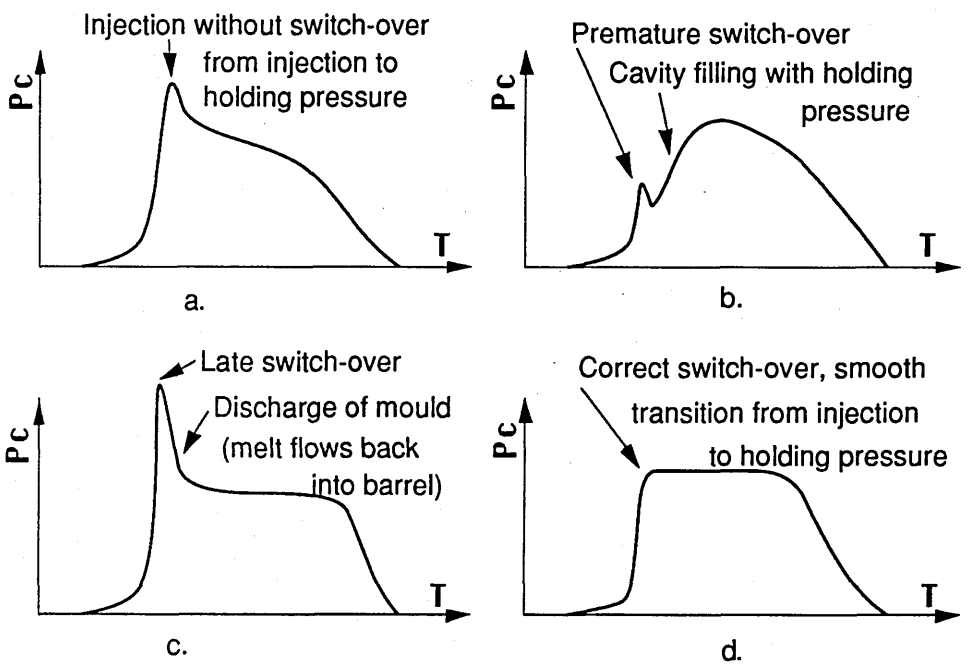

Figure 1.2.2 Four basic possibilities of switch-over.

(a) Injection without switch-over. This is practicable if the necessary final pressure is close to the filling pressure, which is often the case with small gates and with parts having a large flow length to thickness ratio. The hazard of late switch-over exists for with large gate.
(b) Injection with late switch-over. Overpacking is the result which causes back flow which in turn causes undesirable and unfavourable shear stresses because of the combination of flowing and freezing. It is also the principal cause of damage to the mould by deforming cavity edges and overloading the clamping unit.
(c) Injection with premature switch-over. This indicates that the filling process takes place under holding pressure, which is too low for proper filling, and consequently with reduced injection speed. At the moment of switch-over, the flow may stagnate briefly, which produces troublesome surface marks.
(d) Injection with optimum switch-over. Proper selection of this point is particular important. There are four primary methods of determining when to switch over which are discussed in detail in [5].

The hydrostatic pressure itself does not cause stresses but the difference of the pressure does in the cavity. The profile of the pressure shown in the graph can not display the difference. It is only with more comprehensive results given by two- or three-dimensional computer analysis can the pressure difference in the cavity and its consequently results be shown and interpreted.

1.2.3 Velocity

Although flow rate is one of the major parameters in controlling the moulding process, velocity of the melted polymer plays an important role in analysis. Velocity directions in different locations give a preliminary idea of the molecular orientation. In a plastic melt at rest, individual molecular segments are in a random, tangled state of maximum irregularity. During filling stage, molecular chains are deformed by the flow of melt, which causes them to become oriented in the direction of flow. Although at certain conditions (low molecular weight, high temperature, and low pressure), the oriented molecular chains, after some time of standstill, regain their irregular, random state due to their thermal motion (Brownian motion), it usually takes only a fraction of a second, especially in the surface layers, for the material to solidify, and a considerable part of the orientation

produced during the filling is always "frozen-in". The strength of moulded part is always higher in the direction of orientation than perpendicular to it. The same idea is specially important for fibre orientation research when the strength in a particular direction is needed. Velocity differential in space can indicate shear elongation and shear deformation of melt, which can give a whole image of the stress's distribution caused by the combination of viscosity and shear deformation. The viscosity itself is the function of the local velocity difference and its rate, so are the constitutive relations which will be discussed in later sections. This feature of melted polymer becomes extremely difficult in modelling analysis. The velocity information can also give the location of flow front about time, weld lines, and meld lines, which in turn give an intuitive information of the filling. Fig.1.2.3 illustrates the weld line and meld line by means of velocity directions.

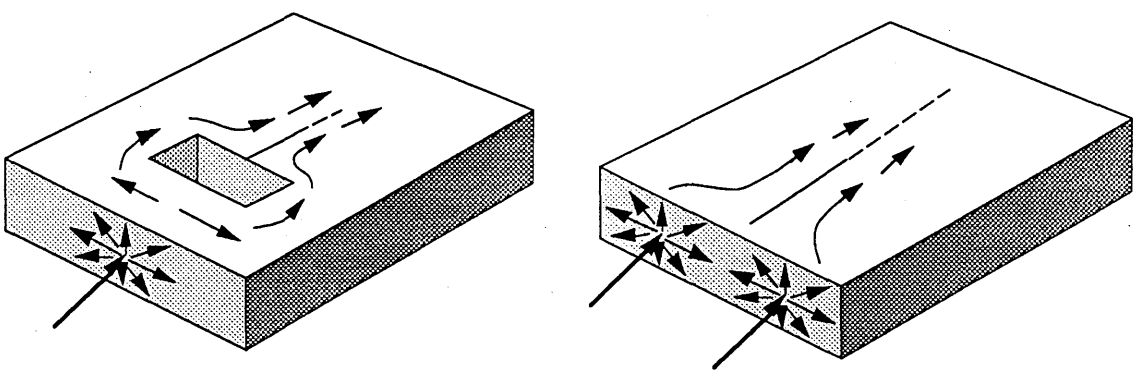

Figure 1.2.3. Weld line and meld line

1.3 General Considerations of Effects

There are many flow and thermal effects which cause different problems in moulded parts. Before more detailed researches about the process are introduced, some general considerations of five major effects for those problems are presented.

1.3.1 Weld / meld lines

As mentioned above, weld line and meld line are obvious flow effects. Weld lines are formed when two melt flow fronts meet and join together, usually with no shear or mixing of the two flows. As well as being visually

unacceptable, they are potential cracks and give areas of local concentrated stresses. Weld lines can be seen around a hole or a thinner area as melt flows join up after surrounding the obstacle, or in the joining area where flows from two or more gates meet together. Although both flows are "welded" together, there is little incentive for molecules to bridge the boundary since the polymer molecules are oriented along the directions of flow. It is so even when pressure is applied. A higher temperature will promote more thermal diffusion, but the weakness of weld-lines will be more pronounced in mineral- or fibre-reinforced polymer compounds because of the absence of fibres bridging the join, as a report[7] stated. From this point of view, meld lines, which are formed by two flow fronts moving in parallel, have the same weakness as weld lines do, but the head-on meeting of two melt fronts may cause some entrapment of air as the join extends through the thickness of the wall to reach the mould faces as shown in Fig. 1.3.1. This is why a short weld line can be seen immediately after the meeting but gradually disappears as it extends in its elongation direction. The entrapment of air is a real risk of crack-like defect, or even burning of the polymer. Venting is a way to avoid the defect. Weld lines are normally inevitable, but they can be repositioned in the least sensitive area by redesigned the gate position.

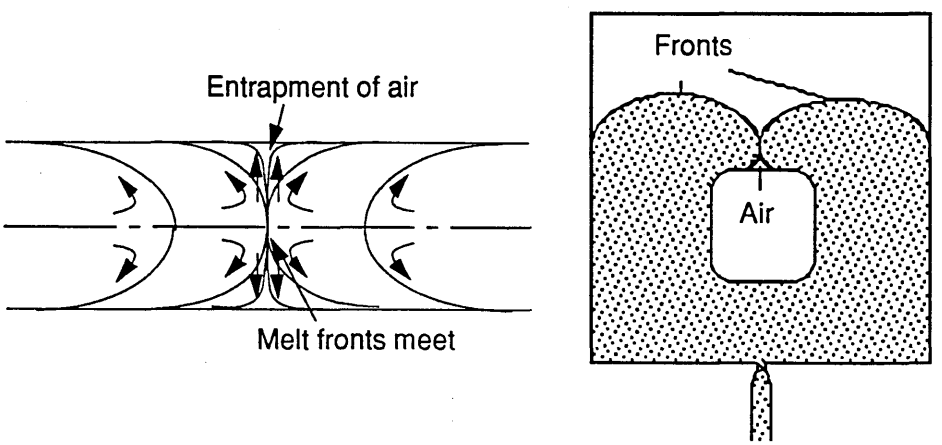

Figure 1.3.1 Weld line and entrapment of air viewed in two directions

1.3.2 Hesitation effects

Hesitation effects are induced when there are significant changes in wall thickness in a part. Under the same pressure, the melt flow always chooses the easier path to fill the cavity. So wherever it has the choices of filling either a thick section or a thin diaphragm, it sits at the edge of the thin section losing heat, goes to the thick section, until the mould almost completely filled when the pressure is then increased sufficient to try to fill the thin section. Often by this time, the front around the thin section is frozen, leave the thin section unfilled. The simple way to solve the problem is to reposition the gate(s), and let the thin section be the last to fill. As long as the melt continues to flow at a steady rate there is no difficulty in filling the thin section[6].

1.3.3 Shrinkage / warpage / sink mark / void

Polymers have high thermal expansion coefficients because of their characteristic microstructures. Thermal expansion is anisotropic if there is molecular orientation present, with the expansion coefficient being smaller in the direction that has the greater fraction of covalent bonding. In the injection moulding process the cooling rate is relatively fast, and it varies with the position in the product, with the outer layers being quicker cooled than the centre. If a polymer is capable of crystallising then the effect of the changing the cooling rate may be dramatic, especially if the maximum rate of the crystal growth is not too high. In this case it may be possible to cool thin sections of the plastic fast enough to avoid any significant crystallisation, whereas in thicker sections the degree of crystallinity is different due to the time spent in the crystallisation temperature range. When a glass forming polymer is cooled, a slower cooling rate gives the polymer more time to relax towards an equilibrium glassy state, this state continues even if the polymer is held at a low temperature. All these reasons cause the variations in density across a product, they are therefore the fundamental factors for the shrinkage. Recent released MF/WARP's introduction[8] indicates the four components for calculating the shrinkage: a). Volumetric shrinkage; b). Crystallisation kinetics; c).relaxation characteristics; d). orientation vector.

Warpage is the phenomenon caused by variations in shrinkage throughout the product. However, how much a part warps depends on the magnitude of

warpage-driving force and the stiffness of the part. A product warps if the driving force is locally sufficiently large, and has residual stress little warping if the driving force is sufficiently small. The flow effect on warpage is mainly the orientation in a moulding, whilst the thermal effect is the temperature and cooling rate difference throughout the component.

As mentioned above, the general remedy for shrinkage / warpage of a moulding is to increase the amount of feeding of the mould to compensate the volume change. This can be controlled either by increasing the holding pressure or the length of the holding time, or by enlarging the gate. Nevertheless, the orientation has to be solved by further shaping on the wall-profiling of the product, and careful design of the mould. The following defects are those which can not be solved by only increasing the amount of feeding.

Sink mark often happens in thick junction area. This is also because of local shrinkage. Fig.1.3.2a illustrates how an island of melt is cut off from the main supply during the solidification. Fig. 1.3.2b shows how solid skin is pulled inwards by the contracting core as it cools, and sink marks can be left in the surfaces of a box. If the skin is strong enough to resist the contracting force, a void may be caused inside the box.

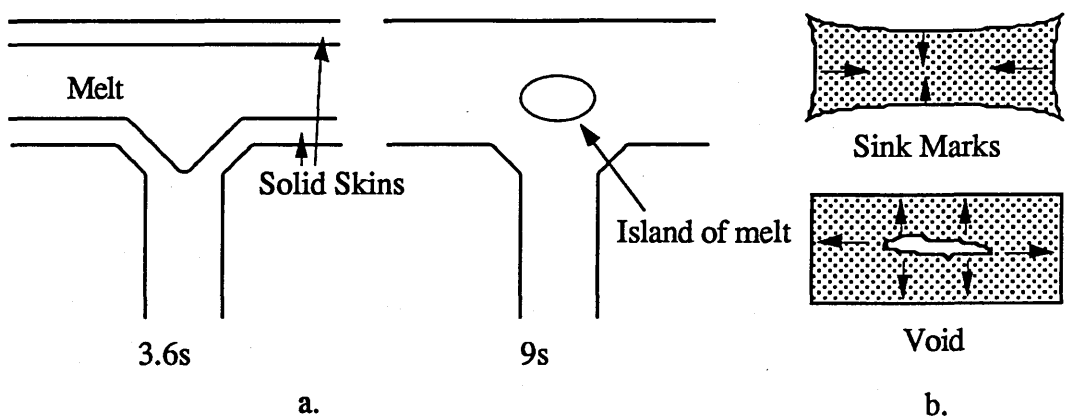

Figure 1.3.2 a. Shrinkage cavity at the intersection of a plate with a reinforcing rib
b. Formation of sinks and voids

1.3.4 Orientation

Orientation in polymers simply refers to alignment of polymer chains, whether they are stretched or not. The shear and extensional flows in injection moulding affect the microstructure of the melt. Polymer chains have a preferred relaxed state. If they are not frozen so stiff to move, it is their

nature to randomly coil up into a "fuzz-ball" configuration. When polymer is pushed through gates and/or runners into mould cavities, these fuzz-balls distort from the stretching and shearing forces. This distortion creates alignment of chains parallel to each other in the flowing directions. If there are rigid additives present, such as glass fibres, these can be aligned with the flow as well. If this non-equilibrium microstructure is "frozen" into the solid state, then there is said to be the orientation of the part. In oriented areas, normally in skins, there are strong and weak directions just like the function of fibres. The strong direction is always along the direction of orientation because the atom-to-atom bonds are much stronger than the weak forces attracting neighbouring chains.

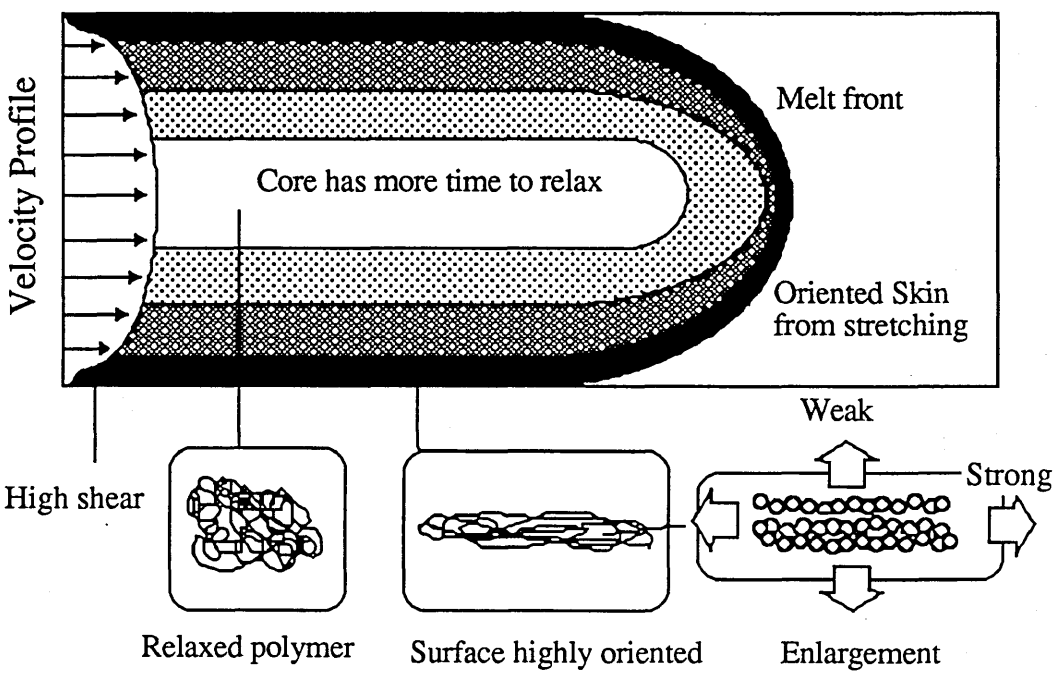

Fig. 1.3.3. Orientation of cavity melt flow in cross section view

The fact is, injection moulded parts are not uniformly oriented. The degree of orientation varies considerably from the surface to the core through the cross section, and from the gate to the extremes. Fig. 1.3.3 shows the orientation in a cross section of a mould where the flow proceeds from left to right. Often a high level of molecular orientation is regarded as a bad feature in injection moulding, since the direction in perpendicular to the flow is weakened, and will be the potential weakness for developing cracks, though the orientation could be beneficial if it were in the direction of the main structural loads. How pronounced these variations are also depends on the moulding conditions—more precisely, the point-to-point flow,

temperature, and pressure conditions at every location in the mould. High residual stress is not a prerequisite for orientation. It is generated from stretching and shearing during the filling stage: fast filling tends to put more orientation on the part surface and less in the core, because the maximum shear always appears near the mould wall where the skin is solidified first, whereas the core freezes later and has more time for melt relaxation. While in the packing and cooling stage, the stretching and shearing essentially disappear, and the polymer orientation can relax out to various degrees. High melt temperature allows the melt to freeze more slowly and allows more time for orientation decay after flow ceases, whereas high holding pressure packs more material into the cavity to compensate for the shrinking melt, and the orientation near the gate and in the core will be exacerbated.

1.3.5 Jetting

When a small gate feeds a plane cavity in the same direction as shown in Fig. 1.3.4, jetting may occur.

A jet of melt is squirted across to the opposite wall without touching the cavity surface. When the jet reaches the wall it buckles and collapses onto the surface. Then the jetting ceases and the melt fills the remaining space in the cavity by spreading disc flow, forming weld-lines as it flows over the cool, buckled jet. Some experiments about jetting have shown that jetting may occur at both lower and higher injection rates, while simple mould filling occurs in the intermediate range of injection rates. The development of simple mould filling is caused by the contact of the extrudate with the mould wall. This can serve as a criterion for jetting. Another way to eliminate jetting is to use barriers near the gate. Detail discussion can be found in reference[9].

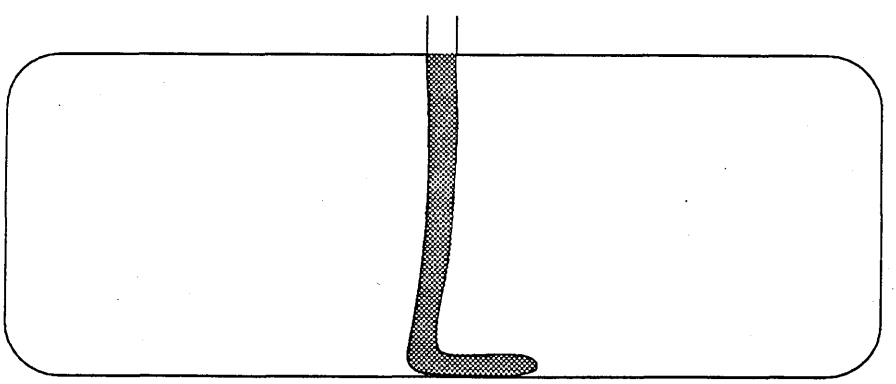

Fig.1.3.4 Jetting

1.4 Mathematical Description and Difficulties

The fluid mechanics and heat transfer of the injection moulding can be generally described by the conservation equations of mass, momentum and energy:

$$\frac{\partial \rho}{\partial t} + (\rho v_i)_{,i} = 0 \tag{1.1}$$

$$\rho\left(\frac{\partial v_i}{\partial t} + v_j v_{i,j}\right) = \sigma_{ij,j} + \rho g_i \tag{1.2}$$

$$\rho c_p\left(\frac{\partial E}{\partial t} + v_j E_{,j}\right) = (kT_{,j})_{,j} + \sigma_{ij} v_{i,j} + \rho v_j g_j + \rho Q \tag{1.3}$$

where ρ, v_i, σ_{ij}, g_i, E, T and Q indicate the density, velocity vector components, stress tensor components, body force vector components, internal energy, temperature and heat source strength of the field, respectively; t represents the time and j is the dummy index for summation; c_p and k are specific heat and thermal conductivity.

The closed system needs two more relations (of which forms can be flow and/or material dependent), that is, the appropriate constitutive equation for the stress tensor, and the equation of state for the internal energy. The associated boundary conditions include:

Solid boundary for the flows:

$$\left.\begin{aligned} v_i &= 0 \\ T_{flow} &= T_{mold} \\ k_f T_{,j} n_j\Big|_{flow} &= -k_m T_{,j} n_j\Big|_{mold} \end{aligned}\right\} \tag{1.4}$$

Flow front boundary for the melt:

$$\left.\begin{aligned} \sigma_{ij} n_j &= 0 \\ T_{,j} n_j &= 0 \end{aligned}\right\} \tag{1.5}$$

Exterior boundary for the mould:

$$T_{,j}n_j = h(T - T_\infty) \qquad (1.6)$$

where h represents the heat transfer coefficient between the mould and the ambient air at a temperature of T_∞.

Thus, the complete system (1.1-1.6) gives us a transient, compressible, non-isothermal, non-Newtonian, three dimensional fluid flow problem with geometric complexity, advancing flow front coupled with a transient heat conduction among the plastic melt, steel mould and cooling liquid.

It is readily seen that the most general, comprehensive formulation of injection moulding results in a very large and complex mathematical problem. While the basic difficulties associated with compressible Navier-Stokes equations remain intact, the constitutive equations of non-Newtonian flows contain higher-order derivatives and non-linear terms, and their best representatives are either of the integral or of the implicit type. The filling stage causes most concern as well as being the most difficult because of the unsteady moving flow front of the melt and the heat transfer through the interfaces between the plastic melt and the mould. Even in cooling stage when the melt is in a state of standstill, the mathematical difficulties include not only the three dimensional transient heat conduction among the melt, mould and the cooling liquid, but also the optimisation of the location and the size of the coolants. What is more, a theory of molecular orientation must be able, at least in principle, to give a complete picture of the process.

However, all the mathematical models that have appeared so far either focus on a specific subset of the general problem or involve major simplifications related to the difficulties mentioned above, or both. Compressibility effects are believed negligible during the filling stage though they may be present due to the large pressure variations involved in the injection moulding. The importance of this simplification is shown from the following advantages: the energy equation can be separately solved; the internal energy is reduced to temperature only; and the divergence of the velocity becomes zero. Another major simplification is that the non-linear terms of convection in the momentum equation can be dropped because polymer melt flows have high viscosity.

1.5 Review on Computer simulation of injection moulding

The highly competitive nature of the plastic industry and the complicated characteristics of polymer processing have served as two impetuses for

computer simulation of injection moulding. Over the last two decades, there has been a tremendous growth in the computer software engineering and intensive research on the numerical methods for serving the injection moulding industry. Some of the products of the software engineering which have evolved over this period are packages that serve to replace the "rules of thumb" of the past with more and more accurate analysis based on sounder theoretical principles. The common feature of the software tools is to combine the relatively matured numerical methods with quickly developed graphical display technologies to aid the engineering analysis. With this feature, the computer simulation has extended from the flow analysis for the filling stage to holding and cooling analysis, stress and creep analysis and shrinkage and warpage analysis for the later stages. As a result, greater emphasis is being placed on the optimisation of the product quality and performance.

Although the general principles in the dynamics of polymer liquid are very intricate and still developing, the modelling of polymer flow processes stemmed from very simple approaches. Colin Austin[6], who laid down the foundation of the Moldflow company in 1978 and who was involved in developing the original software himself, has successfully skipped the complicated mathematics and found the inherent simplicity for the flow analysis. He adopted a very straightforward equilibrium formulation for a thin slice (which could be a rectangular, or a round, or radial section) and assembled all the slices into a whole component following a time marching method. There are some basic ideas behind this simplification. One of them is that the fundamental relation between pressure and the shear stress for a thin slice is quite independent of material or flow characteristics. A second idea is that any errors from predicting shear rate come from the viscosity parameter given and not from any mathematical simplification[10]. Then the accuracy is mainly based on the ways of obtaining the viscosity and the database for them. K.K. Wang *et al.*[11,12] set up a team engaging in an interdisciplinary research on various problems of injection moulding process in Cornell University since 1974, a product of which is another famous commercial package for the injection moulding analysis called C-FLOW. Their two-dimensional model in the 70s was based on Hele-Shaw flow theory (a lubrication model) which was first introduced into this field by Richardson[13], and employed the inelastic generalised Newtonian fluid in a thin cavity by Wang, Shen and Hieber[14]. Other models include the transport models introduced by Harry and Parrott[15] who coupled one-dimen-

sional flow analysis with a heat-balance equation for a rectangular cavity; by Basov and Felipchuk[16] who used the same flow equations but heat conduction equations for the liquid and solid phases; and by Kamal and Kenig[17] and Berger and Gogos[18] using the assumptions of a radial creeping flow for a disc mould filling problem. Since the resulting system of the transport phenomena is quite complex, those various assumptions have to be made by the authors to simplify the mathematical treatment. They are mainly based on two considerations: the first is that the assumptions will not seriously damage the simulation accuracy; and the second is that some questionable items are neglected if they greatly reduce complexity and the error introduced results in more "conservative" solutions. Later on two-dimensional laminar-type flow models were mainly adopted. Broyer *et al.*[19] suggested Hele-Shaw-type model for the flow in a narrow gap mould; Kamal *et al.*[20,21] developed Laplace-type expression for the pressure in a thin cavity; White[22] used the same model to describe the flow in a fully developed flow region. Since the governing equations can be formulated without explicit reference to the rheology of the fluid, these approximations result in the advantage of numerical solving and reach a conclusion that the flow pattern and pressure distribution are independent of the rheological properties of the material. Finite element method was employed for solving the generalised Hele-Shaw flow by Hieber and Shen[23] who had been engaged in the research in the Cornell Injection Molding Group. A few years later, Shen[24,25] reported their new developments of the method which was modified in two aspects: a boundary-integral formulation replaced the finite element treatment of the pressure, and an 'energy integral' approach was used for the transient temperature. A Poisson equation of the pressure potential was solved by the then newly developed boundary integral method[26]. A different but similar modification was given by Jin *et al.*[27] in which a fictitious potential was introduced by using the Kirchhoff transformation, then the Laplace equation of the potential was much easier to be solved by the boundary element method. Almost at the same time as Wang-Hieber-Shen's team, Kamal and Lafleur[28] developed the creeping motion equations for the filling stage, the steady compressible equations for the packing stage and the transient heat transfer equation for the cooling stage with an extra term added for the heat generated by the crystallisation of the polymer (which was developed by Dietz[29]). The simulations of the flow fronts of the melt are considered no less important than the thin cavity flow approximation of the melt. Tadmor[30] was the first to propose a semi-

quantitative model in order to explain the effect of the fountain flow on the orientation distribution. Bhattacharji and Savic[31] presented an analytical solution to the fountain flow in a circular tube, assuming a flat flow front. Castro and Macosko[32] gave a similar solution for the plane flow under the same assumption. However, the assumption of a flat front is unrealistic. Numerical simulations have shown some results much closer to a practical flow front that is actually close to a semicircle. Bigg[33], Huang[34] and Kamal *et al*[35,36] have used the Marker-And-Cell (MAC) method[37] to give the results. The Galerkin finite element technique was employed to give the solution of the fountain flow by Mavridis[38,39]. Most of the modelling methods in the past are collected in a newly published book edited by Tucker III[40].

During the same period, the designs of commercialised packages on simulations for filling stage with more powerful functions as well as other stages of the injection moulding were under the way. In early eighties, the finite element method was introduced into both in C-FLOW and MOLDFLOW. Moldflow, ACAETI (Advanced CAE Technology Inc.), GEC (General Electric Co.), SDRC (Structural Dynamics Research Co.), AEC (Application Engineering Co.) CIMP (Cornell Injection Molding Program) finished the commercialised programs for cooling stage in the mid-eighties, separately, which are called MOLDTEMP, TMCONCEPT, IMES, C-COOL2D, MCAP, POLYCOOL2, MOLDCOOL[41-44] and COOL3D[45], respectively. Other commercially available packages are reviewed in references [46,47]. At this stage, CAD/CAM techniques which were developing in parallel begin to be merged with the processing analysis as these packages appeared to be graphically enhanced, interactive, user-friendly and integrated computer-aided engineering (CAE) systems.

The idea of using a display device to visually show the programmed cutter path was proposed and developed during the 1960's, which was actually the predecessor to today's CAD/CAM/CAE systems. Since then the graphical hardware and software developments have been strongly stimulated because the newcomers to the computer field brought in a totally new price and performance spectrum which created a drastic increase in the acceptance of computers in general, and in the use of computers for scientific, engineering, and manufacturing functions in particular. The rapid development of these technologies has yielded a completely different methodology of engineering analysis and design, especially after the occurrence of the systems that could display three-dimensional objects in high resolution.

The CAD/CAM/CAE products are revolutionising the speed and the efficiency of the plastic design and processing tasks. The "rules of thumb" that governed the designs of the past are giving way to sophisticated computer packages which are enabling major advances in speed, productivity, accuracy and quality. At first, these programs are mainly for manipulation of the complicated geometries, putting ideas into a shape and saving the geometry into a database. The obvious advantages are the intuitively guided creation, manipulation of geometrical information, and the presentations and outputs from the systems. Secondly, they are used as pre- and post-processor of other packages like stress analysis, economic and operation analysis, etc. Many interfaces are designed for transferring the graphical and physical data between the two types of packages. As the requirements grow for computers to evaluate the geometrical designs and productivity, and the computer hardware techniques develop, gradually the evolution of the systems of purely geometrical manipulations merges with the development of the analysis systems. For example, IBM(Greenock)[48] is now building up a highly integrated CIM (Computer Integrated Manufacturing) system for increasing its productivity and competing ability, in which the most beneficial aspects of the applications will be the prototyping the part, the designing of mould, and mould-making. Xerox Co. has already built up a CAE package called ACTFLOW[49] whose flow solvers are based on those of MOLDFLOW, C-FLOW and MEFISTO (developed in Institut für Kunststoffverarbeitung, Germany). The details about what and how benefits are for the designs can be found in the reference written by Gosztyla[50].

The geometrical complexity is a really difficult task in computer simulation of injection moulding. However, the most difficult task, which many researchers tried to avoid, or to simplify, or to simulate with more accurate models, is in the rheological aspects of modelling plastic behaviours. Plastic liquids are non-Newtonian fluids; the non-linear constitutive relations characterised by the rheological properties therefore play a central role in governing the way they flow and deform in response to applied forces and the stresses inside them. Some classic and pioneering works on the polymeric rheology of continuum and combination of the molecular theory and continuum are introduced in several recently published books[51-55]. Kamal and Ryan[56] give a very good review on the rheological aspects. It is pointed out in their paper that in modelling a polymer processing operation, two opposing factors must be carefully considered in selecting a rheological constitutive equation. First, it is desirable to select a constitutive equation

which has the capability of accurately describing the rheological response of material over a broad range of environmental conditions and deformation histories. On the other hand, the constitutive relation must be utilised in conjunction with the governing equations, therefore, the mathematical simplicity of the relationship is of prime concern. Crochet and Watlers[57] also point out that for reasons of tractability, the more complex the flow problem, the simpler has to be the constitutive model used in non-Newtonian fluid mechanics. Tanner[55] gives a table of five reflections of twenty different constitutive models subject to seven types of classified flows. From the table he suggests that it would be wasteful and counterproductive to always insist on using the most complex model of constitutive equation for all purposes. One should choose only those which are suitable for the problems studied. Because of the geometrical complexity in the computer simulation of injection moulding, it is necessary to compromise between the accuracy in the description of material response and the mathematical tractability of the resulting governing equations. Especially on practical applications, easier approaches for prediction of the flow phenomena are preferable.

1.6 Lagrangian Description in the Numerical Simulation

Although most of the formulations mentioned above, or more general — in fluid mechanics, are based on Eulerian description, Lagrangian ideas are found very important in the numerical simulation of injection moulding. From the most intuitive point of view, the filling stage of the problem is a finite fluid flow with a moving boundary, the phenomenon of a quantity of polymeric liquid which moves, deforms from one space to another. On the other hand, the polymeric fluids are viscoelastic materials whose constitutive laws are expressed as integro-differential equations written for a particle. Therefore it is better to trace a particle's trajectory in time to give an effective way for the calculation[58]. Even for some simple models of the constitutive equation, the viscous terms dominate the flow so that the convection terms can be naturally dropped, therefore Lagrangian formulation can be relatively ideal. A further requirement for the Lagrangian description is to give the orientation of plastic particles or even fibre-like particles concerned. The numerical techniques based on a Lagrangian description have been developed for fluid mechanics both in finite difference methods and in finite element methods for many years. They can date back to 1950s,

when the famous work[59] by von Neumann-Richtmyer was developed using a one dimensional Lagrangian description. Although later developments (like Kolsky[60], Wilkins[61], Goudreau and Hallquist[62], etc.) of the Lagrangian techniques in two- and three-dimensions are mainly concentrated on hyperbolic equations of compressible fluid and/or elastic-plastic flows, their extensions to incompressible, non-Newtonian liquids can still be found[63-67]. Since the coordinate system follows the fluid motion, they have significant advantages of sharp resolution of material interface and no convection across the boundary of each element so that the methods are highly accurate and stable, and easily implemented. Therefore they are often used in the studies of multimaterial interaction and the incorporation of surface tension effects. However, the major disadvantage of the techniques is the mesh tangling at severe distortions, and it has been thought to block their developments. Numerous efforts have been made to mitigate the mesh distortion problem, such as various methods of remeshing, and some Lagrangian-Eulerian hybrid methods like Particle-In-Cell method (PIC)[68,69], Marker-And-Cell method (MAC)[37], Arbitrary Lagrangian Eulerian method (ALE)[70], Finite Volume Method (FVM)[71]. Although these combinations of both Lagrangian and Eulerian give successful solutions to the computational fluid mechanics, some of these hybrid methods require enormous computer space to store both the grid and particle information, and double the computing time; Others not only increase the computing time two-fold but also lose both the accuracy and the original characteristics of Lagrangian description which appear to be important in the injection moulding simulations.

1.7 Why Boundary Element Methods

The disadvantage of these pure Lagrangian techniques is because of the FDM's or FEM's grid system in which most of the unknowns are defined and solved explicitly or implicitly. Although it seems that only Free Lagrangian Method (FLM)[72] manages to extend the pure Lagrangian techniques without loss of the accuracy and improve mesh distortion problem by reconnecting mesh based on some connectivity rules, it is worthwhile trying to develop them by a completely new method without the domain grid system involved. Boundary element methods have emerged as a powerful alternative; since the unknowns to be solved are those on the boundaries, the unknowns within the domain in most of cases can be

derived from the boundary values, which give better accuracy and a continuous solution.

Boundary element methods stem from the modern theory of boundary integral equations which could date back to 1903 when Fredholm[73] established the existence of solutions on the basis of his limiting discretisation procedure. Only after the advent of fast digital computers did the possibility of implementing the discretisation process arithmetically opened up. Although there were considerable developments on the numerical implementation of the discretisation of the equations (they were reviewed in [74]), since the finite difference and later the finite element methods had been dominating the numerical analysis in engineering, boundary integral equation methods did not obtain much attention from the engineering circle until 1978 when Brebbia's first book[75] on boundary element method was published, in which the discretisation of the classic boundary integral equations was transferred into the concepts and transformations of the type already known in finite element methods. The advantages of this alternative give an impetus to the rapid development in many areas of which the fundamental solutions of the governing equations are available, such as potential problems and linear elastostatics. There are still some useful features in its extension to non-linear and time-dependent problems, such as accuracy and easy implementation, though its "boundary only mesh" advantages appears to be no longer exist since most of the developments in these areas have suffered from the application of finite element concepts in the domain. However, the potential promotion remains as some papers show efforts to preclude the domain integrals by the dual reciprocity principle[76-78] and the multiple reciprocity method[79-82].

The first numerical application of boundary methods to fluid mechanics was in the amazing paper by Trefftz[83]. The integral equations governing flows of incompressible viscous fluids and the fundamental solutions to classic Stokes equations, time-dependent creeping motion equations, and even the Stokes equations with one simplified convection term can be found in Oseen's remarkable monograph[84]. However, there are various ways to deal with different problems in fluid mechanics so that the integral equations can take several forms. The early notable numerical approximations of boundary integral equations in fluid mechanics started in potential flow, when Hess and Smith[85] developed their pioneering work in aerodynamics. In early 1970s, Wu[86] began his investigations with a velocity-vorticity formulation, which separates the kinematics from the kinetics of the incom-

pressible problem. Later on, Coleman[87,88] has done some researches on steady Newtonian and non-Newtonian flows with a formulation of the stream and stress functions; Bush and Tanner[89], Tosaka and Onishi[90] have used the fundamental solutions of primitive variables to develop the formulation for steady viscous flows; Tosaka and Onishi[91] have also given their integral formulations and the fundamental solutions for unsteady viscous flows by time-differencing; Kitagawa and Brebbia[92,93] have developed the penalty function method. Dargush and Banerjee[94] have followed Oseen's fundamental solutions of both steady and unsteady viscous flows to give their applications of boundary element methods. Some other recent works related to various fluid dynamics are reviewed in newly published books[94,95].

It is not surprising that all these developments in boundary element methods are based on Eulerian coordinate system, trying to face the non-linearities rather than to avoid them. As far as the author knows the only exception is Hebeker's work[96] in which he uses the Lagrangian form to drop the convection terms. In this regard this thesis emphasises developing boundary element approaches in Lagrangian description, both for steady and unsteady incompressible viscous flows. Boundary element methods are also used to solve some simplified models for non-Newtonian flow in ducts and in thin cavities.

From another point of view, the boundary element methods are really manifesting themselves as better roles in Computer Aided Engineering systems, especially for those three dimensional problems. Hence in a long term, the methods should be at least one part of the basis of a new system, such as CASIM, the system this thesis is establishing, which brings these new and better ideas into the computer simulation of injection moulding, and is expected to be able to solve various practical processing problems in injection moulding.

1.8 The Arrangement of the Thesis

This thesis is arranged roughly according to the degree of modelling complexity. The second chapter concerns mainly the non-isothermal non-Newtonian flow in a pipe, and gives a boundary element model for other shapes based on the analytical solutions for the pipe flow. Chapter Three reviews a boundary element model which is based on a group of simplified governing equations for the filling stage in thin cavities, and shows a

boundary solution of the velocity potential and a further development of modelling the temperature field of the stage. Two examples are given for testing the effectiveness and accuracy in predicting the flow front patterns. Transient temperature field of the cooling stage is simulated in Chapter Four by using a time-dependent boundary element method for multimedia problems. Discussions are given on the use of interfacial elements and the concave domain calculations. In Chapter Five, the governing equations of steady viscous flow are transferred into boundary integral equations and the unknown pressure is decoupled from the equations; problems concerning the particle and fibre orientations and free moving surface related to fountain flow are simulated by using the boundary element method resulted from creeping model. Chapter Six gives a detail formulation of boundary integral equations on unsteady viscous flow. Two unsteady problems with free moving surface are given to demonstrate the effectiveness of the resulting boundary element method. The practical simulations of some IBM's computer parts with geometrical complexity are given in Chapter Seven by using MOLDFLOW; A useful principle is suggested there for simulating complicated multicavity mouldings.

Chapter Eight outlines the CASIM program design which includes the basic techniques in writing graphical enhanced pre-, post-processors, image processor and in all the modules of BEM models mentioned in Chapter Three, Four, Five and Six.

It is noted that the aim of the development of the boundary element methods is to solve the complicated problem effectively and accurately. The most headache obstacle in the development is the involvement of domain integrals. Although the author treats the domain integrals by domain meshing in the thesis, the last contribution to the thesis is a new dual reciprocity theory which, in author's view, will be the next step in boundary-only scheme. This is the reason the author mentions the developments in chapter two, three, four, five and six but leaves the numerical implementations and examples for his future work. Yet it is not the only challenge in this computer simulation of injection moulding since there are so many outstanding problems. Therefore in the last chapter, the author wishes to suggest the immediate next step of the research, the difficulties and the modelling potentials.

Chapter Two

Nonisothermal Laminar Flow in Ducts

2.1 Introduction

In the injection moulding process one first encounters viscous flows in ducts. Plastic melt is forced through confined channels at relatively high speed so as to minimise the cycle time. The flows inside the confined channels such as sprues or runners are typically laminar. Because most polymers have a low thermal conductivity and a high viscosity which is dependent on the shear-rate, pressure and temperature, the entanglement of these factors in the flows results in various concerns. One of the phenomena is the choking possibility[97,98] caused by the high pressure involved and its dependence of the viscosity. Others include the velocity profile and the temperature increases caused by the shear-rate dependence. As mentioned before, severe rise in temperature can result in degradation in thermoplastics, or trigger premature reactions in thermosets. Therefore it is very important to be able to estimate the local temperature change in ducts due to viscous heating and heat transfer so that the processing melt temperature and the injection speed can be properly controlled.

Although the controlling equations for general viscous flow are very complicated, when the flow occurs in straight ducts with constant cross section, it can be assumed as a fully developed steady flow, and then the nonlinear convective terms in the momentum equations vanish identically. For Newtonian fluids with an isothermal assumption in some regular cross sections, even exact solutions of the resulting linear equations can be easily worked out[99]. However, the cross section is not often regular and the fluid inside is completely non-Newtonian or viscoelastic. The nonisothermal characters of the flows require the energy equation to be taken into account and solved simultaneously with the other equations. Since this fully developed tube flow is characterised with simple shearing, and very close to steady viscometric, a generalised Newtonian fluid (GNF) model can be suitable to give quite good results for flow rate and shearing stress[55,53]. The high dependence of the non-Newtonian viscosity on the pressure, shear rate and temperature can then be expressed in simple ways.

For flows in a circular tube, much work has been done by using different models. It is simply because fully developed flow implies that $\partial V_z/\partial z=0$, and on the basis of symmetry, there is no θ dependence at all. Therefore from the continuity equation and no slip boundary condition it can be seen that $V_r=0$. With an isothermal assumption, the controlling equations are then reduced to

$$\frac{dP}{dz} = -\frac{1}{r}\frac{d}{dr}(r\tau_{rz}) \qquad (2.1.1)$$

together with proper relation between the stress and the strain-rate. The Newtonian relation between them gives the simplest form

$$\tau_{rz} = \mu\frac{dV_z}{dr} \qquad (2.1.2)$$

in which μ is the viscosity constant. The exact solution for a Newtonian fluid is given as follow:

$$V_z = \frac{(P_o - P_L)R^2}{4\mu L}\left[1-\left(\frac{r}{R}\right)^2\right] \qquad (2.1.3)$$

where V_z is the velocity component in the axial direction, R is the radius of the tube, P_o and P_L are the pressure from both ends of the tube with length L. From this result the relation between the volume rate of flow and the pressure drop can be obtained:

$$Q = \int_0^{2\pi}\int_0^R rV_z\,dr\,d\theta = \frac{\pi(P_o - P_L)R^4}{8\mu L} \qquad (2.1.4)$$

which is the famous result of Hagen[100] and Poiseuille[101].

The idea of generalised Newtonian fluid models is to modify the viscosity of Newton's law by varying it with the shear rate. One of the GNF models is the well known power-law model[102]

$$\eta = \eta_o\dot{\gamma}^{n-1} \qquad (2.1.5)$$

in which η_o and n are two parameters and γ is the square root of the half second scalar invariant of the strain-rate tensor

$$\dot{\gamma} = \sqrt{\frac{1}{2}\dot{\gamma}_{ik}\dot{\gamma}_{ki}} \qquad (2.1.6)$$

Replacing Newtonian viscosity by expression (2.1.5), equation (2.1.1) now results in[103]

$$V_z = \left(\frac{R}{s+1}\right)\left(\frac{R(P_o - P_L)}{2\eta_o L}\right)^s\left[1 - \left(\frac{r}{R}\right)^{s+1}\right] \qquad (2.1.7)$$

where s=1/n. For n<1 this gives a velocity profile that is flatter than the parabolic profile in equation (2.1.3) for Newtonian fluids. It is easy to obtain the volume rate of flow Q

$$Q = \left(\frac{\pi R^3}{s+3}\right)\left(\frac{R(P_o - P_L)}{2\eta_o L}\right)^s \qquad (2.1.8)$$

For n=1 it reduces to the Hagen-Poiseuille "law".

Clearly the temperature rise by viscous heating and heat transfer is appreciable because of the high viscosity for polymeric fluids and the large velocity gradients. The isothermal assumption is no longer appropriate and the energy equation for temperature distribution must be taken into account

$$\rho C_p V_z \frac{\partial T}{\partial z} = k\left(\frac{1}{r}\frac{\partial}{\partial r}\left(r\frac{\partial T}{\partial r}\right) + \frac{\partial^2 T}{\partial z^2}\right) + \tau_{zr}\frac{dV_z}{dr} \qquad (2.1.9)$$

where T is temperature, ρ is density, C_p is specific heat and k is thermal conductivity. In general those physical properties are temperature dependent, but they are assumed to be constants for most polymeric flow and heat transfer calculations, according to the information obtained[104] for some materials. Only the specific heat is found to be a strong function of temperature for some semi-crystalline materials.

Although it is reasonable in many calculations to assume that k, C_p, and ρ do not vary with temperature, the same cannot be said for the parameters in the generalised Newtonian fluid model for η. Apart from the temperature and shear-rate, pressure is also found to have influence on the viscosity[105].

A useful empirical equation for these dependences of the power-law form of viscosity is:

$$\eta = \eta_o e^{\beta(p-p_o)-\alpha(T-T_o)}\dot{\gamma}^{n-1} \qquad (2.1.10)$$

where p_o and T_o are reference pressure and temperature, respectively; and η_o, β, α and n are considered as constants and are determined for each fluid from experimental data.

In general, the governing equations (2.1.1), (2.1.2), (2.1.9) and (2.1.10) are difficult to solve. By making different simplifications, however, solutions for the each case can be obtained. By neglecting the heat conduction and convection in the axial direction, Kearsley[106] obtained the solution for n=1 case. By assuming that the viscous-heating is unimportant, ignoring the axial heat conduction in equation (2.1.9), and the velocity profile as given by equation (2.1.7), an asymptotic solution of the temperature distribution for small z can be obtained[107]. By ignoring the axial heat conduction and assuming α=0, that is, the viscosity expressed as equation (2.1.5), Dinh and Armstrong[108] obtained analytic solution with an infinite set of eigenfunctions corresponding to the infinite set of eigenvalues. By assuming that the temperature is independent on z, Martin[109] obtained the exact solution for the fully developed flow in a pipe for $\alpha\neq0$ and $n\neq1$ case. Recently Richardson[110-113] extended the solutions to developing flows in several different shapes of the ducts. However, the pressure dependence of the viscosity was not taken into account in all these solutions.

In this chapter, the exact solution for the case of fully developed flow (both temperature and velocity) is extended to an exact solution for $\alpha\neq0$, $n\neq1$ and $\beta\neq0$ case, and an approximate solution in the axial direction is developed. They are then generalised for slightly tapered pipe. The possibility of choking is discussed in different cases. In later sections starting from 2.6, boundary element formulations for nonisothermal laminar flows in ducts of arbitrary cross sections are developed, in which a dual reciprocity method is introduced.

2.2 Fully Developed Flow in a Pipe

Assume first that the temperature is fully developed, then the energy equation (2.1.9) reduces to

$$k\frac{1}{r}\frac{d}{dr}(r\frac{dT}{dr}) = \tau_{zr}\frac{dV_z}{dr} \qquad (2.2.1)$$

where the right hand side is actually a negative value since we define

$$\tau_{zr} = -\eta\frac{dV_z}{dr} \qquad (2.2.2)$$

with proper boundary conditions given as follows (no frozon layer):

$$T = T_w,\ V_z = 0 \quad \text{when } r = R \qquad (2.2.3a)$$

$$\frac{dT}{dr} = 0,\ \frac{dV_z}{dr} = 0 \quad \text{when } r = 0 \qquad (2.2.3b)$$

then equations (2.1.1), (2.1.10), (2.2.1-3) construct a complete controlling system for this nonisothermal steady flow in a pipe of radius R.

From equation (2.1.1) the stress can be expressed as a function of pressure gradient and, combining with (2.2.2), yields the following relation

$$\tau_{zr} = \frac{r}{2}\frac{dp}{dz} = -\eta_o \exp[\beta\Delta p - \alpha(T - T_w)]\dot{\gamma}^{n-1}\frac{dV_z}{dr} \qquad (2.2.4)$$

From the expression (2.1.6), the strain-rate can be worked out easily as $\dot{\gamma}$=-dV_z/dr. Substituting this relation into (2.2.4) results in

$$\frac{dV_z}{dr} = -\left(\frac{rP_z}{2\eta_o}\right)^s \exp[\alpha s(T - T_w) - \beta s\Delta p] \qquad (2.2.5)$$

where s = 1/n, P_z=-dp/dz and Δp is the pressure drop along the pipe.

Substituting equations (2.2.4) and (2.2.5) into equation (2.2.1) yields

$$k\frac{1}{r}\frac{d}{dr}(r\frac{dT}{dr}) = -\eta_o \exp[\alpha s(T - T_w) - \beta s\Delta p]\left(\frac{rP_z}{2\eta_o}\right)^{s+1} \qquad (2.2.6)$$

The solution to this equation, according to Martin's solution[109], can be written in the following form:

$$T = T_w + \frac{1}{\phi}\ln\{\exp(\phi\Delta T) + [1 - \exp(\phi\Delta T)]x^{s+3}\} \qquad (2.2.7)$$

where $\phi=-\alpha s/2$, $x=r/R$ and

$$\Delta T = \frac{1}{\phi}\left[\ln\left(1 \pm \sqrt{1-4Na_p}\right) - \ln 2\right] \qquad (2.2.8)$$

in which $Na_p = \dfrac{\eta_o \alpha s R^{s+3}}{2(s+3)^2 k \exp(\beta s \Delta p)}\left(\dfrac{P_z}{2\eta_o}\right)^{s+1}$ is defined as a dimensionless parameter called Nahme number based on the pressure drop, which is often used to interpret the ratio of heat generation to heat required to alter the viscosity in non-isothermal problems.

It can be seen that the variation of Na_p can only be between 0 and 1/4, ΔT has two roots corresponding to any value in the range other than 1/4. However the range for pressure drop can be very large.

Substituting the temperature solution into (2.2.5) produces

$$\frac{dV_z}{dr} = \frac{-\exp(-\beta s \Delta p) x^s}{\left\{\exp(\phi \Delta T) + [1 - \exp(\phi \Delta T)] x^{s+3}\right\}^2}\left(\frac{RP_z}{2\eta_o}\right)^s \qquad (2.2.9)$$

By using the velocity boundary conditions in (2.2.3), the volumetric flow rate can be obtained as follow

$$Q = -\pi R^3 \int_0^1 x^2 \frac{dV_z}{dr}\, dx = \frac{\pi R^3}{(s+3)\exp(\phi \Delta T + \beta s \Delta p)}\left(\frac{RP_z}{2\eta_o}\right)^s \qquad (2.2.10)$$

This relation, according to (2.2.8), indicates that the same pressure distribution (or drop) along the axis can have two values of the flowrate. This is similar to the discussion in reference [112], however, the pressure drop corresponding to a single value of flowrate may never be reached if parameter β is not zero, therefore two curves case may occur.

Eliminating the pressure related factors, the velocity function can be expressed as

$$V_z(x) = \frac{Q(s+3)}{\pi R^2} \int_x^1 \frac{-\exp(\phi \Delta T) x'^s\, dx'}{\left\{\exp(\phi \Delta T) + [1 - \exp(\phi \Delta T)] x'^{s+3}\right\}^2} \qquad (2.2.11)$$

Expressions (2.2.7,10&11) are the complete solutions of the temperature, volumetric flow rate and velocity within the pipe. Both equations (2.2.7) and (2.2.11) are two parameter dependent functions, they are $\phi\Delta T$ and s, or more basically, $\alpha\Delta T$ and s. $\alpha\Delta T$ is often defined as a dimensionless parameter called Pearson number which in the present case is interpreted as the ratio of the heat flux resulting from the temperature difference between the centre and the wall to heat required to alter the viscosity. Fig.2.2.1 and 2.2.2 show schematically the temperature and velocity curves in terms of these two parameters, respectively.

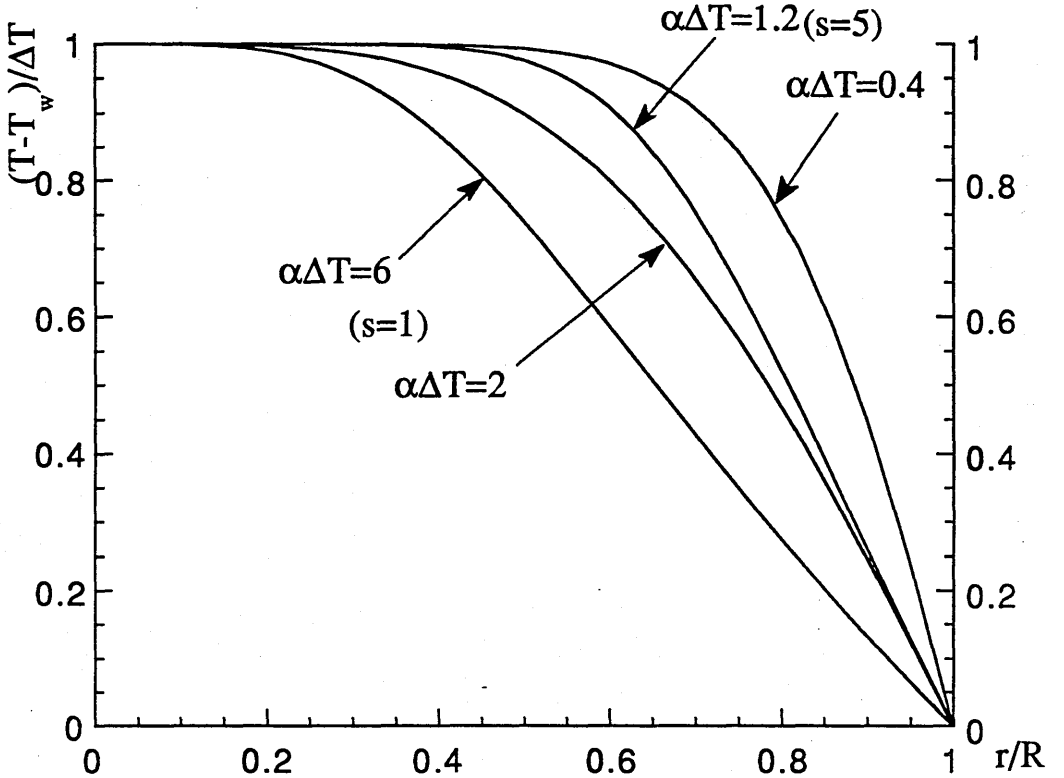

Fig.2.2.1 Dimensionless temperature profile

Differentiating equation (2.2.9) it can be seen that there is a zero point of the second derivative of the velocity which can be expressed as follow:

$$x^{s+3} = \frac{(s+1)\exp(\phi\Delta T)}{(s+5)(1-\exp(\phi\Delta T))} \qquad (2.2.12)$$

Clearly, if the zero point is about a half, as shown in Fig.2.2.2, the velocity in the boundary layer is much slower than that in the centre part. This profile requires the Pearson number higher than a critical value. When the Pearson number is above that value, even though it cannot indicate that

there must a "frozen" layer existing next to the wall, the profile can quite smoothly extend to the stagnant boundary layer. The frozen layer can be taken into account by introducing a melting temperature T_m which can be located with R_m if $T_w<T_m<T_w+\Delta T$. Thus the dimensionless r/R becomes r/R_m in Fig.2.2.2, and upper bond of the integration in (2.2.11) changes to R_m/R. A full discussion of frozon layer can be found in reference [112].

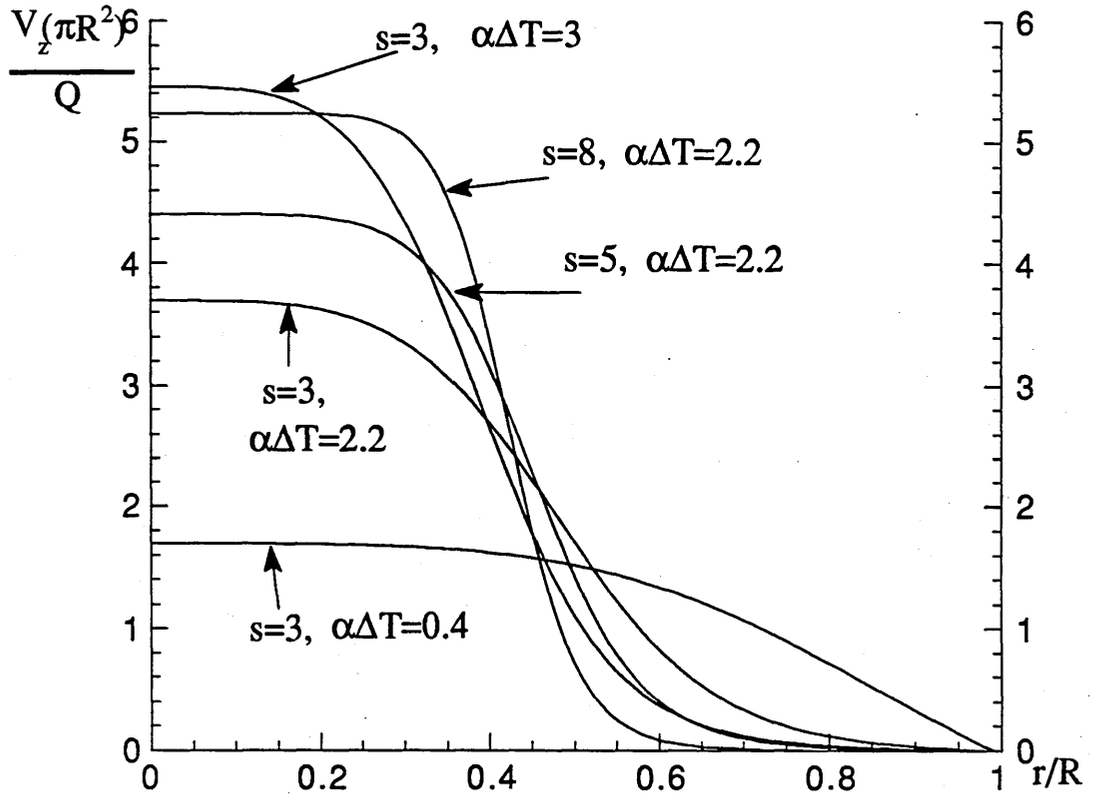

Fig.2.2.2 Dimensionless velocity profile

2.3 Choking Possibility

From solution (2.2.10) it can be seen that when the flowrate has a single value (which means that $Na_p=1/4$), the pressure drop has to satisfy the following equation

$$\frac{d(\Delta p)}{dz} = -K\exp\left(\frac{\beta s\Delta p}{s+1}\right);\quad \text{where } K=\left[\frac{(s+3)^2 k(2\eta_o)^s}{\alpha s R^{s+3}}\right]^{\frac{1}{s+1}} \qquad (2.3.1)$$

If the boundary conditions ($\Delta p=0$, when $z=L$; $\Delta p=\Delta p_o$, when $z=0$) are used, this equation leads directly to the following solution

$$\Delta p_o = -\frac{s+1}{\beta s}\ln\left[1-\frac{\beta s KL}{s+1}\right] \qquad (2.3.2)$$

This solution predicts a rapid increase in the required pressure to reach a certain distance from the inlet, and because of the pressure dependence, choking of the flow occurs when $\beta sKL/(s+1)$ approaches to unity. If $\alpha=0$ ($\phi=0$), a similar equation can be derived from solution (2.2.10) which is the same conclusion as that from reference [97]; If s=1, (2.3.2) reduces to the same solution as equation (22) in reference [98].

It is interesting to see that even if $\alpha\neq0$ and the pipe is longer than a critical length, $(s+1)/\beta sK$, choking would still be predicted to occur at $L=(s+1)/\beta sK$. In practice, however, choking never happens[98]. Therefore it is fully justified to repudiate the assumption* of fully developed temperature, though in some cases the critical length could be very long.

In order to use the fully developed solutions to obtain an approximate solution for the temperature distribution in the z direction, some new assumptions must be made. First the mean temperature $\bar{T}$ and a new reference temperature T_n are introduced, and a relation

$$\Delta T = 2(\bar{T} - T_n) \qquad (2.3.3)$$

is assumed in which ΔT is a function of z, and T_n is a function of s and α.

Substituting this relation into (2.2.10) and then differentiating the equation results in

$$-\alpha P^*_z d\bar{T} = dP^*_z \qquad (2.3.4)$$

where $P^*_z = \exp(-\beta\Delta p)P_z$.

One more equation to relate the mean temperature and the pressure along the axial direction is needed. The simplest model is to assume that the heating along the axis is adiabatic, for which the first law of thermodynamics leads to an expression for the temperature rise in the form[114]

$$\rho C_p Q d\bar{T} = Q dp \qquad (2.3.5)$$

in which ρ and C_p are density and heat capacity per unit mass. However, this equation does not show the direction of the increasing pressure. In the filling process the pressure decreases in the positive z direction while the temperature increases. Therefore, a negative sign should be added in either side when the differentiation is with respect to z.

The boundary conditions are as follows

* Actually $\partial T/\partial z$ is not zero, the temperature field is thus fully developed in the sense that convection and axial conduction are negligible but not in the sense that the temperature field is independent of z.

$$\left.\begin{array}{ll} \Delta p = \Delta p_o;\ \bar{T} = \bar{T}_o & \text{when } z = 0 \\ \Delta p = 0 & \text{when } z = L \end{array}\right\} \qquad (2.3.6)$$

A complete system for both the pressure and the mean temperature along the z axis is constructed through (2.3.4-2.3.6). If the constant part of K is defined as K'

$$K' = \frac{2\eta_o}{R}\left[\frac{Q(3n+1)}{n\pi R^3}\right]^n \qquad (2.3.7)$$

then, by simple manipulations, the following relation is produced

$$\left(\beta + \frac{\alpha}{\rho C_p}\right)\Delta p_o = \ln\left[1 + \left(\beta + \frac{\alpha}{\rho C_p}\right)K' L \exp(-\alpha \bar{T}_o)\exp(\beta \Delta p_o)\right] \qquad (2.3.8)$$

from which it can be seen that choking never occurs.

Like expression (18) in the reference[97], equation (2.3.8) can be written in a more useful form:

$$\left(\beta + \frac{\alpha}{\rho C_p}\right)K' L \exp(-\alpha \bar{T}_o) = \exp\left(\frac{\alpha \Delta p_o}{\rho C_p}\right) - \exp(-\beta \Delta p_o) \qquad (2.3.9)$$

If β=0, the pressure drop can be explicitly expressed as

$$\frac{\alpha}{\rho C_p}\Delta p_o = \ln\left[1 + \frac{\alpha K' L}{\rho C_p}\exp(-\alpha \bar{T}_o)\right] \qquad (2.3.10)$$

If α=0, (2.3.8) reduces to equation (9) in reference [97].

2.4 Axial Approximate Solutions for Temperature and Pressure

Expression (2.3.9) is the approximate relation between the length L of the tube and the pressure drop Δp_o which is the pressure difference p_o-p_L. Therefore the pressure at z=L can be expressed in terms of the starting pressure and the starting mean temperature. According to the reference[97],

however, only if L is longer than a certain length can the equation be useful.

The approximate distributions of the pressure and the mean temperature within the range (0,L) are given as follows:

$$p = p_L - \frac{1}{\left(\beta + \frac{\alpha}{\rho C_p}\right)} \ln\left\{\frac{z}{L} + \left(1 - \frac{z}{L}\right)\exp\left[-\left(\beta + \frac{\alpha}{\rho C_p}\right)\Delta p_o\right]\right\} \quad (2.4.1)$$

$$\bar{T} = \bar{T}_o + \frac{p_o - p}{\rho C_p} \quad (2.4.2)$$

The last relation indicates that the mean temperature at z=L can also be expressed in terms of the starting pressure and the starting mean temperature:

$$\bar{T}_L = \bar{T}_o + \frac{\Delta p_o}{\rho C_p} \quad (2.4.3)$$

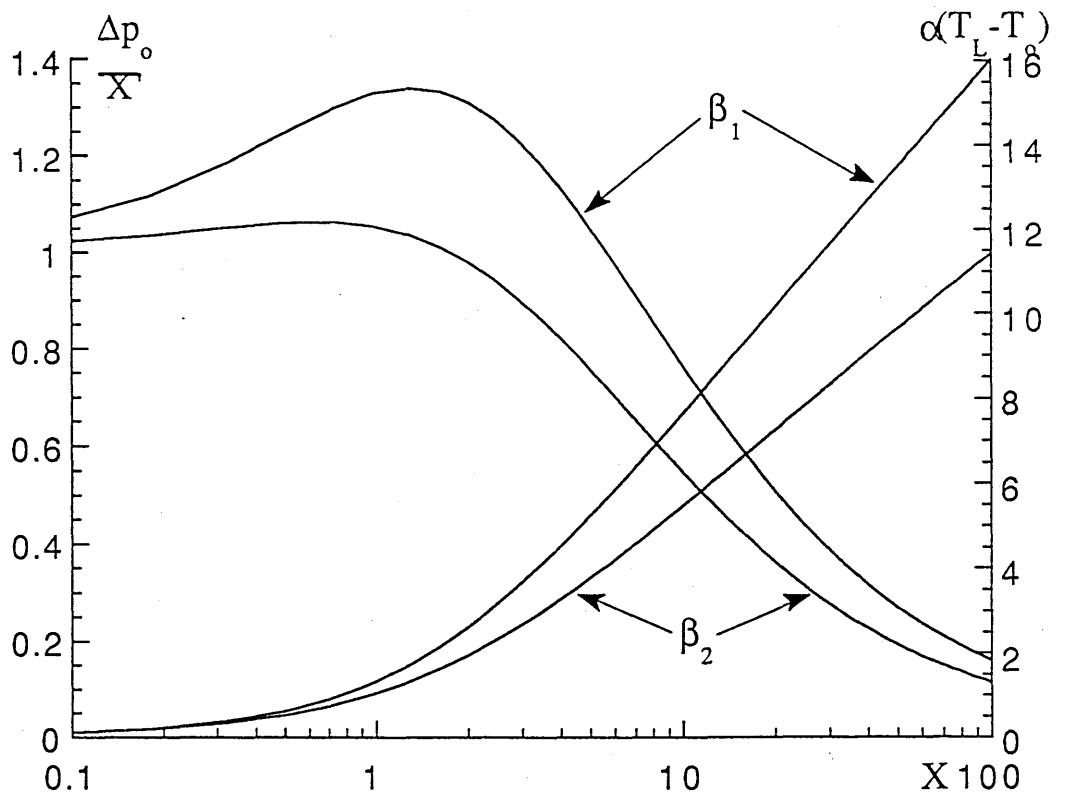

Fig.2.4.1 The pressure drop and the mean temperature.

$$\left(X = \frac{\alpha}{\rho C_p} K' L \exp(-\alpha \bar{T}_o);\ X' = X\frac{\rho C_p}{\alpha};\ \beta_1 = 2.5\frac{\alpha}{\rho C_p};\ \beta_2 = 1.5\frac{\alpha}{\rho C_p}\right)$$

Equations (2.3.9) and (2.4.3) are very useful explicit expressions for the mean temperature and the pressure in terms of inlet conditions and other parameters such as the flow-rate, radius and those for viscosity. Fig.2.4.1 shows the distributions of the mean temperature and the pressure.

2.5 Approximate Solution for Slightly Tapered Circular Tube

In practical injection moulding, a tapered tube is often designed for a sprue or a runner in order to be easily ejected with the moulding connected. The flow in a tapered tube requires consideration of both the radial direction and an acceleration in the axial direction, but it is still reasonable to assume that the flow will maintain axial symmetry. Therefore it can be assumed that the velocity is independent of θ direction. The continuity equation and the r- and z-components of the equation of motion are then

$$\frac{1}{r}\frac{\partial}{\partial r}(rV_r) + \frac{\partial V_z}{\partial z} = 0 \qquad (2.5.1)$$

$$\rho\left(V_r\frac{\partial V_r}{\partial r} + V_z\frac{\partial V_r}{\partial z}\right) = \frac{1}{r}\frac{\partial}{\partial r}(r\tau_{rr}) + \frac{\partial \tau_{zr}}{\partial z} - \frac{\partial P}{\partial r} \qquad (2.5.2)$$

$$\rho\left(V_r\frac{\partial V_z}{\partial r} + V_z\frac{\partial V_z}{\partial z}\right) = \frac{1}{r}\frac{\partial}{\partial r}(r\tau_{zr}) + \frac{\partial \tau_{zz}}{\partial z} - \frac{\partial P}{\partial z} \qquad (2.5.3)$$

These nonlinear equations are difficult to solve in general. However the advantage of the fact can be taken that the geometry changes slowly to show that these equations are dominated by only a few terms, and if the small terms are neglected, the problem is easy to solve.

At first the sizes of the velocities is estimated. The axial velocity is determined by the volumetric flow rate and must be of order $(Q/\pi R^2)$. This is written as

$$V_z \approx O(Q/\pi R^2) \qquad (2.5.4)$$

The size of V_r is dictated by the continuity equation which gives.

$$\frac{1}{r}\frac{\partial}{\partial r}(rV_r) = -\frac{\partial V_z}{\partial z} \approx O\left[\frac{Q}{\pi R_o^2 L}\left(1-\frac{R_o^2}{R_L^2}\right)\right] \qquad (2.5.5)$$

Clearly if the tube is slightly tapered which means that $(R_o-R_L)/L<<1$, then this derivative is very small. If it is approximately assumed that the derivative is zero, then the controlling equations reduce to equation (2.1.1) again. The same assumption can also be used as it has been used in section 2.2 for the temperature so that the solutions (2.2.8-10) for the circular tube case can still be used here.

Differentiating expression (2.3.1) with respect to z again, noticing that this time R is a linear function of z such that $R=R_o+(R_L-R_o)(z/L)$, then the relation between the pressure gradient and the temperature difference is obtained as follow

$$\frac{dP_z^*}{P_z^*} = \frac{dK'}{K'} - \alpha d\bar{T} \qquad (2.5.6)$$

By using the first law of thermodynamics and the boundary conditions again, a differential equation for the pressure drop is obtained

$$\frac{d(\Delta p)}{dz} = -K'\exp\left[-\alpha\bar{T}_o - \frac{\alpha\Delta p_o}{\rho C_p} + \left(\beta+\frac{\alpha}{\rho C_p}\right)\Delta p\right] \qquad (2.5.7)$$

The solution to this equation can be written in a similar form as equation (2.3.9)

$$\left(\beta+\frac{\alpha}{\rho C_p}\right)K''\exp(-\alpha\bar{T}_o) = \exp\left(\frac{\alpha\Delta p_o}{\rho C_p}\right) - \exp(-\beta\Delta p_o) \qquad (2.5.8)$$

in which K'' is the integration

$$K'' = \int_0^L K'\,dz = 2\eta_o\left[\frac{Q(3n+1)}{n\pi}\right]^n \frac{L}{3n(R_L-R_o)}\left[\frac{R_L^{3n}-R_o^{3n}}{(R_L R_o)^{3n}}\right] \qquad (2.5.9)$$

from which it can be easily seen that in the extreme case when R_L approaches R_o, K" approaches K'L. Thus solution (2.5.8) reduces to (2.3.9).

The solution of the pressure in the range of (0,L) is given as follow:

$$p = p_L + \frac{1}{\psi}\ln\left\{\frac{R^{3n} - R_o^{3n}}{R_L^{3n} - R_o^{3n}}\left(\frac{R_L}{R}\right)^{3n}\left(1 - e^{\psi\Delta p_o}\right) + e^{\psi\Delta p_o}\right\} \qquad (2.5.10)$$

in which $\phi=(\beta+\alpha/(\rho C_p))$. The mean temperature expression is the same as (2.4.2), but the pressure should be obtained from (2.5.10).

Equations (2.4.1) and (2.5.10) can be easily written in a dimensionless form. Fig.2.5.1 shows the pressure distribution in three cases: $\omega=1$, $\omega=0.5$ and $\omega=0.2$ ($\omega=R_o/R_L$), with the power law index n=0.5.

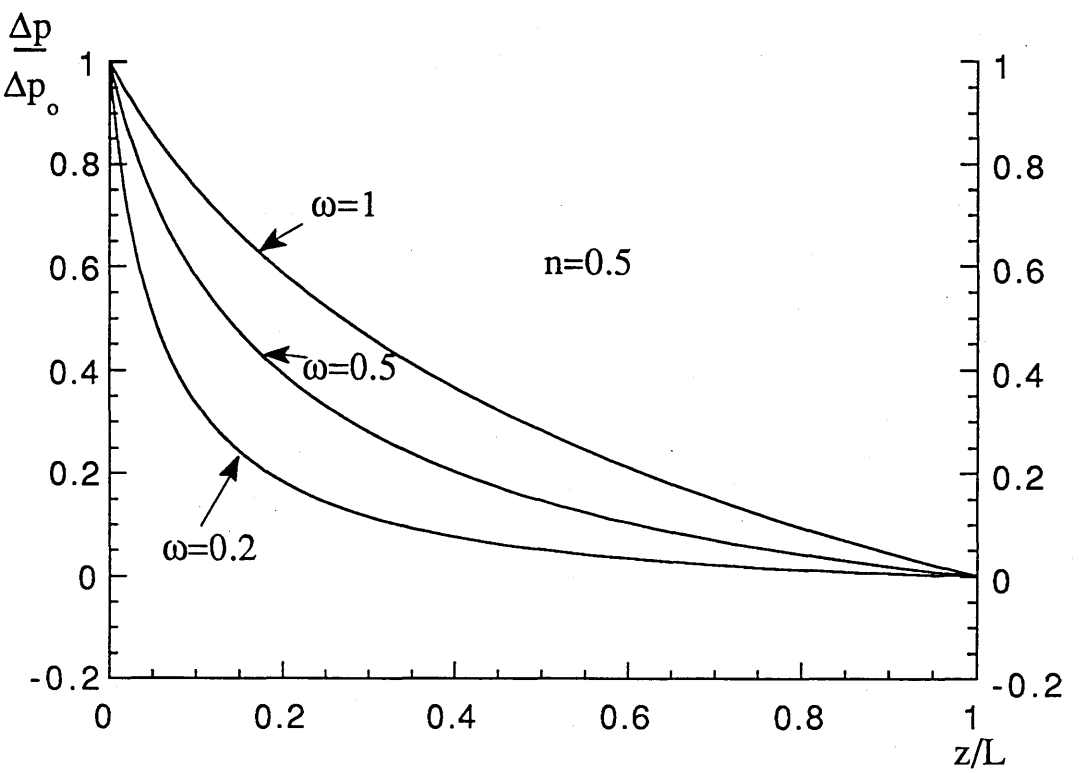

Fig.2.5.1 Dimensionless pressure curves within the range (0,z/L),$\omega=R_o/R_L$.

2.6 Non-isothermal Steady Flow in a Cross Section of Any Shape

A runner system in injection moulding often consists of ducts with cross sections other than circular. For flow through other conduits of constant cross section, the assumption of fully developed flow can still be used. The equations of momentum conservation reduce to a single equation

$$\frac{\partial \tau_{xz}}{\partial x} + \frac{\partial \tau_{yz}}{\partial y} = \frac{dP}{dz} \qquad (2.6.1)$$

in which

$$\tau_{xz} = \eta_o \exp[\beta\Delta p - \alpha(T - T_w)]\left[0.5(V_{z,x}^2 + V_{z,y}^2)\right]^{\frac{n-1}{2}} V_{z,x} \qquad (2.6.2)$$

$$\tau_{yz} = \eta_o \exp[\beta\Delta p - \alpha(T - T_w)]\left[0.5(V_{z,x}^2 + V_{z,y}^2)\right]^{\frac{n-1}{2}} V_{z,y} \qquad (2.6.3)$$

If it is still assumed that the temperature is independent of z, then the energy equation reduces to

$$k\nabla^2 T = -\tau_{xz} V_{z,x} - \tau_{yz} V_{z,y} \qquad (2.6.4)$$

Equations (2.6.1-4) together with proper boundary conditions construct a controlling system for the non-isothermal steady flow in a straight duct of arbitrary cross section.

From equations (2.6.2) and (2.6.3) the velocity derivatives can be inversely expressed in terms of the stresses, temperature and pressure differences

$$\frac{\partial V_z}{\partial x} = \frac{\exp[\alpha s(T - T_w) - \beta s\Delta p]\tau_{xz}}{\eta_o^s\left[0.5\left(\tau_{xz}^2 + \tau_{yz}^2\right)\right]^{\frac{1-s}{2}}} \qquad (2.6.5)$$

$$\frac{\partial V_z}{\partial y} = \frac{\exp[\alpha s(T - T_w) - \beta s \Delta p]\tau_{yz}}{\eta_o^s \left[0.5\left(\tau_{xz}^2 + \tau_{yz}^2\right)\right]^{\frac{1-s}{2}}} \qquad (2.6.6)$$

Substituting these two relations into the energy equation, the following equation is produced

$$k\nabla^2 T = -2^{\frac{1-s}{2}} \eta_o^{-s} \exp[\alpha s(T - T_w) - \beta s \Delta p]\left(\tau_{xz}^2 + \tau_{yz}^2\right)^{\frac{s+1}{2}} \qquad (2.6.7)$$

As is known, equation (2.6.1) for a Newtonian fluid can be a form of Poisson's equation with a constant in right hand side

$$\nabla^2 V_z = \frac{1}{\mu}\frac{dP}{dz} \qquad (2.6.8)$$

The exact solutions of this equation for cross sections of many shapes can be obtained[99]. The velocity V_z can always be expressed as

$$V_z = \psi + \frac{1}{4\mu}\frac{dP}{dz}(x^2 + y^2) \qquad (2.6.9)$$

in which the function ψ satisfies

$$\nabla^2 \psi = 0 \qquad (2.6.10)$$

with the boundary condition

$$\psi = -\frac{1}{4\mu}\frac{dP}{dz}(x^2 + y^2) \qquad (2.6.11)$$

Such an idea can be adopted for non-Newtonian flows, since it can be assumed that the stresses are the derivatives corresponding to a potential function ϕ

$$\tau_{xz} = \frac{\partial \phi}{\partial x}; \quad \tau_{yz} = \frac{\partial \phi}{\partial y} \qquad (2.6.12)$$

which enable equation (2.6.7) to solved independently.

Equation (2.6.7) can be expressed in integral equation form as follow

$$cT(\xi,\zeta)+\int_{\Gamma}T\frac{\partial T^{*}}{\partial n}\,d\Gamma=\int_{\Gamma}T^{*}\frac{\partial T}{\partial n}\,d\Gamma+B(\xi,\zeta) \qquad (2.6.13)$$

in which c is a constant based on the location (ξ, ζ) (1/2 on the smooth boundary, 1 inside the domain), and the function $B(\xi,\eta)$ is a domain integral as follows

$$B(\xi,\zeta)=C\int_{\Omega}T^{*}\exp[\alpha s(T-T_{w})]\left(\tau_{xz}^{2}+\tau_{yz}^{2}\right)^{\frac{s+1}{2}}d\Omega \qquad (2.6.14)$$

where Ω is the whole cross section domain, and C is a constant. T* is the fundamental solution of the two dimensional Laplace equation

$$T^{*}=-\frac{1}{4\pi}\ln\left[(x-\xi)^{2}+(y-\zeta)^{2}\right] \qquad (2.6.15)$$

Since the unknown temperature is involved in the domain integration (2.6.14), equation (2.6.13) requires iteration. Having known the temperature solution of a circular cross section, one can easily give an approximate solution of the cross section for the first step. For example, for flow through a duct of elliptical cross section of major and minor semiaxes a and b, the first trial function of the temperature distribution can be a form as follow

$$\exp[-\alpha s(T-T_{w})]=\left[C_{1}+C_{2}\left(\frac{x^{2}}{a^{2}}+\frac{y^{2}}{b^{2}}\right)^{\frac{s+1}{2}}\right]^{2} \qquad (2.6.16)$$

where C_1 and C_2 are two constants.

But this is only an approximate solution because it does not satisfy the energy equation (2.6.6) unless a=b.

The stress potential function ϕ for the elliptical cross section is given in the reference[99]

$$\phi = \frac{dP}{dz}\frac{a^2b^2}{2(a^2+b^2)}\left(\frac{x^2}{a^2}+\frac{y^2}{b^2}-1\right) \qquad (2.6.17)$$

By using equation (2.6.11), the temperature solution can be worked out through the iteration of equation (2.6.13).

The axial temperature rise in a duct of arbitrary cross section should be more or less like the distribution in a circular duct, therefore from an engineering point of view equation (2.4.3) can still be used to estimate the temperature rise. For more accurate results of the temperature, pressure and velocity, one has to resort three dimensional models.

2.7 Dual Reciprocity Method

The existence of a domain integral (2.6.14) requires the whole domain to be discretised into cells which loses the elegance and computational efficiency of the boundary integral equation method. However, a new and effective technique, the so-called "dual reciprocity method" can be used to transform the domain integral into the boundary. The method was first proposed by Brebbia and Nardini[115] for elastodynamic problems, and extended by Wrobel *et al* [77,78,116,117] to transient heat conduction problems. The method is explained through its application to nonisothermal laminar flow problems below.

Assume that the domain integral (2.6.14) is expressed as follow:

$$B = \int_{\Omega} T^* \, G d\Omega; \text{ where } G(x,y) = C\exp[\alpha s(T-T_w)]\left(\tau_{xz}^2+\tau_{yz}^2\right)^{\frac{s+1}{2}} \qquad (2.7.1)$$

The function G(x,y) can now be replaced by a sum of a series of N coordinate functions to reduce it to a boundary only form:

$$G(x,y) = \sum_{i=1}^{N} A_i f_i(r) \qquad (2.7.2)$$

The indices i indicate that the function series is based on different polar origins, r_i which are chosen to correspond to all the boundary nodes and some internal points. In order to reduce the domain integral to a boundary one, each of the functions must to satisfy the following Laplace equation:

$$\Delta f_i(r) = \delta(r - r_i) \qquad (2.7.3)$$

Thus, equation (2.6.13) can be rewritten as follows

$$cT = \int_\Gamma \left(T^* \frac{\partial T}{\partial n} - T \frac{\partial T^*}{\partial n} \right) d\Gamma + \sum_{i=1}^{N} A_i \left[\int_\Gamma (f_i \Phi_{,j} n_j - f_{i,j} n_j \Phi) d\Gamma + c_1 \Phi(r_i) \right] \qquad (2.7.4)$$

where c_1 is a constant based on the location of polar origins r_i, Φ is the fundamental solution of the biharmonic equation.

Φ and f_i are given as follows

$$\Phi = \frac{1}{16\pi} \left[(x - \xi)^2 + (y - \zeta)^2 \right] \ln \left[(x - \xi)^2 + (y - \zeta)^2 \right] \qquad (2.7.5)$$

$$f_i = -\frac{1}{4\pi} \ln \left[(x - x_i)^2 + (y - y_i)^2 \right] \qquad (2.7.6)$$

A_i is obtained as follow

$$\{A_i\} = [F]^{-1} \{G_i\} \qquad (2.7.7)$$

where $\{G_i\}$ is a vector of the values on the boundary nodes and the internal points, and [F] is a matrix:

$$[F] = \left[\frac{-1}{4\pi} \ln r_{ij} \right] \qquad (2.7.8)$$

It can be seen that the position of the polar origin r_i should not be chosen to coincide with any of the boundary nodes or internal points because the distances r_{ij} in matrix [F] cannot be zero. r_{ij} is expressed as follow

$$r_{ij} = \sqrt{(x_i - x_j + \chi)^2 + (y_i - y_j + \chi)^2} \qquad (2.7.9)$$

where χ is an arbitrary positive constant, and $(x_i+\chi, y_i+\chi)$ are the positions of those boundary nodes and internal points.

2.8 Concluding Remarks

The above developments on the non-isothermal laminar flow in ducts are based on some previous models. Although the analytical solutions can only be obtained for simple geometry such as a circular tube, they can reveal phenomena which could be easily missed in numerical solutions. On one hand it should be said that all the analytical or semi-analytical models can readily supply solutions to temperature, pressure and velocity in terms of some known parameters for different simplified cases, or approximate estimates of these variables, which form the basis of the understanding of the fluid and heat transfer problems and provide testing examples for other methods. On the other hand, though these models are gradually more and more comprehensive, it must be realised that the accurate and complete solutions of the whole governing equations for this complicated problem cannot be obtained in this way. In the last two sections, the boundary integral equation method has been applied for the extension to ducts of constant arbitrary cross section and made use of a boundary element method. There are some other numerical methods available in getting the approximate results. In later chapters, the author emphasises the numerical approaches, especially the boundary element methods, which are the main techniques to obtain the solutions.

Although the dual reciprocity method mentioned in the last section has not been implemented in this chapter, it will be the basis for later developments on the applications of the boundary element methods because the time-dependent problems, non-linearity in Navier-Stokes equations and non-Newtonian constitutive models need the domain integrals transferred onto boundary.

Chapter Three

BEM for Filling Process in Thin Cavities

3.1 Introduction

Although the equations to govern the three dimensional non-Newtonian, non-isothermal flows are very complicated, possible approximations can be made. In the filling process slowly varying, relatively narrow viscous flow in thin cavities is dominant. These flows usually can be simplified by using the well-known lubrication approximation, which originated with the famous work[118] by Osborne Reynolds who laid the theoretical foundations of hydrodynamic lubrication. A significant assumption of the lubrication approximation is that any motion of the fluid in a direction normal to the surfaces can be neglected in comparison with motion parallel to them. Apart from this assumption, originally there are others as follows: (a) the fluid is incompressible; (b) inertial forces are neglected in comparison with the shear viscous forces because of the slowness of the flow; (c) there is no slip on the walls; (d) the fluid is Newtonian; (e) the flow is isothermal. In order to describe the polymer behaviours more effectively, however, the last two assumptions are no longer available, since the viscosity is rate- and temperature-dependent. This model with a concept of gapwise-average velocity was first proposed by Hieber and Shen[23] who provided a rigorous derivation of the governing equations for the nonisothermal non-Newtonian flow, and called their model a generalised Hele-Shaw flow. A distinct advantage of this model is that the governing equations of the flow can be combined to yield a single equation for a single variable which does not vary across the cavity thickness. Although their model was first solved by a finite element/difference method, they soon applied a boundary integral method to solve the resulting equation[24-26].

In this chapter, the boundary element method for the filling process of thin cavities in the injection moulding is first reviewed. The method was first introduced in the calculation by Kwon[26], and the Kirchhoff transformation was used later on for improving the boundary integral formulation by Jin and Samuelsson[27]. Based on the method a further development on the energy equation is suggested, and the feasibility for practical applications is discussed. In the last section, two examples are

given to show the effectiveness and accuracy of the model for the moving front pattern, and comparisons are done between the modelling results and the corresponding experimental results from reference [119].

3.2 Simplified Governing equations

All those assumptions mentioned in the above section give rise to the simplifications of the governing equations to the form

$$(\eta u_{k,z})_{,z} - P_{,k} = 0 \qquad k = x, y \qquad (3.2.1)$$

where u_x and u_y are the velocity components in x- and y-directions, comma denotes the space derivative, P is the pressure, and η is the viscosity which can be a rate-, temperature- and even pressure-dependent function

$$\eta = f_1(T, \dot{\gamma}, P) \qquad (3.2.2)$$

The incompressible continuity condition can be expressed as:

$$u_{k,k} = 0 \qquad (3.2.3)$$

The boundary conditions for the velocity field are

$$u_k = 0 \qquad \text{on walls} \qquad (3.2.4)$$
$$u_{k,z} = 0 \qquad \text{at } z = 0 \qquad (3.2.5)$$
$$P = 0 \qquad \text{along the flow front} \qquad (3.2.6)$$
$$P = P_e \qquad \text{along the inlet} \qquad (3.2.7)$$

The pressure is independent of z direction except in the narrow area immediately behind the flow front. However the fountain flow effects in the area are assumed to be neglected (the effects is discussed in Chapter Five), therefore equation (3.2.1) can be integrated with respect to z as follow

$$u_{k,z} - \frac{z}{\eta} P_{,k} = 0 \qquad (3.2.8)$$

in which the boundary conditions (3.2.5) have been used.

After differentiating them with respect to k(=x,y), and using equation (3.2.2), the following relation is yielded

$$\left(\frac{z}{\eta}P_{,k}\right)_{,k}=0 \qquad (3.2.9)$$

From this equation, it seems that the whole thing between the brackets might be replaced by the corresponding derivatives of a function, that is,

$$\Psi_{,k}=\frac{z}{\eta}P_{,k} \qquad (3.2.10)$$

which could be substituted into (3.2.9) to form a Laplace equation. However, it can be readily seen that Ψ is a z-dependent function unless the velocity distribution in z direction were proportional to z. Thus further integrations should be carried out in order to eliminate the dependence of z. A gapwise-average velocity results from integrating equations (3.2.8) twice:

$$\bar{u}_k=\frac{1}{b}\int_0^b u_k(z)dz\,; \quad \text{where} \quad u_k(z)=\int_z^b u_{k,z'}dz' \qquad (3.2.11)$$

and then the governing equation becomes:

$$\bar{u}_k-SP_{,k}=0 \qquad (3.2.12)$$

where $S=\frac{1}{b}\int_0^b\int_z^b\frac{z'}{\eta}dz'\,dz$. Differentiating (3.2.12) with respect to k(=x,y), and using (3.2.2), the following equation can be obtained:

$$\left(SP_{,k}\right)_{,k}=0 \qquad (3.2.13)$$

Since S is no longer a z-dependent function, the Kirchhoff transformation can be applied on equation (3.2.13), that is,

$$S=\frac{d\Psi}{dP};\quad \Psi_{,k}=SP_{,k} \qquad (3.2.14)$$

from which the velocity components can be directly obtained according to (3.2.12). The governing equation finally becomes:

$$\Psi_{,kk} = 0 \qquad (3.2.15)$$

and boundary conditions (in x-y plane)

$$\Psi_{,k} = 0 \quad \text{on walls} \qquad (3.2.16)$$

$$\Psi = 0 \quad \text{along the flow front} \qquad (3.2.17)$$

$$\Psi = C_1 \quad \text{along the inlet} \qquad (3.2.18)$$

where C_1 is an arbitrary constant.

Equation system (3.2.15-18) should be considered for the velocity field rather than for the pressure field because S is a function of the position which cannot be determined by this system. Equation (3.2.15) is merely the gapwise-average velocity potential equation which can also be directly obtained from integration of the continuous equation with respect to z. From this system it can be seen that the gapwise-average velocity field depends only on the boundary of the thin cavity, and it can be solved independently.

The pressure field, however, depends on the viscosity which, due to its temperature dependence, requires the energy equation to be taken into account. It seemed because of the difficulties in solving both connected equations that the concept of the thermal layer was introduced in references [26,27]; an assumption of linear variation of the temperature in the layer was made, and an approximate expression for the thickness of it was derived from the energy equation. In spite of such a simplification, the calculation of the thickness required the pressure gradients to be known, and a finite difference method was used for the computation.

In fact, for a certain type of the viscosity models, the pressure gradients and the temperature fields can be solved separately as well. In the following part of the section, the energy equation is reformulated, and an easier way for solving the pressure gradients and the temperature fields is given for one case. The energy equation can be written as

$$\frac{DT}{Dt} = \alpha T_{,kk} + \eta\dot{\gamma}^2 \qquad k = x, y, z \qquad (3.2.19)$$

where $\frac{D}{Dt}$ means the Lagrangian time derivative, α thermal diffusivity.

Integrating this equation with respect to z over the half-gap thickness, the governing equation for the gapwise-average temperature can be obtained:

$$\frac{D\bar{T}}{Dt} = \alpha\left(\frac{1}{b}T_{,z}\Big|_{z=b} + \bar{T}_{,kk}\right) + H \qquad k = x, y \qquad (3.2.20)$$

in which $T_{,z}\Big|_{z=0} = 0$ has been used due to the symmetry, $\bar{T} = \frac{1}{b}\int_0^b T dz$ and

$$H = \frac{1}{b}\int_0^b \eta\dot{\gamma}^2 dz = P_{,k}\bar{u}_k = \frac{1}{S}\bar{u}^2 \qquad (3.2.21)$$

The boundary conditions for the gapwise-average temperature field are

$\bar{T} = \bar{T}_e$ along the inlet (3.2.22)
$\bar{T} = \bar{T}_w$ along the wal ls (3.2.23)
$\bar{T} = \bar{T}_w$ along the flow front (3.2.24)

It can be seen that there are the pressure gradients or the viscosity involved in (3.2.21), naturally the expression of the viscosity has to be given for any attempt for the solution. A power-law model is used for the description of the strain-rate and temperature dependence of the viscosity:

$$\eta = \eta_0 g(T)\dot{\gamma}^{n-1} \qquad (3.2.25)$$

where g(T) is an arbitrary function of temperature.

The strain rate is defined as

$$\dot{\gamma} = +\sqrt{u_{x,z}^2 + u_{y,z}^2} \qquad (3.2.26)$$

and by using (3.2.8) and (3.2.25), after rearrangement it can be expressed as

$$\dot{\gamma} = \left[\frac{\Lambda z}{\eta_0 g(T)}\right]^s \qquad (3.2.27)$$

where s is 1/n and $\Lambda = +\sqrt{P_{,x}^2 + P_{,y}^2}$.

By substitution of (3.2.27) into (3.2.25), S and H can be expressed as follows:

$$S = \Lambda^{s-1}\delta; \quad H = \Lambda^{s+1}\delta \tag{3.2.28}$$

where

$$\delta = \frac{1}{b\eta_0^s}\int_0^b \frac{z^{s+1}}{[g(T)]^s}\,dz \tag{3.2.29}$$

From expressions (3.2.21) and (3.2.28), Λ can be obtained as follow

$$\Lambda = \left|\frac{\bar{u}}{\delta}\right|^n \tag{3.2.30}$$

Thus S and H in (3.2.28) can be expressed without involving the pressure gradients though they are dependent on the pressure gradients. This result decouples equation (3.2.20) which can be solved separately after the velocity field is obtained. From (3.2.28-30) it can be seen that the temperature distribution in the z direction becomes essential in determining S and H, and subsequently in solving the pressure gradients and the gapwise-average temperature fields. However, the temperature distribution in the z direction does not affect both fields very much, and it can always be expressed by a function of the local gapwise-average temperature. Therefore an approximation can be made for it. For $g(T)=\exp[-\beta(T-T_w)]$, which is often used in modelling polymer flows. It is assumed that

$$T = T_w - \frac{2}{\beta s}\ln\left[C + (1-C)\left(\frac{z}{b}\right)^{s+2}\right] \tag{3.2.31}$$

where C is a gapwise-average temperature dependent parameter.

Thus, following expressions can be easily obtained:

$$\delta = \frac{b^{s+1}}{(s+2)C\eta_0^s} \tag{3.2.32}$$

$$\left.\frac{\partial T}{\partial z}\right|_{z=b} = -\frac{2}{\beta s}(s+2)(1-C) \tag{3.2.33}$$

and the relation between the gapwise-average temperature and C can be approximately expressed as

$$\bar{T} \approx T_m + \frac{1}{\beta s}\ln C \tag{3.2.34}$$

where T_m is a parameter dependent on s and β. A more accurate relation between $\bar{T}$ and C can be found by integrating equation (3.2.31) (or a temperature function) over the thickness.

By substitution of all these expressions into (3.2.20), the governing equation of the gapwise-average temperature field finally becomes

$$\frac{D\bar{T}}{Dt} = \alpha\bar{T}_{,kk} - \frac{2(2n+1)\alpha}{\beta}(1-C) + \eta_0\left[C\left(\frac{2n+1}{n}\right)\right]^n\left(\frac{|\bar{u}|}{b}\right)^{n+1} \tag{3.2.35}$$

in which the magnitude of the velocity appears in the last term. Therefore the temperature should be solved after the velocity field is obtained.

From (3.2.12) the pressure equation can be obtained as follows

$$P_{,kk} = -\frac{S_{,k}\bar{u}_k}{S^2} = -\frac{S_{,k}}{S}P_{,k} \tag{3.2.36}$$

Since S involves the parameter C which is a position function, the pressure field can be worked out after the temperature field is solved.

3.3 The Boundary Integral Expressions

For the potential Ψ at any point ξ in a given domain bounded by its boundary Γ, the boundary integral equation corresponding to Laplace equation (3.2.15) can be written as

$$c(\xi)\Psi(\xi) + \int_{\Gamma} \Psi \Phi_{,i} n_i d\Gamma = \int_{\Gamma} \Phi \Psi_{,i} n_i d\Gamma \qquad (3.3.1)$$

where $c(\xi)$ is geometrical dependent constant, $c(\xi)=0.5$ for ξ on a smooth boundary and $c(\xi)=1$ for ξ inside the domain. Φ is the fundamental solution of the Laplace equation, which can be written as

$$\Phi = \frac{1}{2\pi} \ln \frac{1}{r} \qquad (3.3.2)$$

where r is the distance between the source point and observing point.

Differentiating equation (3.3.1) with respect to k (k=x,y) results in the gapwise-average velocity components:

$$c(\xi)\bar{u}_k(\xi) + \int_{\Gamma} \Psi \Phi_{,ik} n_i d\Gamma = \int_{\Gamma} \Phi_{,k} \bar{u}_i n_i d\Gamma \qquad (3.3.3)$$

In fact this expression is only necessary for points inside the domain. The velocity components on the free surface boundary can be obtained by using the following relations

$$\bar{u}_k = \Psi_{,i} n_i n_k \qquad (3.3.4)$$

where $\Psi_{,i}n_i$ is the flux on the boundary which is obtained from equation (3.3.1).

The integral equation corresponding to equation (3.2.35) can also be written as follows

$$c\bar{T}(\xi, t) = \int_{t_o}^{t} \left[\int_{\Gamma} \alpha(\bar{T}_{,i} T^* - \bar{T} T^*_{,i}) n_i d\Gamma - \int_{\Omega} F(\bar{T}) T^* d\Omega \right] dt' + \int_{\Omega_o} [\bar{T} T^*]_{t_o} d\Omega \qquad (3.3.5)$$

where Ω and Γ are the domain and its boundary at time t', Ω_o is the domain at time t_o, and

$$F(\bar{T}) = \frac{2(2n+1)\alpha}{\beta}(1-C) - \eta_0 \left(C \frac{2n+1}{n} \right)^n \left(\frac{|\bar{u}|}{b} \right)^{n+1} \qquad (3.3.6)$$

Also, T^* is the fundamental solution of classical diffusion equation which can be found in Chapter Four. The condition for this formulation is that the difference between t and t_0 is very small. Details of the formulation of equation (3.3.5) are similar to those for time dependent viscous flow field in Chapter Six, and they are therefore not given here.

The unknown pressure, governed by a Poisson equation given by (3.2.36), can be solved by a similar integral equation to equation (3.3.1) but with a domain integral involved:

$$c(\xi)P(\xi) + \int_\Gamma P\Phi_{,i}n_i d\Gamma = \int_\Gamma \Phi P_{,i}n_i d\Gamma + \int_\Omega \Phi S^{-2}S_{,i}\bar{u}_i d\Omega \qquad (3.3.7)$$

3.4 Discussions on the Equations

Equations (3.3.1), (3.3.3), (3.3.5) and (3.3.7) can be used to solve the whole flow field of the three major physical variables in the filling process of a thin cavity. Despite the apparent advantages in implementing equation (3.3.1) for the velocity potential, it is readily seen that the involvement of domain integrals are the main difficulties in implementing the other equations, especially for this moving boundary problem. Because the domain has to be remeshed for the evaluation of the integrals when the previous grid is distorted, it has eliminated the key advantage of the boundary element method, and results in virtually no difference from the finite element method. The better solution to the domain integral involvement is to use a dual reciprocity method which is already introduced in the last chapter.

An intrinsic feature of this gapwise-average velocity potential is that the mould filling pattern, in terms of the shape of the front, is independent of the rheological properties of the polymers, even independent of the thickness of the cavity. Although in practical thermoplastic injection moulding, it is observed that the rheological properties do not affect much on the flow pattern in mould cavities with uniform thickness, the hesitation effect is a typical phenomenon of the dependence of the flow pattern on the variation of thickness, which also strongly reflects the rheological influence. Thus it is difficult to apply this model to mouldings with variable thickness.

A second restriction is that the model cannot, at least in theory, be extended to the mould cavities with turnings in the third dimension. An approximation method used in some packages is to lay flat a three dimensional

mould cavity for calculation. However, the turnings have, rigorously speaking, effects on the flow field. Also if the flow meets a "T" or a "+" shape joint, the model seems powerless. Geometrical complexity is one of the basic features in simulation of injection moulding, this boundary element model therefore has to be further developed to fit the real situation.

The integral equation for the temperature field is set up following a Lagrangian description. In the Lagrangian description, the trajectory of a particle is actually the coordinate curve. Therefore the convection terms under an Eulerian coordinate system vanish since each particle is "carrying" its mass, momentum and energy with it all the way through a fixed coordinate system. However, the trajectory has to be approximated by small segments of straight lines each of which is formed in each time increment. Therefore the time increment has to be small enough for following the particle trajectory. If otherwise it would lead to a wrong way and the whole calculation result would be distorted.

In spite of these limitations, this model is considered very effective in obtaining the flow front shape for a plane thin cavity or for a simple three dimensional cavity with uniform thickness. In the following section, two simple examples are given to show the effectiveness and accuracy.

3.5 Numerical Implementation and Testing Examples

The simplest problem is a plane part moulded with an isothermal Newtonian fluid, and based on experimental evidence for injection moulding there is reason to hope that it will give good estimates of flow front shapes for nonisothermal and non-Newtonian flows. The parameter S can be easily obtained in this case

$$S = \frac{b^2}{3\eta_o} \qquad (3.5.1)$$

This is the constant factor between the velocity potential Ψ and pressure P, and equations (3.2.15) and (3.2.36) become identical so that only one Laplace equation is required to be solved.

The numerical implementation of a boundary element method is straightforward, since a sample program is given in Brebbia's book[75]. A general purpose boundary element program is coded for this potential function, and linear element approximation is used. The program is a part

of the package CASIM, which is introduced in Chapter Eight. The basic feature for this moving boundary type problem is that the free surface boundary nodes move at their local speed in each time step. Therefore the program is designed to have functions of insertion and deletion of nodes. When any of the elements is stretched longer than a critical length, one more node is inserted between the two nodes which define two new elements to replace the old one. On the other hand, if two adjacent elements are shrunk to be less than another critical length, the sharing node is then taken away. Any node meets the wall of the cavity, it is stopped moving by assigning a zero to its velocity components. This procedure is much easier than a remesh routine for a finite element method.

It is not necessary to nondimensionalise a Laplace equation since there would be no dimensionless parameters produced, and as explained in the last section, this is precisely the reason why the advancing front is independent of rheological properties and thickness but the shape of the boundary itself. Also the length of a time increment is not so critical as it for a time-dependent equation, but for this moving boundary problem, the time increment should not be chosen very large otherwise it would cause unacceptable errors in predicting the shape of the flow front, such as "ripples" or sharp vertex corners developed. Once the first time increment is found suitable for a stable calculation, the rest of the time increment can be chosen either the same as the first time increment, or a calculated value following a principle that the average displacement is kept the same as it during the first time increment. Obviously the latter scheme is faster in most of the injection moulding problems since the velocity of a flow front becomes slower while the front is stretched longer.

The first example is a mould filling process of a disc, which diameter is assumed much longer than its thickness. The gate position is at the bottom edge of the disc. Since this example has been carried out by the some previous researchers, it is easier for verifying the model and the program. In the initial state, the flow front is assumed as a circular segment with the gate at the centre, and the inlet flow is assumed to keep a flow rate all the time so that the fill time is a function of the initial velocity and its local radius. No slip condition is adopted on the cavity wall. If the effect of circumferential wall were neglected, the flow front would continuously move radially into the cavity from the gate. From the flow front pattern shown in Fig. 3.5.1, it can be seen that in the early stage of the filling, the wall exerts a retarding force, and the flow front in the vicinity of the wall

bends back towards the gate. As the flow progresses, that area moves faster than the centre of the front because the curved wall deflects the melt. Gradually the shape of the front becomes linear and then in the later stages curves away from the gate.

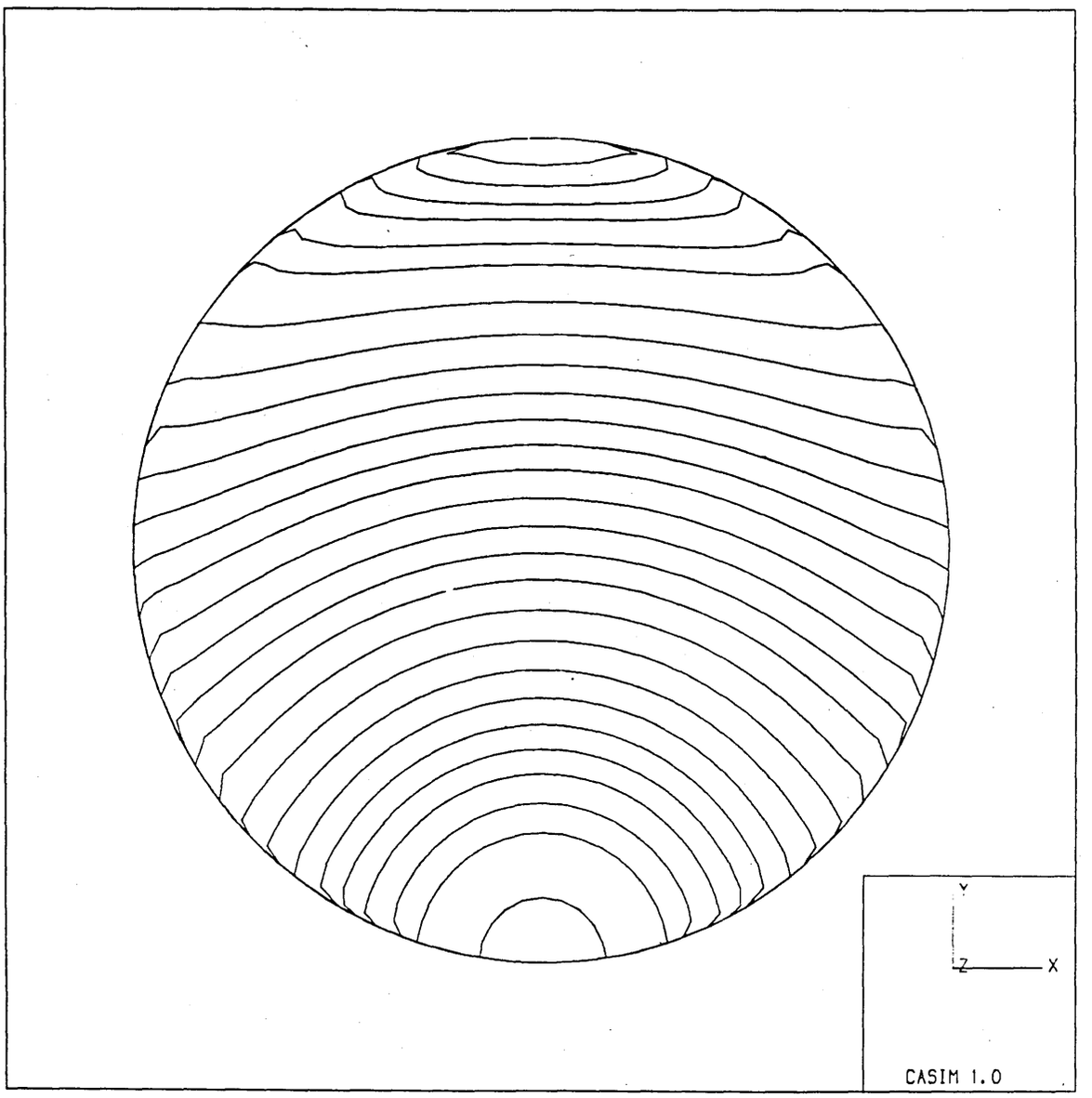

Fig. 3.5.1 Flow front pattern during filling a disc mould.

The computer simulation result shown above is very close to an experimental result given by Beyer and Spencer[119]. In order for comparison, the successive photographics of the flow front of the experimental result are given in Fig.3.5.2. (Carefully observed of the pictures one would find that there are some dark particles which were deliberately put inside the polymer. In the fifth frame of the pictures, a

streak of them is shown entering the cavity, and in subsequent frames as it travels across the mould, the particles move faster than the advancing front. "When it catches up the advancing front it is forced outward against the mold wall." Then a black smear is left behind it against the wall. The phenomena of particles moving towards the front and being stretched near the walls viewed transversely are fully discussed later in Chapter Five). In spite of the quality of the pictures, the polymer front at each frame can be recognised. The detail of the front surface shape near the wall is not clear enough for comparing the corresponding part of the computed graphical result, where the curving-back front shape is approximated by a segment of straight line.

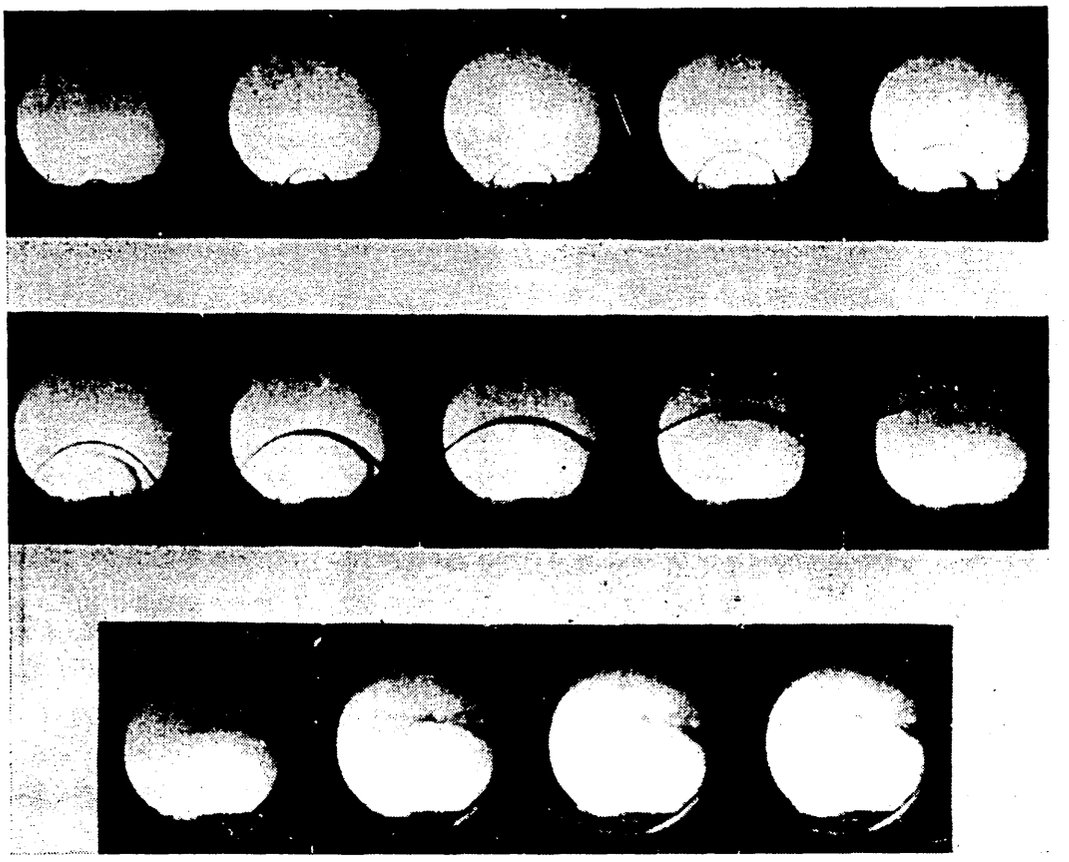

Figure 3.5.2. Sequence of flow front moving across the mould.

One of the other experimental examples shown in reference [119] is the filling process in the same disc but with a circular insert in the middle to show the formation of a weld line. The sequence of flow around the circular insert is shown in Fig.3.5.3.

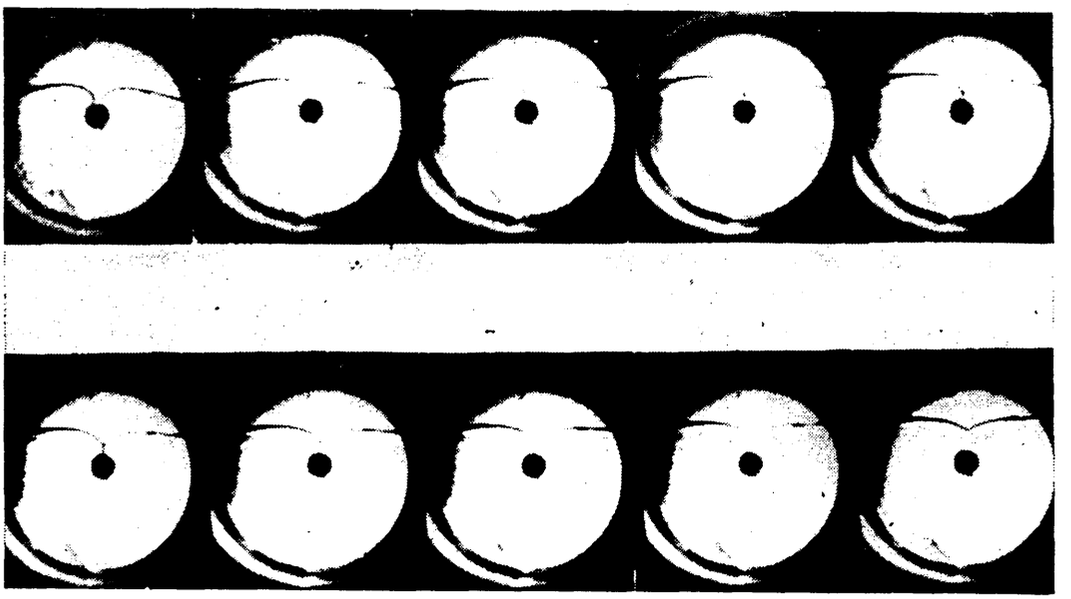

Figure 3.5.3. Sequence of flow around a circular insert.

In general, a numerical modelling of a weld line formation is not easy since once two fronts meet together, the resulting weld line requires not only the potentials but also the potential gradients approached from both sides to be identical. In a boundary element method, if the domain is a single-connected, any node on the weld line will be used twice following the normal procedure. Because of the two unknowns on the weld line, the program has to be carefully designed for setting a different equation in each time. In this example the weld line is assumed on the symmetric line, thus zero normal gradient condition can be given to the weld line node(s). The same diameter ratio is used in the calculation as the experiment. Fig.3.5.4 shows the development of the flow front of the computer modelling.

It is clear from the computer graphical result that the flow of polymer adjacent to the insert is greatly retarded. As a result the two flow streams produced by the insert first meet at a distance from the insert. The weld line then forms in toward the insert as well as in the direction of the flow. It can be seen that a small pocket of air may be trapped between the insert and the joining fronts unless means are provided in practical process for allowing the entrapped air to escape. The butt-in streams soon become one and form a common front moving up. The rest of the development of the front has little difference from the normal pattern without the insert shown in Fig.3.5.1.

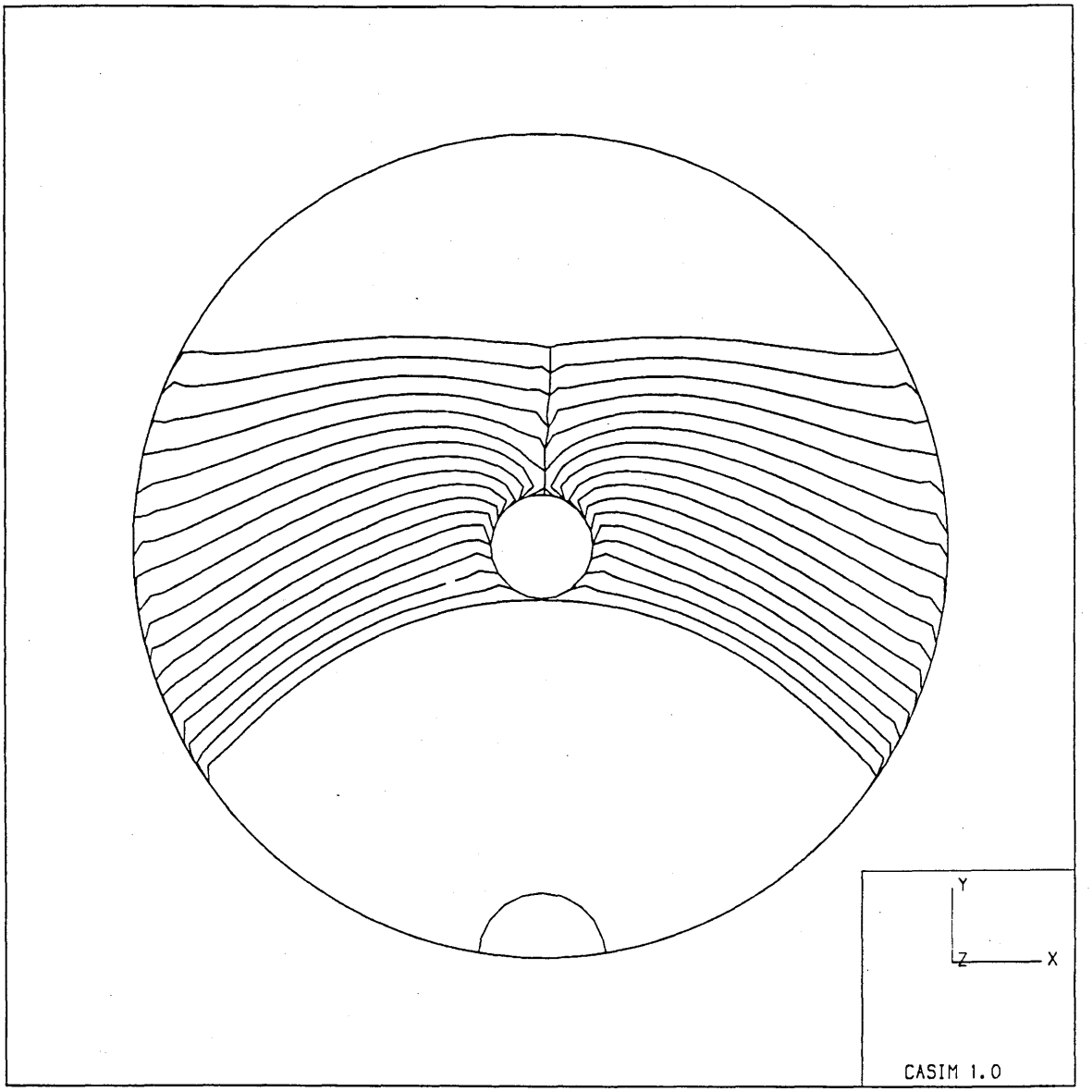

Figure 3.5.4 Computer result of the flow front pattern around the circular insert and forming a weld line.

The boundary elements give an advantage to trace the formation of the weld line in the beginning, but those elements on the weld line would soon become redundant for rest of the calculation if a cavity were much bigger. A remaining problem is how to eliminate the elements and set up a double-connected region for rest of the calculation and leave a track of the weld line for recognition in post-processing.

In both examples the character of symmetry has not been used. This is because the velocity on the symmetrical line could not be directly worked out from the flux value, if the symmetrical line were discretised with

boundary elements. Since the normal component of the velocity is zero, the tangential component has to be worked out by using a finite difference method. It would not save many elements but possibly produce bigger errors because the accuracy of the computed component would actually depend on the size of the elements on the symmetrical line. The errors produced from the full-scale calculations can be detected carefully from these two diagrams: both sides are not exactly identical, and the computed weld line is not a straight line, slightly offset from the symmetrical line.

Chapter Four

BEM for Cooling Analysis

4.1 Introduction

Cooling-system design affects both the part quality and productivity very significantly. Normally more than three quarters of the cycle time in the injection moulding is taken by the cooling stage. Hence, there is a substantial incentive for reducing cycle time by improving the cooling system. On the other hand, a good cooling system should also extract heat from the melt uniformly throughout the mould. Two major problems in quality can be avoided if an uniform cooling is designed for a mould. Warpage of a moulded product is one of them whose roots may lie in the proper design of the cooling system. Another problem is that the homogeneity of properties in parts moulded from crystalline resins is strongly dependent on temperature history and cooling time. Minor changes in these variables can result in major differences in crystal formation and thus in the mechanical properties of the moulded product. In addition, the quality also depends on the repeatability of the moulding machine used. Therefore the objective of an optimum cooling system design is to achieve a maximum rate, uniform and balanced cooling. The basic design variables of such a system include the sizes of the cooling channels, their locations, cooling fluid flow rate and its inlet temperature. Then the requirements for an analysis tool should be able to give an accurate picture of the distribution and history of the temperature development on which the mould designers can revise their design of a cooling system. A further requirement for a package may associate the cooling analysis with the optimum design, so that a rough design is the input, and a possible ideal design is the output of the package. Although the discussion of the optimum design is beyond the range of this thesis, the common fundamental is an accurate and efficient numerical method.

Most of previous works on the cooling analysis are based on some empirical and/or simplified heat transfer models. These models are still playing very important roles in quick evaluation of a proposed cooling system in some commercialised packages. However, the rapid development of the boundary element techniques in the last two decades has made both

accurate and fast calculation possible. The designers of both COOL3D and MOLDTEMP have adopted boundary element methods for their three dimensional modellings of the process. Recent papers[45,120] of CIMP group showed that in COOL3D, a local one-dimensional transient analysis was used for the plastic part, and the steady-state equation of the temperature distribution was adopted for a cycle-average three-dimensional mould analysis.

The intention of this chapter is to develop the boundary element techniques for a fully, coupled transient heat conduction analysis of the cooling stage. Although only the two-dimensional case is carried out in this chapter, the techniques can be easily extended into three dimensional problems. In the last section of this chapter, a new dual reciprocity method for the transient boundary element method with a time dependent fundamental solution is introduced.

4.2 Governing Equations

During the cooling stage of the injection moulding process, the polymer liquid inside the mould is brought to a standstill, being cooled down and solidified. The transient heat conduction in the whole system is then dominating the period of the process. The media in the analysis include the melt polymer, the solid mould and the cooling fluid. Thermal diffusivity of polymer is typically much smaller than that of the mould material, therefore the cooling time depends largely upon the rate at which the melt polymeric material transfers heat from its inner region to its interface with the mould. Another feature of the problem is that the specific heat of polymeric materials may be a strong function of temperature especially in the case of semi-crystalline materials[121]. To express the problem mathematically, one has to consider the following initial-boundary value controlling equation for the heat conduction in the finite time interval $0 < t \leq \tau$, where the term of strain energy is assumed to be too small to be taken into account:

$$\rho C_p \frac{\partial T}{\partial t} = (kT_{,i})_{,i} \quad \text{in} \quad \Omega \times (0, \tau) \tag{4.2.1}$$

with initial condition:

$$T(P, 0) = T_0(P) \cdot \text{on} \ \Omega \tag{4.2.2}$$

and boundary conditions:

$$T(P,t) = \underline{T}(P) \quad \text{on } \Gamma_T x(0,\tau) \tag{4.2.3}$$

$$q(P,t) = \underline{q}(P) \quad \text{on } \Gamma_q x(0,\tau) \tag{4.2.4}$$

$$q(P,t) = h[T(P,t) - \underline{T_1}(P)] \quad \text{on } \Gamma_h x(0,\tau) \tag{4.2.5}$$

where Ω is the domain concerned which is bounded by boundary $\Gamma=\Gamma_T\cup\Gamma_q\cup\Gamma_h$, P is any point within the domain or on the boundaries, and q is the boundary heat flux defined by $q=-\partial T/\partial n$ in which $\mathbf{n}$ is the unit outward normal vector at the boundary. $\underline{T}$, $\underline{q}$, h and $\underline{T_1}$ are given smooth functions on their corresponding boundaries and T_o is a smooth function on Ω. ρ, C_p, k and h are density, specific heat, thermal conductivity and convective heat transfer coefficient, respectively. The thermal properties are obviously discontinuous from one medium to another. The boundary conditions between two adjacent media are given as following types:

$$T(P^+,t)=T(P^-,t) \quad \text{and } q(P^+,t)=-q(P^-,t) \tag{4.2.6}$$

There is a convection term added in the governing equation for the cooling liquid:

$$\rho C_p\left(\frac{\partial T}{\partial t} + v_i T_{,i}\right) = (kT_{,i})_{,i} \quad \text{in} \quad \Omega x(0,\tau) \tag{4.2.7}$$

where v_i are the velocity components.

In most heat conduction calculations it is assumed that the thermal conductivity, specific heat and density do not change appreciably with temperature. The information in reference [104] gives the temperature dependence of those thermal properties for some polymer materials; only the specific heat is found to vary appreciably with temperature for some polymers in the range of temperature of interest. Therefore the governing equation (4.2.1) can be rewritten as

$$\frac{\partial T}{\partial t} = \alpha T_{,ii} \quad \text{in} \quad \Omega x(0,\tau) \tag{4.2.8}$$

where α is the thermal diffusivity. Equation (4.2.7) can be rewritten correspondingly.

4.3 Boundary Integral Formulations

The time-dependent fundamental solution T* of the adjoint equation of (4.2.8), which has its singularity at (x,t), is given by

$$T^*(x,t;x',t') = \frac{H(t-t')}{4\pi\alpha(t-t')^{d/2}} \exp\left[-\frac{r^2}{4\alpha(t-t')}\right] \qquad (4.3.1)$$

where r represents the Euclidean distance between the two points x and x' ($x \in R^d$), and H is the Heaviside function.

Based on this fundamental solution (4.3.1), equation (4.2.8) can be transformed into the following integral equation, as mentioned in references[122-128]:

$$cT(x,t) = \int_{t_0}^{t}\int_{\Gamma}\alpha(qT^* - Tq^*)d\Gamma\, dt' + \int_{\Omega}T(x',t_0)T^*(x,t,x',t_0)d\Omega \qquad (4.3.2)$$

where c = 1 if x is inside the domain Ω; c = 0.5 if x is on the smooth boundary Γ of the domain, and

$$q^* = \frac{\partial T^*}{\partial n} = -\frac{r_i n_i}{2\alpha(t-t')}T^* \qquad (4.3.3)$$

This relation shows that the value of the function T at any point x inside the domain or on the boundary for any instant $t > t_0$ can be expressed explicitly by the integration, once the initial and boundary conditions are known.

It is not possible to work out analytically the fundamental solution to the adjoint equation of (4.2.7) due to the nonlinear velocity being involved. However, if it is assumed that the velocity is a constant, the governing equation would then become:

$$\frac{\partial T}{\partial t} + \tilde{u}_1 \frac{\partial T}{\partial x_1} - \alpha \nabla^2 T = 0 \qquad (4.3.4)$$

where $\tilde{u}_1$ is the magnitude of the velocity of the flow along x_1 direction. The fundamental solution to the adjoint equation of (4.3.4) is given by Vick and Golan[129]; it is presented here for three dimensional case as follow:

$$T^* = \frac{H(t-t')}{4\pi\alpha(t-t')^{\frac{3}{2}}} \exp\left[\frac{(x_1 - x_1' - x_c)^2 + (x_2 - x_2')^2 + (x_3 - x_3')^2}{4\alpha(t'-t)}\right] \qquad (4.3.5)$$

where $x_c = \int_{t_0}^{t} \tilde{u}_1(t')dt'$.

The integral equation for this case can be written as follow:

$$cT(x,t) = \int_{\Omega} TT^*\Big|_{t'-t_0} d\Omega + \int_{t_0}^{t}\left[\int_{\Gamma}\left(\alpha\frac{\partial T}{\partial n} - \tilde{u}_1 n_1 T\right)T^* d\Gamma - \int_{\Gamma}\alpha T\frac{\partial T^*}{\partial n} d\Gamma\right]dt' \qquad (4.3.6)$$

The detailed formulation of this integral equation can be found in Appendix A.

4.4 Numerical Implementation of the Integral Equations

The basic features of the numerical implementation of the boundary integral equation are virtually the same as those in finite element approximations, that is, discretising both T and q over the spatial and time domain of concern, and establishing a system of linear equations by collocation at a sufficient number of nodes on the boundary at each time step to determine the nodal values.

In two-dimensional case, suppose there are N_Γ nodal points $\{P_j\}_{j=1,N_\Gamma}$ along Γ. Any two adjacent points P_iP_{i+1} ($i \in \{1,N_\Gamma\}$) are linked by a small line segment Γ_i which is called a boundary element. Here P_{N_Γ} is regarded as P_1. Hence the boundary Γ is approximated by the union of the boundary elements Γ_i ($i=1,N_\Gamma$). The time interval $[t_0, \tau]$ is divided into N_t subintervals. Let $t_F = F(\tau - t_0)/N$ ($0 \le F \le N_t$). Furthermore, for calculating the domain integral, the domain Ω is divided into N_Ω cells $\{\Omega_e\}_{e=1,N_\Omega}$,

where Ω_e is a triangle. Ω is divided in such a way as the nodal points of the cells coincide with the nodal points of the boundary elements taken on Γ. If $\phi_i(x)$ $(i=1,....,N_\Gamma)$ is denoted as the basic functions over Γ and $\psi_F(t)$ $(F=1,....,N_t)$ as the basic functions over $[t_0, \tau]$, the approximations end up as follows:

$$T \approx \tilde{T} = \tilde{T}_{iF}\phi_i(x)\psi_F(t); \quad q \approx \tilde{q} = \tilde{q}_{iF}\phi_i(x)\psi_F(t) \tag{4.4.1}$$

The index iF represent the nodal values of T and q at node i on x and node F on t. Substituting equations (4.4.1) into (4.3.2), the boundary element equation is established for the temperature at any point in the domain at any instant τ:

$$\begin{aligned} c\tilde{T}(x,\tau) + \alpha \sum_{j=1}^{N_T}\sum_{F=1}^{N_t}\int_\Gamma \left[\tilde{T}^j_{iF}\phi_i(x')\int_{t_{F-1}}^{t_F}\psi_F q^*(x,\tau,x',t')dt'\right]d\Gamma(x') \\ = \alpha \sum_{j=1}^{N_T}\sum_{F=1}^{N_t}\int_\Gamma \left[\tilde{q}^j_{iF}\phi_i(x')\int_{t_{F-1}}^{t_F}\psi_F T^*(x,\tau,x',t')dt'\right]d\Gamma(x') \\ + \sum_{e=1}^{N_\Omega}\int_{\Omega_e} T(x',t_0)T^*(x,\tau,x',t_0)d\Omega(x') \end{aligned} \tag{4.4.2}$$

The interpolation functions can be vectors if they are linear or higher order. In this chapter, a linear interpolation function is used for the spatial approximation and a constant for the time approximation, that is

$$\phi_i = \frac{1}{2}\begin{bmatrix}1-x\\1+x\end{bmatrix}; \quad \psi_F = 1; \quad T_i = \begin{bmatrix}T_1\\T_2\end{bmatrix}; \quad q_i = \begin{bmatrix}q_1\\q_2\end{bmatrix} \tag{4.4.3}$$

The time integrals in (4.4.2) can be integrated analytically as follow

$$\int_{t_{F-1}}^{t_F} q^*(x,\tau,x',t')dt' = \frac{r_{,i}n_i}{2\pi\alpha r}\left[\exp(-s_{F-1}) - \exp(-s_F)\right] \tag{4.4.4}$$

$$\int_{t_{F-1}}^{t_F} T^*(x,\tau,x',t')dt' = \frac{1}{4\pi\alpha}\left[E_1(s_{F-1}) - E_1(s_F)\right] \qquad (4.4.5)$$

where $E_1(s) = \int_s^\infty \frac{e^{-u}}{u}du$; $s_F = \frac{r^2}{4\alpha(\tau - t_F)}$.

If the integrations over each boundary and domain element are defined as follows

$$\left.\begin{aligned} h_{jk}^F &= \frac{1}{2\pi\alpha}\int_{\Gamma_k}\phi_i(x')\frac{r_{,i}n_i}{r}\left[\exp(-s_{F-1}) - \exp(-s_F)\right]d\Gamma(x') \\ g_{jk}^F &= \frac{1}{4\pi\alpha}\int_{\Gamma_k}\phi_i(x')\left[E_1(s_{F-1}) - E_1(s_F)\right]d\Gamma(x') \\ b_{le}^0 &= \int_{\Omega_e}\tilde{T}^1(x',t_0)T^*(x,\tau,x',t_0)d\Omega(x') \end{aligned}\right\} \qquad (4.4.6)$$

, then equation (4.4.2) can be rewritten into the following matrix form:

$$\sum_{F=1}^{N_t}\left(H^F T_F - G^F Q_F\right) = B^0 \qquad (4.4.7)$$

where the coefficients of the matrices H, G and B are assembled by the terms resulting from integration over each element using (4.4.6), T_F and Q_F are the vectors of the temperature and heat flow values at all boundary nodes.

There are two different time-marching schemes[126] which can be employed to solve the equation established above. The first is the "boundary-only" scheme. This scheme consists in starting all time integrations from the initial instant t_0 up to the current time step t_n. Then the domain integration is only needed at the initial instant. If the temperature distribution at the initial instant is a function of a harmonic type, the domain integration can even be transformed into equivalent boundary integrals[128]. In this way no domain integrations are needed during the time-marching process. In each time step, however, the nodal values have to be stored and two more square matrices have to be calculated

for evaluating the time integrations. Such requirements for the storage and the computing time during the time-marching process make the scheme impractical. The second scheme is to treat the temperature distribution of each previous time step as the initial condition for the current time step. The influence of the previous step's distribution on the current step is carried by the domain integration. In this way, the coefficient matrices at each time step are exactly the same as those at the first time step, only the domain integral is needed for updating the right-hand side terms. Yet it is precisely this domain integral that takes the most of the computing time. Up until now, there have been some efforts to preclude the domain integral such as dual reciprocity methods based on the time independent fundamental solution[77,78] and the recurrent algorithm[130]. In the author's point of view, neither of them is accurate enough to replace the direct numerical domain integration, though a substantial computing time is reduced. Since the numerical domain integration can be easily replaced in a program if a better method appears (e.g. a new dual reciprocity method based on time dependent fundamental solution introduced in 4.8), the second scheme is applied here.

For the temperature at any instant t_F in the scheme, equation (4.4.7) can be rewritten as following:

$$HT_F - GQ_F = B^{F-1} \tag{4.4.8}$$

When the source point is not on the element, the coefficients h_{jk} and g_{jk} can be evaluated by standard Gaussian formulae, i.e.

$$\left.\begin{aligned} h^i_{jk} &= \frac{d_{jk}}{4\pi}\sum_{l=1}^{L}\frac{1}{r^2_{jl}}\exp(-s_{F-1})\phi_i(x'_l)W_l \\ g^i_{jk} &= \frac{R_k}{8\pi}\sum_{l=1}^{L}E_1(s_{F-1})\phi_i(x'_l)W_l \end{aligned}\right\} \tag{4.4.9}$$

where d_{jk} is the distance between the source point j and the element k, R_k is the element length, and L represents the number of integration points.
When the source point collocates with the element, h_{jj} becomes c (on smooth boundary c=0.5) due to the distance vanishing. The integration for g_{jj} can be done analytically[125] since the exponential integral function can be expanded in a series[131]. The series and approximation forms of the

exponential integral function as well as the analytical integrations of g^i_{jj} are all given in Appendix B.

The coefficients for vector B is formed by evaluating the domain integration over the triangular elements. The Hammer's integration formulae is used, and the interpolation functions of the finite element type are introduced in order to save the storage and computing time, i.e.

$$B^n_e = A_e \sum_{k=1}^{K} \frac{1}{4\pi\alpha(t_F - t_{F-1})} \exp\left(\frac{-r^2_{ik}}{4\alpha(t_F - t_{F-1})}\right) W_k \Phi^n_k \qquad (4.4.10)$$

where $\Phi^n = \begin{Bmatrix} \eta_1 \\ \eta_2 \\ \eta_3 \end{Bmatrix}$, $\eta_1, \eta_2, \eta_3 = 1-\eta_1-\eta_2$ are area coordinates defined as $\eta_i = \frac{A^i_e}{A_e}$, A_e is the area of the triangular element and K is the number of integration points.

4.5 Treatment of Boundary Conditions

Since the boundary Γ may consist of three types of boundary conditions (4.2.3-5), it can be described in the following form

$$\int_{\Gamma_T \cup \Gamma_q \cup \Gamma_h} (qT^* - Tq^*)d\Gamma = \left[\int_{\Gamma_T} qT^* d\Gamma - \int_{\Gamma_q} Tq^* d\Gamma + \int_{\Gamma_h} (hT^* - q^*)T d\Gamma\right]$$

$$+ \left(\int_{\Gamma_q} \underline{q} T^* d\Gamma - \int_{\Gamma_T} \underline{T} q^* d\Gamma - \int_{\Gamma_h} h\underline{T}_1 T^* d\Gamma\right) \qquad (4.5.1)$$

in which all the unknowns are put between the square brackets and the known boundary values are put between the parentheses. The following operators are introduced to simplify the notation:

$$\tilde{H}T = c_2 T + \int_{t_{F-1}}^{t_F} \alpha \left[\int_{\Gamma_q} Tq^* d\Gamma - \int_{\Gamma_h} (hT^* - q^*) T d\Gamma \right] dt' \qquad (4.5.2)$$

$$\tilde{\Theta}q = \int_{t_{F-1}}^{t_F} \int_{\Gamma_T} \alpha q T^* \, d\Gamma \, dt' \qquad (4.5.3)$$

and a function defined by

$$\tilde{b} = \int_{t_{F-1}}^{t_F} \alpha \left(\int_{\Gamma_q} qT^* d\Gamma - \int_{\Gamma_T} Tq^* d\Gamma - \int_{\Gamma_h} hT_1 T^* d\Gamma \right) dt' + \int_{\Omega} [TT^*]_{F-1} d\Omega - c_1 T \qquad (4.5.4)$$

where $c_1=c$, $c_2=0$ if $x \in \Gamma_T$, and $c_1=0$, $c_2=c$ if $x \in \Gamma_q$ or Γ_h.

In this way, the boundary integral equation is finally obtained

$$\tilde{H}T - \tilde{\Theta}q = \tilde{b} \qquad (4.5.5)$$

where all the unknowns are in the left hand side. Notice that there are N_1 values of T on Γ_T and N_2 values of the other conditions on Γ_q and/or Γ_h, hence there are only N ($=N_1+N_2$) unknowns in the system of equation (4.5.5).

If more than one medium are considered, the interfacial boundary conditions (4.2.6) have to be taken into account. If an interface is denoted as Γ_I, the rest of the boundary as Γ_{Ri}, c_i for the location dependent parameters and Ω_i for the domains (i=1,2 for both sides, $c_1+c_2=1$), one should have the following boundary integral equations for the media from both sides of the interface:

$$c_1 T(x, t_F) = \alpha_1 \int_{t_{F-1}}^{t_F} \int_{\Gamma_{R1} \cup \Gamma_I} (qT^{1*} - Tq^{1*}) d\Gamma \, dt' + \int_{\Omega_1} T_{F-1} T^{1*}_{F-1} d\Omega \qquad (4.5.6a)$$

$$c_2 T(x, t_F) = \alpha_2 \int_{t_{F-1}}^{t_F} \int_{\Gamma_{R2} \cup \Gamma_I} (qT^{2*} - Tq^{2*}) d\Gamma \, dt' + \int_{\Omega_2} T_{F-1} T^{2*}_{F-1} d\Omega \qquad (4.5.6b)$$

According to the interfacial boundary conditions, one can work out the unknown temperature and heat flux on the interface by taking both summation and subtraction of the above two equations, i.e.

$$T(x,t_F)=\int_{t_{F-1}}^{t_F}\int_{\Gamma_I}\left[q'\left(\frac{T^{1*}}{\rho_1 C_{p1}}+\frac{T^{2*}}{\rho_2 C_{p2}}\right)-T(\alpha_1 q^{1*}-\alpha_2 q^{2*})\right]d\Gamma\,dt'$$
$$+\alpha_1\int_{t_{F-1}}^{t_F}\int_{\Gamma_{R1}}(qT^{1*}-Tq^{1*})d\Gamma\,dt'+\alpha_2\int_{t_{F-1}}^{t_F}\int_{\Gamma_{R2}}(qT^{2*}-Tq^{2*})d\Gamma\,dt'$$
$$+\int_{\Omega_1}T_{F-1}T^{1*}_{F-1}d\Omega+\int_{\Omega_2}T_{F-1}T^{2*}_{F-1}\,d\Omega \qquad (4.5.7)$$

where $q'=k_1q_1=-k_2q_2$ and

$$(c_1-c_2)T(x,t_F)=\int_{t_{F-1}}^{t_F}\int_{\Gamma_I}\left[q'\left(\frac{T^{1*}}{\rho_1 C_{p1}}-\frac{T^{2*}}{\rho_2 C_{p2}}\right)-T(\alpha_1 q^{1*}+\alpha_2 q^{2*})\right]d\Gamma\,dt'$$
$$+\alpha_1\int_{t_{F-1}}^{t_F}\int_{\Gamma_{R1}}(qT^{1*}-Tq^{1*})d\Gamma\,dt'-\alpha_2\int_{t_{F-1}}^{t_F}\int_{\Gamma_{R2}}(qT^{2*}-Tq^{2*})d\Gamma\,dt'$$
$$+\int_{\Omega_1}T_{F-1}T^{1*}_{F-1}d\Omega-\int_{\Omega_2}T_{F-1}T^{2*}_{F-1}\,d\Omega \qquad (4.5.8)$$

If denote the number of interfacial points are denoted as N_i, then the total number of unknowns N is $N_1+N_2+2N_i$. Only with equations (4.5.6-8) can all the unknowns be solved. Similarly, all the unknowns are put on the left hand side and the knowns on the other. Finally a boundary integral equation system like (4.5.5) can be obtained. The internal temperature can be worked out by applying (4.5.6) after all the unknowns on both the exterior and interfacial boundaries are solved.

4.6 Examples

A computer program of the boundary element method on transient heat conduction among multi-medium has been coded in FORTRAN. This program is a part of the package CASIM which will be introduced in Chapter Eight. The program was tested with simple geometries, and the

results were compared with analytical ones. Hereafter, two simple examples concerning the problems in the cooling stage of the injection moulding are presented.

Example 4.1

Fig.4.6.1 is a problem of a thin plate of melted polymer material being cooled down in a mould of which there are some cooling channels in each side of the melt. Suppose the melt temperature at the initial instant is 220 °C, and the mould temperature is 25 °C. The cooling water flows constantly through the channel, and the temperature on the interface of the cooling channel is kept at 25 °C all the time.

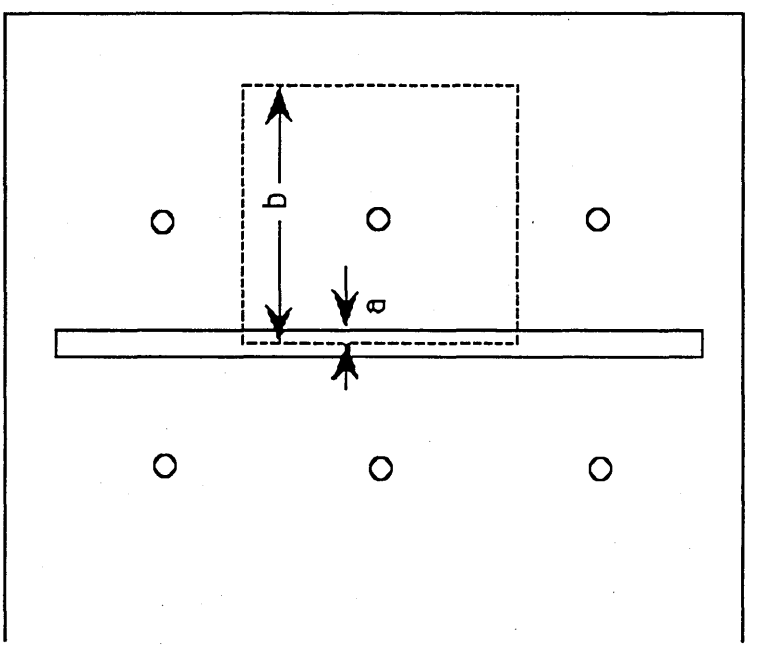

Figure 4.6.1. Schematic of the transverse section of the cooling

Although the whole problem could be computed by using the boundary element mesh over all the boundaries and interfaces, only the dotted part was taken for the calculation for simplicity. The heat flux at the boundaries around the square is assumed to be zero. The height ratio a/b of the plastic melt and the mould in this part is 6:100, the ratio of the corresponding thermal diffusivities is 1:150, and the ratio of the diameter of the cooling channel and the mould height is 8:100. The location of the cooling channel is in the centre of the square. The initial condition of the temperature field is assumed as shown in the first frame.

Fig.4.6.2 shows the development of the temperature field in terms of contours and time intervals. It can be seen that the temperature gradient at the interface is always very high. The coolant absorbs the heat and causes

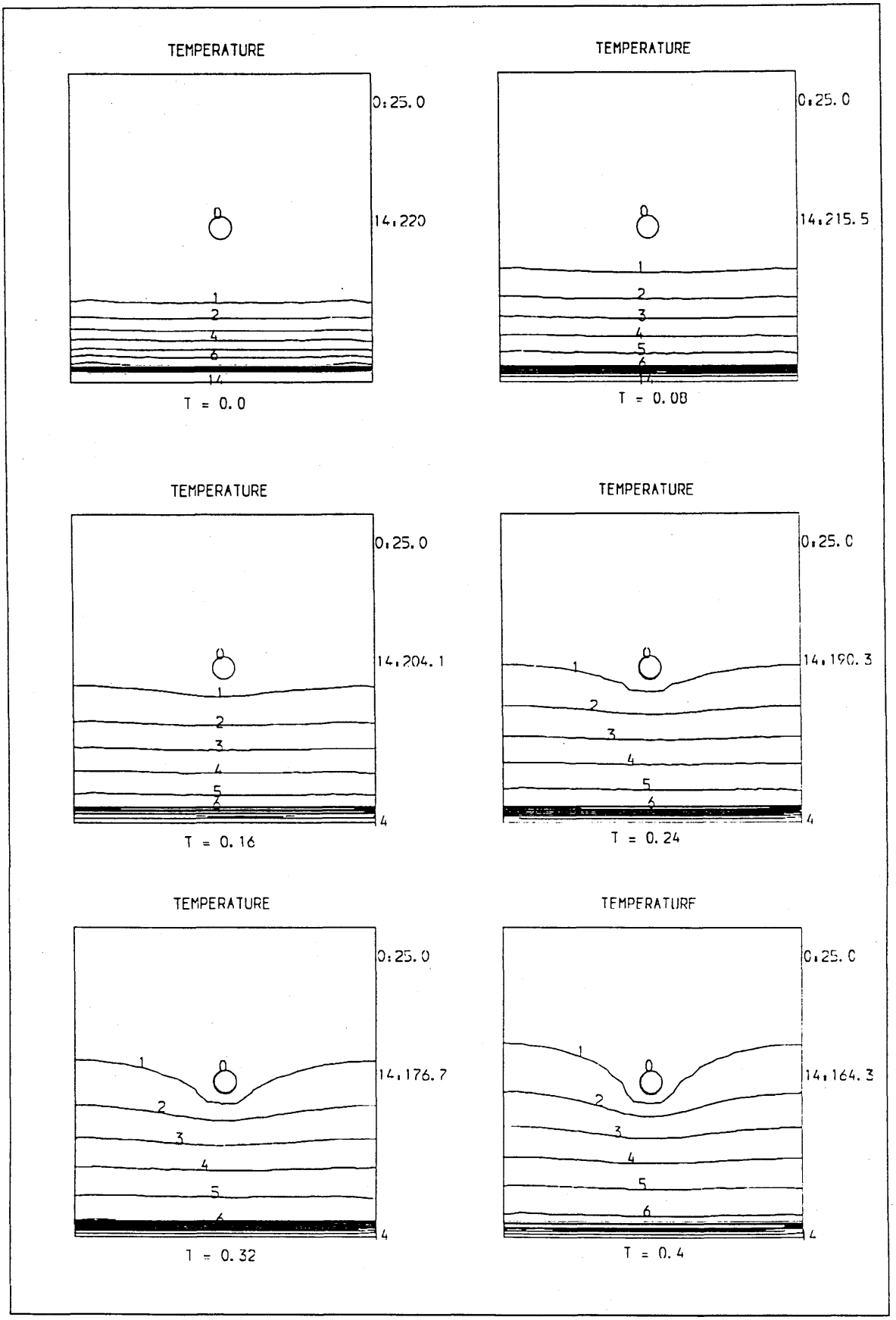

Fig.4.6.2. The development of the temperature field (continued)

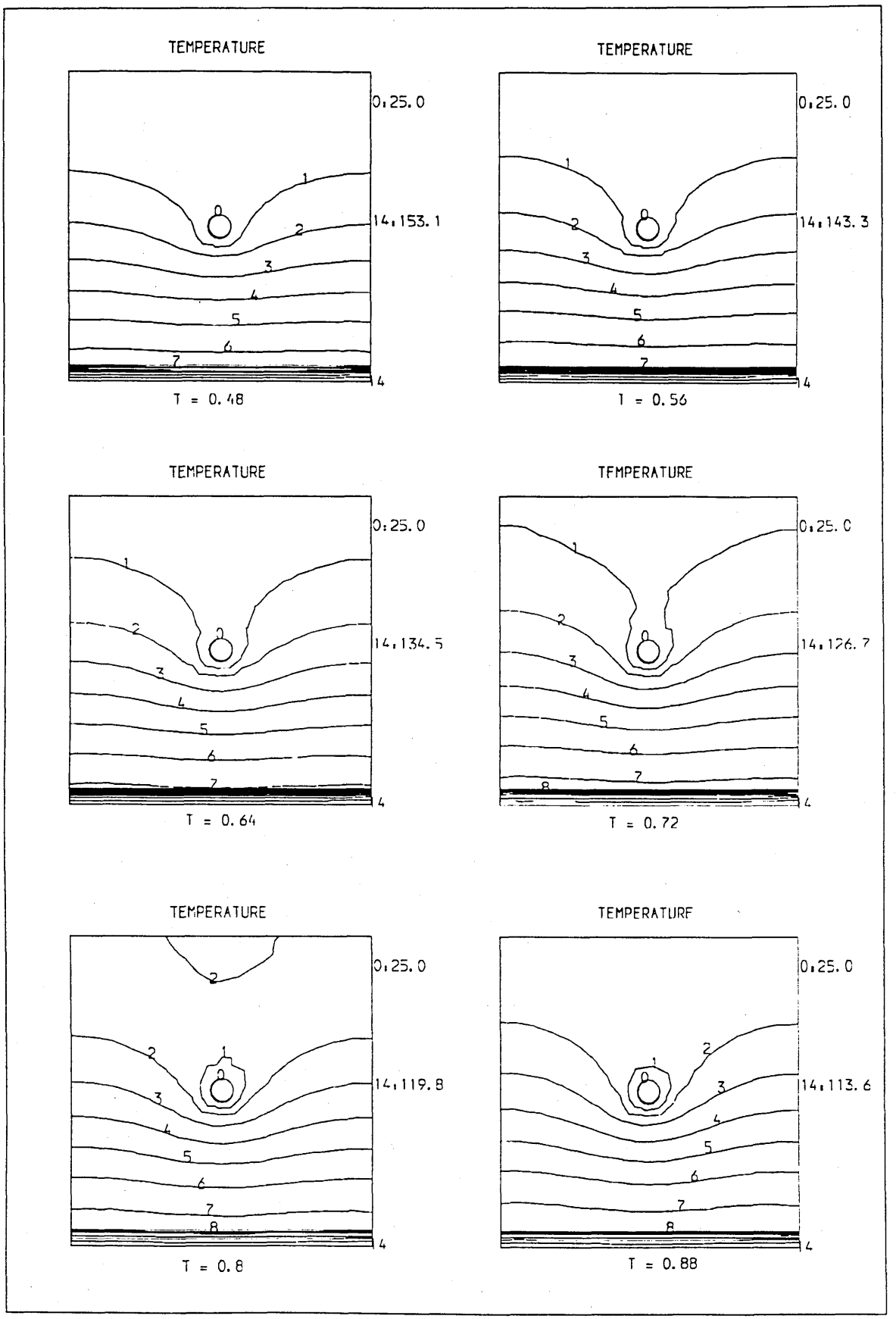

Fig.4.6.2. Continued from the last page (continued)

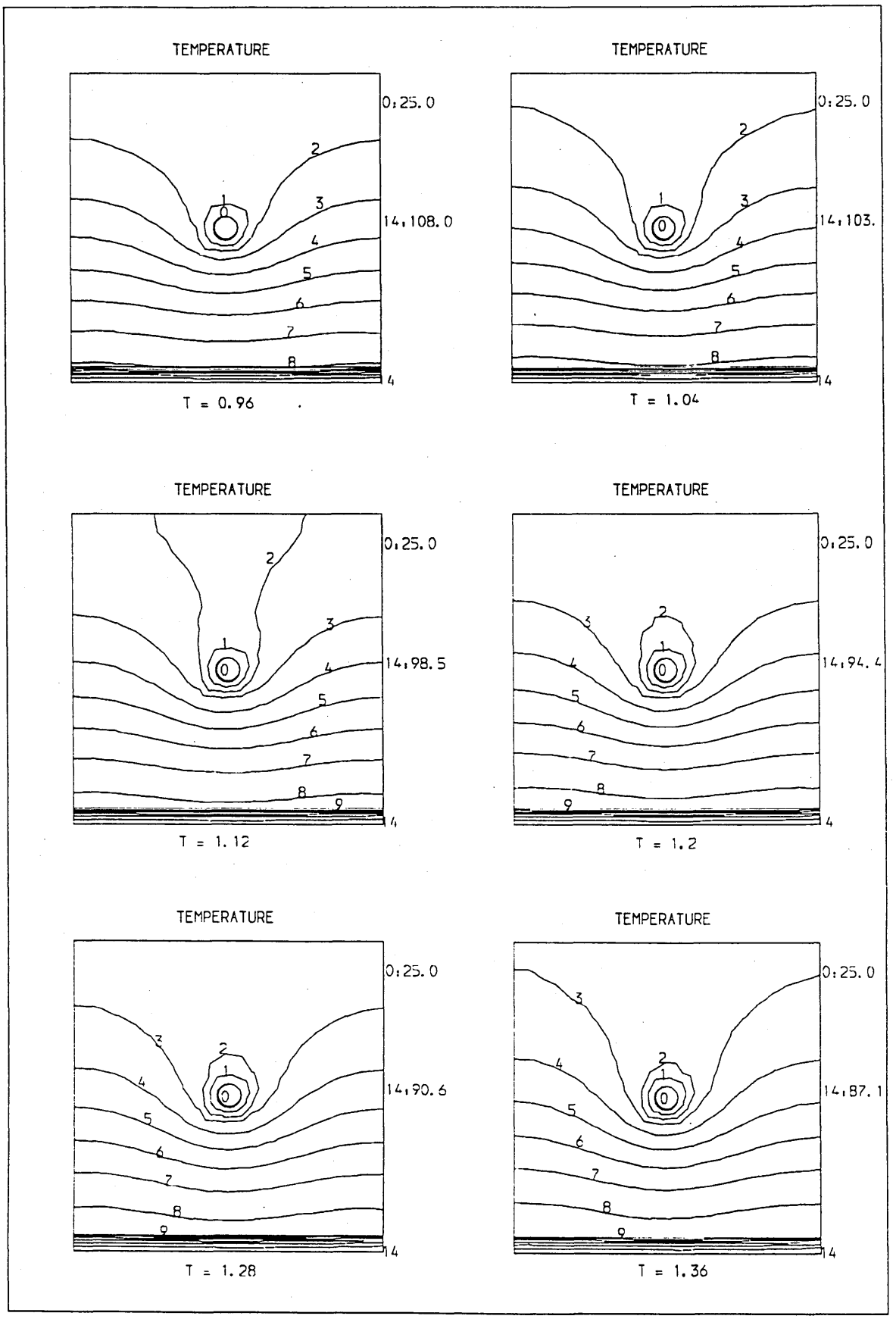

Fig.4.6.2. Continued from the last page (continued)

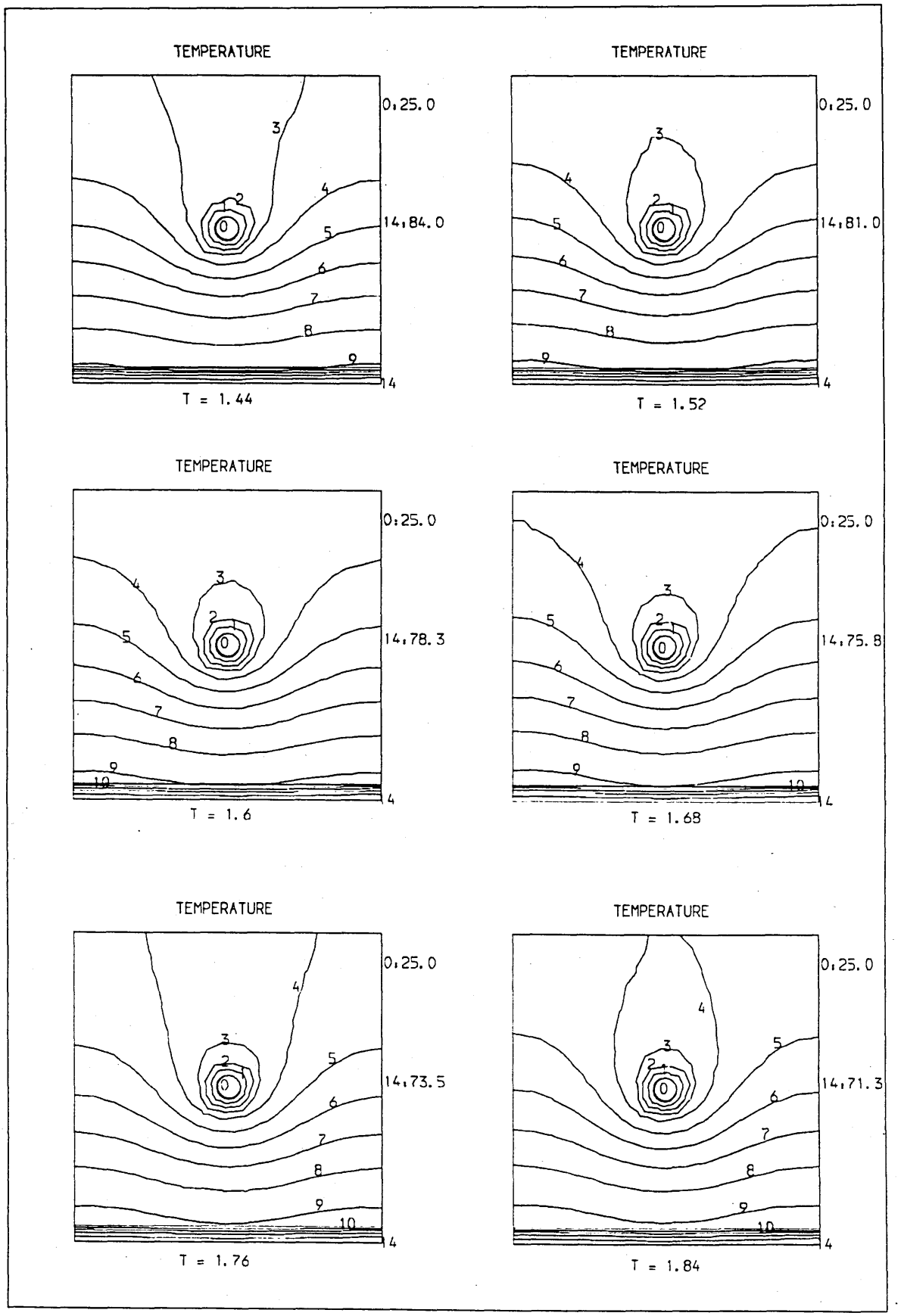

Fig.4.6.2. Continued from the last page (continued)

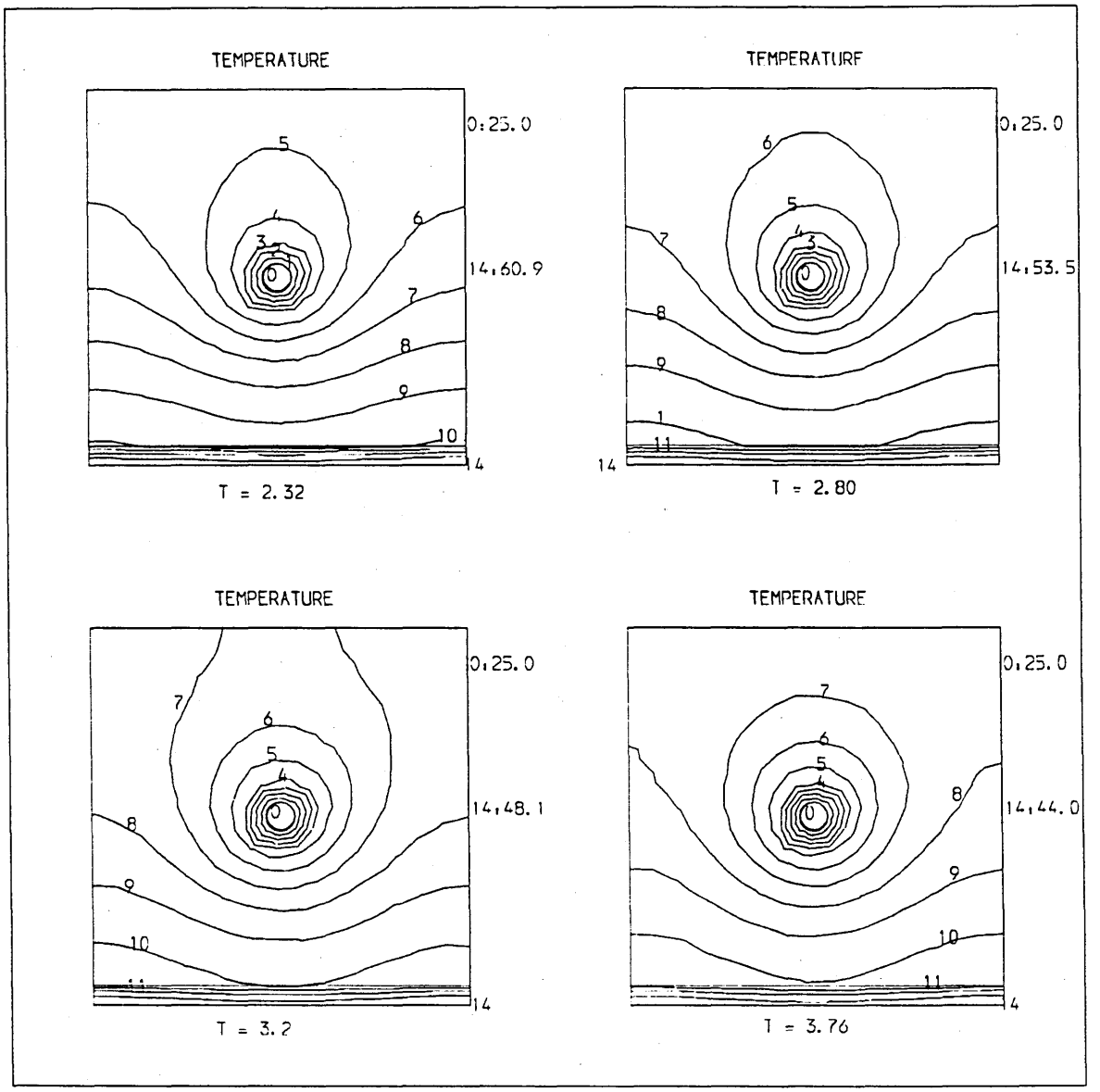

Fig.4.6.2. The development of the temperature field from 0 to 3.76 seconds

the temperature gradient around it very high in the later stage. The speed of decreasing of the maximum temperature (in the centre of the thin part) decelerates since 0.16 second, with 13.8 °C difference in the following time interval comparing 4.1 °C difference in the last 7 time intervals.

Example 4.2

Fig.4.6.3 shows a cross section of a part with a "+" joint in a mould in which there is a cooling channel in each quad of the joint. The temperature distribution around the joint is especially of concern because often a sink mark occurs in the end of the joint or a void happens inside it. Again only a square of a quarter of the cross section is taken to approximate the problem

for simplicity. The zero heat flux condition is again given to the boundaries of the square. The rib is slightly tapered and the corner is rounded. The ratio of the diameter of the coolant to the thickness of the horizontal part is 1:1. The ratio of the radius to the distance between the centre of the coolant and the edge of the part is 1:10. The diffusivity ratio is identical with it in the last example. The initial temperature field is given as shown in the first frame which indicates that most of the melt is at 220 °C, and the coolant is at 25 °C. The cooling liquid is assumed to take the heat away in such a speed that the surface of the coolant is kept this temperature.

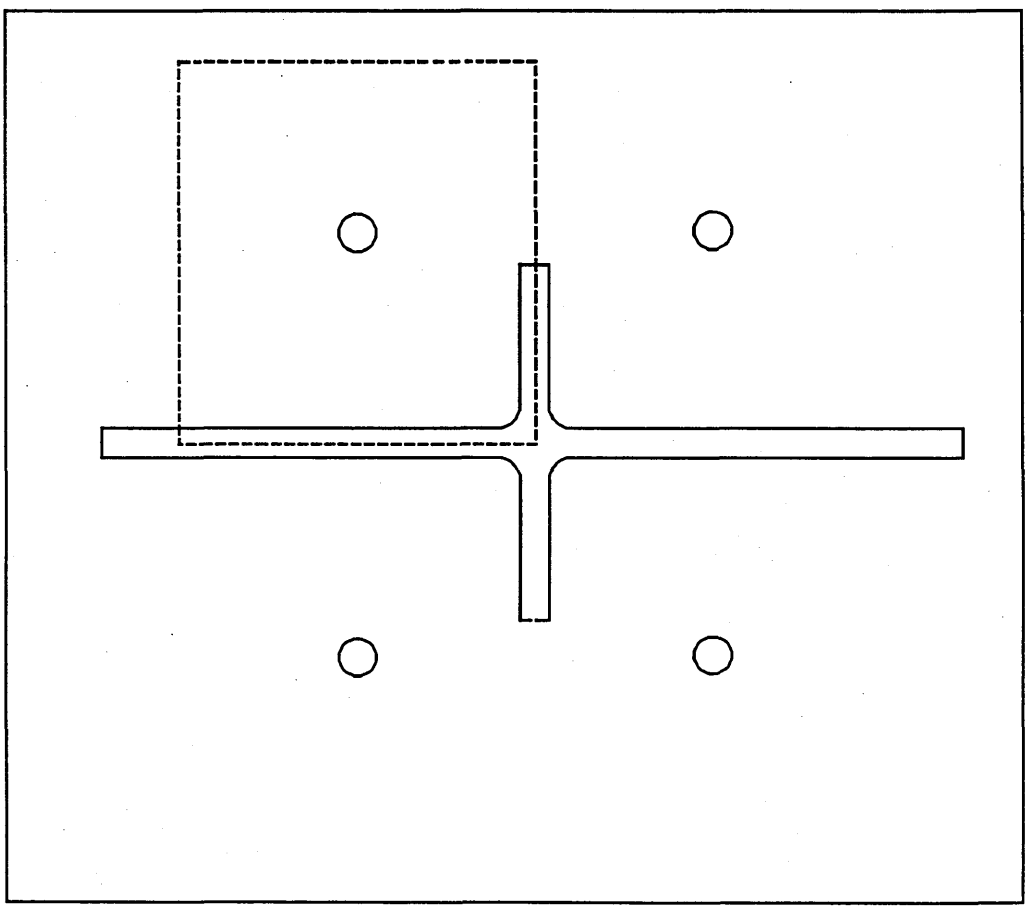

Figure.4.6.3. Schematic of the "+" joint with coolants in its four quads.

The history of the evolvement of the temperature field is shown in Fig.4.6.4. There are similarities to the example 4.1 in the temperature gradients at the interfaces but the maximum temperature decreases much slower because of its geometrical location (in the centre of the joint). The sequence of these frames clearly indicates the reason for sealing off an island of melt inside the joint which may cause a sink mark or a void unless high pressure is maintained or other means for resolving the problem.

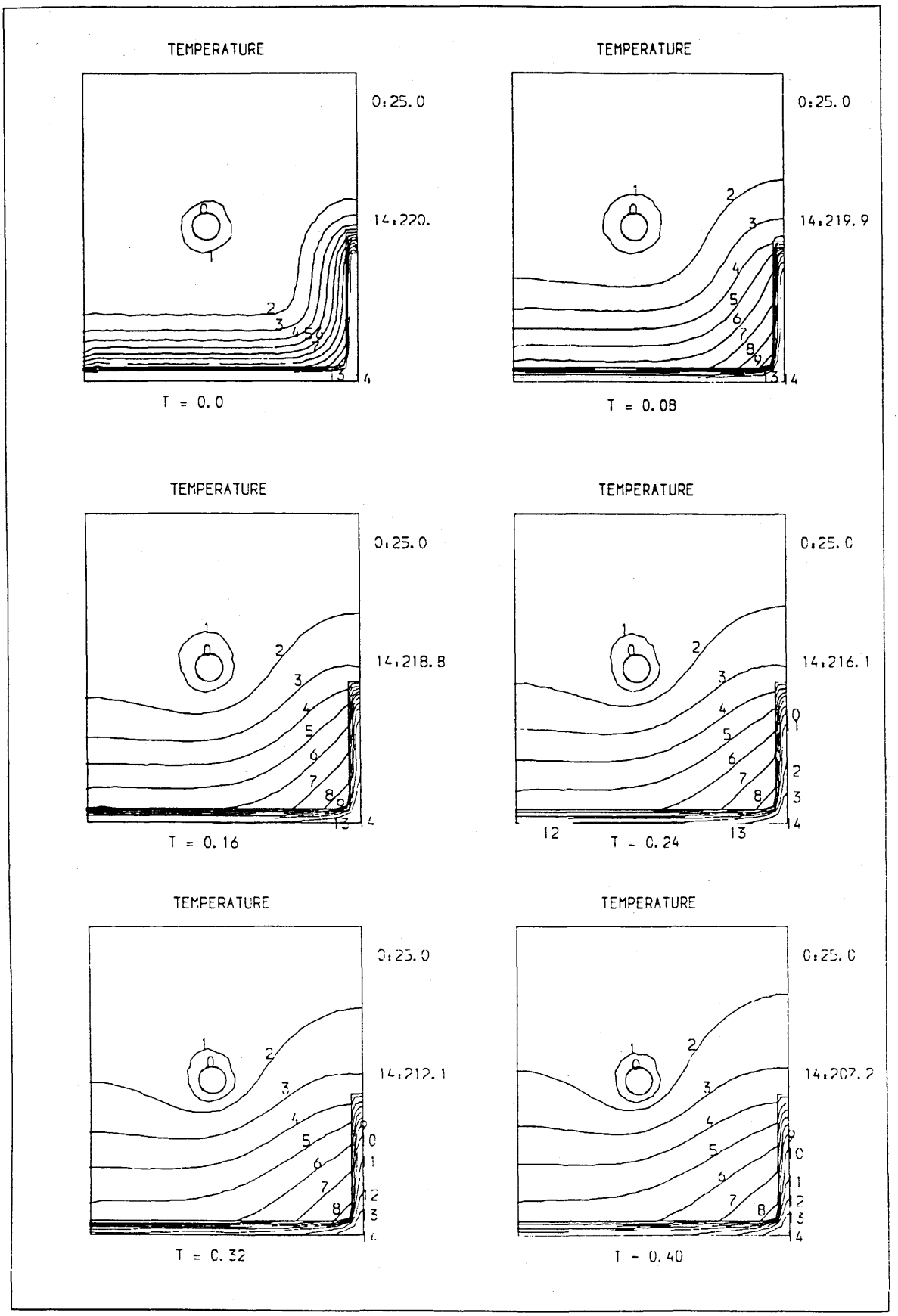

Fig.4.6.4.The temperature evolvement in terms of contours and time intervals (continued).

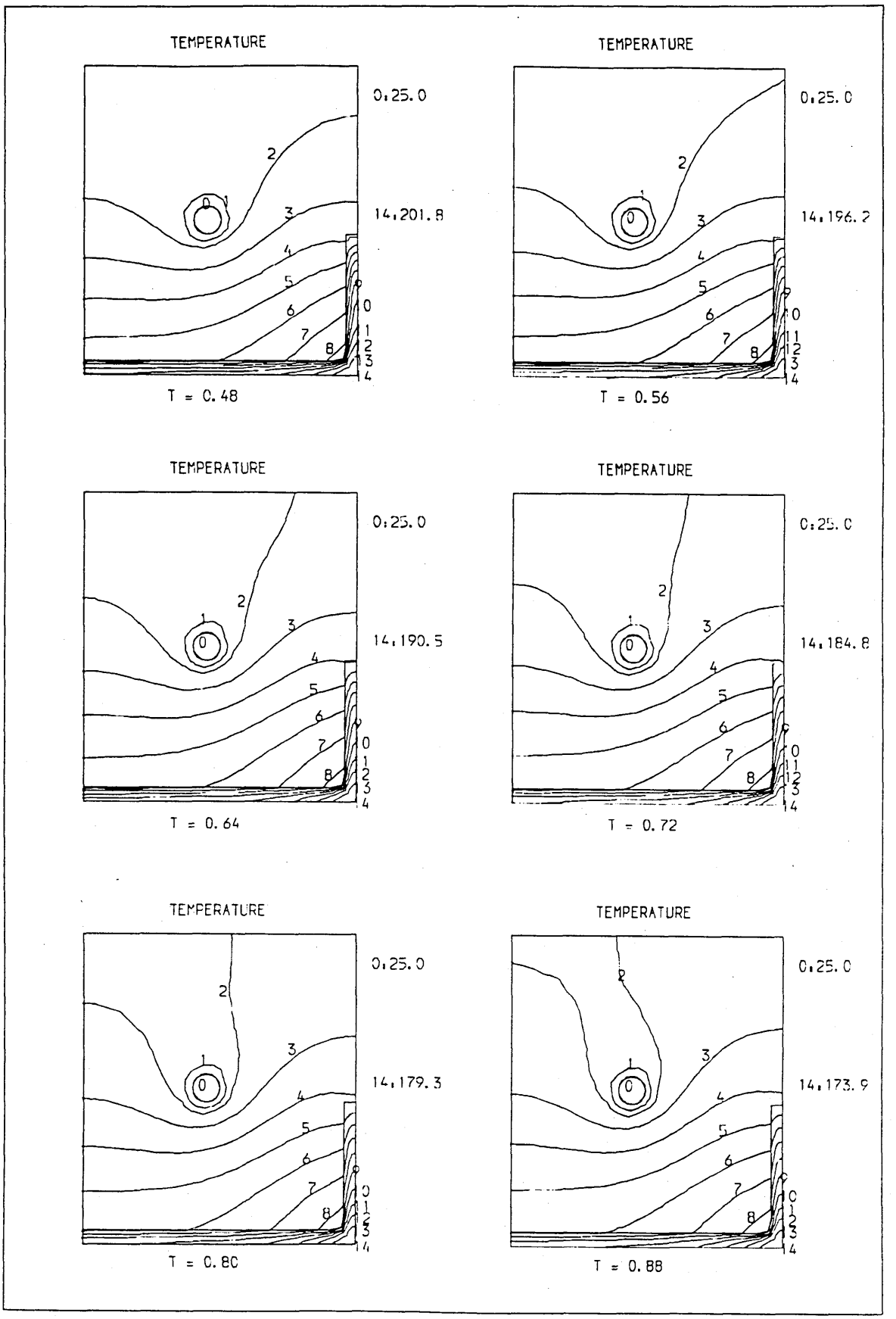

Fig.4.6.4. Continued from the last page (continued)

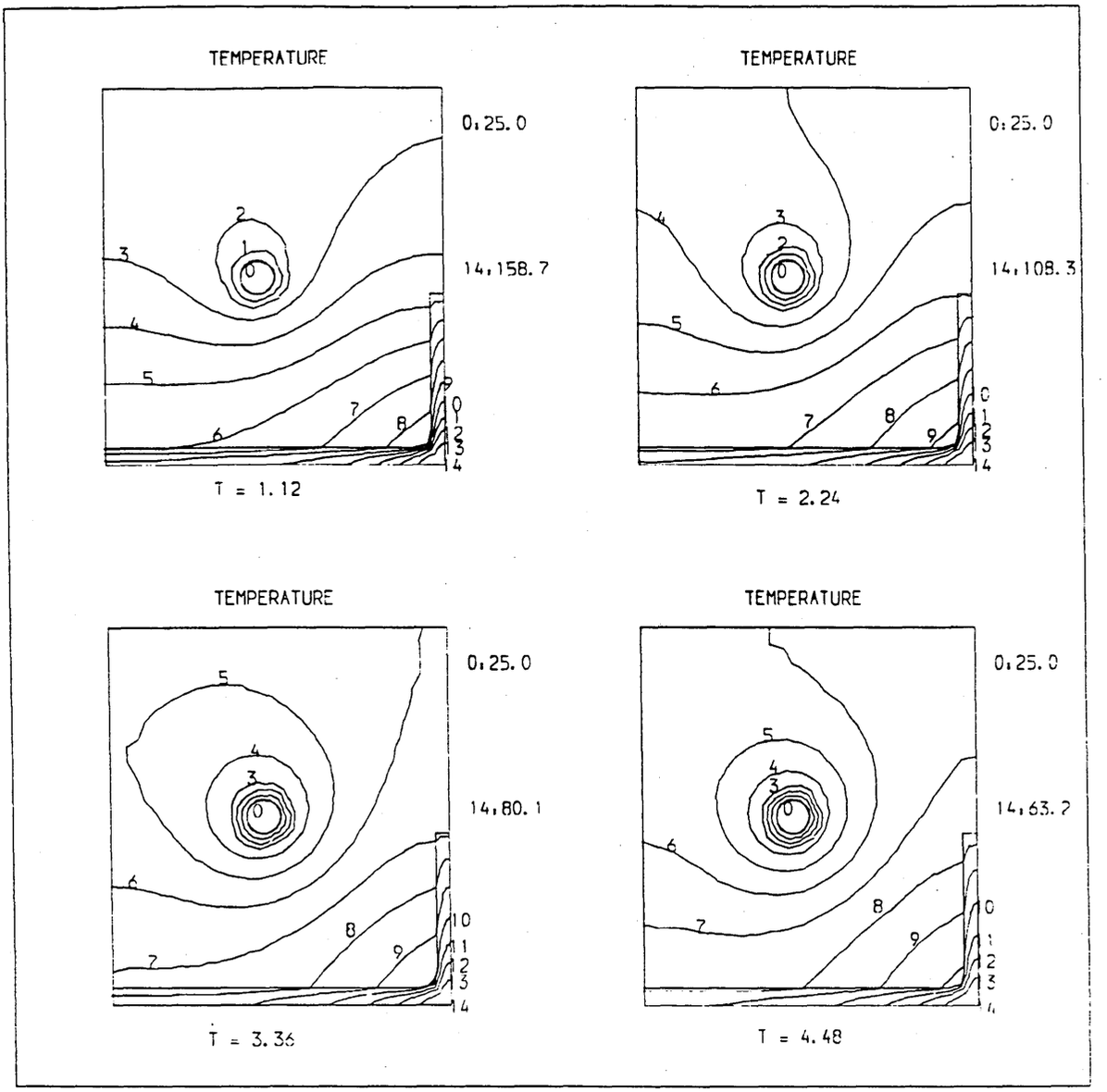

Fig.4.6.4. Continued from the last page.

Fig.4.6.5 shows the enlargement of the temperature field at 5.6 second from which it can be seen that the joint centre is 52.3 °C, though most of the part is under 50 °C.

From this example it can be concluded that from a geometrical view point it is very difficult to design an ideal cooling system to cool down the polymer with a joint of this type uniformly. The location, size of the coolants and initial temperature of the cooling liquid can be designed to speed up the cooling, then the whole cycle time can be reduced.

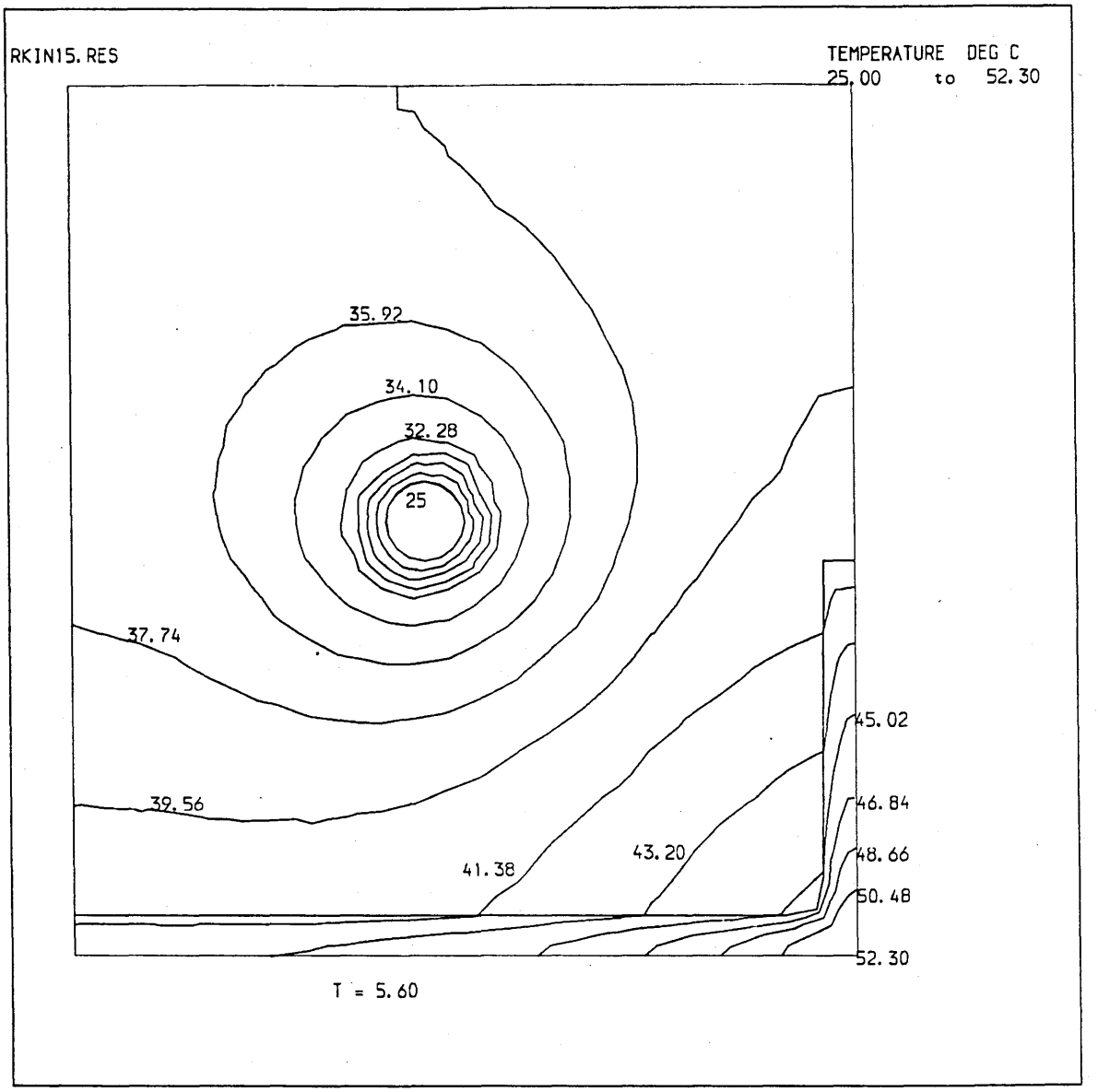

Fig.4.6.5. The enlargement of the temperature field at 5.6 second.

4.7 Further Discussions

Although all kinds of transient heat conduction problems can be solved by using the program, there are some limitations in the application for the cooling of the plastic parts. One of them is that the number of interfacial elements would be massive due to the geometrical complexity of the parts. Despite the significant reduction by one dimension, the resulting system could still be sizable, and the computing resources might not be satisfactory. In the author's point of view, it is possible to overcome the limitation by a further and reasonable simplification.

Let us consider the following transformation:

$$\zeta_i = \frac{x_i}{\sqrt{\alpha_k}};\ (k = 1, 2, \cdots) \qquad (4.7.1)$$

After this transformation, the coordinates are normalised. Thus there is no physical property involved in the governing equation in this new space. Equations (4.5.6a-b) become identical, no more equations are needed for the points on the interfacial boundaries. In return for this, a special attention must be paid to the distance between the source point and the observing point. Any straight line between these two points across a interfacial boundary is split in such a way as given in the following:

$$\rho^2 = \left(\frac{x_1 - \hat{x}_1}{\sqrt{\alpha_1}} + \frac{\hat{x}_1 - x'_1}{\sqrt{\alpha_2}} \right)^2 + \left(\frac{x_2 - \hat{x}_2}{\sqrt{\alpha_1}} + \frac{\hat{x}_2 - x'_2}{\sqrt{\alpha_2}} \right)^2 \qquad (4.7.2)$$

where $\hat{x}_1$ and $\hat{x}_2$ are the coordinates of the intersection point between the straight lines and the interface, α_1, α_2 are the two corresponding thermal diffusivities in both sides of the interface, and ρ is the distance in this new space.

However, the resulting boundary integral equation in this space is not identical to the equation group (4.5.7-8). The derivative of the boundary integral equation becomes discontinuous on the interface because of the discontinuity of the new coordinates on the interface. In order to smooth the sharp change of the heat flux q', a tiny artificial zone is introduced along the interface in which the thermal diffusivity change continually from α_1 to α_2. In this way, the calculation of the distance is much easier because no intersection coordinates need to be calculated. Only when the source point is on the interface, the formulae of the distance is:

$$\rho^2 = \left(\frac{\sqrt{2}\, x_1}{\sqrt{\alpha_1 + \alpha_2}} - \frac{x'_1}{\sqrt{\alpha_2}} \right)^2 + \left(\frac{\sqrt{2}\, x_2}{\sqrt{\alpha_1 + \alpha_2}} - \frac{x'_2}{\sqrt{\alpha_2}} \right)^2 \qquad (4.7.3)$$

where an average thermal diffusivity is used, and the observing point is assumed in domain 2. Fig. 4.7.1 shows the two different transformations schematically.

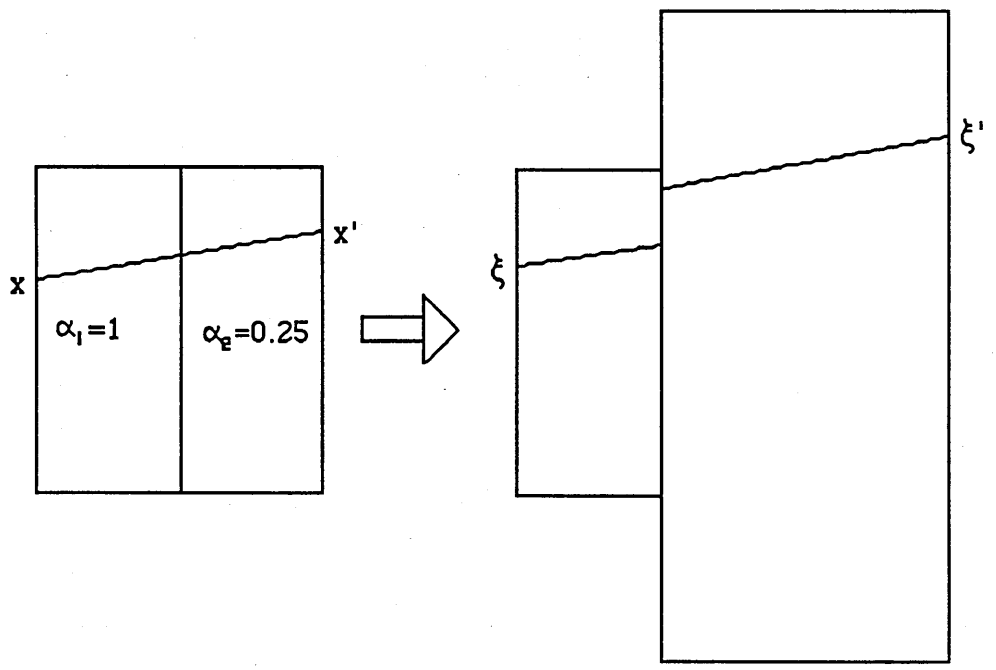

a. The transformation by equation (4.7.1) and the distance between two points in both sides.

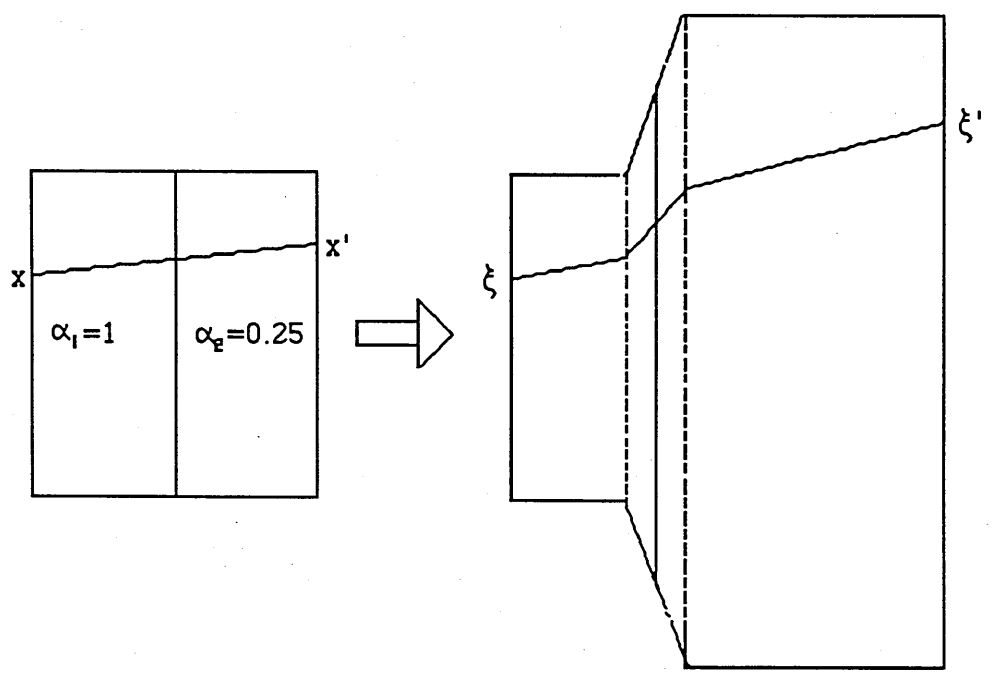

b. A thin artificial zone is assumed along the interface, the coordinates become continues

Fig.4.7.1 A new scheme without interface elements

A comparison between the BEM scheme with interface elements and the BEM scheme without interface elements is given in example 4.3.

Example 4.3

Two adjacent media of the same size are heated up from one end as shown in Fig.4.7.2. The ratio of the diffusivities is 1:10. Fig.4.7.2 is the temperature evolvement resulting from the boundary element scheme with interfacial elements, and Fig.4.7.3 is the temperature evolvement resulting from the boundary element scheme without the interfacial elements.

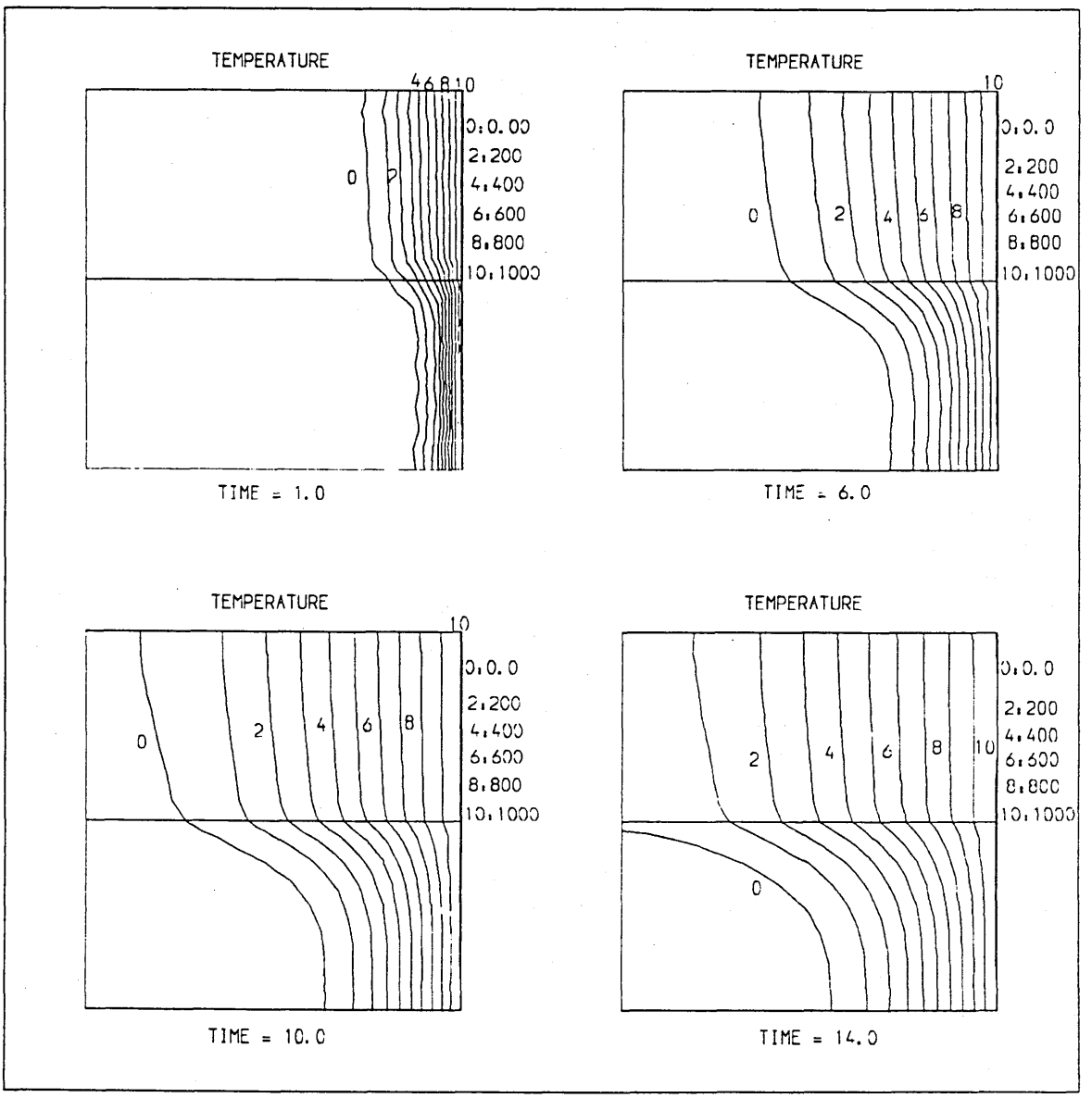

Fig.4.7.2. BEM scheme with interfacial elements for two media heat conduction

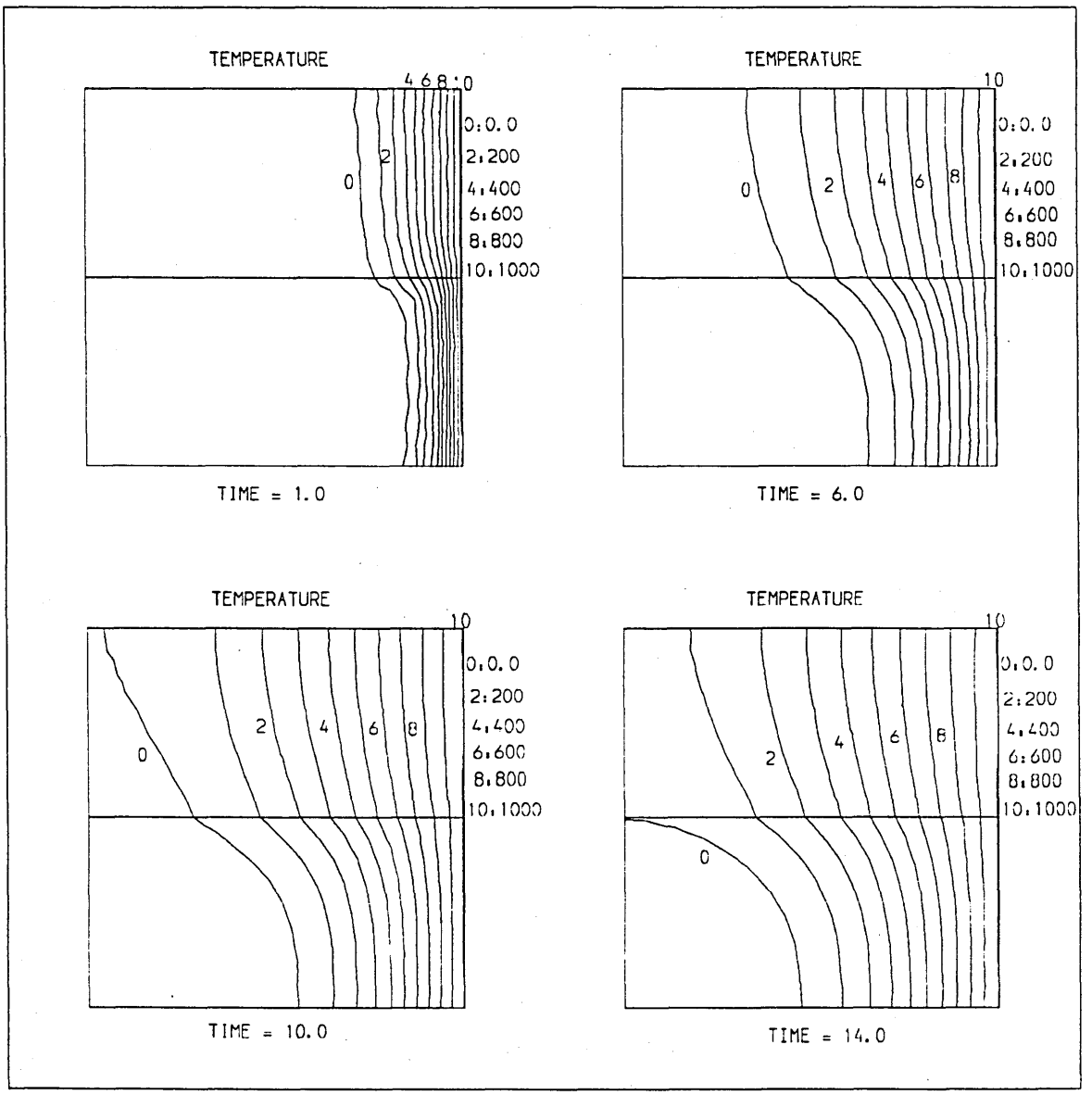

Fig.4.7.3. BEM scheme without interfacial elements for two media heat conduction

It becomes very interesting if this new idea is extended to a problem with a concave domain in which the boundary element methods have another limitation to apply. Let us still consider a problem with two media which have different thermal diffusivities as shown in Fig.4.7.4. If the second thermal diffusivity approaches zero which means that the medium is an insulated block, the distance between two points sitting at both sides of the concave corner in the other medium goes to infinity according to equation (4.7.2). However, there is heat transferred through medium one, therefore the distance between the two points has to be a new concept.

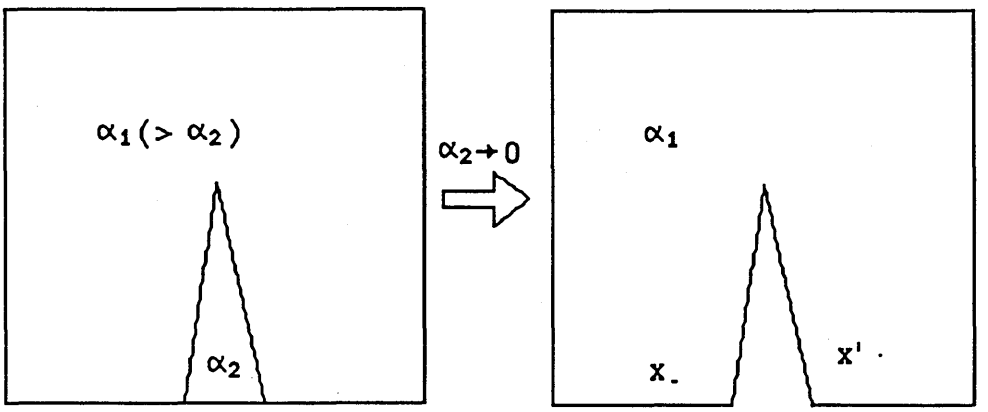

Fig.4.7.4 What is the distance between x and x' in this extreme case?

Normally, the boundary element methods can not be directly applied in this concave domain problem with an insulated boundary condition along the concave side. The domain has to be divided up into two convex sub-domains, and an artificial interface has to be constructed as shown in Fig.4.7.5. Obviously, this interface precludes the possibility of a straight line which belongs to the domain from bridging across the concave corner. Intuitively, this treatment is the same as a new concept of an effective distance between the two points which can be stated as follow:

***Definition*: An effective distance between any two points in a domain is the shortest curve within the domain connecting these two points.**

Following this definition, the effective distance between the two points is the curve around the concave corner as shown in Fig.4.7.6.

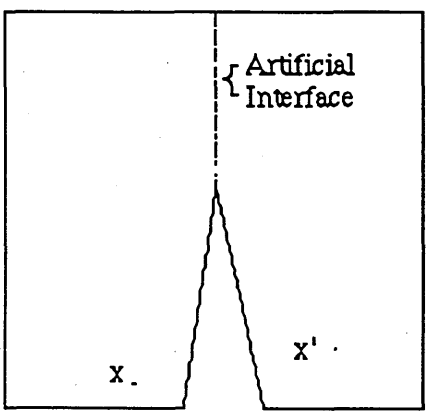

Fig.4.7.5 An interface to divide the domain into two convexes

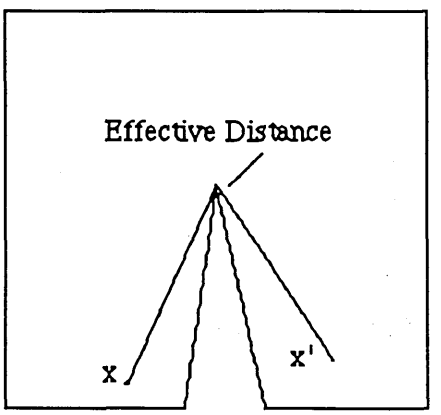

Fig.4.7.6 Effective distance within the concave domain

All these can be drawn to a conclusion: **There is no difference between using the effective distance and using convex sub-domains for a concave domain problem with an insulated boundary condition along the concave side(s) in a boundary element method.** This new idea, which needs to be mathematically proved, permits significant extending of the boundary element methods to the concave domain problems without interface elements, and saving both manual work of dividing the concerning concave domain into convex sub-domains and computing resources. Based on this new idea, a program is coded and a example is given to prove the suitability and effectiveness below.

Example 4.4

A square domain with a crack from the midpoint of its right side to its centre. All the boundaries are insulated except the right side where the temperature is kept 1000 °C in the upper half and 0 °C in the lower half. The development of the temperature field is shown in Fig.4.7.7. When the time is approaching to infinity the temperature field is identical to the temperature field in steady state. The contours should be then symmetrical about the crack. From the enlargement of the temperature field at 176 second shown in Fig.4.7.8, it can be seen the contours are very close to symmetric about the crack.

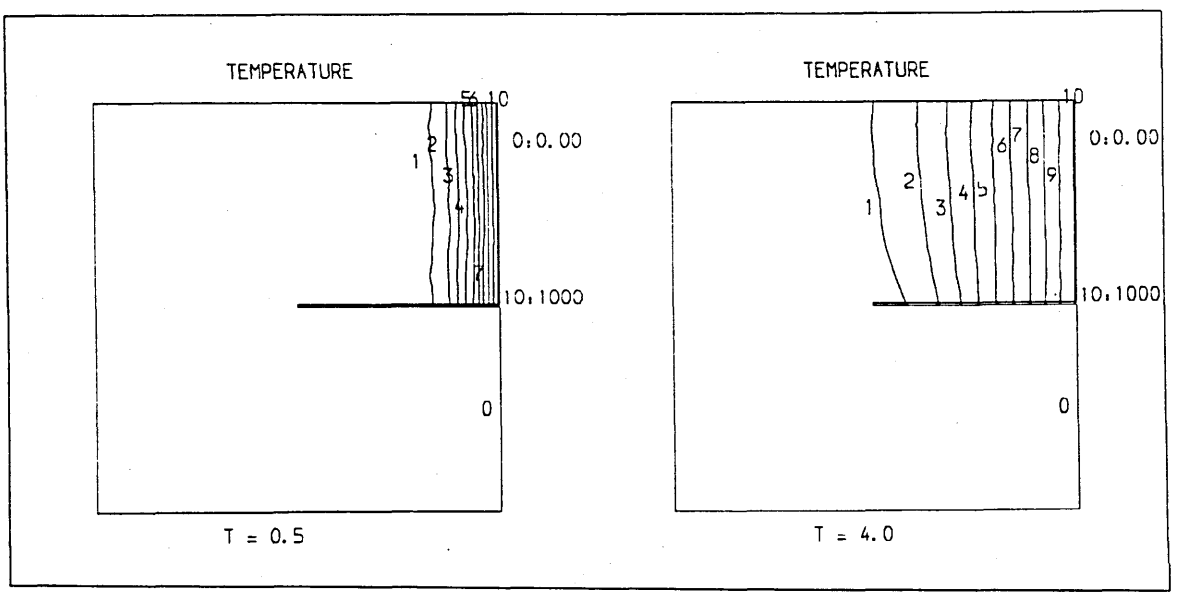

Fig.4.7.7. The development of the temperature field in a concave domain. (continued)

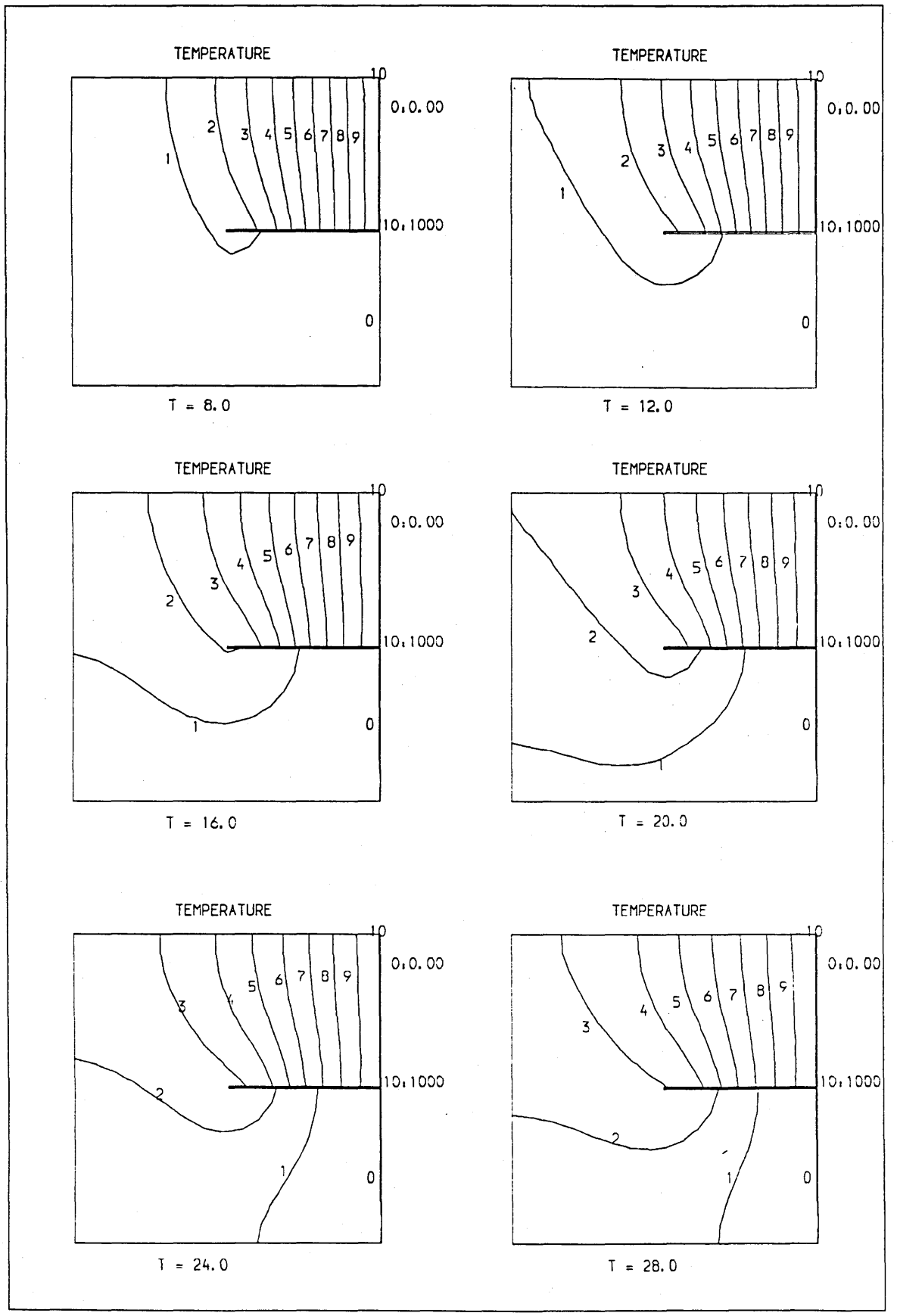

Fig.4.7.7. Continued from the last page.

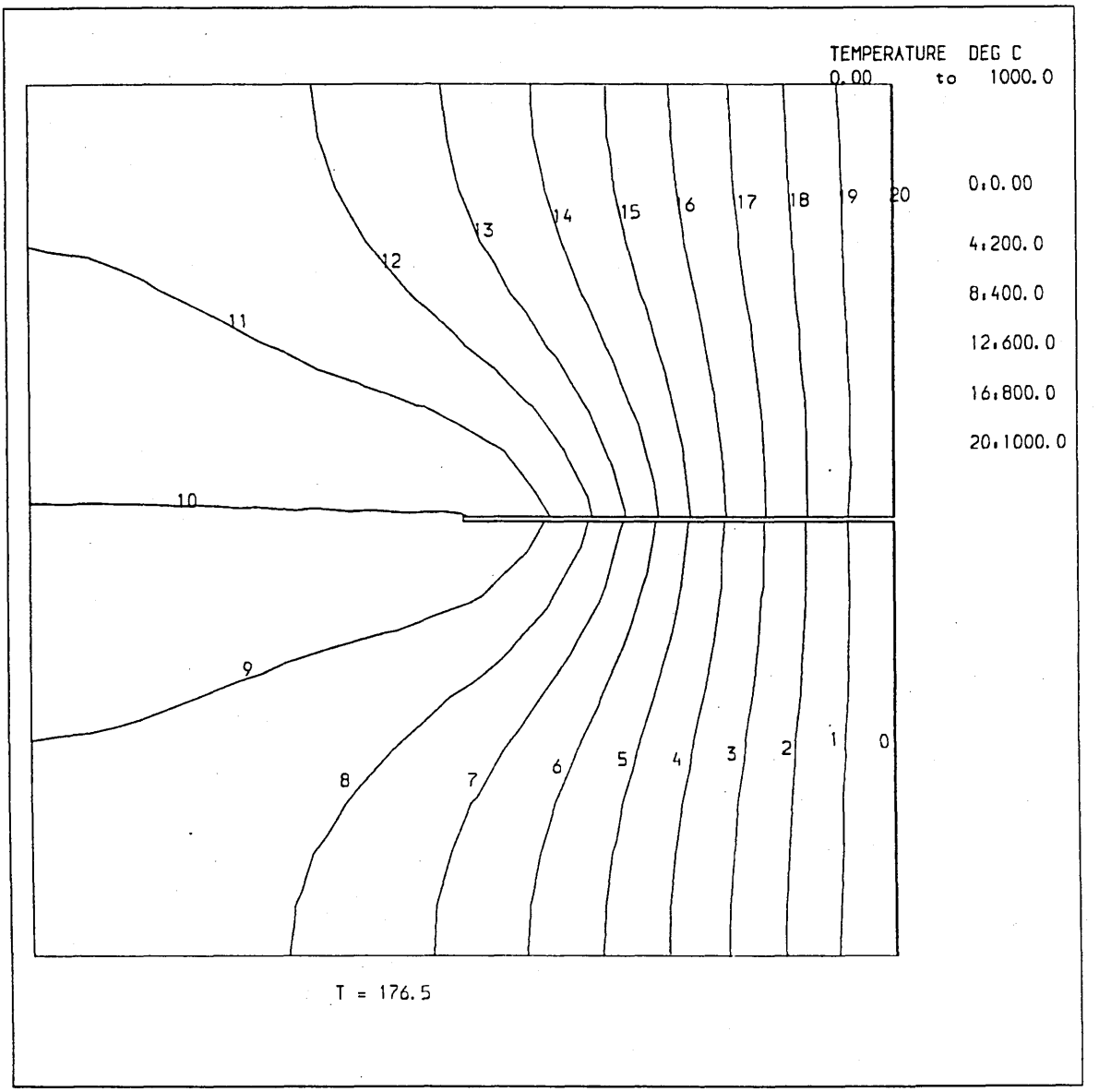

Fig.4.7.8. The temperature field at 176 second.

4.8 Transformation of the Domain Integral into Boundary Integrals

As mentioned in section 2.7, the existence of domain integral loses the elegance and efficiency of the boundary element method. The idea of the dual reciprocity principle can also be used in this time-dependent case to transform the domain integral into boundary integrals. Let us consider the domain integral in equation (4.3.2). Following the idea, the temperature field $T(x',t_0)$ is replaced by following N coordinate function series:

$$T(x', t_0) = \sum_{i=1}^{N} A_i f_i(r) \qquad (4.8.1)$$

in which $f_i(r)$ satisfies the Laplace equation (2.7.3), and r_i are the polar origins for the functions.

Equation (4.3.2) can then be rewritten into the following form

$$cT = \int_{t_o}^{t}\int_{\Gamma} \alpha(qT^* - Tq^*)d\Gamma\, dt' + \sum_{i=1}^{N} A_i\left[\int_{\Gamma}(f_i\Phi_{,j}n_j - f_{i,j}n_j\Phi)d\Gamma + c_1\Phi(r_i)\right] \qquad (4.8.2)$$

where c_1 is a constant based on the location of the polar origins, and Φ is the fundamental solution of the following Poisson equation

$$\Phi_{,ii} = \frac{1}{4\pi\alpha\Delta t^{d/2}}\exp\left[-\frac{r^2}{4\alpha\Delta t}\right] \qquad (4.8.3)$$

For both two and three dimensional cases, Φ are given by Pina and Fernandes[128]

$$\left.\begin{aligned} \Phi &= -\frac{1}{4\pi}\left[E_1\left(\frac{r^2}{4\alpha\Delta t}\right) + \ln\left(\frac{r^2}{4\alpha\Delta t}\right) + \gamma\right] && 2D \\ \Phi &= -\frac{1}{4\pi r}\mathrm{erf}\left[\frac{r}{(4\alpha\Delta t)^2}\right] && 3D \end{aligned}\right\} \qquad (4.8.4)$$

The coefficients A_i are obtained in the same way as mentioned in section 2.7 of Chapter Two.

Chapter Five

BEM for Steady Viscous Flow

5.1 Introduction

The limitations of the models based on the thin cavity approximation must be realised though they have been effective in predicting quantities such as pressure, flow front position, and velocity. For cavities with high aspect ratios, or some localised problems, more accurate models should be used. Also, it is the phenomena that happen in the flow field near the advancing front that have a profound effect on the properties of the moulding and must be taken into account. This flow effect is described as "fountain effect" due to the phenomena of deceleration and outward motion of fluid particles as they approach a slower moving surface.

Polymer flow can also be simplified as a creeping flow. This is a reasonable simplification because the Reynolds number in dimensionless Navier-Stokes equations

$$\mathrm{Re}\left[\dot{u}_i + (u_j u_i)_{,j}\right] = \sigma_{ij,j} + \mathrm{Re} f_i \qquad (5.1.1)$$

is so small that the inertia terms in the left hand side can then be omitted. For Newtonian fluids such an omission results in so-called *creeping motion* or Stokes equations as follows

$$\sigma_{ij,j} + \mathrm{Re} f_i = 0 \qquad (5.1.2)$$

in which the constitutive equation is the Newtonian relation. Polymer flow is characterised as high viscosity; many flow problems in polymer processing satisfy the low Reynolds number conditions. Therefore, to approximate the flows by the creeping motion equation in the filling stage of the injection moulding technique is reasonable. The incompressible condition can be reasonably used for the flow field during the filling stage of the injection moulding, though the compressibility may be present due to the large

pressure variation involved. Therefore the continuity equation is given as follow

$$u_{i,i}=0 \qquad (5.1.3)$$

If only the time-derivative term of the inertia terms is neglected, equations (5.1.1) become *steady viscous flow* as follows

$$\mathrm{Re}(u_j u_i)_{,j} = \sigma_{ij,j} + \mathrm{Re} f_i \qquad (5.1.4)$$

which can give a more accurate approximation of the filling flow of the injection moulding. Yet it is precisely this non-linearity that is the principal mathematical difficulty pervading classical hydrodynamics.

If the non-linear constitutive relationship is introduced, that is, the non-Newtonian models for the polymer fluids, equations (5.1.2) or (5.1.4) are even more difficult to solve. What is more, the energy conservation equation has to be added into the simultaneous equations if the non-isothermal effect on viscosity is taken into account.

However, as mentioned in Chapter One, several authors, notably Wu[86], Coleman[87,88], Bush and Tanner[89], Tosaka and Onisaka[90,91], Kitagawa and Brebbia[92,93], Tran-Cong and Phan-Thien[132,133] have developed the boundary element methods for solving the incompressible steady viscous flows, even for attacking some non-Newtonian flows. In this chapter, the boundary integral equation method for incompressible steady viscous flows in primitive variables is presented and applied for solving the fountain flow, particle and fibre orientations in the area and some free surface problems.

5.2 Boundary Integral Representations

It is the Green's function technique which forms the basis of the equations in integral forms. However, the first systematic developments for the steady, incompressible creeping flows stem from the work of Lorentz[134] who proved the following reciprocal theorem

$$\int_S dS \cdot \Sigma' \cdot v'' = \int_S dS \cdot \Sigma'' \cdot v' \qquad (5.2.1)$$

any two motions of the same fluid conforming to equations (5.1.2) and (5.1.3). Ten years later Oseen in his classic book[84] gave the solutions of such a motion in which the velocity and stress fields were caused by a disturbed source at a variable point, and obtained the integral formulations not only for the creeping flow but also for some more complicated flows.

It can be clearer and easier, however, to derive the integral equations by using the weighted residual method nowadays. Let us employ a Cartesian tensor weight function for equation (5.1.4).

$$\int_{\Omega}\left[\sigma_{ij,j} + \mathrm{Re}f_i - \mathrm{Re}(u_j u_i)_{,j}\right]V_{ik}\,d\Omega = 0 \qquad (5.2.2)$$

where Ω is the domain in which the medium occupies with the following conditions on the medium boundary Γ:

$$\left.\begin{aligned} u_i &= \underline{u}_i & \Gamma_1 \\ \tau_i &= \underline{\sigma}_{ij,j} n_j = \underline{\tau}_i & \Gamma_2 \end{aligned}\right\} \qquad (5.2.3)$$

and $\Gamma_1+\Gamma_2=\Gamma$, $\underline{u}_i$ and $\underline{\tau}_i$ are prescribed velocities and tractions on the corresponding boundaries. Whatever the shape or position of the domain Ω is in a fixed frame system the integral always applies over the medium.

A requirement for these tensor functions V_{ik} (i,k=1,2,3) is that the determinant of the corresponding matrix is not zero, that is:

$$\det[V_{ik}] \neq 0 \qquad (5.2.4)$$

This is the prerequisite and sufficient condition for the trivial solution of a group of homogeneous equations. Equations (5.2.2) can be regarded as such a homogeneous matrix equation where each k row is required to be zero, and the weight functions can be regarded as the coefficients.

According to the Gauss theorem, the following relation can be obtained by integration by parts:

$$\int_{\Omega}\left[\sigma_{ij,j} - \mathrm{Re}(u_j u_i)_{,j}\right]V_{ik}\,d\Omega =$$

$$\int_{\Gamma}\left[\sigma_{ij} - \mathrm{Re}\, u_j u_i\right] n_j V_{ik}\, d\Gamma - \int_{\Omega}\left[\sigma_{ij} - \mathrm{Re}\, u_j u_i\right] V_{ik,j}\, d\Omega \qquad (5.2.5)$$

in which n_j (j=1,2,3) are components of the unit outward normal to the boundary of the medium, and Γ is the boundary which will change as the medium changes.

A constitutive equation must be given for the fluid material considered. The relation of Newtonian fluid is given for the formulation:

$$\sigma_{ij} = -\mathrm{Re} p\delta_{ij} + u_{i,j} + u_{j,i} \qquad (5.2.6)$$

By substituting this equation into the second term on the right-hand side of equation (5.2.5), and after integration by parts, equation (5.2.2) becomes following form:

$$\int_{\Gamma}(u_i n_j V_{ik,j} + u_j n_i V_{ik,j})\, d\Gamma - \int_{\Gamma}(\tau_i - \mathrm{Re}\, u_j u_i n_j) V_{ik}\, d\Gamma =$$

$$\int_{\Omega}\left[u_i V_{ik,jj} + u_j V_{ik,ji} + \mathrm{Re}(p V_{ik,i} + f_i V_{ik} + u_j u_i V_{ik,j})\right] d\Omega \qquad (5.2.7)$$

in which τ_i (i=1,2,3) are the components of the surface traction which are equal to $\sigma_{ij}n_j$.

The weight functions for the incompressible continuity equation (5.1.3) are a group of vector functions since equation (5.1.3) is a scalar equation with three unknown velocity components

$$\int_{\Omega} u_{i,i} \Pi_k\, d\Omega = 0 \qquad (5.2.8)$$

Integration by parts yields

$$\int_{\Omega} u_{i,i} \Pi_k\, d\Omega = \int_{\Gamma} u_i n_i\, \Pi_k\, d\Gamma - \int_{\Omega} u_i\, \Pi_{k,i}\, d\Omega = 0 \qquad (5.2.9)$$

By adding this relation into equation (5.2.7), after rearrangement, yields

$$\int_\Gamma u_i n_j (V_{ik,j} + V_{jk,i} - Re\,\Pi_k \delta_{ij}) d\Gamma - \int_\Gamma (\tau_i - Re\,u_j u_i n_j) V_{ik} d\Gamma =$$

$$\int_\Omega Re\, p V_{ik,i} d\Omega + \int_\Omega u_i (V_{ik,jj} + V_{jk,ij} - Re\,\Pi_{k,j} \delta_{ij}) d\Omega$$

$$+ \int_\Omega Re(f_i V_{ik} + u_i u_j V_{ik,j})\, d\Omega \qquad (5.2.10)$$

The requirements for the weight function V_{ik} and P_k are clear now. They should result in the elimination of the first two body integrals in the right hand side and supply the weight functions to solve the unknowns. Both

$$V_{ik,jj} + V_{jk,ij} - Re\,\Pi_{k,j} \delta_{ij} = \delta_{ik} \delta(x - x') \qquad (5.2.11)$$

$$V_{ik,i} = 0 \qquad (5.2.12)$$

and

$$V_{i,jj} + V_{j,ij} - Re\,\Pi_{,j} \delta_{ij} + Re\,U_j V_{i,j} = 0 \qquad (5.2.13)$$

$$V_{i,i} = \delta(x - x') \qquad (5.2.14)$$

can satisfy the requirements. Equations (5.2.11) and (5.2.12) are similar to those in reference [90], but equations (5.2.13) and (5.2.14) are the weight functions which are degraded for solving the scalar unknown, pressure. $\delta(x-x')$ is the Dirac delta function for observation point x and source point x'. The functions V_{ik} are called fundamental tensor solutions as they imply the velocity components in i-direction at the point x when a source of unit strength is applied in k-direction at the point x'. The equations (5.2.13) and (5.2.14), however, indicate a fictitious velocity field in which V_i are the components at the point x under a source of unit strength acting at the point x'.

The body force components f_i are often those of gravitational loads in which case they can be expressed by a potential function as follow:

$$f_i = \Psi_{,i}; \quad \Psi = -g x'_3; \quad b = \begin{Bmatrix} 0 \\ 0 \\ -g \end{Bmatrix}; \quad \nabla^2 \Psi = 0 \qquad (5.2.15)$$

where g is the gravitational acceleration. This results in the transformation of the body force integral onto boundary:

$$\int_{\Omega} \mathrm{Re} f_i V_{ik}\, d\Omega = -\int_{\Gamma} \mathrm{Re} g x'_3\, V_{ik} n_i d\Gamma + \int_{\Omega} \mathrm{Re}\, g x'_3 V_{ik,i}\, d\Omega \qquad (5.2.16)$$

in which the last integral is zero due to (5.2.12) or $\mathrm{Re}gx_3$ due to (5.2.14).

Finally the integral representations both for the velocity components and the pressure are obtained:

$$u_k(x) = \int_{\Gamma} u_i \sigma^*_{ikj} n_j d\Gamma - \int_{\Gamma} (\tau_i - \mathrm{Re}\, u_j u_i n_j) u^*_{ik} d\Gamma + \int_{\Gamma} \mathrm{Re}\, g x'_z\, u^*_{ik} n_i d\Gamma$$

$$- \int_{\Omega} \mathrm{Re} u_i u_j u^*_{ik,j}\, d\Omega \qquad (5.2.17)$$

$$p(x) = \frac{1}{\mathrm{Re}}\left(\int_{\Gamma} u_i \left(\sigma^{**}_{ij} + \mathrm{Re}\, u_j u^{**}_i \right) n_j d\Gamma - \int_{\Gamma} \tau_i u^{**}_i d\Gamma \right)$$

$$- g x_z + \int_{\Gamma} g x'_z\, u^{**}_i n_i d\Gamma \qquad (5.2.18)$$

where x_z indicates the vertical distance from the zero gravitational surface, and σ^{**}_{ij} are defined in the same way as equations (5.2.6), correspondingly σ^*_{ikj} are defined as

$$\sigma^*_{ikj} = u^*_{ik,jj} + u^*_{jk,ij} - \mathrm{Re}\, p^*_{k,j} \delta_{ij} \qquad (5.2.19)$$

and an asterisk in the superscript means the solutions from equations (5.2.11) and (5.2.12) while two asterisks means the solutions from equations (5.2.13) and (5.2.14).

Since the integral equations of velocity components (5.2.17) are continuous and differentiable about the space coordinates x, the integral expressions of the strain rates can be worked out easily from the following derivatives of the velocity components:

$$u_{k,l} = \int_\Gamma u_i \sigma^*_{ikj,l} n_j d\Gamma - \int_\Gamma (\tau_i - Re\, u_j u_i n_j) u^*_{ik,l} d\Gamma + \int_\Gamma Re\, gx'_z\, u^*_{ik,l} n_i d\Gamma$$

$$- \int_\Omega Re\, u_i u_j u^*_{ik,jl}\, d\Omega \qquad (5.2.20)$$

This tensor expression together with (5.2.18) can be used to obtain the stress tensor by using (5.2.6).

It can be readily seen that if the convective terms are neglected, equations (5.2.17,18,20) are then reduced to the linear boundary integrals only, which gives a great deal of advantages in saving the computing resources.

5.3 Fundamental solutions

The derivation of the fundamental solutions for equations (5.2.11) and (5.2.12) was given in detail in reference [90]. The form of the fundamental solutions to these equations is well known, it is identical to those of incompressible elasticity. Hereafter the components of both velocity and stress are given as follows:

$$u^*_{ik} = \delta_{ik} \Delta\Phi - \Phi_{,ik} \qquad (5.3.1)$$

$$Re\, p^*_k = -\Delta\Phi_{,k} \qquad (5.3.2)$$

where Φ is given as the fundamental solution of the biharmonic equation

$$\nabla^4 \Phi = 0 \qquad (5.3.3)$$

The explicit form of the fundamental solutions for two-dimensions and three dimensions are given by the expressions:

$$\left.\begin{aligned} \Phi &= \frac{1}{8\pi} r^2 \ln r \qquad 2D \\ \Phi &= \frac{r}{4\pi} \qquad 3D \end{aligned}\right\} \qquad (5.3.4)$$

in which r is the distance from the observation point x to the source point x'.

Substituting Φ into equations (5.3.1) and (5.3.2), the following results can be obtained:
2D case:

$$u^*_{ik} = \frac{1}{8\pi}\{(2\ln r + 3)\delta_{ik} - 2r_{,i}r_{,k}\} \tag{5.3.5}$$

$$\sigma^*_{ik} = \sigma^*_{ikj}n_j = \frac{1}{\pi r}r_{,i}r_{,k}r_{,j}n_j \tag{5.3.6}$$

$$u^*_{ik,j} = \frac{1}{4\pi r}\left(2r_{,i}r_{,k}r_{,j} + \delta_{ik}r_{,j} - \delta_{ij}r_{,k} - \delta_{kj}r_{,i}\right) \tag{5.3.7}$$

$$\sigma^*_{ik,j} = \frac{1}{\pi r^2}\left[n_j r_{,i}r_{,k} + \left(\delta_{ij}r_{,k} + \delta_{kj}r_{,i} - 4r_{,i}r_{,j}r_{,k}\right)r_{,l}n_l\right] \tag{5.3.8}$$

3D case:

$$u^*_{ik} = \frac{1}{4\pi r}(\delta_{ik} - r_{,i}r_{,k}) \tag{5.3.9}$$

$$\sigma^*_{ik} = \frac{3}{2\pi r^2}r_{,i}r_{,k}r_{,j}n_j \tag{5.3.10}$$

$$u^*_{ik,j} = \frac{1}{4\pi r^2}(3r_{,i}r_{,k}r_{,j} + \delta_{ik}r_{,j} - \delta_{ij}r_{,k} - \delta_{kj}r_{,i}) \tag{5.3.11}$$

$$\sigma^*_{ik,j} = \frac{3}{2\pi r^3}\left[n_j r_{,i}r_{,k} + \left(\delta_{ij}r_{,k} + \delta_{kj}r_{,i} - 5r_{,i}r_{,j}r_{,k}\right)r_{,l}n_l\right] \tag{5.3.12}$$

The fundamental solutions of equations (5.2.13) and (5.2.14) can be easily obtained. Firstly, due to the fact that equation (5.2.13) can be rewritten as

$$(\sigma^{**}_{ij} + \mathrm{Re}u_j u^{**}_i)_{,j} = 0 \tag{5.3.13}$$

it can be found that $\sigma^{**}_{ij} + \mathrm{Re}u_j u^{**}_i$ is an arbitrary constant tensor which is enough for the first integral in equation (5.2.18). Secondly, the velocity potential can be assumed:

$$u_i^{**} = \Psi_{,i} \qquad (5.3.14)$$

Substituting this relation into equation (5.2.14) yields the equation for the function Ψ as follow:

$$\Delta\Psi = \delta(x-x') \qquad (5.3.15)$$

The fundamental solution of this equation is well known:

$$\left.\begin{aligned} \Psi &= \frac{1}{2\pi}\ln\left(\frac{1}{r}\right) \quad 2D \\ \Psi &= \frac{1}{4\pi r} \quad 3D \end{aligned}\right\} \qquad (5.3.16)$$

in which r is the distance from the observation point x to the source point x'.

Finally the fundamental solutions of equations (5.2.13-14) are written as the following expressions

$$\left.\begin{aligned} u_i^{**} &= -\frac{r_{,i}}{2\pi r};\ \sigma_{ij}^{**} + Re\, u_j u_i^{**} = 0 \quad 2D \\ u_i^{**} &= -\frac{r_{,i}}{4\pi r^2};\ \sigma_{ij}^{**} + Re\, u_j u_i^{**} = 0 \quad 3D \end{aligned}\right\} \qquad (5.3.17)$$

which leads the pressure equation (5.2.18) being much easier to solve.

5.4 Boundary points

When the observation point x is taken to the boundary, the integrals have a singularity. No matter what the boundary is like at x, one can always supplement it by a small spherical surface, such that the second integral of the right hand side in equation (5.2.17) is:

$$\lim_{\varepsilon\to 0}\left\{\int_{\Gamma_\varepsilon} \tau_i u_{ik}^* d\Gamma\right\} = \tau_i \lim_{\varepsilon\to 0}\left\{\int_{\Gamma_\varepsilon} u_{ik}^* d\Gamma\right\} \qquad (5.4.1)$$

Substituting any of the velocity fundamental solutions into the right hand side of this equation and making use of mid-value theorem, this integral goes to zero as ε approaches zero.

The first integral in equation (5.2.17) however behaves differently. One can see that the limit of the integral over a small spherical surface can be written as

$$\lim_{\varepsilon \to 0} \int_{\Gamma_\varepsilon} u_i \sigma^*_{ikj} n_j d\Gamma = u_i \lim_{\varepsilon \to 0} \int_{\Gamma_\varepsilon} \sigma^*_{ikj} n_j d\Gamma \qquad (5.4.2)$$

The term σ^*_{ikj} values are now of $1/\varepsilon^2$ order while the terms resulting from integration over the surface are of order ε^2. Hence the integral (5.4.2) does not vanish when ε goes to zero but produces a free term. It can be proved that:

$$\lim_{\varepsilon \to 0} \int_{\Gamma_\varepsilon} \sigma^*_{ikj} n_j d\Gamma = \delta_{ik}(1 - C) \qquad (5.4.3)$$

where C is the fraction of the local space occupied by the point, which is 1/2 for the smooth boundary, and 1 for any internal point. Consequently, a general tensor equation for both internal and boundary points is produced:

$$Cu_k(x) = \int_\Gamma u_i \sigma^*_{ikj} n_j d\Gamma - \int_\Gamma (\tau_i - Re\, u_j u_i n_j) u^*_{ik} d\Gamma + \int_\Gamma Re\, g x'_z u^*_{ik} n_i d\Gamma$$
$$- \int_\Omega Re\, u_i u_j u^*_{ik,j} d\Omega \qquad (5.4.4)$$

For equation (5.2.18), there is a different story for the boundary point. Since the boundary integral involved is only of the fictitious velocity, for two dimensional case, it becomes:

$$\lim_{\varepsilon \to 0} \left\{ \int_{\Gamma_\varepsilon} \tau_i u^{**}_i d\Gamma \right\} = \lim_{\varepsilon \to 0} \int_{\Gamma_\varepsilon} (Rep - u_{j,k} n_k n_j - u_{k,j} n_k n_j) \frac{d\Gamma}{2\pi r} \qquad (5.4.5)$$

The pressure and velocity derivative components can be expanded with their values in the centre of the circle:

$$p = p^{(0)} + \varepsilon\phi; \qquad u_{j,k} = u^{(0)}_{j,k} + \varepsilon\phi \tag{5.4.6}$$

They obviously approach their centre values when ε goes to zero. Due to the following fact for a half circle

$$\int_{\Gamma_\varepsilon} n_k n_j \frac{d\Gamma}{2\pi r} = \frac{\delta_{kj}}{2} \tag{5.4.7}$$

the limit becomes

$$\lim_{\varepsilon \to 0} \left\{ \int_{\Gamma_\varepsilon} \tau_i u_i^{**} d\Gamma \right\} = \frac{Re\, p^{(0)}}{2} + \left(u^{(0)}_{j,k} + u^{(0)}_{k,j} \right) \frac{\delta_{kj}}{2} = \frac{Re\, p^{(0)}}{2} \tag{5.4.8}$$

where the incompressible condition has been used.

The three dimensional case can be worked out in the same way, so that for both boundary and internal points equation (5.2.18) becomes:

$$Cp(x) = -\frac{1}{Re} \int_\Gamma \tau_i u_i^{**} d\Gamma - Cgx_z + \int_\Gamma gx'_z u_i^{**} n_i d\Gamma \tag{5.4.9}$$

Once the values of the traction and velocity components on the boundary have been worked out, the pressure, stresses and strain rates on the boundary can be easily calculated. Therefore the singularity which appeared in the above equation is not a problem at all. The details of the formulations are given in Appendix C.

5.5 Boundary Element Implementation

Although equations (5.4.4) and (5.4.9) are exact statements, boundary element approximations have to be used for most of the boundary value problems. The boundary discretisation process begins by subdividing the whole boundary into individual elements of simple shape. The geometry of

the boundary element and the variation of velocity and traction components on it are completely defined by the nodal values and associated shape function. They are expressed as follows:

$$x_i(\zeta) = N_w(\zeta)x_{iw};\ u_i(\zeta) = N_w(\zeta)u_{iw};\ \tau_i(\zeta) = N_w(\zeta)\tau_{iw} \qquad (5.5.1)$$

where ζ are the intrinsic coordinates, N_w shape functions, and x_{iw}, u_{iw}, and τ_{iw} the nodal values of coordinates, velocity and traction components, respectively.

Only the two dimensional case is considered hereafter, and the linear approximation is applied in which the shape functions are written as follows

$$N_1(\zeta) = \frac{1}{2}(1-\zeta);\ N_2(\zeta) = \frac{1}{2}(1+\zeta) \qquad (5.5.2)$$

For a creeping flow (and the body force is neglected), the resulting equations are written as follows:

$$Cu_k = \sum_{e=1}^{M}\left(u_{iw}\int_{\Gamma e} N_w\sigma^*_{ik}d\Gamma - \tau_{iw}\int_{\Gamma e} N_w u^*_{ik}d\Gamma\right) \qquad (5.5.3)$$

$$Cp = -\frac{1}{Re}\sum_{e=1}^{M}\tau_{iw}\int_{\Gamma} N_w u_i^{**}d\Gamma \qquad (5.5.4)$$

In fact, equations (5.5.3) form the only system to be implicitly solved, (5.5.4) can be used to solve the pressure explicitly after the values of the traction components on the boundary are worked out.

The boundary integration can be numerically calculated for all the elements by Gaussian formulae except the collocation elements in which the analytical integrations have to be employed. They are given as follows:

$$\left.\begin{aligned}\int_{-1}^{1} N_1(r)\left[\left(\ln r + \frac{3}{2}\right)\delta_{ik} - r_{,i}r_{,k}\right]dr &= R\left[\left(\ln R^2 - \frac{3}{2}\right)\delta_{ik} - R_iR_k\right]\\ \int_{-1}^{1} N_2(r)\left[\left(\ln r + \frac{3}{2}\right)\delta_{ik} - r_{,i}r_{,k}\right]dr &= R\left[\left(\ln R^2 - \frac{1}{2}\right)\delta_{ik} - R_iR_k\right]\end{aligned}\right\} \qquad (5.5.5)$$

For the steady viscous flow case, the domain has to be discretised into elements and an iteration scheme must be carried out. Thus, for any point within a domain triangular element both coordinates and values of the velocity components are defined as follows:

$$x_i(\zeta) = A_w(\zeta)x_{iw};\ u_i(\zeta) = A_w(\zeta)u_{iw} \qquad (5.5.6)$$

where A_w are the area coordinates.

From the fundamental solutions (5.3.7) it can be seen that the kernel functions for the domain integral have a singularity when r approaches zero. This singularity is the main error source when Hammer's formulae is used for the numerical integration. However, this error can be reduced significantly by introducing the following expressions.

At first a constant velocity field is introduced. It is obvious that the following integral is always zero: u^c_i

$$\int_\Omega u^*_{ik}(u^c_i u^c_j)_{,j}d\Omega = \int_\Gamma u^c_i u^c_j n_j u^*_{ik}d\Gamma - \int_\Omega u^c_i u^c_j u^*_{ik,j}d\Omega = 0 \qquad (5.5.7)$$

Subtracting equation (5.5.7) from equation (5.4.4) produces

$$Cu_k(x) = \int_\Gamma u_i\sigma^*_{ikj}n_j d\Gamma - \int_\Gamma \tau_i u^*_{ik}d\Gamma + \int_\Gamma Re(u_i u_j - u^c_i u^c_j)n_j u^*_{ik}d\Gamma$$
$$+ \int_\Gamma Re\, g x'_z\, u^*_{ik}n_i d\Gamma - \int_\Omega Re(u_i u_j - u^c_i u^c_j)u^*_{ik,j}\,d\Omega \qquad (5.5.8)$$

Equations (5.5.8) are used for iteration and the velocity components at the previous step can be chosen as u^c_i for each node. Therefore the error caused by the singularity is effectively reduced.

The flow chart of the implementation is introduced in Chapter Eight, and a general purposed code has been designed. In the following sections, several problems are solved by the applications of the boundary element method.

5.6 Particle Orientation Caused by Fountain Flow Effect

As mentioned in Chapter One, the orientation in polymers in injection moulding is caused by stretching and shearing forces, especially in the skins of the mouldings. These phenomena involve the flow kinematics in the transition region between the fully developed flow and the flow front. The characteristics of this region are that the flow elements near the centreline move faster but decelerate as they approach the free surface, and then move outwards towards the walls. Since the melt sticking on the wall soon solidifies, the melt near the wall is then stretched and sheared creating a highly oriented skin.

In a special visualisation study of the particle orientation, Schmidt[135-137] found that for a thin-walled moulding coloured particles introduced along the centreline come out at the surface in contact with the mould walls and in reverse order of the colours, and producing a series of "V" marks in the skin area as shown in Fig.5.6.1. In a finite element simulation, Mavridis *et al* [38,39] put some Lagrangian fluid elements in the central area of the flow field near the advancing front to investigate the deformation and orientation of them, and illustrated the phenomena of the elements splitting in the front and stretching along the walls which were caused by the fountain effect. The "V" shape marks formed in the skin area were illustrated as a "rolling-type" motion which occurred far behind the advancing front, and the turning over of the fluid elements was illustrated as the result of shear flow in the fully developed region.

The shortcomings of the conclusion obtained by using the finite element analysis cannot be easily detected. However, the turning over of the fluid elements cannot happen in the fully developed region because the vertical velocity component is virtually zero. Therefore it can be presumed that the "V" marks formed in the skin area are also a direct consequence of the fountain effect. The fluid elements used in Maviridis et al's work actually captured only a portion of the phenomenon.

It is obvious that the complex fountain flow includes the non-Newtonian and non-isothermal characteristics. If only viewing from the point of the general Navier-Stokes equations, there are the compressibility and the inertia terms. However, the fountain flow effects are influenced, but not determined, by these features. At first, the hydrodynamic phenomenon contributes to the essential characteristic of the fountain flow, so the Newtonian model of the constitutive equation can provide an overwhelming

a. Coloured particles orientation in finished part viewed from top.

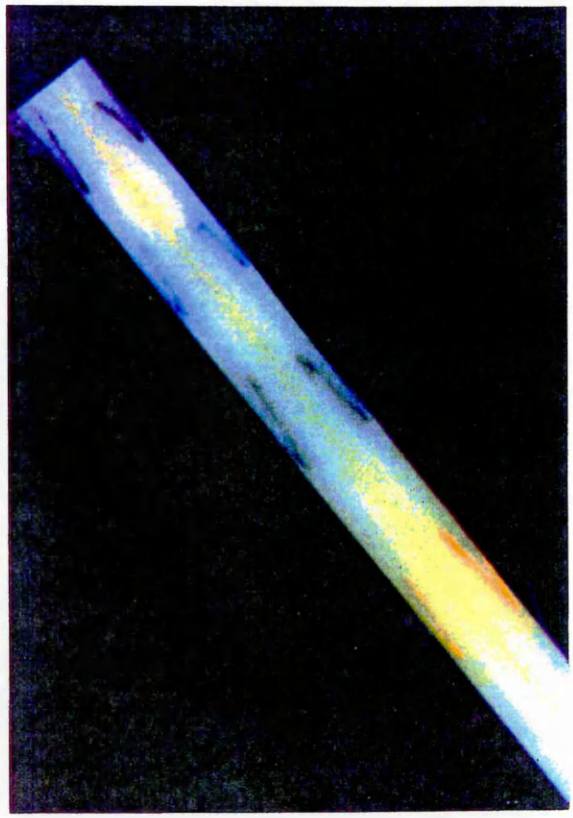

b. "V" marks of the coloured particles in finished part viewed transversely.

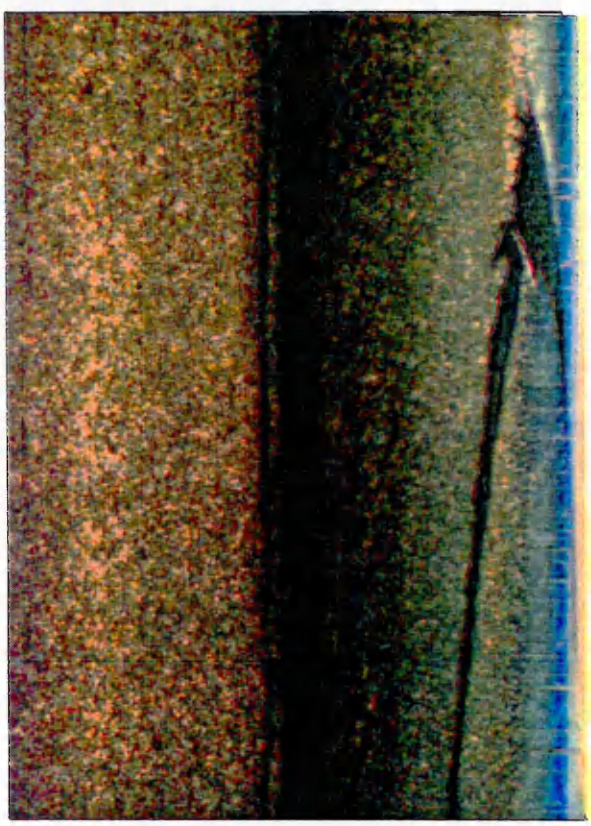

c. Enlargement of the green "V" mark.

d. Enlargement of the yellow "V" mark.

Fig.5.6.1 Schmidt's experimental result on particle orientation[140]. (Original colour pictures)

information of the effects. Secondly, there is almost no compressibility near the advancing front because of the low pressures involved; thirdly, if the coordinate system is moving at the same speed as it at the front tip, the flow becomes a steady-state problem. Also, most polymer flows are characterised as high viscosity, thus the inertia terms can be considered too small to be taken into account compared with other terms due to the low Reynolds number. Consequently, the creeping motion equations can be used for the approximation of the fountain flow. This gives a great advantage in fulfilling an idea of particle-in-domain since only the boundary integrals are involved in the integral equations, and the solution inside the domain of the flow field can have an unlimited analytical resolution.

The idea of particle-in-domain is similar to the idea of Particle-In-Cell (PIC) which was originally introduced by Harlow[68] for finite difference methods in early sixties. The later developments of the idea have evolved to some other methods[69] such as Marker-And-Cell (MAC)[37] methods which were also used in calculating the fountain flow and predicting the orientations[138,139]. The efficiency and accuracy of the boundary element method and the particle-in-domain idea used for this simulation are really tremendous, as once the boundary values are solved, the positions and velocities of the Lagrangian particles at any moment can be worked out explicitly by using the boundary values, thus much more detail of the fountain flow effects on the particle orientation can be given without using a large amount of computing resources.

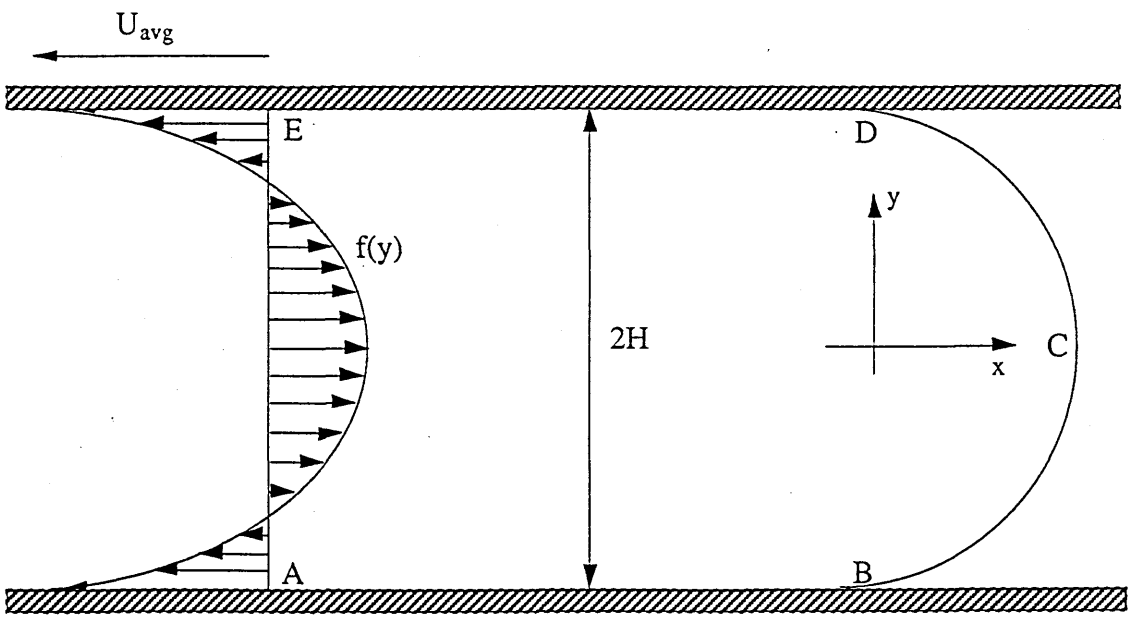

Fig.5.6.2. Fountain flow in a moving frame of reference

The problem is shown schematically in Fig.5.6.2. Referring to this diagram, the boundary condition on AE is the velocity distribution as follows:

$$U_x=f(y),\ U_y=0 \qquad (5.6.1)$$

in which the function f(y) is the solution for the fully developed Newtonian flow which is given in a form as

$$f(y)=\left(\frac{H^2P_x}{2}\right)\left[1-\left(\frac{y}{H}\right)^2\right]-U_{avg} \qquad (5.6.2)$$

in which H is half of the gap height, P_x the pressure gradient along the axial direction, U_{avg} the average velocity in the cross section (as a symbol, zero U_{avg} means the problem is defined in a fixed frame of reference).

The boundary conditions (AB and DE) on the walls are the velocity - U_{avg}, assuming that the walls moving backward in the reference frame; and on the free surface BCD the traction components vanish:

$$\sigma_{ij}n_j=\tau_i=0 \qquad (5.6.3)$$

where $\sigma_{ij}=-\delta_{ij}p+\eta[U_{i,j}+U_{j,i}]$.

The efficiency of the boundary element method can also be shown in the determination of the shape of the flow front, because only the boundary values are involved. The method of determining the free surface shape is, however, based on the fixed frame. By moving the front at its own speed, we can obtain the shape until the velocity on the central point C of the moving front equals the average velocity U_{avg}. The scheme is interpreted schematically in Fig.5.6.3. Some more boundary nodes are inserted automatically in the stretched free surface during the iteration for the sake of accuracy, therefore the number of the nodes is increased from 80 to 106 finally.

Fig.5.6.4 shows the velocity vector field in the moving frame of reference, from which it can be seen that the fluid particles in the centre area approaching the flow front, decelerating, spilling over and moving backwards in both the skin areas. If a constant velocity vector field U_{avg} is

superposed onto this vector field, the real velocity field can be yielded as shown in Fig.5.6.5.

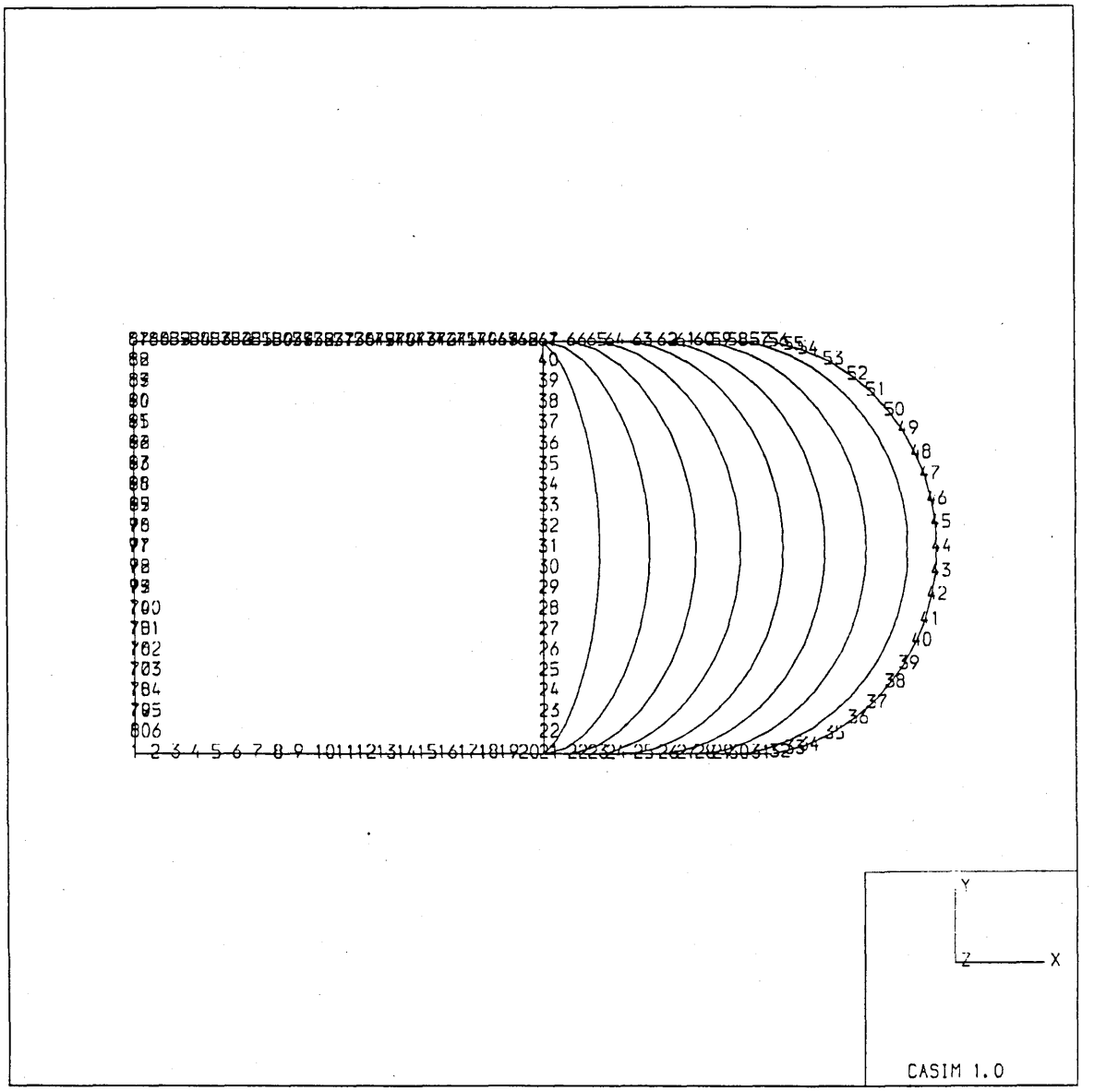

Fig.5.6.3 Moving the free surface to a stable shape.

However, both pictures cannot show exactly how the "V" marks are formed. Only through a tracer-in-domain technique can the phenomenon be illustrated. Therefore some tracers are put in the central area near the inlet boundary AE.

Most of the evolution of the particle orientation was very similar to that reported in reference[39] when the same size of the tracer area was given. However, the "rolling"-type motion which was indicated responsible for forming "V" shapes in [39] could never happen in the fully developed area

far behind the flow front. The tracers moving backward at slightly different speeds in the skin areas could be observed. The latter is undoubtedly the reason for the particles shearing and stretching in the skin areas. It could also be, presumably, the cause for the formation of "V" marks. It was this phenomenon that inspired the author to put some more tracers in the area farther off the centreline. The orientation history of the particles is shown in Fig.5.6.6.

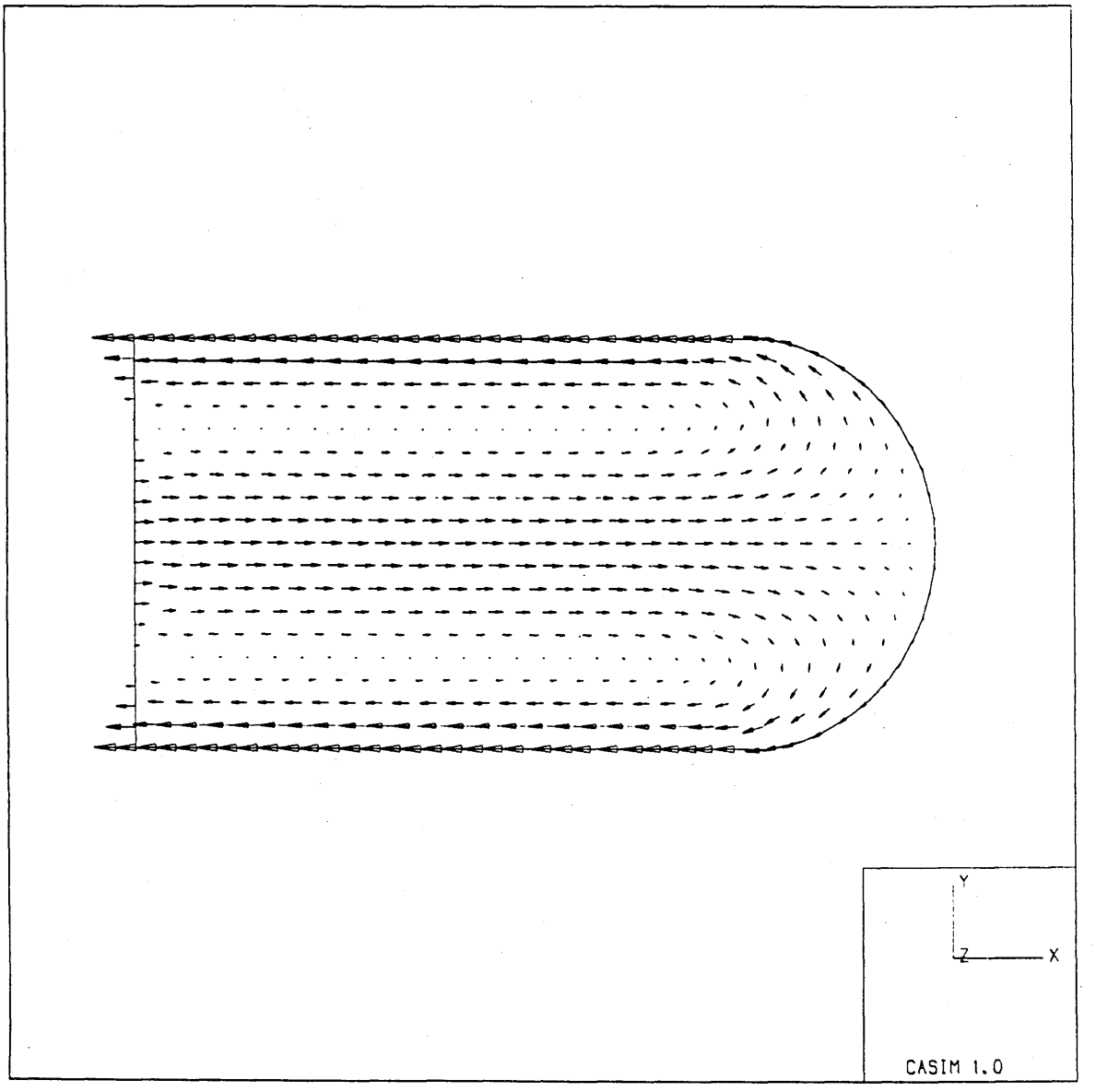

Fig.5.6.4 The velocity vector field in the moving frame of reference.

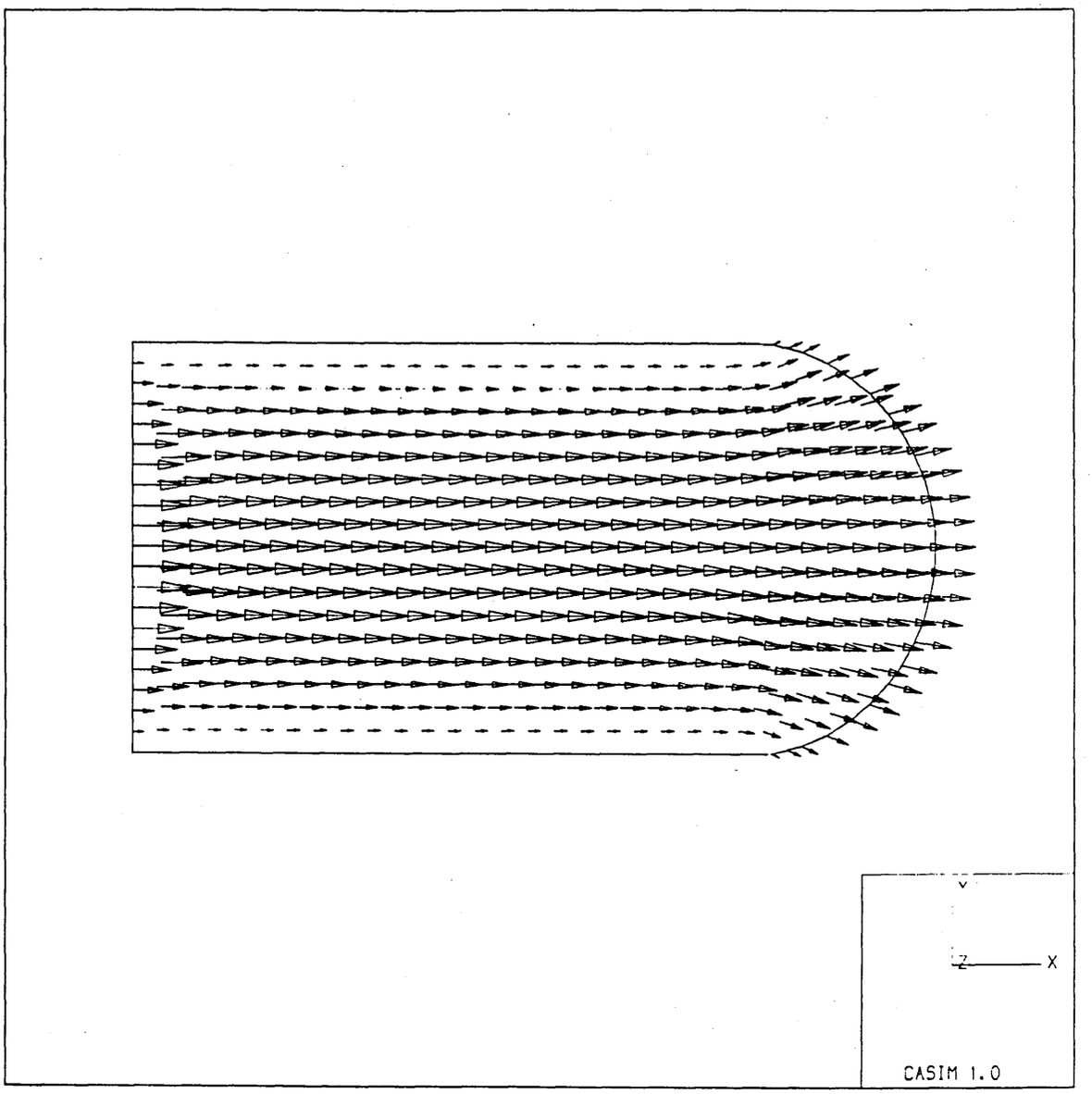

Fig.5.6.5 The velocity vector field in the fixed frame of reference.

It is just like some runners starting racing in rows in a track field, though those who are closer to the centreline run faster at first straight line period, they slow down and soon are left behind in the front area because of longer arc tracks. Those who are farther from the centreline run slowly all the time, therefore they are also left behind in spite of shorter arc tracks. Only those in the middle rows can gradually lead the race in the front area, and therefore the "V" marks are formed in the duration when all of them are turning around in the front area and running along the walls. This formation can be shown clearer if a closer look is taken at the tracers velocity pictures at individual moments.

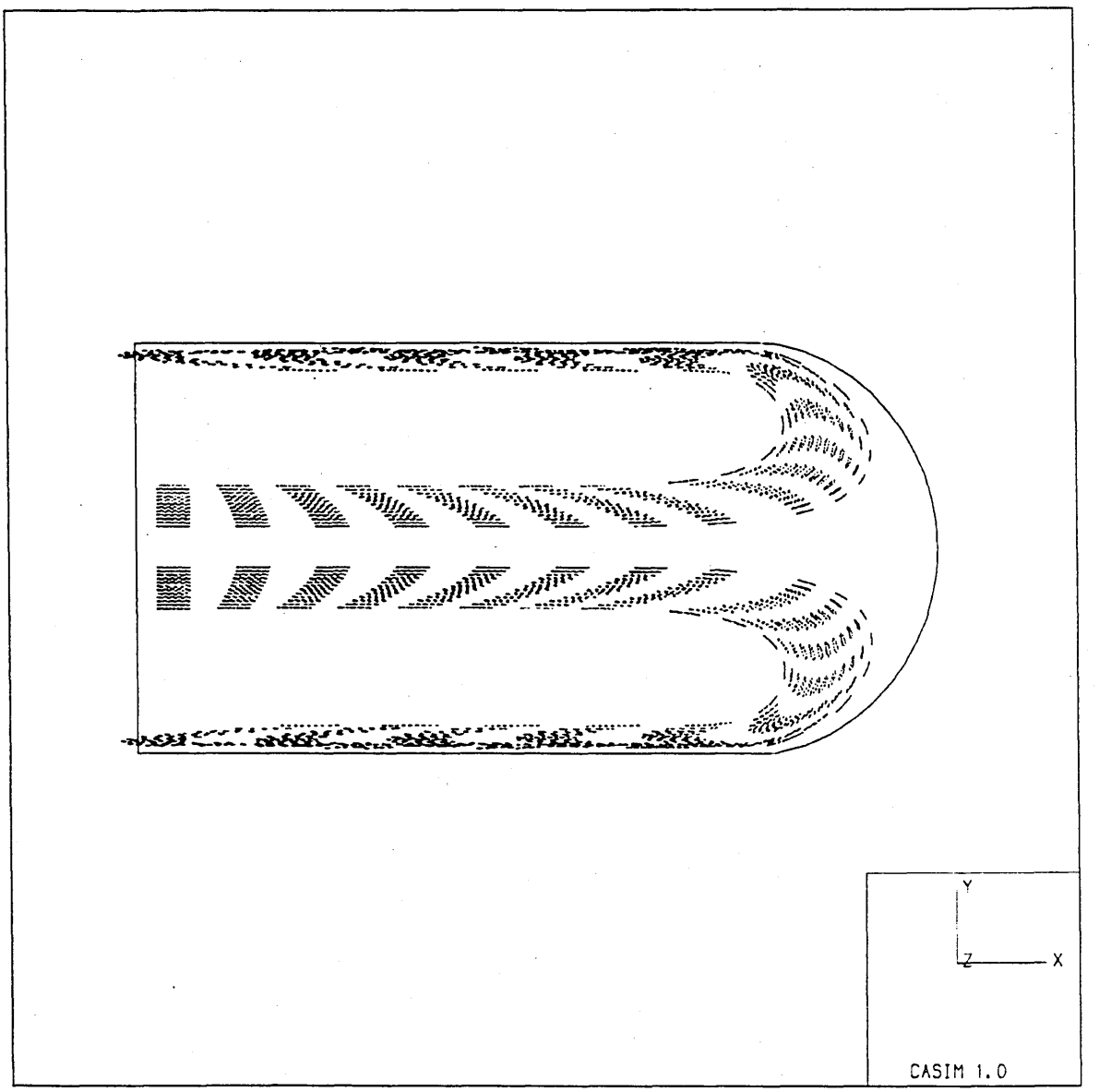

Fig.5.6.6 Orientation history of the particles in the moving frame of reference.
(In every two seconds from 0.-12., and 15.-33. seconds)

Fig.5.6.7-8 are the vector plots at 25 seconds and 29 seconds, respectively. From these pictures it can also be seen that the farther from the front, the sharper the "V" marks will be, and the longer they will be stretched. Clearly the phenomena are caused by the shearing effects in the skin areas which enhance the forming of the "V" marks. The temperature effect is responsible for freezing the "V" marks in the skin areas, and the frozen layer on the walls should start to form soon behind the flow front. In spite of this, the strong shearing force still exists all along the skin and

could stretch the softer half of the "V" shape longer. Although lack of this non-isothermal proof, the "V" shapes of the tracers presented here are closely in agreement with Schmidt's experiments.

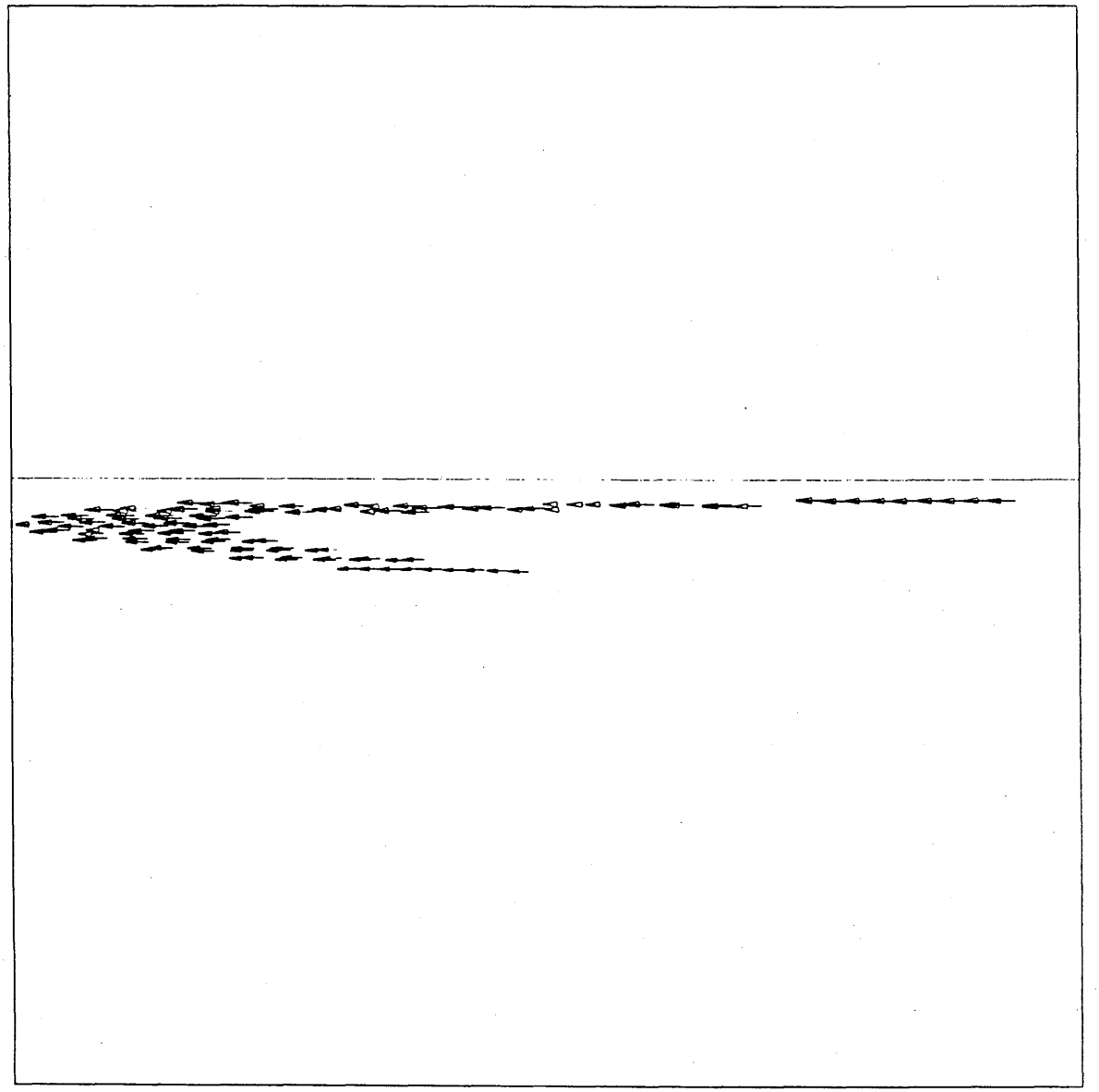

Fig.5.6.7. Enlargement of the tracer region at T=25 seconds

The tracers in a particular row can never exceed each other since they all have the same velocity history. After turning around in the flow front area, they still line up parallel to the wall surface but moving backward. This is the reason for the phenomenon of the tracers appearing in the skin in the opposite order to their entering in the gate.

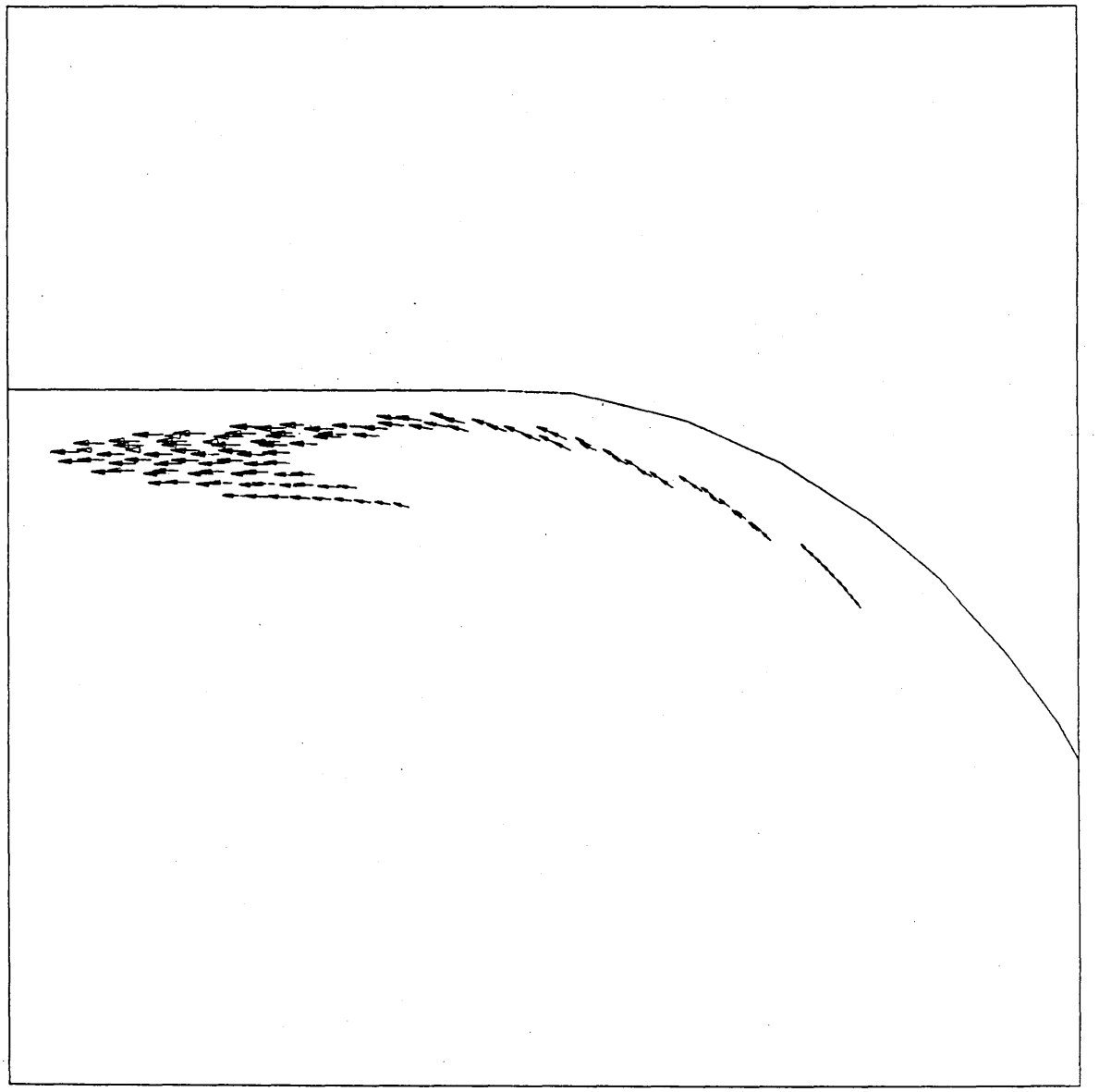

Fig.5.6.8. Enlargement of the tracer region at T=29 seconds

5.7 Fibre Orientation

The above application can be extended to fibre orientation in a creeping flow field. It is well known that short fibre-like particles are often added into a polymeric matrix to enhance the mechanical properties of the resulting composite material. The mechanical properties of the reinforced plastics are a strong function of the orientation of the fibres. This kind of reinforcement is mainly done by a injection moulding operation, therefore it is desirable to predict the orientation of the fibres through the computer

modelling based on hydrodynamic theory of suspensions of rigid in creeping flows.

The first study on a small ellipsoidal particle in a creeping flow was done by Jeffery[141], who extended Einstein's treatment for the case of spherical particles, and gave the expressions for the time dependence of the orientation of ellipsoids of revolution under the hydrodynamic torque resulting from fluid stresses. Since his investigation several other authors have given some developments on the suspensions which are reviewed in references [142,99]. The numerical methods for predicting the fibre orientation are mainly based on those which are used for fluid fields. Although finite difference (FD) and finite element methods (FE) are not limited in offering a quantitative analysis (e.g. reference [143]), they pose difficulties in performing the domain discretisation when the flow field needs updating. The boundary element methods are well suited to this class of problems. Examples can be found in recent applications to the similar problems[144-147].

The main concern here is the prediction of fibre orientation in an arbitrary plane flow in which the axis of symmetry of the fibres remains. It should not be difficult to extend the prediction of fibre orientation to three dimensional case since the equations obtained by Jeffery were for that case. In order to use Jeffery's equations we assume that the fibres are represented by a prolate spheroid with 2a as the length of the axis of revolution and 2b as the equatorial diameter. There are some other assumptions which were used in Jeffery's formulation: i) the non-linear convection terms are neglected (creeping motion); ii) no-slip between fibre-liquid interface; iii) apart from the disturbance produced in the immediate neighbourhood of the fibre, the flow is steady; iv) there is no interaction between fibres; v) the fibre is non-sedimentary and has its centre at a point in the fluid where its translational velocity is zero; vi) the distance between the fibre centre and the wall of the cavity is not appreciable compared to the fibre size.

Since the axis of revolution lies in the x-y plane, the orientation is fully characterised by the angle ϕ between its axis of symmetry and the x-axis as shown in Fig.5.7.1. This angle is governed by a differential equation reduced from Jeffery's equations in the following form[142]:

$$\frac{d\phi}{dt} = \omega + B\left[\gamma_{xy}\cos 2\phi - \frac{1}{2}(\gamma_{xx} - \gamma_{yy})\sin 2\phi\right] \qquad (5.7.1)$$

where γ_{xx}, γ_{xy}, γ_{yy} are the components of strain rate tensor, ω is the vorticity, i.e.

$$\gamma_{xx} = \frac{\partial u_x}{\partial x}, \gamma_{yy} = \frac{\partial u_y}{\partial y}, \gamma_{xy} = \frac{1}{2}\left(\frac{\partial u_y}{\partial x} + \frac{\partial u_x}{\partial y}\right), \omega = \frac{1}{2}\left(\frac{\partial u_y}{\partial x} - \frac{\partial u_x}{\partial y}\right) \tag{5.7.2}$$

and B is a scalar related to the aspect ratio of the fibre,

$$B = \frac{r_p^2 - 1}{r_p^2 + 1}, \quad r_p = \frac{a}{b} \tag{5.7.3}$$

from which it can be seen that the parameter B approaches asymptotically to one for a slender fibre.

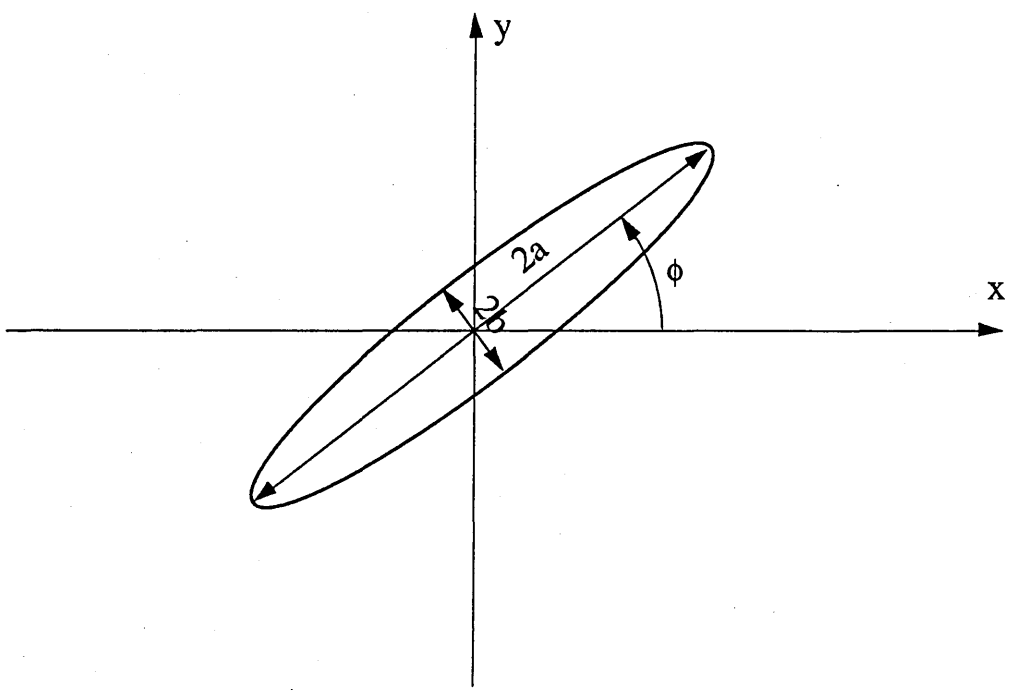

Fig.5.7.1 A fibre representation and its orientation angle in a reference frame.

As a simple test, consider the case of a uniform shear flow in the x-direction with a velocity gradient $\dot{\gamma}$. Equation (5.7.1) can be written in a much simpler way:

$$\frac{d\phi}{dt} = \frac{\dot{\gamma}}{2(r_p^2 + 1)}(r_p^2 \sin^2\phi + \cos^2\phi) \qquad (5.7.4)$$

With an initial condition $\phi=\phi_o$, one can obtain the solution[142,143]

$$\phi = -\tan^{-1}\left[\frac{1}{r_p}\tan\left(\frac{2\pi t}{T}\text{sign}(\dot{\gamma})\right) - \tan^{-1}(r_p \tan\phi_o)\right] \qquad (5.7.5)$$

where T is a period of rotation given by

$$T = \frac{2\pi}{|\dot{\gamma}|}\left(r_p + \frac{1}{r_p}\right) \qquad (5.7.6)$$

Fig.5.7.2 and 5.7.3 show the fibre orientation for two cases: r_p=1000 and r_p=3, respectively. For r_p=1000 case the fibre gradually aligns along the horizontal line and does not flip over within this limited length. In r_p=3 case, however, one can observe the flip-over of the fibres when they pass the half wave-length at each y position. The numerical prediction is fully in agreement with the theoretical result.

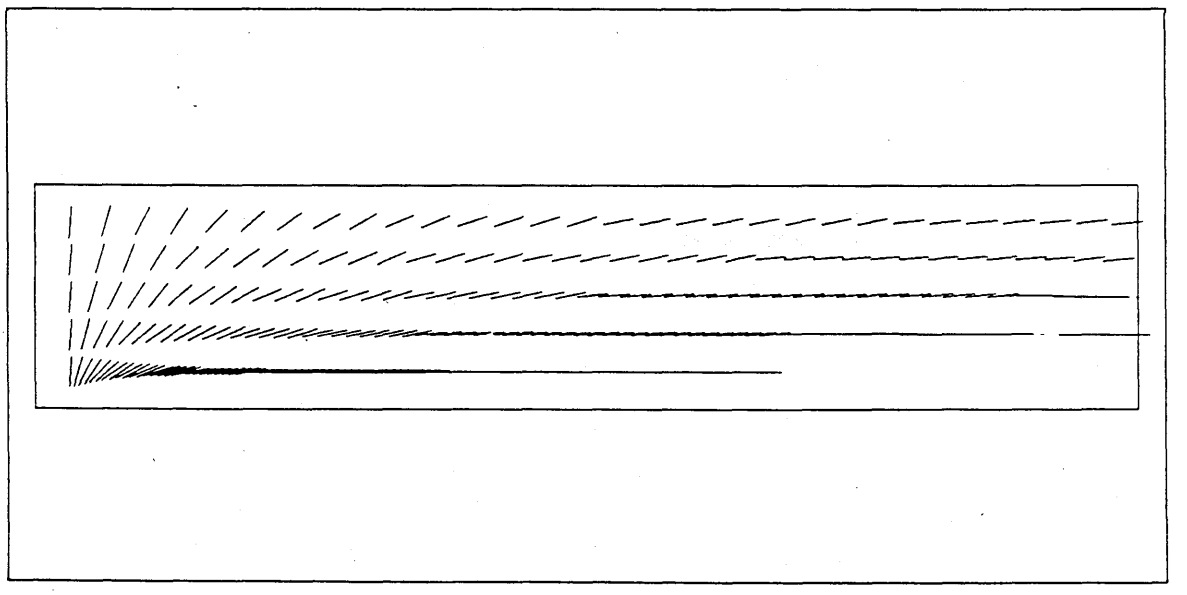

Fig.5.7.2. Fibre orientation in steady shear flow for r_p=1000.

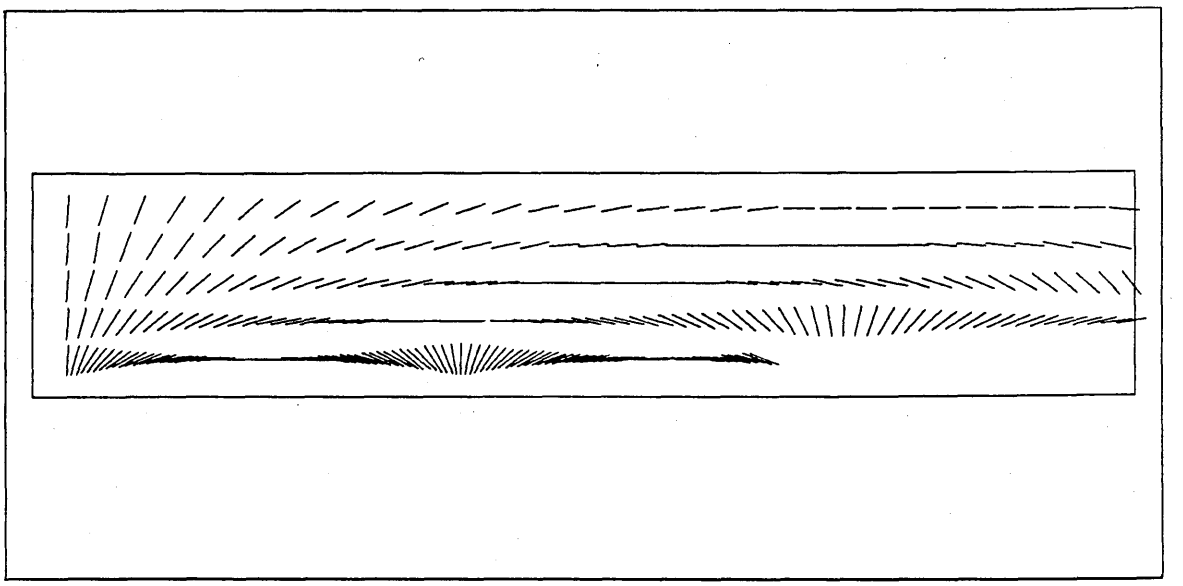

Fig.5.7.3. Fibre orientation in steady shear flow for r_p=3.

Let us consider the fibre orientation in a fountain flow which, as discussed in the last section, is of practical importance in injection moulding. The boundary conditions of the viscous flow field remain the same as those described in the last section but the field is slightly longer than that in the last section, and 118 boundary elements are employed in this calculation. Instead of dimensionless tracers, some fibre-like particles are put in the centre inlet area. At first, investigation is done for the motion of the slender fibres (r_p=1000) which are injected in the inlet area parallel to the flow direction there. In this case, it can be readily seen from equation (5.7.1) that the orientation angle remains zero in the fully developed flow region, because $\partial u_y/\partial x=0$ which results in $d\phi/dt=0$. In the fountain flow region, as shown in Fig.5.7.4, the fibres basically align along the flow directions.

It is remarkable to see that even though the initial orientation angle of the fibres is perpendicular to the flow direction as shown in Fig.5.7.5, the fibres gradually align along with the velocity vectors in the fully developed flow region both in the centre and near the wall. Although some fibres do not quickly flip over in the fountain flow region as they do in zero initial orientation angle case, all the fibres soon align up along the walls. Presumably, the fibres will be frozen up along the walls and the orientation will remain intact. Both zero and right initial orientation cases should cover all the other possible initial orientations. Fig.5.7.6 shows the history of the

fibre orientation starting from random orientations and reveals the history of the flip-over of each fibre by tracing them with labels.

From Fig.5.7.6 it can be seen that the fibres in the upper half flip over in counter-clockwise way while those in the lower half rotate clockwise. The farther from the centreline, the quicker they flip over.

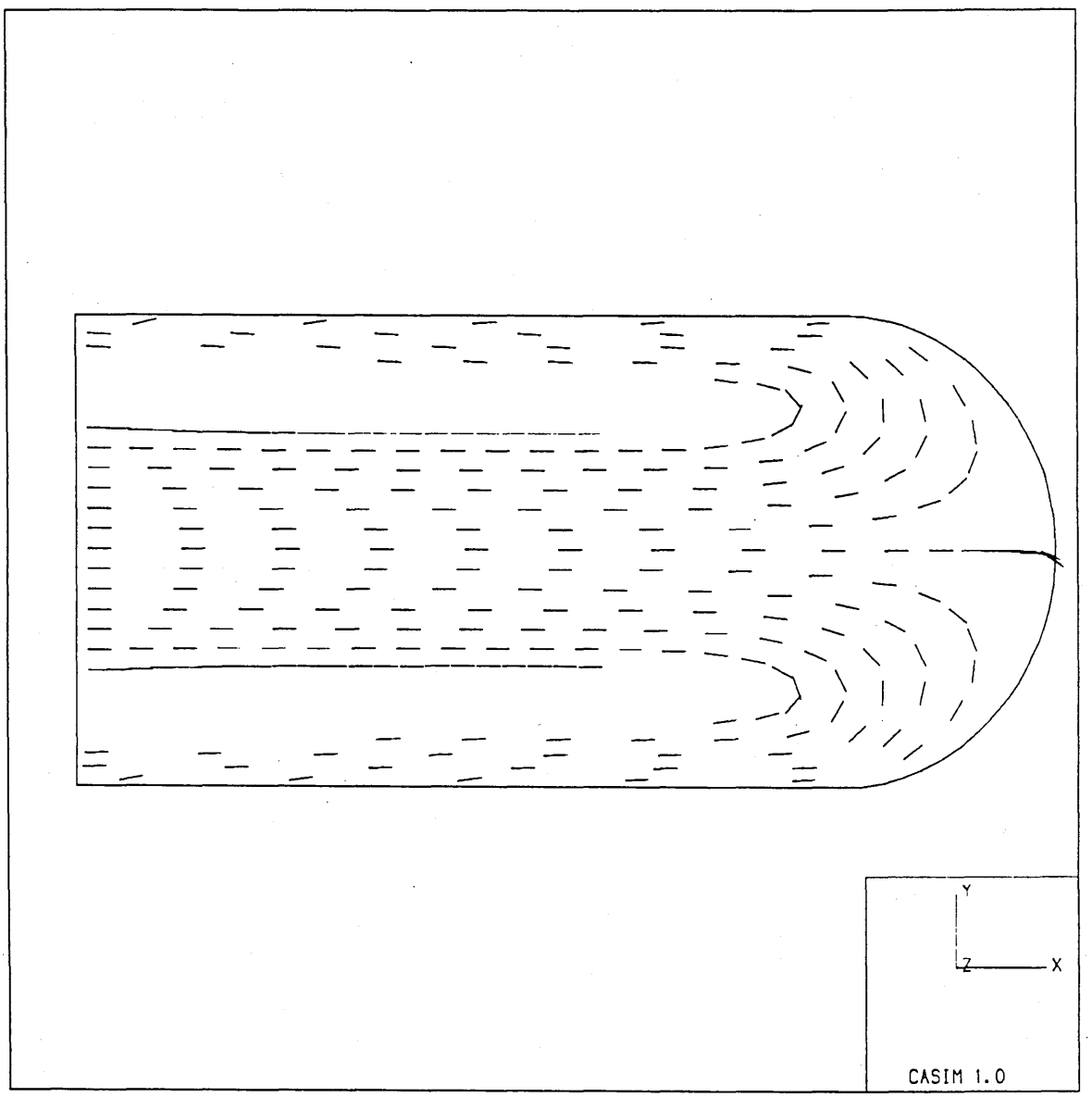

Fig.5.7.4 Fibre orientation resulting from fountain flow effects.
(r_p=1000, ϕ_o=0)

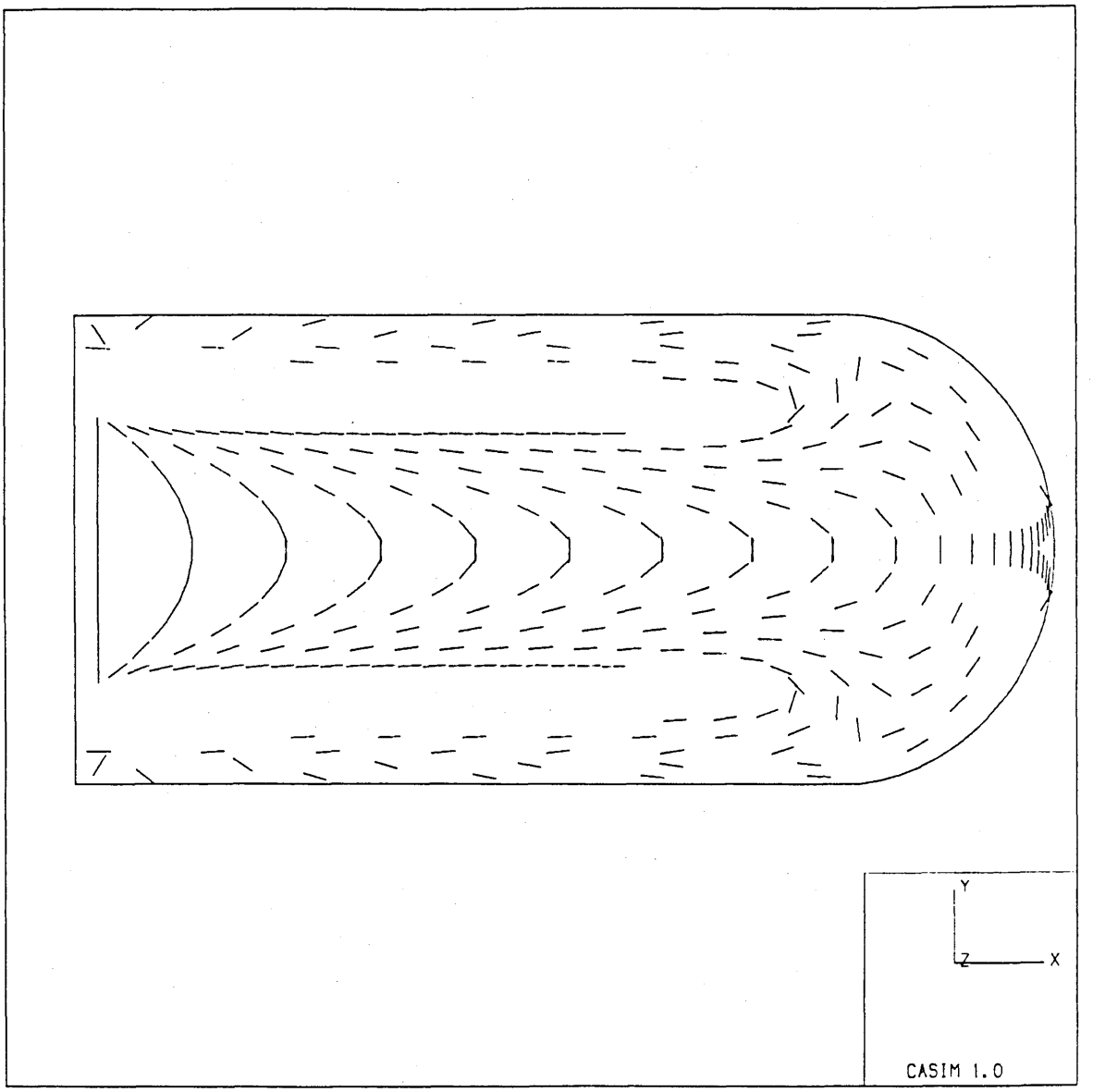

Fig.5.7.5. Fibre orientation history resulting from fountain flow effects. (r_p=1000, ϕ_o=π/2)

However, the exceptions can be readily seen in the area immediately behind the free surface. The reason for those in that area turning the other way around is because the velocity gradient about the direction perpendicular to the velocity direction alters from negative to positive in the upper half, and from positive to negative in the lower half. In order to confirm the phenomena, another simulation is done for the case that r_p=3, and ϕ_o=π/2 which history of fibre orientation is shown in Fig.5.7.7. If observed carefully there should be a curve representing a zero-gradient

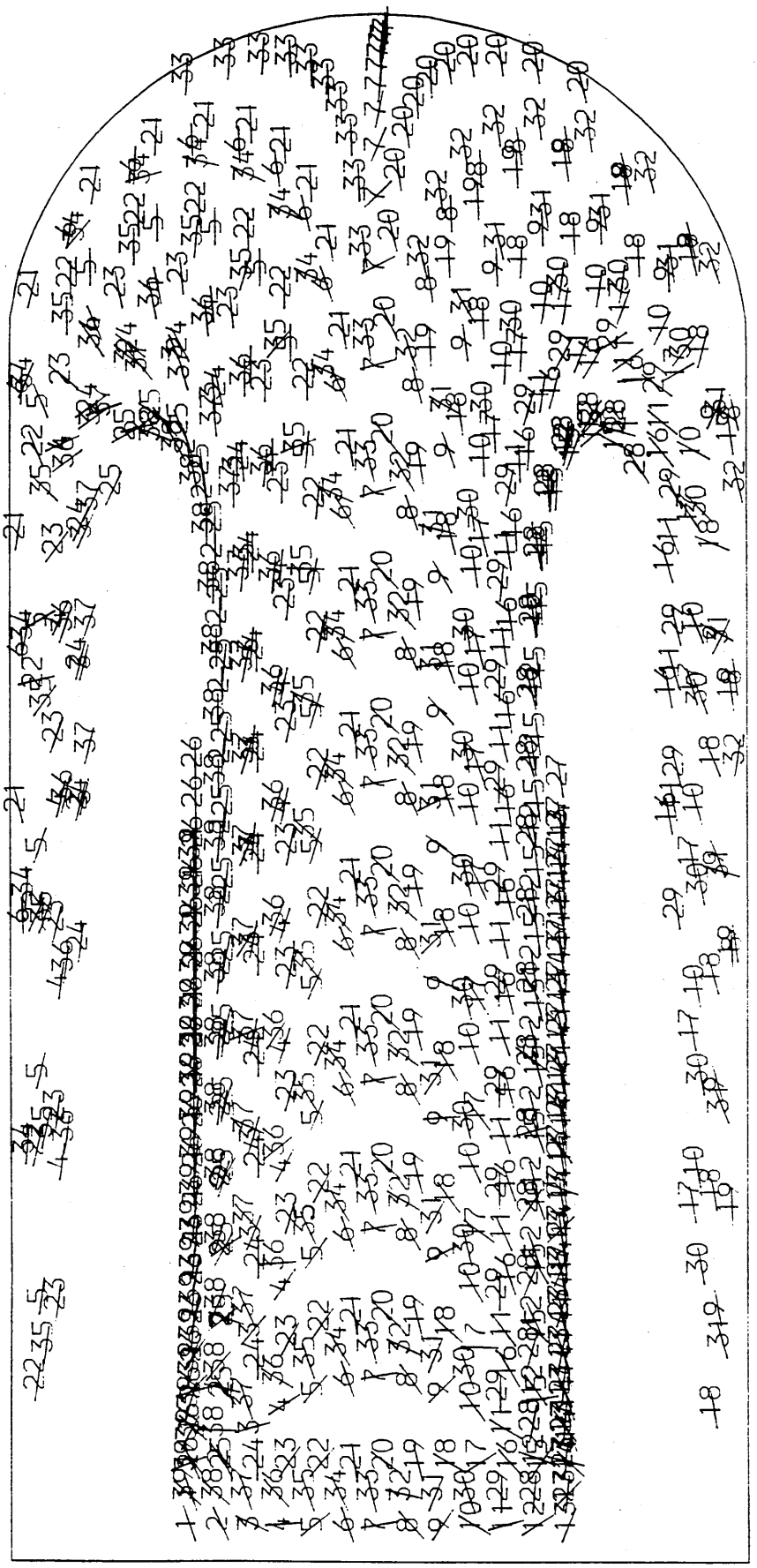

Fig.5.7.6. The history of the flip-over of the fibres.

(with respect to the perpendicular direction of the velocity) of the velocity, which goes along the centreline in the fully developed region and splits into two curves near the free surface. Referring to Fig.5.7.6 one is approximately between fibre 34 and fibre 6 in the upper half; the other is roughly between fibre 32 and 31 in the lower half, and both curves disappear at the ends of the free surface. The zero-gradient curves including other two are shown schematically in Fig.5.7.8. These phenomena clearly indicate that the periodic flip-over depends strongly on the velocity gradient perpendicular to the velocity, and the velocity itself. This is very similar to the flip-over period in the steady shear flow.

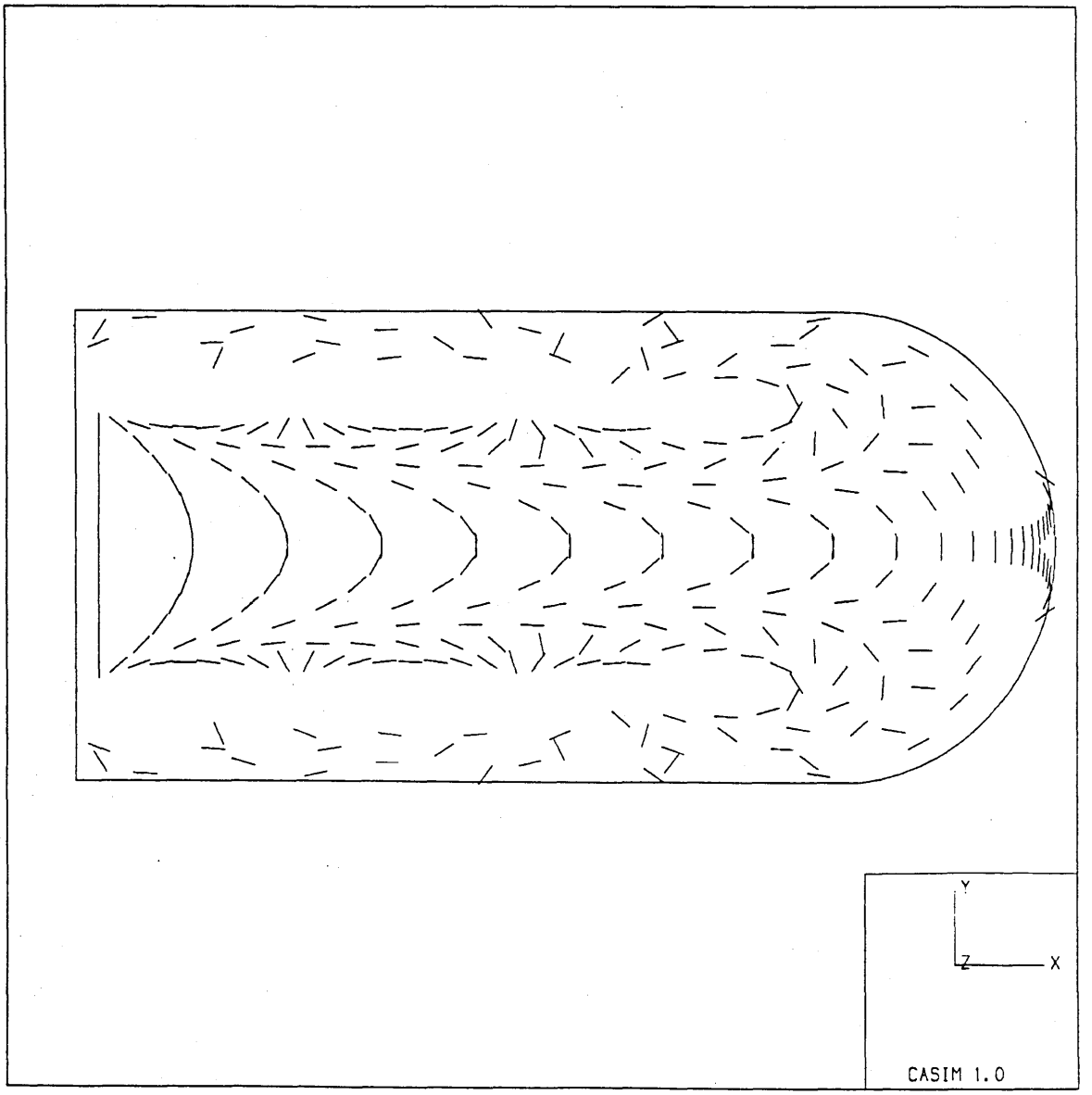

Fig.5.7.7 The history of the orientation of fibres (r_p=3, ϕ_o=π/2)

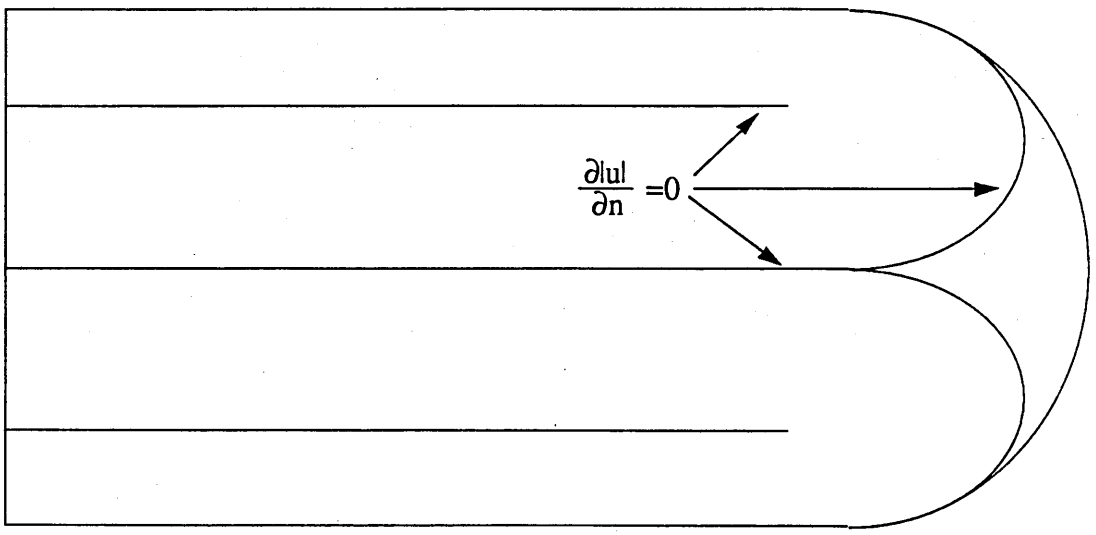

Fig.5.7.8. The zero-velocity-gradient curves. **n** is the normal vector of streamlines.

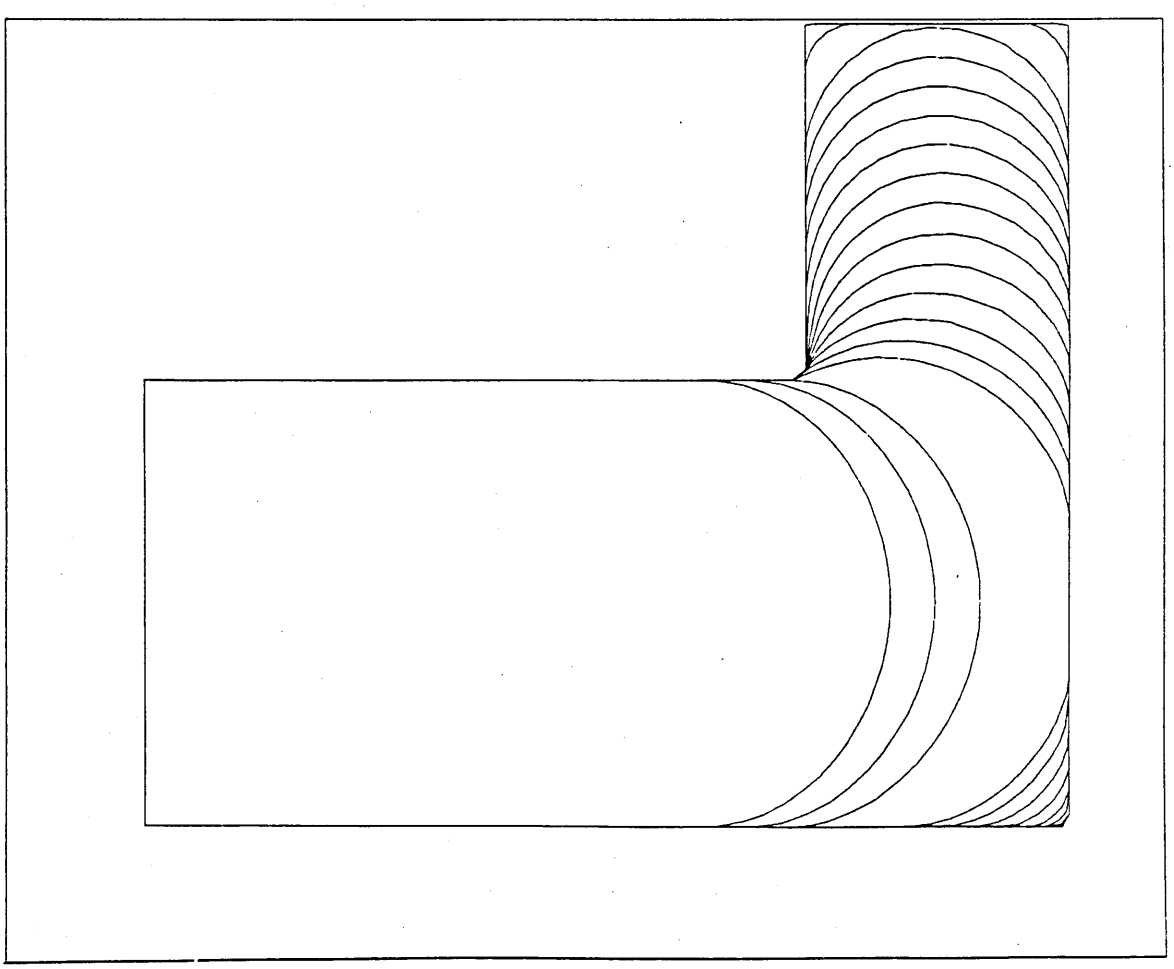

Fig.5.8.1. The history of the free surface in a L shape.

5.8 Modelling of Moving Free Surface

The applications can be further extended into determining the free surface positions viewed transversely. As is already described in section 5.6, the free surface is formed by moving the boundary nodes at their own speeds. If the free surface in the last two sections moves further in a rectangular cavity, it will hit the wall and squeeze into corner. If there is a rib standing in the end, the flow will turn around and move into the rib as shown in Fig. 5.8.1.

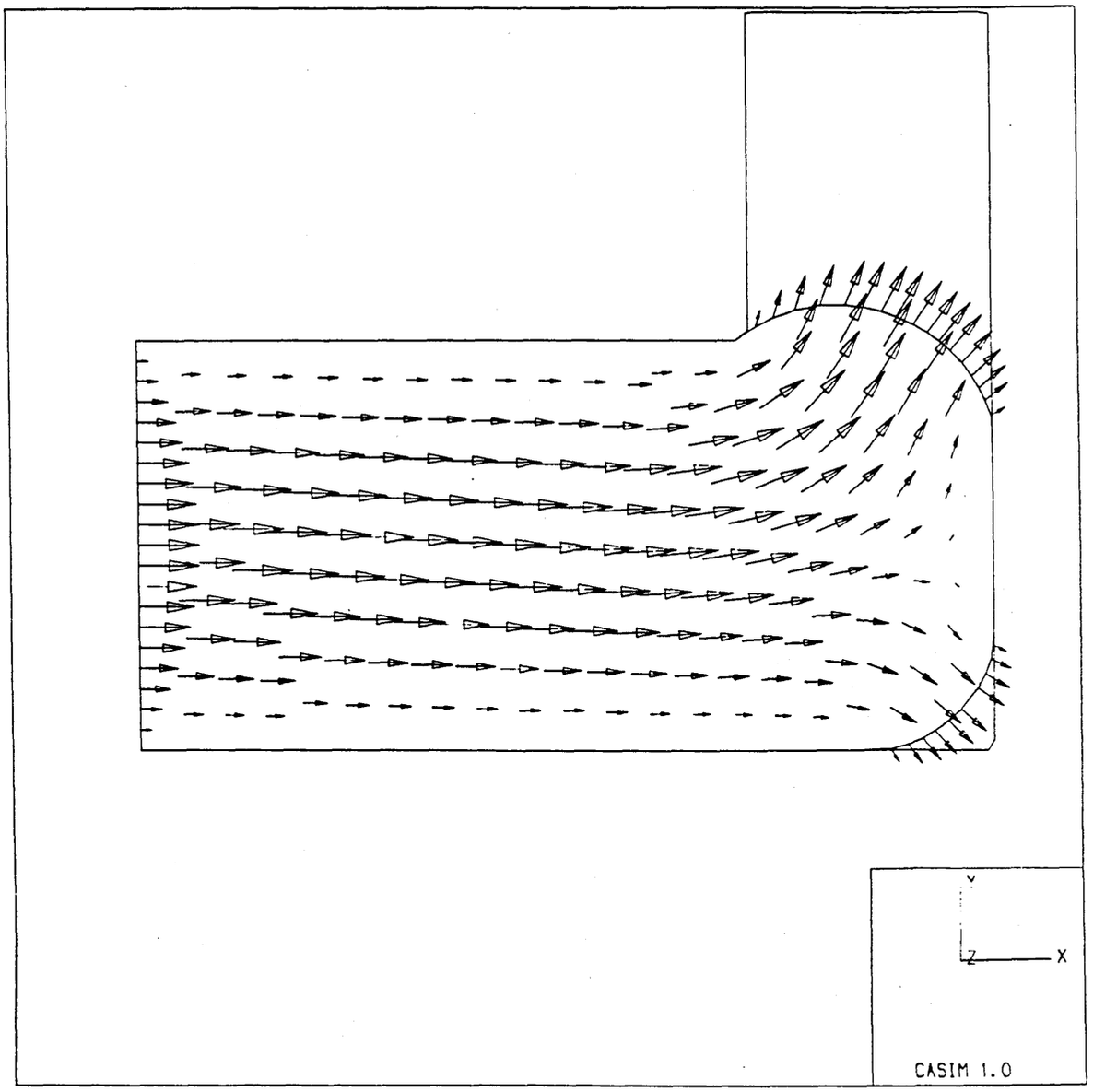

Fig.5.8.2. The velocity field at an intermediate moment of the free surface flow in an L shape.

At any moment of the progression of the free surface, the velocity and pressure field can be easily calculated. Fig.5.8.2-3 are the velocity and pressure fields at an intermediate moment. From the velocity field it can be clearly seen that the flow encountering the wall is forced to split into two streams: the smaller one is squeezing into the down-right corner getting its shorter front line; the other one is turning 90 degrees and getting longer free surface. The pressure distribution reflects the building-up of pressure in the front wall, and the pressure gradients in both free surfaces. Although there are still some problems to overcome for the pressure calculation in corners, the corners between the free surface and the solid wall are the real pressure singularities. To clearly give the pressure transitions in the areas,

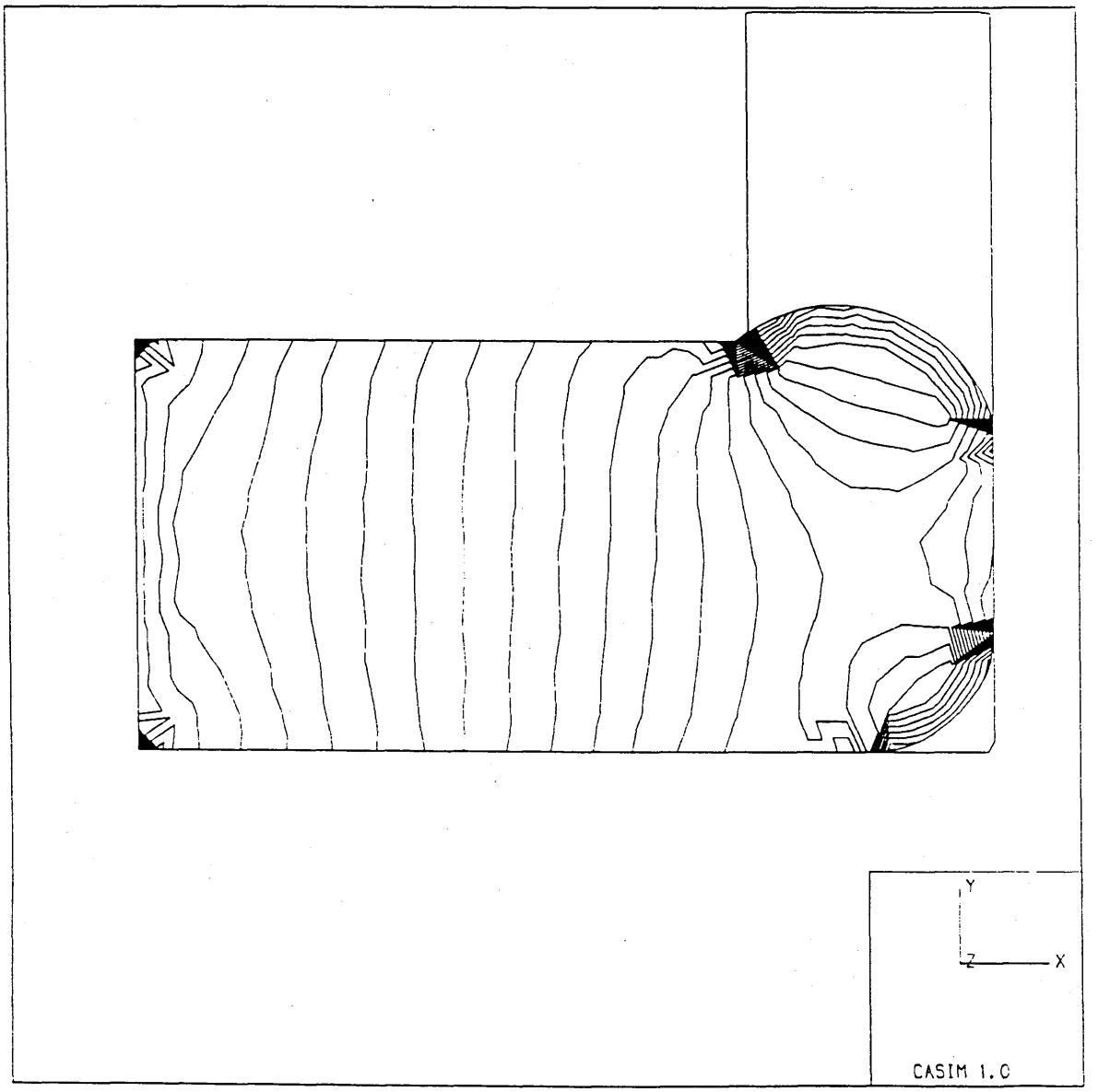

Fig.5.8.3. The pressure field at the moment.

special treatments have to be done. In theory, a boundary element method can give a better result than the one shown here. Thus the author hopes to work it out in near future. The last diagram is about the flow moving into two channels with different thicknesses. This is a purely hydrodynamic flow without any surface tension being taken into account. Even so the small front has obviously a different speed from the other one. This is because, as can be seen in the above pressure field, the pressure near the transition area of the short front restrains the flow stream stronger, and forces less liquid flow into the channel, while the other has more space to release the pressure around it.

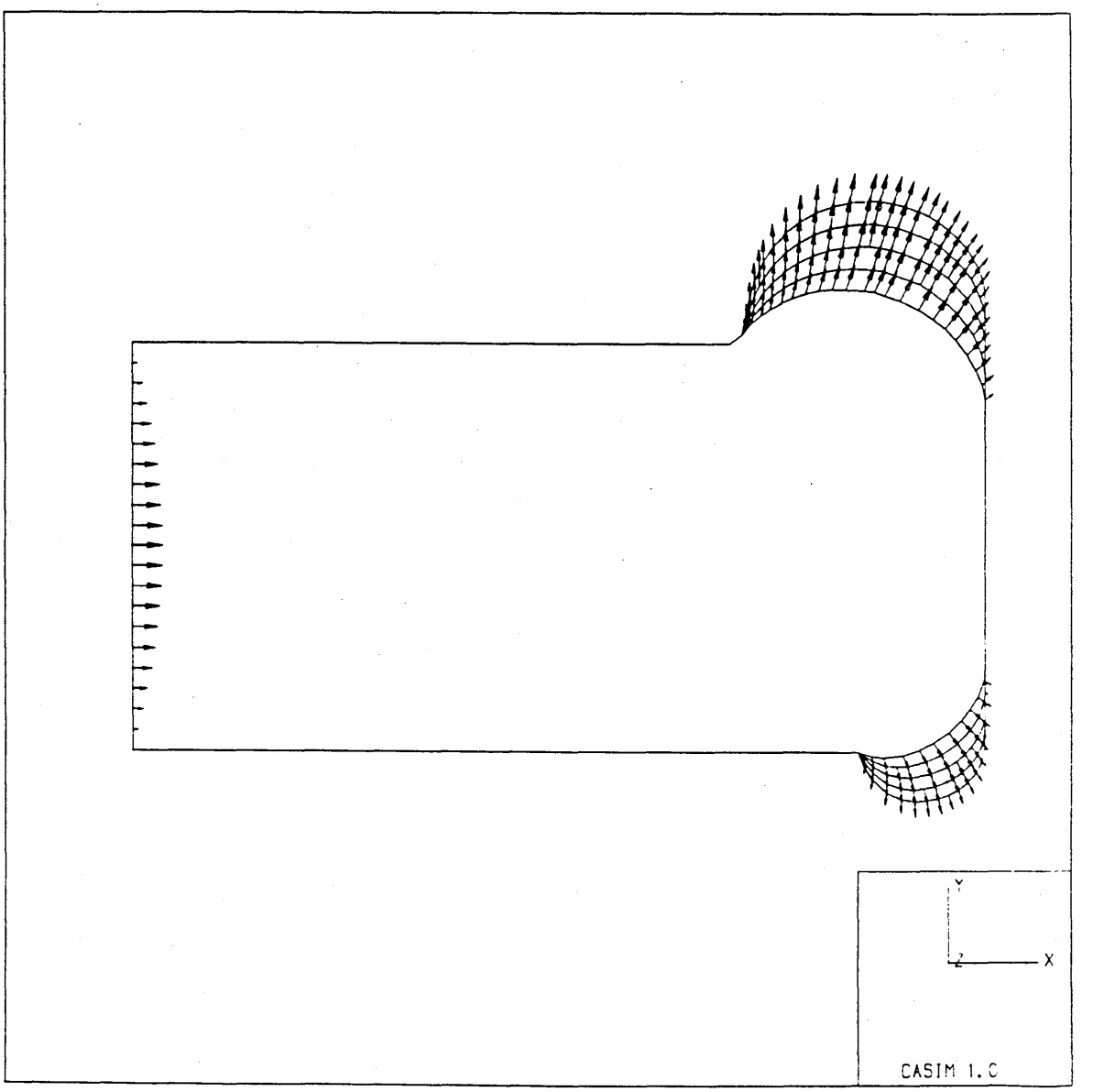

Fig.5.8.4. The history of the velocity of a free surface moving into two channels with different thickness.

5.9 Concluding Remarks

In this chapter the linear boundary element method for two dimensional steady viscous flows has been successfully implemented. The method is found accurate and effective especially in creeping motion type problems such as fountain flow effects on particle and fibre orientations, and determination of a free moving surface.

Although the creeping motion model is somehow not perfect, the applications in this chapter suggest a greater potential for more general problems. One naturally would consider that it would be much better to extend the method to non-Newtonian fluid problems, at least for generalised Newtonian models. A second useful extension is for the transient problems. Ultimately it is ideal if the model can be extended to compressible equations, then the packing stage can be simulated. In the next chapter, the transient viscous flow is being solved by a newly developed boundary element method described in Lagrangian form.

Chapter Six

BEM for Unsteady Viscous Flow

6.1 Introduction

For more accurate and more general simulation of the polymeric flow, unsteady viscous flow should be considered. For the filling stage of the injection moulding process, the flow front, or the free surface, is actually time-dependent. Traditionally, this type of problem is treated by a finite difference or finite element method. The unsteady viscous flow problems with free surface modelled by a boundary element method has not appeared due to the difficulties in handling non-linearity, time-dependence and in constructing of the fundamental solutions for the corresponding non-linear Navier-Stokes equations.

In this chapter, the Lagrangian approach is used to establish the boundary integral equation model for unsteady viscous flow and two numerical examples are given for demonstrating the effectiveness.

6.2 Governing Equations and Oseenlet

The governing equations for unsteady viscous flow can be described by the conservation equations, and constitutive equations as mentioned in previous chapters. For incompressible Newtonian fluid, the equation of continuity and Newtonian constitutive equation remain unchanged:

$$u_{i,i} = 0 \tag{6.2.1}$$

$$\sigma_{ij} = -\mathrm{Re}\,P\delta_{ij} + u_{i,j} + u_{j,i} \tag{6.2.2}$$

The difference from steady flow is the inertia force involved:

$$\sigma_{ij,j} - \mathrm{Re}\frac{Du_i}{Dt} + b_i = 0 \tag{6.2.3}$$

in which the second term is the "substantial derivative" of the mass flow.

Equations (6.2.1)-(6.2.3) together with a proper description of initial and boundary conditions comprise a complete system for unsteady viscous flow problems. The initial conditions are of the types shown below:

$$\left.\begin{aligned} u_i &= u_i^0(x) \quad \text{or} \\ \sigma_{ij} &= \sigma_{ij}^0(x) \end{aligned}\right\} \tag{6.2.4}$$

The boundary conditions on the medium boundary Γ are of the types:

$$\left.\begin{aligned} u_i(x,t) &= \bar{u}_i(x,t) \quad \Gamma_1 \\ \tau_i(x,t) &= \bar{\tau}_i(x,t) \quad \Gamma_2 \end{aligned}\right\} \tag{6.2.5}$$

where $\Gamma_1+\Gamma_2 = \Gamma$.

It is well known that the analytic solution of this system is impossible except for a few of the simplest cases. It is possible, however, to construct an analytic solution in an unbounded time-spatial region for a similar system called *unsteady creeping equations*. The basic feature of this system is that the convection terms do not exist. Therefore it is a linearised Navier-Stokes system. The solutions of the system are known as Oseenlet that were presented in Oseen's monograph[84]. Oseen did not give the details of the derivation of the solutions in his book. For reasons of completion and later developments of the integral equation method, the derivations have been done in this thesis by resorting the Hörmander's operator matrix method[148]. The details of the re-derivation are given in Appendix D.

The velocity and stress components of the fundamental tensor solutions can be written as follows:

$$u_{ik}^* = \delta_{ik}\Phi_{,jj} - \Phi_{,ik} \tag{6.2.6}$$

$$\sigma_{ikj}^* = \delta_{ik}\Delta\Phi_{,j} + \delta_{jk}\Delta\Phi_{,i} + \delta_{ij}\Delta\Phi_{,k} - 2\Phi_{,ikj} - \mathrm{Re}\,\delta_{ij}\frac{\partial}{\partial t}\Phi_{,k} \tag{6.2.7}$$

and Φ is the fundamental solution of the equation

$$\left(\mathrm{Re}\frac{\partial}{\partial t} - \Delta\right)\Delta\Phi = \delta(x-x')\delta(t-t') \tag{6.2.8}$$

6.3. Integral Formulation in Lagrangian Description

Based the fundamental solutions of the unsteady creeping motion equations, a group of integral equations can be established for replacing the original Navier-Stokes equations. The Green's function technique can be applied to such an approach, and forms the basis for Oseen's classic book on low Reynolds number hydrodynamics. However, if the formulation is done in a Lagrangian description, the coordinate system must be crucial. The above equations are all derived in a Cartesian coordinate system. Thus if the equations are defined in a time dependent deformable coordinate system, the deformation in time t-t' must be small enough to keep the coordinate perpendicularity. In such a coordinate system, both groups of equations can be rewritten as followings:

$$\left.\begin{aligned} \mathrm{Re}\frac{\partial u^*_{ik}}{\partial t'} &= -\sigma^*_{ikj,j} + \delta_{ik}\delta(x-x')\delta(t-t') \\ \mathrm{Re}\frac{\partial u_i}{\partial t'} &+ \mathrm{Re}(u_j - w_j)u_{i,j} = \sigma_{ij,j};\quad x' \in \Omega(t');\quad t' \geq 0 \end{aligned}\right\} \qquad (6.3.1)$$

where w_j are the velocity components of the deformable reference system, and the left hand side of the second groups are the expansion of the substantial derivative. From equation (6.3.1) following expression can be easily derived

$$\mathrm{Re}\frac{\partial(u^*_{ik}u_i)}{\partial t'} = \mathrm{Re}\left(u^*_{ik}\frac{\partial u_i}{\partial t'} + u_i\frac{\partial u^*_{ik}}{\partial t'}\right)$$

$$= u^*_{ik}\left[\sigma_{ij,j} - \mathrm{Re}(u_j - w_j)u_{i,j}\right] - u_i\sigma^*_{ikj,j} + u_i\delta_{ik}\delta(x-x')\delta(t-t') \qquad (6.3.2)$$

Integrating both sides of this equality over the time-spatial region $\Omega(t')\times(t_o,t_1)$, where $\Omega(t')$ is the space which the medium occupies at time t', and $t_o \leq t' \leq t_1$, $t_1 = t+\varepsilon$ ($\varepsilon > 0$), produces

$$\mathrm{Re}\int_{t_o}^{t_1}\int_{\Omega(t')}\frac{\partial(u^*_{ik}u_i)}{\partial t'}\,d\Omega dt' = \int_{t_o}^{t_1}\int_{\Omega(t')} u_i\delta_{ik}\delta(x-x')\delta(t-t')\,d\Omega dt' +$$

$$\int_{t_o}^{t_1}\int_{\Omega(t')}\left\{u^*_{ik}\left[\sigma_{ij,j}-\mathrm{Re}\left(u_j-w_j\right)u_{i,j}\right]-u_i\sigma^*_{ikj,j}\right\}d\Omega dt' \qquad (6.3.3)$$

Because the reference system deforms with time, the left hand side of this equation can be expanded as follow:

$$\int_{t_o}^{t_1}\int_{\Omega(t')}\frac{\partial(u^*_{ik}u_i)}{\partial t'}d\Omega dt'=\int_{t_o}^{t_1}\left(\frac{d}{dt'}\int_{\Omega(t')}u^*_{ik}u_i\,d\Omega-\int_{\Gamma(t')}w_jn_ju^*_{ik}u_i\,d\Gamma\right)dt' \qquad (6.3.4)$$

where w_j is the velocity components of the moving boundary and n_j is the unit outward vector normal to the boundary. The first integral in the right hand side of this expression can be further integrated

$$\int_{t_o}^{t_1}\frac{d}{dt'}\int_{\Omega(t')}u^*_{ik}u_i\,d\Omega\,dt'=\int_{\Omega(t')}u^*_{ik}u_i\,d\Omega\Big|_{t'=t_1}-\int_{\Omega(t')}u^*_{ik}u_i\,d\Omega\Big|_{t'=t_o} \qquad (6.3.5)$$

in which the first integral disappears because u^*_{ik} is zero when $t_1 > t$.

Following the property of delta functions, the first integral of the right hand side of equation (6.3.3) becomes $u_k(x,t)$. The first and third terms of the second integration can yield boundary integrals after integrations by parts twice, which procedures are the same as explained for steady viscous flow in Chapter Five:

$$\int_{t_o}^{t_1}\int_{\Omega(t')}\left(u^*_{ik}\sigma_{ij,j}-u_i\sigma^*_{ikj,j}\right)d\Omega\,dt'=\int_{t_o}^{t_1}\int_{\Gamma(t')}(u^*_{ik}\sigma_i-u_i\sigma^*_{ik})d\Gamma\,dt'$$

$$-\int_{t_o}^{t_1}\int_{\Omega(t')}\left[\mathrm{Re}\,Pu^*_{ik,i}+u_i(u^*_{ik,jj}+u^*_{jk,ij}-\mathrm{Re}\,P^*_{k,j}\delta_{ij}-\sigma^*_{ikj,j})\right]d\Omega\,dt' \qquad (6.3.6)$$

According to equations (6.2.6-7), the last integral is zero. Assembling all the results from (6.3.4-6), the integral equations can now be rewritten as:

$$u_k(x,t)=\int_{t_o}^{t}\left[\int_{\Gamma(t')}(u_i\sigma^*_{ik}-u^*_{ik}\sigma_i)d\Gamma+\mathrm{Re}\int_{\Omega(t')}u^*_{ik}(u_j-w_j)u_{i,j}d\Omega\right]dt'$$

$$-\mathrm{Re}\left[\int_{t_o}^{t}\int_{\Gamma(t')}w_jn_ju^*_{ik}u_i\,d\Gamma\,dt'+\int_{\Omega(t_o)}u^*_{ik}u_i\Big|_{t_o}d\Omega\right] \qquad (6.3.7)$$

It can be readily seen that the second domain integral can be eliminated if $w_j=u_j$. This is to say that the reference system is the Lagrangian one which is fixed on the deforming and moving medium. The coordinates of the reference system, when viewed as functions of particles and time, are expressed as the displacement functions $x_i=x_i(x_{0i},t_0,t)$, where x_{0i} is the initial location of the fluid particles at reference time t_0. On the contrary, if the velocity function of the boundary, $\boldsymbol{w}$, is zero, the Eulerian reference is used. Equation (6.3.7) then reduces to the conventional form which Oseen[84] obtained many years ago and some researchers (e.g. Dargush and Banerjee[148]; Piva and Morino[149]; Tosaka and Kakuda[150]) have developed and/or tried numerical implementations recently. For the more general case, equation (6.3.7) can be considered as the basis for an Eulerian and Lagrangian combination.

The result of the integral equations under the Lagrangian reference can be written as follow:

$$u_k(x,t)=\int_{t_o}^{t}\int_{\Gamma(t')}(u_i\sigma^*_{ik}-u^*_{ik}\sigma_i-\mathrm{Re}\,u_jn_ju^*_{ik}u_i)d\Gamma\,dt'$$

$$-\mathrm{Re}\int_{\Omega(t_o)}u^*_{ik}u_i\Big|_{t_o}d\Omega(x'_o) \qquad (6.3.8)$$

The last domain integral can be simpler if the velocity fundamental solutions (6.2.20) and the continuity equation (6.2.1) are used again. It becomes

$$\int_{\Omega(t_o)}u^*_{ik}u_i\,d\Omega=\int_{\Omega(t_o)}u_k\Delta\Phi d\Omega-\int_{\Gamma(t_o)}\Phi_{,k}u_in_i\,d\Gamma \qquad (6.3.9)$$

Finally, the boundary integral representations are set up for the components of velocity in Lagrangian form:

$$C_{ik}u_i(x,t) = \int_{t_o}^{t_1}\int_{\Gamma(t')} (u_i\sigma^*_{ik} - u^*_{ik}\sigma_i - Reu_j n_j u^*_{ik} u_i)d\Gamma\, dt'$$
$$+ Re\left(\int_{\Gamma(t_o)} \Phi_{,k} u_i n_i d\Gamma - \int_{\Omega(t_o)} u_k \Delta\Phi d\Omega\right) \qquad (6.3.10)$$

where the constants C_{ik} are δ_{ik} for x inside the medium body, and $C\delta_{ik}$ for x on the boundary. The accurate value of C is discussed in section 6.5.

It can be readily seen that the last domain integral is exactly the same form as it appeared in the boundary integral equation for transient heat transfer problem which was introduced in Chapter Four. It can be, needless to say, transferred to boundary if the dual reciprocity theory introduced in section 4.8 can be successfully proved and implemented. It is really a promising development for the boundary element methods since no domain mesh involving in the calculation.

This group of equations (6.3.10) provides a required relationship in a Lagrangian description between the velocity-stress field inside the medium and the corresponding velocity and traction boundary values. Based on the equations, the motion of a finite fluid medium or multimedia interactions can be solved, as well as that for infinite fluid motion. The major difference from the conventional Eulerian description is the disappearance of the time-spatial integral about the convection terms.

6.4 Integral Equation for Pressure

The above idea can be easily extended to the decoupled integral formulation for the unknown pressure. Notice the domain integral in equation (6.3.6), the second term disappears according to equation (6.2.7), whereas the pressure can be integrated if the velocity components of the fundamental solutions satisfy

$$u^{**}_{i,i} = \delta(x - x')\delta(t - t') \qquad (6.4.1)$$

where it has to be an one-order tensor because the pressure is a scalar function. Two asterisks are used in order to distinguish it from the fundamental solution given in section 6.2.

A group of supplemental equations have to be given for completing the system for the fundamental solutions:

$$\mathrm{Re}\frac{\partial u_i^{**}}{\partial t} = \sigma_{ij,j}^{**} \qquad (6.4.2)$$

Replacing the fundamental solutions in equations (6.3.6) by these new set yields:

$$\mathrm{Re}P(x,t) = \int_{t_o}^{t_1}\int_{\Gamma(t')} (u_i\sigma_i^{**} - u_i^{**}\sigma_i)\,d\Gamma\,dt' - \int_{t_o}^{t_1}\int_{\Omega(t')} \left(u_i^{**}\sigma_{ij,j} - u_i\sigma_{ij,j}^{**}\right)d\Omega\,dt' \qquad (6.4.3)$$

Using equations (6.4.2) and (6.3.3) the domain integral can be replaced as follows:

$$\int_{\Omega(t')} \left(u_i^{**}\sigma_{ij,j} - u_i\sigma_{ij,j}^{**}\right)d\Omega = \mathrm{Re}\int_{\Omega(t')} \left[\frac{\partial(u_i^{**}u_i)}{\partial t'} + u_i^{**}(u_j - w_j)u_{i,j}\right] d\Omega \qquad (6.4.4)$$

Similarly, the first term can be expanded and the second term of the domain integral vanishes due to the deforming reference. After rearrangement, the integral equation for pressure is written as follow:

$$CP(x,t) = \int_{\Omega(t)} u_i^{**}u_i\Big|_{t'=t_1} d\Omega(x') - \int_{\Omega(t_o)} u_i^{**}u_i\Big|_{t'=t_o} d\Omega(x'_0) + \frac{1}{\mathrm{Re}}\int_{t_o}^{t_1}\int_{\Gamma(t')} (u_i\sigma_i^{**} - u_i^{**}\sigma_i - \mathrm{Re}\,u_j n_j u_i^{**}u_i)\,d\Gamma\,dt' \qquad (6.4.5)$$

where C is the parameter which has the same meaning as mentioned in the previous section.

The new set of the fundamental solutions governed by equations (6.4.1-2) can be obtained easily, because it can always be assumed that u_i^{**} is a

derivative of a potential function multiplied by a delta function of time, that is,

$$u_i^{**} = \Theta_{,i}\delta(t-t') \tag{6.4.6}$$

which can be substituted into equation (6.4.1) to form a Laplace type equation. The fundamental solution of the Laplace equation, Θ, is expressed as follows:

$$\left.\begin{aligned}\Theta &= \frac{1}{2\pi}\ln\left(\frac{1}{r}\right) \quad 2D\\ \Theta &= \frac{1}{4\pi r} \quad 3D\end{aligned}\right\} \tag{6.4.7}$$

Substituting (6.4.6) into equation (6.4.2) and using the Newtonian relation yields

$$2\delta(t-t')\Theta_{,knn} - Re\,P^{**}_{,k} - Re\,\Theta_{,k}\frac{\partial\delta(t-t')}{\partial t} = 0 \tag{6.4.8}$$

from which the traction components can be derived:

$$\sigma_i^{**} = n_i\left[Re\,\Theta\frac{\partial\delta(t-t')}{\partial t} - 2\delta(t-t')\delta(x-x')\right] + 2\delta(t-t')\Theta_{,ij}n_j \tag{6.4.9}$$

According to the solution (6.4.6), the integral equation of the unknown pressure is a boundary only form:

$$CP(x,t) = \int_{\Gamma(t)}\left[\frac{2u_i\Theta_{,ij}n_j}{Re} - n_i\left(\Theta\frac{\partial u_i}{\partial t} + \frac{2u_i}{Re}\right) - \Theta_{,i}\left(\frac{\sigma_i}{Re} + u_j n_j u_i\right)\right]d\Gamma \tag{6.4.10}$$

This is an explicit integral representation that gives pressure anywhere in the field or on the boundary in terms of **u** and σ, which values are all known after the solution of equations (6.3.10).

6.5 Boundary Element Implementation

The boundary element system for solving equations (6.3.10),(6.4.10) rests on the discretisation of the boundary of the medium of concern and the time interval during which the medium deforms and moves. Because the fundamental solutions are zero after t due to the property of the Heaviside function, the upper bound of the time integration, $t_1=t+\varepsilon$, can then be replaced by t. In fact, the only equations to be solved are (6.3.10) for the unknown velocity and traction components on the boundary, and then the rest of the unknowns can be explicitly worked out by using those boundary values.

Time-marching

From equation (6.3.10) it can be seen that the velocity of the particles are determined by the functions based on the velocity-traction values on the boundary, the position of which may be unknown, and the velocity field at time t_0 which the position is known. Since the velocity of a particle is the time derivative of the position vector

$$u_i = \frac{dx_i}{dt} \tag{6.5.1}$$

The position of the particle after time $t-t_0$ is then given by

$$x_i = x_i^0 + \int_{t_0}^{t} u_i(t')dt' \tag{6.5.2}$$

The time interval must be small enough. In fact, a constant approximation is chosen, and the time interval is so small that both the boundary position and the variables on the boundary within the duration can be assumed independent of the time. Thus the position can be expressed in a simple way as follow

$$x_i = x_i^0 + (t - t_0)u_i^0 \tag{6.5.3}$$

that is, the position of the boundary at time t can be expressed by the position and the velocity at time t_0. Also, the order of the first integration in equations (6.3.10) can be interchanged and the unknowns can be brought outside of the time integrals:

$$\int_{t_o}^{t}\int_{\Gamma(t)}(u^*_{ik}\sigma_j - u_i\sigma^*_{ik})d\Gamma dt' = \int_{\Gamma(t)}\left(\sigma_j\int_{t_o}^{t}u^*_{ik}\,dt' - u_i\int_{t_o}^{t}\sigma^*_{ik}\,dt'\right)d\Gamma \qquad (6.5.4)$$

With $U^*_{ik} = \int_{t_o}^{t} u^*_{ik}\,dt'$ and $\Sigma^*_{ik} = \int_{t_o}^{t}\sigma^*_{ik}\,dt'$, equations (6.3.10) becomes

$$Cu_k = \int_{\Gamma(t)}\left(u_i\Sigma^*_{ik} - U^*_{ik}\sigma_i - Re\,u_j n_j U^*_{ik}u_i\right)d\Gamma + Re\left(\int_{\Gamma(t_o)}\Phi_{,k}u_i n_i d\Gamma - \int_{\Omega(t_o)}u_k\Delta\Phi d\Omega\right) \qquad (6.5.5)$$

It can be seen that based on the velocity field at the beginning of the time interval, equations (6.5.5) gives the flow field at the end of the time interval. If this small time interval is defined as a time step, that is, $\Delta t=t_m-t_{m-1}$ ($t=t_m$, $t_0=t_{m-1}$), and the flow field at the end of the previous time step is the flow field at the beginning of the current time step, thus the velocity field at any time can be obtained.

Iteration

Since the third term is a non-linear one, an iteration procedure is necessary in each time step. Let u_i^{m-1} be the known velocity field at time step t_{m-1}. The algorithm for the iterative process for the unknown u_i^m and σ_i^m values at time step t_m is briefly explained in the following paragraph.

At first the following implicit functions for the velocity and stress fields are defined as f

$$f(u_i^m, \sigma_i^m, \bar{u}_i^m, u_i^{m-1}) = Cu_k^m - \int_{\Gamma_m}\left(u_i^m\Sigma^*_{ik} - U^*_{ik}\sigma_i^m - Re\,\bar{u}_j^m n_j U^*_{ik}u_i^m\right)d\Gamma - Re\left(\int_{\Gamma_{m-1}}\Phi_{,k}u_n^{m-1}d\Gamma - \int_{\Omega_{m-1}}u_k^{m-1}\Delta\Phi d\Omega\right) \qquad (6.5.6)$$

where U^*_{ik} and Σ^*_{ik} can be analytically expressed:

$$U^*_{ik} = \int_{t_{m-1}}^{t_m} u^*_{ik}dt' = \frac{1}{8\pi}\left\{\delta_{ik}[E_1(s) - S_o(s)] + \frac{2x_i x_k}{r^2}S_o(s)\right\} \qquad (6.5.7)$$

$$\Sigma^*_{ik} = \int_{t_{m-1}}^{t_m} \sigma^*_{ik} dt' = \frac{1}{2\pi r^2}\left\{\left(\delta_{ik}x_j n_j + x_i n_k\right)\left[S_0(s) - e^{-s}\right]\right.$$
$$\left. - \frac{2x_i x_j n_j x_k}{r^2}\left[2S_0(s) - e^{-s}\right] + x_k n_i\left[S_0(s) - 1\right]\right\} \qquad (6.5.8)$$

in which $S_0(s) = \frac{1}{s}(1 - e^{-s})$, $E_1(s) = \int_s^\infty \frac{e^{-u}}{u} du$, and $s = \frac{Re r^2}{4\Delta t}$.

At the initial step of the iteration, the velocity value at time t_{m-1} is used for the velocity $\bar{u}_i^m$ in equation (6.5.6). Thus the first iteration is computed as

$$f(u_i^{m(1)}, \sigma_i^{m(1)}, u_i^{m-1}, u_i^{m-1}) = 0 \qquad (6.5.9)$$

Then we have

$$f(u_i^{m(L)}, \sigma_i^{m(L)}, u_i^{m(L-1)}, u_i^{m-1}) = 0 \qquad (6.5.10)$$

The iteration is repeated until the computed velocity components satisfy the convergence criterion

$$\left|u_i^{m(L)} - u_i^{m(L-1)}\right| \le \varepsilon_1 \qquad (6.5.11)$$

where ε_1 is a prescribed small value. If the process converges then the both the velocity and traction values obtained at the L^{th} iteration are assigned to those of m^{th} time step.

Singularities and Geometrical Dependent Parameter C

If velocity components are constants, we can prove that

$$Cu_k^c = \int_\Gamma u_i^c \Sigma^*_{ik} d\Gamma - Re\left(\int_\Omega u_k^c \Delta\Phi d\Omega - \int_\Gamma \Phi_{,k} u_i^c n_i d\Gamma\right) \qquad (6.5.12)$$

This relation gives a very useful tool to handle the singularities and the geometrical parameter C. First of all, if u_1=1 and u_2=0, then we have

$$C=\int_{\Gamma}\Sigma^{*}_{11}d\Gamma-\mathrm{Re}\int_{\Gamma}\Phi_{,2}n_2d\Gamma\;;\quad 0=\int_{\Gamma}\Sigma^{*}_{12}d\Gamma+\mathrm{Re}\int_{\Gamma}\Phi_{,2}n_1d\Gamma \qquad (6.5.13)$$

Similarly, if $u_2=1$ and $u_1=0$, then we have

$$C=\int_{\Gamma}\Sigma^{*}_{22}d\Gamma-\mathrm{Re}\int_{\Gamma}\Phi_{,1}n_1d\Gamma\;;\quad 0=\int_{\Gamma}\Sigma^{*}_{21}d\Gamma+\mathrm{Re}\int_{\Gamma}\Phi_{,1}n_2d\Gamma \qquad (6.5.14)$$

6.6 Examples

A computer program of the boundary element method on the unsteady incompressible flow with free surface has been coded in FORTRAN. The program is a part of the CASIM package scheme which will be introduced in Chapter Eight. The insertion and deletion of boundary nodes for moving free surface are the basic feature of the coding which is similar to that of the programs for thin cavity flow and steady viscous flow introduced in Chapter Three and Five, respectively. Two examples have been tried for testing the effectiveness and accuracy of the method and the program.

Example1: Simulation of Compression Mould Filling

In recent years, the need for high volume production of large, lightweight, strong and stiff parts, particularly for automotive applications, has made compression moulding an important process for fibre reinforced polymers. This is largely responsible for the increased interest in computer modellings for compression moulding. In the past few years some researchers have studied ways of the simulation in order to know more about the characteristics and properties of a final part before it is actually manufactured. Emphasis of the simulations is on the fluid mechanics of the mould filling, the features of which stage are very close to those in the filling stage of injection moulding process. The models adopted for the stage of compression moulding are also referred to the models for the filling stage of injection moulding. A generalised Hele-Shaw model on thin charges was first adopted by Lee, Folgar and Tucker[152] for the filling stage, and a finite element method was implemented for the model. Following the applications of boundary element methods for the modelling, Osswald and Tucker[153] soon used a boundary element method based on an extension of the GHS model to analyse the filling stage of the compression

moulding. However, as introduced in Chapter Three [the difference is a non-homogeneous term representing the compression velocity appeared in the right hand side of equation (3.2.15)], the GHS models can only apply to a thin charge of uniform thickness. A more general boundary integral formulation was employed by Barone and Osswald[154] recently. This model is based on a newly developed flow model by Barone and Caulk[155] which is valid for both thick and thin charges. The newly determined fundamental solutions in the reference [153] for the model served the basis for the boundary only scheme in their numerical approximation. To date, almost all the models are for predicting the front progression and/or the flow field in the coordinate plane perpendicular to the pressing direction. In order to know the flow field viewed transversely, and to demonstrate the unsteady viscous model introduced in this chapter, the mould filling of the compression moulding is simulated hereafter. The model can obviously be extended to three dimensional simulation for the filling process so that the details of the flow field can be simulated without further simplifications.
The compression mould filling process is shown schematically in Fig.6.6.1. A pre-measured chopped fibre reinforced polymer compound is placed between the heated halves of a mould; these halves are then brought together to squeeze the charge and fill the mould, after which pressure is maintained while the polymer cures. The distinguishing features of this process include that the material is pre-prepared with layers of film and fibres and other additives, and the volume fraction and the size of the fibres can be relatively large.

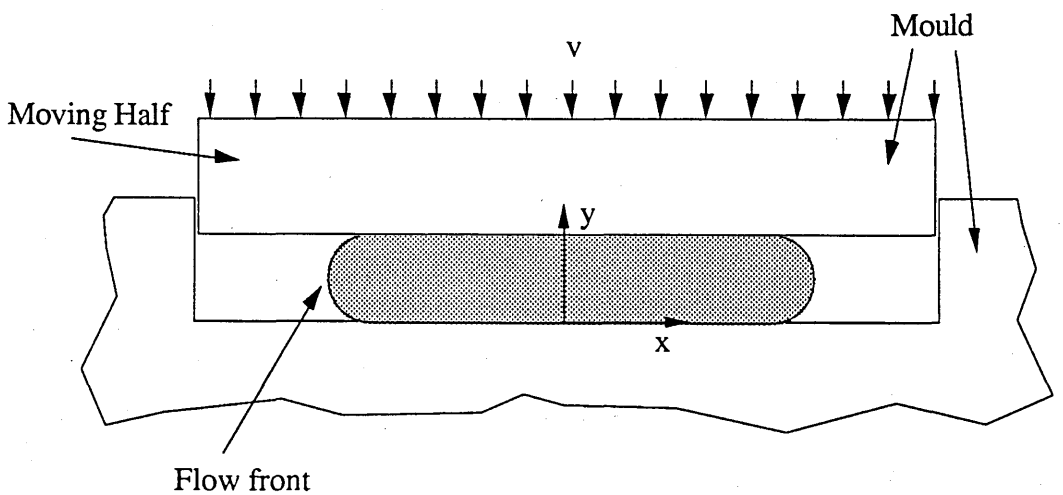

Fig.6.6.1. Schematic of a compression mould filling process.

Just like the diagram, the problem viewed transversely is a block of charge being squeezed towards the cavity extremes. The upper half moves at speed v_0, the lower half is fixed. No-slip condition is assumed on both walls. The advantage of symmetry is taken, so only half of the charge is simulated. On the symmetrical line the normal component of the velocity is set zero, and on the free surface, the traction components are zero.

Similar to the features in the programs for models discussed in Chapter Three and Five, a node inserting scheme is designed to the program, and any node touches on the walls is set the corresponding boundary conditions on it. Therefore during the simulation the nodes to define the free surface are being changed, and the number of the nodes on the walls are increasing. In order to trace each node both on the boundary and inside the domain, the nodes are not re-numbered. Unlike the other two programs, the interior nodes must be used for the time marching. The succession of boundary variation is shown in Fig.6.6.2.

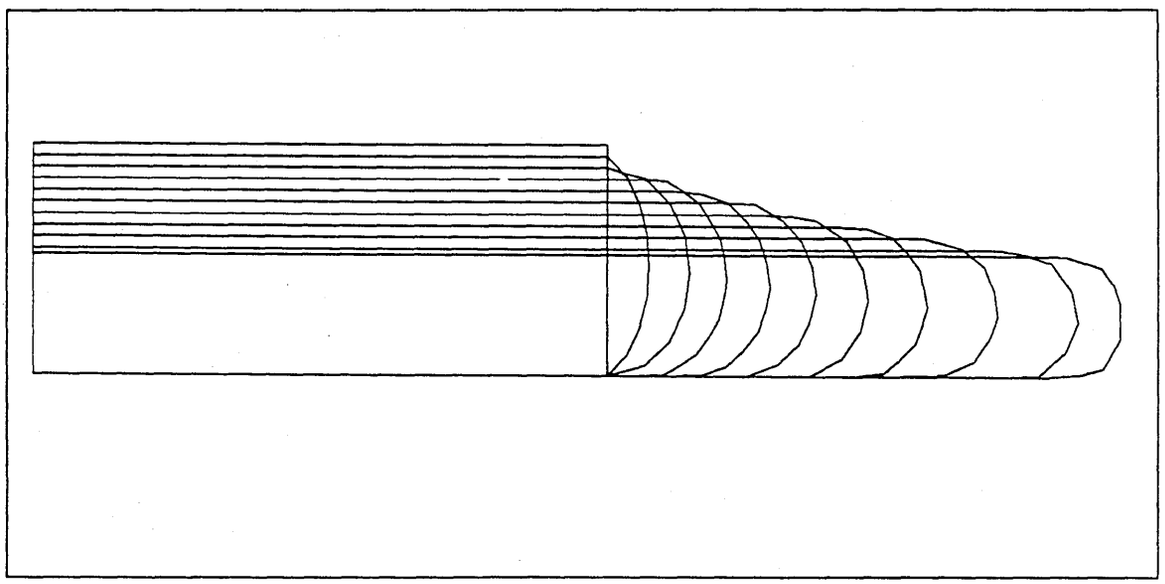

Fig.6.6.2 Succession of boundary positions in compression moulding.

The velocity fields are shown successively in Fig.6.6.3. From those graphs it can be seen that the particles in the central area just behind the flow front are accelerating with the horizontal components of the velocity much higher than their vertical components. The original front is soon stretched and becomes a curve close to a semi-circle with a little bit more touching the lower wall first. The particles on and behind it soon split about a horizontal line slightly below the central line, and those in the upper half

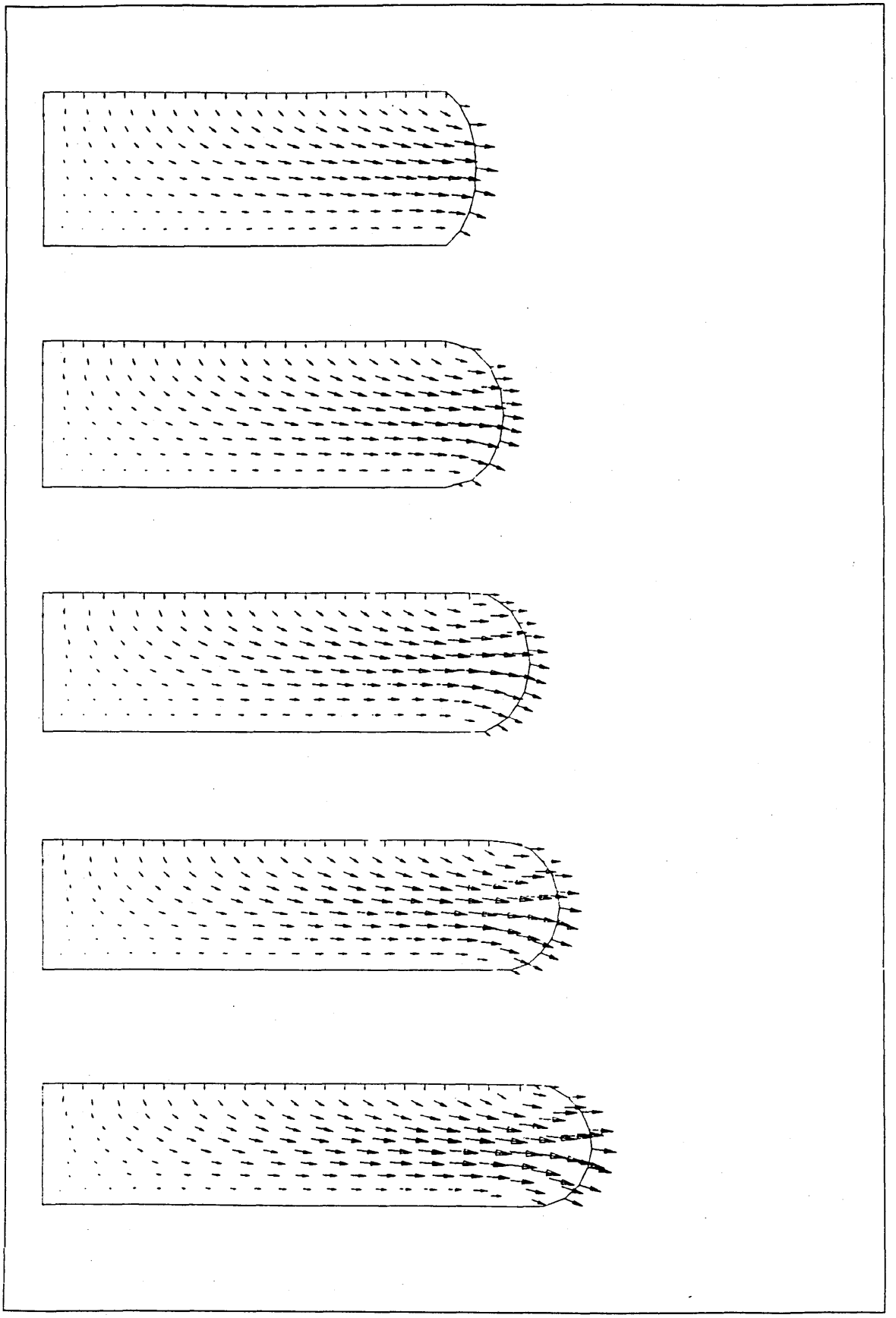

Fig.6.6.3. Velocity fields (Continued).

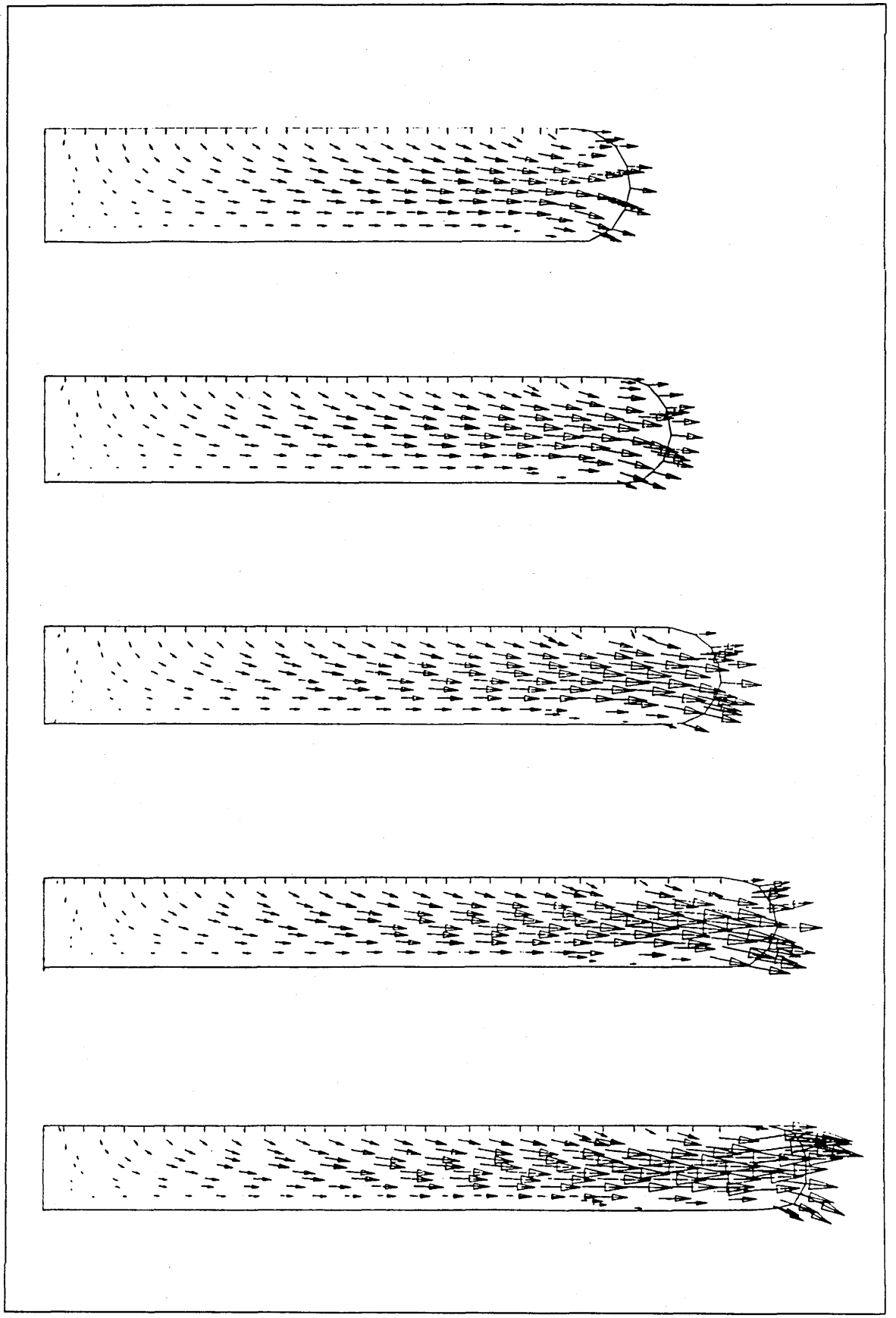

Fig.6.6.3. Velocity fields (Continue from the last page).

move almost horizontally to meet the downward-moving half of the mould, while those in the lower half move down forward to meet the fixed half.

In the last graph, the particles on and just behind the flow front meet the side wall at about eight times as much as the speed of the moving half. Obviously, the first bit to meet the side wall is slightly below the central point of the front, and the rest of the front is squeezed into extremes of the cavity. The dimension at last is 0.21:1.9 which is almost the same volume as its original dimension (0.4:1).

Example 2: Squeezing without a mould cavity

If the above charge is squeezed by two blocks without side restrictions and wall extensions, the resulting flow fields will be interesting. Of course this is not for an existing polymer process, since it is hard to find a suitable example to verify the model, this example is just for demonstrating the potentials of this boundary element model for unsteady viscous flow with free moving boundary.

The original size is the same as the above example. The time increment used here is twice as much as it used in the above example. A succession of seven graphs of the flow front progression is shown in Fig.6.6.4. The velocity fields corresponding to the flow front graphs are shown in Fig.6.6.5.

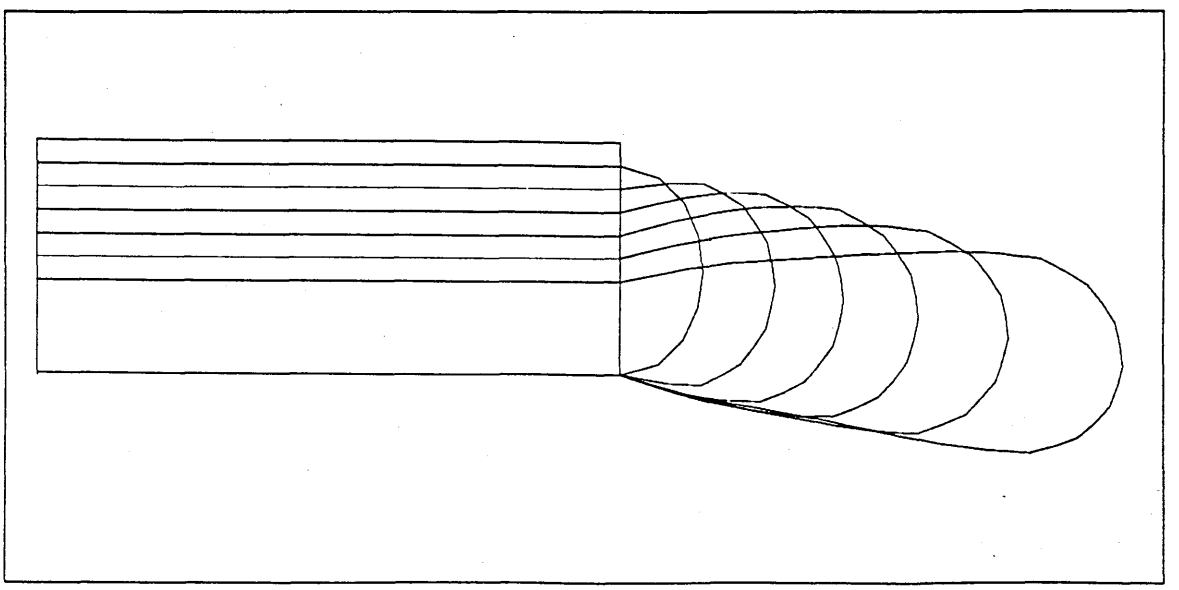

Fig.6.6.4. Succession of the flow front progression

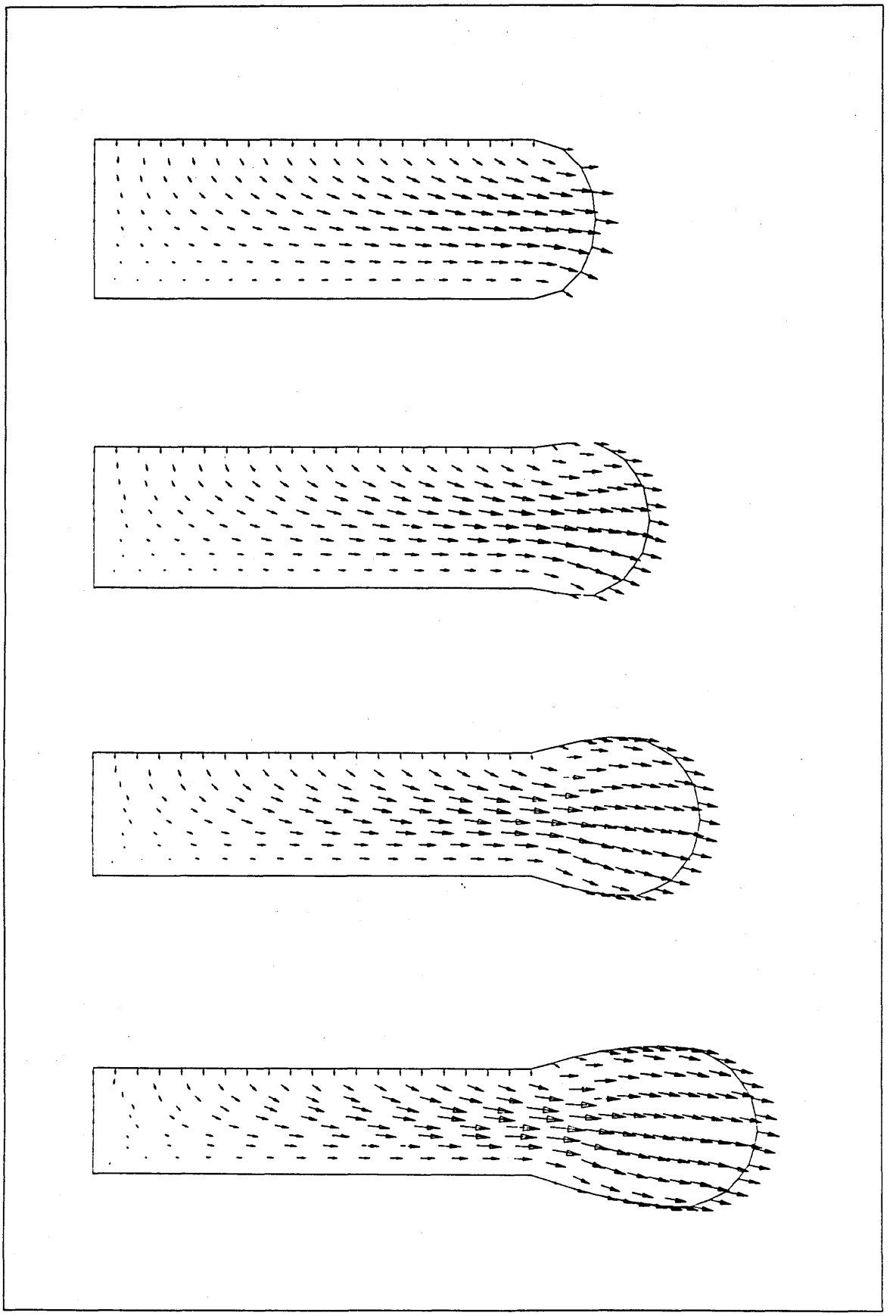

Fig.6.6.5. The velocity field (Continued)

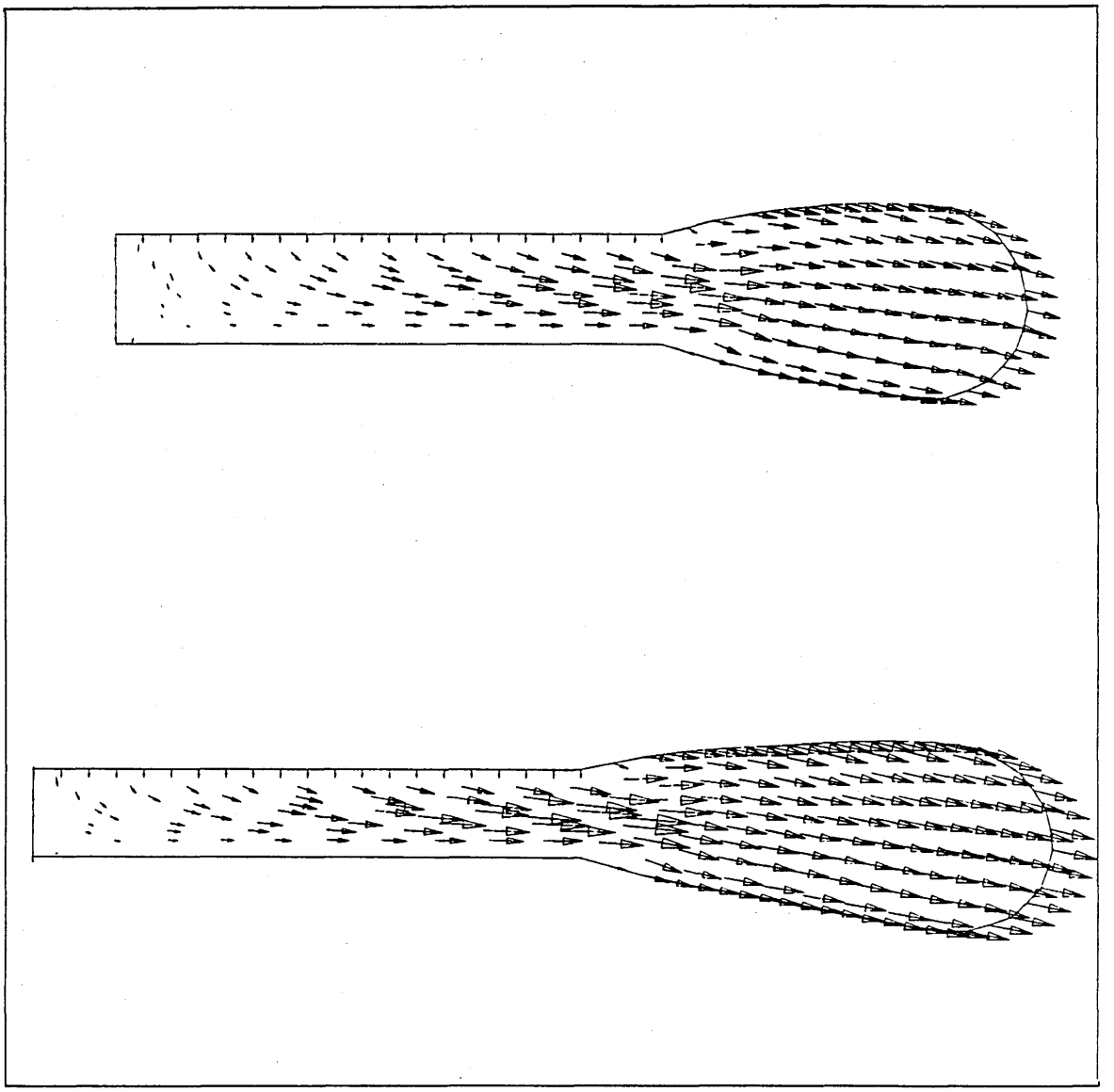

Fig.6.6.5. The velocity field (continued from the last page).

6.7 Concluding Remarks

In this chapter, a boundary element method for transient incompressible viscous flow with free moving surface is presented. The formulation is derived in Lagrangian description, the convection terms therefore vanish and no unknown field variables involved in the resulting system. For polymer flows which are characterised with high viscosity or low Reynolds number, this formulation is particularly effective. The only remaining domain integral is about the flow field in the previous time step, which is exactly the same form as it in the boundary integral formulation for transient heat conduction equation. Although the dual reciprocity method is

not introduced here, it should have no major difference from what was introduced in Chapter Four. Therefore the boundary only scheme is potential, and the computational advantage of the boundary element method has not lost. Two examples have been shown the effectiveness and accuracy of the model, especially for the compression mould filling. Three dimensional case can be extended and then the details of the flow field can be obtained for interpreting the process.

Chapter Seven

Processing Analysis by MOLDFLOW

7.1 Introduction

Some real moves in the field of computer simulation of injection moulding have already been made by MOLDFLOW, C-FLOW and some other program designers. Fortunately, the author has been supplied with the first part of the MOLDFLOW package, which has long been used for practical processing analysis. The exercises of the simulation by MOLDFLOW not only give much experience of the engineering analysis but also inspire some ideas for the simulation itself.

In this chapter, the author wishes to introduce MOLDFLOW, its philosophy and powerful functions, and some ideas incurred by interpreting the simulation analyses of four practical IBM's computer components.

7.1.1 General Description of MOLDFLOW

MOLDFLOW is a computer package which supplies computer-aided engineering methods for studying the design and production of plastic parts, improving the quality of the parts, and reducing the manufacturing costs. As mentioned in Chapter One, the injection moulding technique includes many aspects. From a macroscopic point of view, it can be classified as three stages. The filling stage is the period when the plastic melt is injected into mould until the whole cavity is filled. The major characteristic of this stage is the fluid flow. The second stage concerns mainly the compressibility because of the pressurisation after the mould is filled, and the third is the cooling stage in which the thermal characteristic is overwhelming. MOLDFLOW not only covers the three stages by its series of programs but also emphasises the effects caused by the characteristics. In fact, MOLDFLOW is its original name for only the flow analysis program. As the requirements increase, not only the flow analysis itself is updated several times, but also cooling, holding, shrinkage and warpage, stress and creep analyses are produced in succession so that the package gradually becomes an integrated MOLDFLOW system. The system uses the finite element method as its major means for the flow analysis, finite difference

method for the holding and cooling analysis, and boundary element method for three dimensional cooling analysis. The shrinkage and warpage analysis are mainly based on the results from the flow, holding and cooling analyses, and the material shrinkage coefficients from the database determine the thermal extraction from each stage to give the shrinkages on both the parallel and perpendicular directions to the flow. Besides the application of these approximate numerical methods, the important part of the package is its own standard raw material database called MATDB. MOLDFLOW's flow and thermal analyses are based on the database and the data of which come from practical experiments in many laboratories and companies, particularly raw material suppliers. They have helped Moldflow to establish

Table 7.1.1

PRODUCT	VENDOR	HARDWARE
AUTOTROL	Autotrol Technology	APOLLO
BRANVO	Schlumberger Application	APOLLO / VAX
CADAM	Cadam Inc.	IBM VM / IBM MVS
CADDS	Computervision Corp.	CDS4000 / CADDStation
CADKEY	Cadkey Inc.	IBM PC XT / AT
CADES	IBM	IBM VM / IBM MVS / IBM RT
CATIA	Dassault Systems	IBM VM / IBM MVS
DOM	Calma Company	APOLLO / VAX
DUCT	Deltacam	APOLLO / VAX
EUCLID	Matra Datavision	VAX
ICEM	Control Data	CYBER
I-DEAS	SDRC	VAX / APOLLO
I / FLOW	Intergraph	CLIPPER
PATRAN	PDA Engineering	VAX/APOLLO/HP9000/IBM
SABRE	Gerber Technology	HP9000
Unigraphics	McDonnell Douglas	VAX / DG / HP9000
VDA-FS	SI (Norway)	VAX

the database and formulate uniform testing procedures of its own laboratory. Because of ever-increasing range of material, Moldflow has a plan to update the database every four months. It also has its own powerful pre- and post-processors for generating and meshing the geometrical surfaces, and displaying the results in multicoloured contour lines or solid modes. However, the integrated engineering product demands the

association functioning with better developed CAD/CAM systems. The following table[156] gives the interfaces of MOLDFLOW with some of such systems:

From this table it can be seen that the MOLDFLOW designers have put a great deal of effort in the connecting CAD packages to construct the commercialised CAE package as a powerful tool. Experiences gained by using the flow and thermal analyses feedback to the design work and made the package more and more efficient and accurate. Comparisons between the software predictions and laboratory trials to date, have shown that accurate results can be achieved[157]. More details about the first part of MOLDFLOW are given through the following examples in later sections.

7.1.2 MOLDFLOW's Structure

The structure of MOLDFLOW is shown in Fig. 7.1.1:

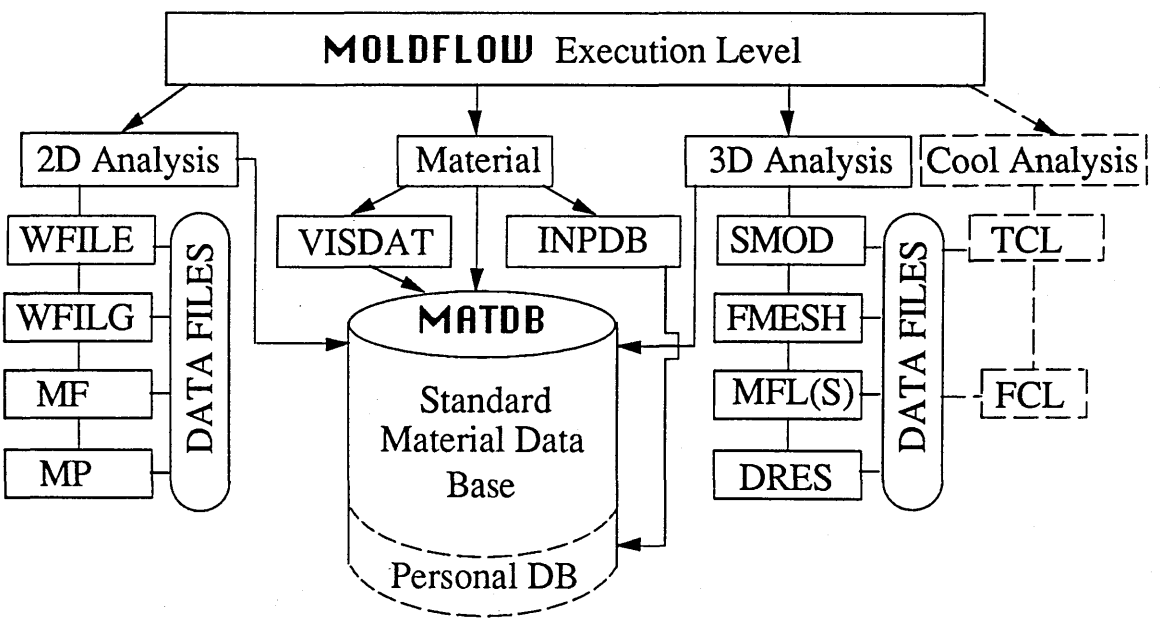

Fig. 7.1.1 The structure of MOLDFLOW, the dotted boxes are not in the present package.

MOLDFLOW execution level is actually a menu written in ISPF (Interactive System Productivity Facility) statements. Other modules are stored in a big library. The data files are the media between the modules in the same sub-menu, also the media for transferring the data with other packages. The standard material database, MATDB, has just over 1,100

dated polymer materials' properties from various suppliers. A user can setup his / her own personal database by using INPDB. 2D ANALYSIS provides a quick estimate of the processing window, pressure gradient, temperature and so on. The methods used in the modules are obviously the original simplified formulations. SMOD and FMESH are the three dimensional pre-processors for setting up geometrical surface model and generating finite element mesh, respectively. The mesh generator can generate up to 10,000 triangular elements or 6,000 nodes for a problem. These numbers are also the limitations of the package capacity in IBM3090(CMS). DRES is a powerful graphical enhanced post-processor which can be used for displaying the result files. Both SMOD and DRES are apparently supported by graPHIGS system. Functions and methods of using each module can be found in detail in MOLDFLOW Manuals[158].

7.2 Brief Introduction to MOLDFLOW's Simulation Algorithms

The theory behind the MOLDFLOW package has evolved from surprisingly simple formulations. Instead of solving the complicated Navier-Stokes equations, it adopted a very straightforward formulation for a thin slice (which could be a rectangular, or a round, or radial section) and assembled all the slices into a whole component following a time marching method. The formulation is the equilibrium equation between the pressure and the stresses, that is, the force pushing the block along is the pressure drop along the block multiplying the section area, and this force is resisted by the shear stresses acting on both faces, that is, shear stress multiplies the two face areas. That is,

Stress=pressure drop*thickness/(2*length) (7.2.1)

There is no physical property involved in this formula. If the pressure across the flow field is known, then the shear stress can be obtained by such a simple formula. If the viscosity is known, the shear rate can then be calculated, since it is the parameter of the linear relation between the shear stress and shear rate. Any errors from predicting shear rate come from the viscosity parameter given and not from any mathematical simplification[10]. Then the accuracy is mainly based on the ways of obtaining the viscosity. Although in practice the viscosity is a complicated function of temperature, shear rate, pressure, etc., it can always be found reasonably accurate if the

data in several cases are supplied. For example, viscosity supplied from MATDB are at least in three cases for a power law model, and six cases for a second order model. The increase in velocity over a slice is the shear rate multiplied by the thickness. Then from known velocity at the solid boundary (which is assumed to be zero because the plastic is frozen at the wall), the next face of each slice over a block will then be known. The same procedure can be done for each block; the complete velocity distribution is then known across the section. Multiplying the velocity of each slice by its cross-sectional area gives the volumetric flow, which can then be added together to give the total flow rate.

The three dimensional finite element techniques used in MOLDFLOW are the further developments of the above ideas. The finite element method is well known in stress analysis. The basic procedure in this package is to break up the moulding into a number of small triangular elements, which are connected at their nodes. The basic variables (flow rate, pressure) of each element are connected by a similar relation to equation (7.2.1) and a constitutive model, and an element resistance matrix like a "stiffness matrix" is formed which is dependent on the geometry of the element and the local viscosity. Assembling these matrices together for all the elements gives a large family of equations, which can then be solved to give the nodal flow rates and pressures by assuming the viscosity as a constant for the first iteration step. The viscosity is revised based on these calculated variables, and the constitutive law for reassembling the equations is used for a second solution. This procedure is repeated until a stabilised pressure distribution is obtained.

The crux of the finite element process is setting the boundary condition for each node. Either a pressure is specified and the flow rate will be calculated, or a flow rate is given and the pressure is then calculated. Because the mesh is under an Eulerian description, there is a "front nodal growth logic" designed in the package for the moving boundary. The method involves calculating the "control volume" which is based on the volume of all elements connected to a given nod, and subsequently each "node fill time" can be calculated. The algorithm is shown schematically in Fig. 7.2.1.

Simultaneously the temperature is being developed along with the flow pattern. After the nodal variables are obtained, the elemental variables — stresses and strains can be calculated throughout the moulding.

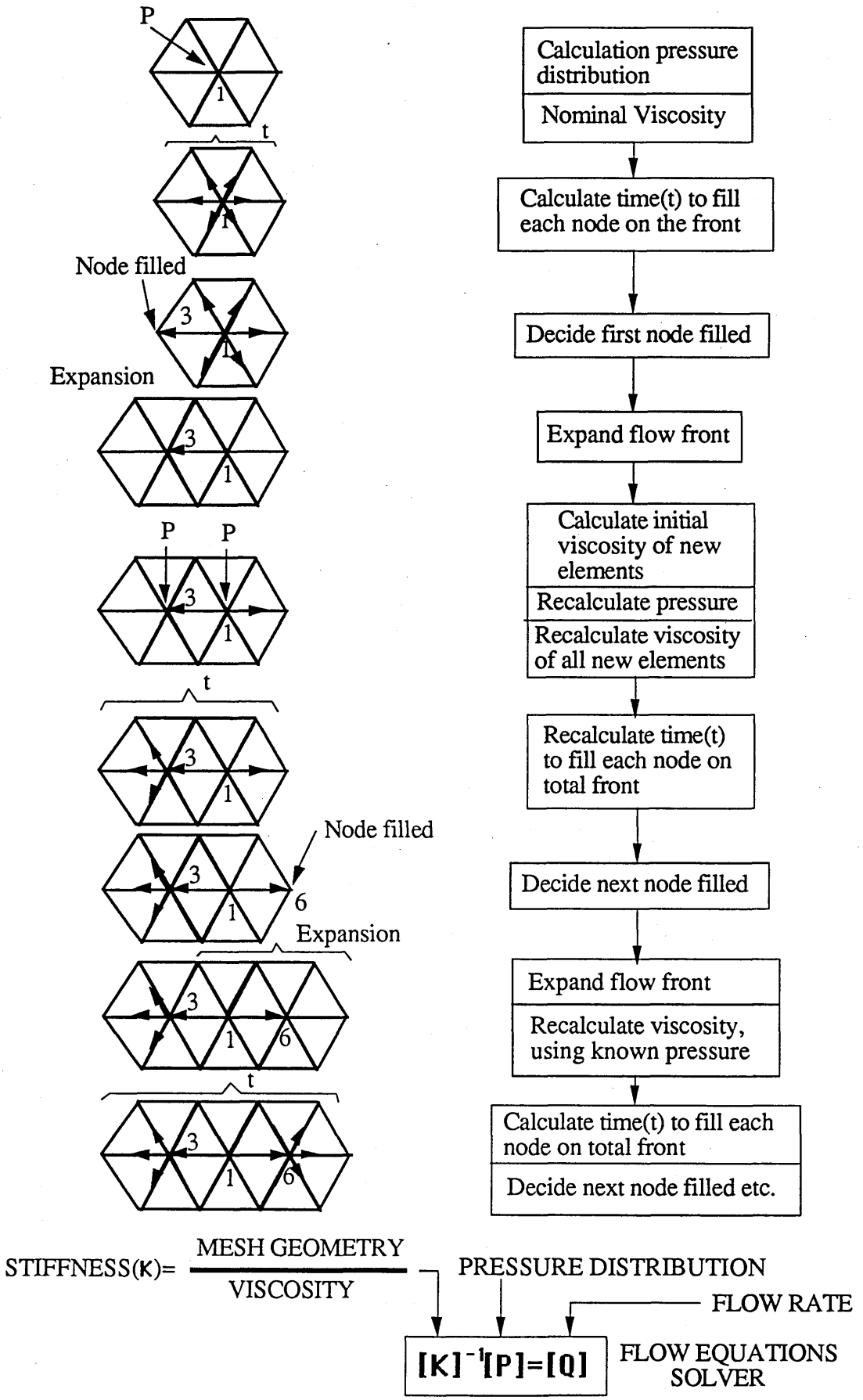

Fig.7.2.1 The nodal growth logic and the FE algorithm for the flow analysis

7.3 Simulation on Injection Moulding a Computer Part with PVC

Some examples can help explain what MOLDFLOW does. Hereafter is a 12" monitor plate-base (part number: 6319015) of a type of IBM computer as shown in Fig.7.3.1a. The material required for this part is polyvinyl chloride (PVC). It is important to understand the moulding characteristics of the material first.

7.3.1 Material Aspect

PVC is chemically inert, water-corrosion, weather-resistant, and an electrical and thermal insulator. It has a high strength-to-weight ratio, and it maintains its properties over long periods of time. The most important

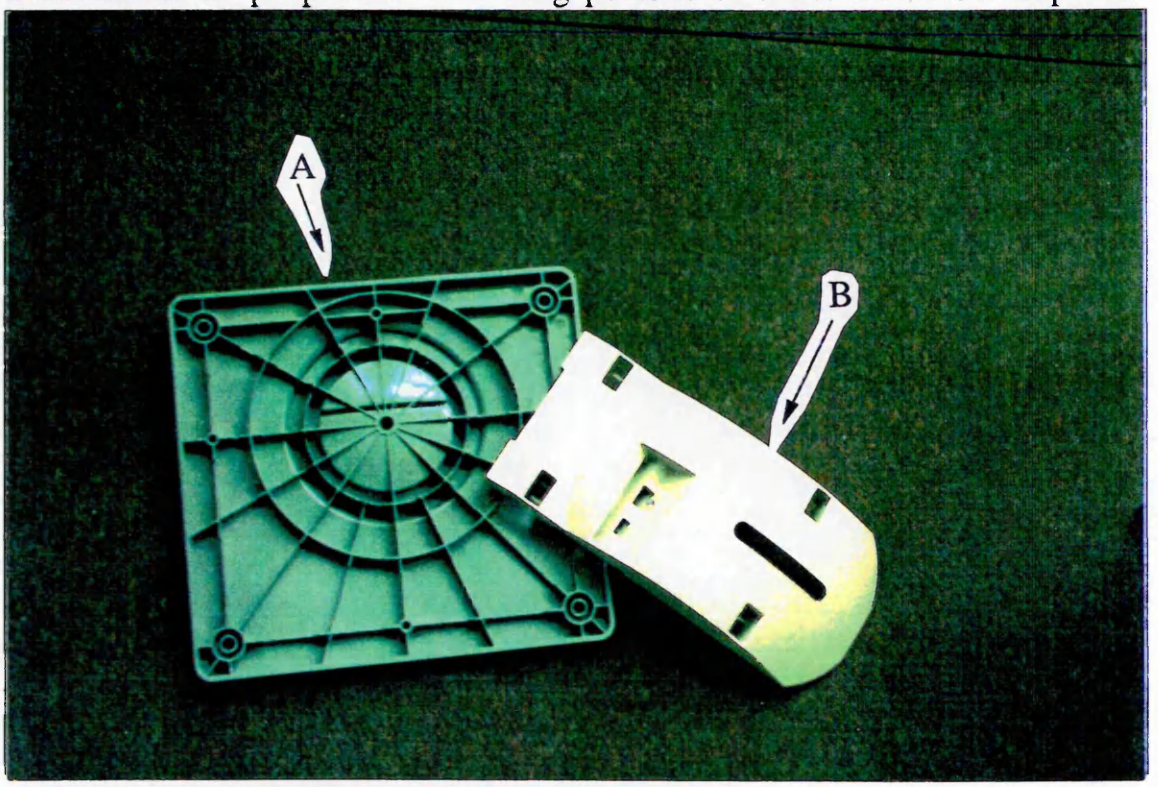

Fig. 7.3.1. 12" Monitor's plate base (a) and pivot plate (b)
(Original colour picture)

consideration of using PVC perhaps, is the low material costs in volume terms and good price stability in the market. However, it is important to remember that there is only a small difference between PVC's melting temperature and the temperature at which it degrades and burns, which is thought to be the challenge to the processor. PVC homopolymers have a melting point between 198 and 205 °C and begin to decompose rapidly at

200 °C. Copolymers are somewhat more forgiving. They begin to melt between 140 °C and 175 °C and offer significant processing advantages; Degradation remains at the high level. PVC is also classified as flexible and rigid. In general, injection moulding of flexible PVC is relatively easy, but special treatments for processing the rigid material should be taken to ensure part quality and long lasting life for the equipment. Rigid PVC is far more heat-sensitive than a flexible product, therefore heat control and flow-path design are more critical for rigid PVC.

MOLDFLOW has a guide menu in which it is indicated that both flexible and rigid PVC have the same barrel melt temperature range (140-200 °C), mould temperature (20 °C) and shear rate limit (20,000 1/s), but flexible PVC has lower maximum stress allowable (150,000 Pa) than the rigid does (200,000 Pa).

MOLDFLOW database gives various PVCs from five suppliers to choose from. However, not every PVC can be used for this particular moulding. Later on it will be seen that the PVC whose viscosity is higher than 300 (Pa.sec) simply can not be used for this moulding. Only two PVCs can be used. H550 is a flexible PVC, and it has extremely low viscosity. It is very easy to find a wide range of processing conditions for H550. H550 may not meet the performance requirements, therefore a rigid PVC, EV103, has been tried as well. The lists of the major properties of H550 and EV103 are as follows:

Table 7.3.1
MATERIAL FILE NAME < Moldflow Standard Database >
==========
HUELS
Material Grade Description

H550 PVC-P VESTOLIT SP 50 CRST.CLR. HUELS AG VI(180)65 HUELS AG JUN88
Material Grade Data
==========
CONDUCTIVITY J/(m.sec.degC) ==> 0.130
SPECIFIC HEAT J/(kg.degC) ==> 1500.
DENSITY kg/cu.m ==> 986.0
FREEZE TEMPERATURE degC ==> 60.00
NO-FLOW TEMPERATURE degC ==> 110.0

VISCOSITY

TEMPERATURE	SHEAR RATE	VISCOSITY
degC	1/sec	Pa.sec
160.0	100.0	536.0
180.0	1000.	64.89
190.0	1.000E+04	11.40

Table 7.3.2
MATERIAL FILE NAME < Moldflow Standard Database >
==========
EVC
Material Grade Description

EV103 PVC PRIMA RI5022 ALLOY EVC VI(180)295 EVC NOV88
Material Grade Data
==========
CONDUCTIVITY J/(m.sec.degC) ==> 0.150
SPECIFIC HEAT J/(kg.degC) ==> 1820.
DENSITY kg/cu.m ==> 1182.
FREEZE TEMPERATURE degC ==> 77.00
NO-FLOW TEMPERATURE degC ==> 130.0

VISCOSITY

TEMPERATURE	SHEAR RATE	VISCOSITY
degC	1/sec	Pa.sec
160.0	1000.	578.4
180.0	100.0	947.7
180.0	1000.	295.1
180.0	1.000E+04	60.55
200.0	100.0	483.6
200.0	1000.	150.6

From these two tables which are directly from MATDB of the package, the differences between these two PVC materials are obvious. It is noted that H550 has three parameters to define its viscosity curve, whereas EV103 has six. The latter is for the second order model of the constitutive equation which is supposed to give a more accurate result than the three parameter's power law one does.

7.3.2 Geometrical Aspect

The geometry of this part is not suitable from structural point of view, also not good for simplification in computer data input due to the unsymmetrical feature. Anyway the geometrical data input is relatively simple except the central part, which has spherical surface to be generated. MOLDFLOW pre-processor, SMOD, can generate any shape of flat polygon surface in three dimensional space, and circles with at most twenty points to define. Its copy-rotating function saves the shortcomings of the points to define a more accurate circle if it is necessary. It also has copy-translating, copy-mirror functions which have been used for generating the geometry. Some points of the spherical surface part in the central area have to be calculated by hand then input into the program. In next chapter a

subroutine of CASIM will be introduced which is coded special for this kind of difficulty. Only one gate position is given in the centre, otherwise two or more gates would produce potential weakness in weld lines. The geometry defined by surfaces in different views are given in Fig. 7.3.2.

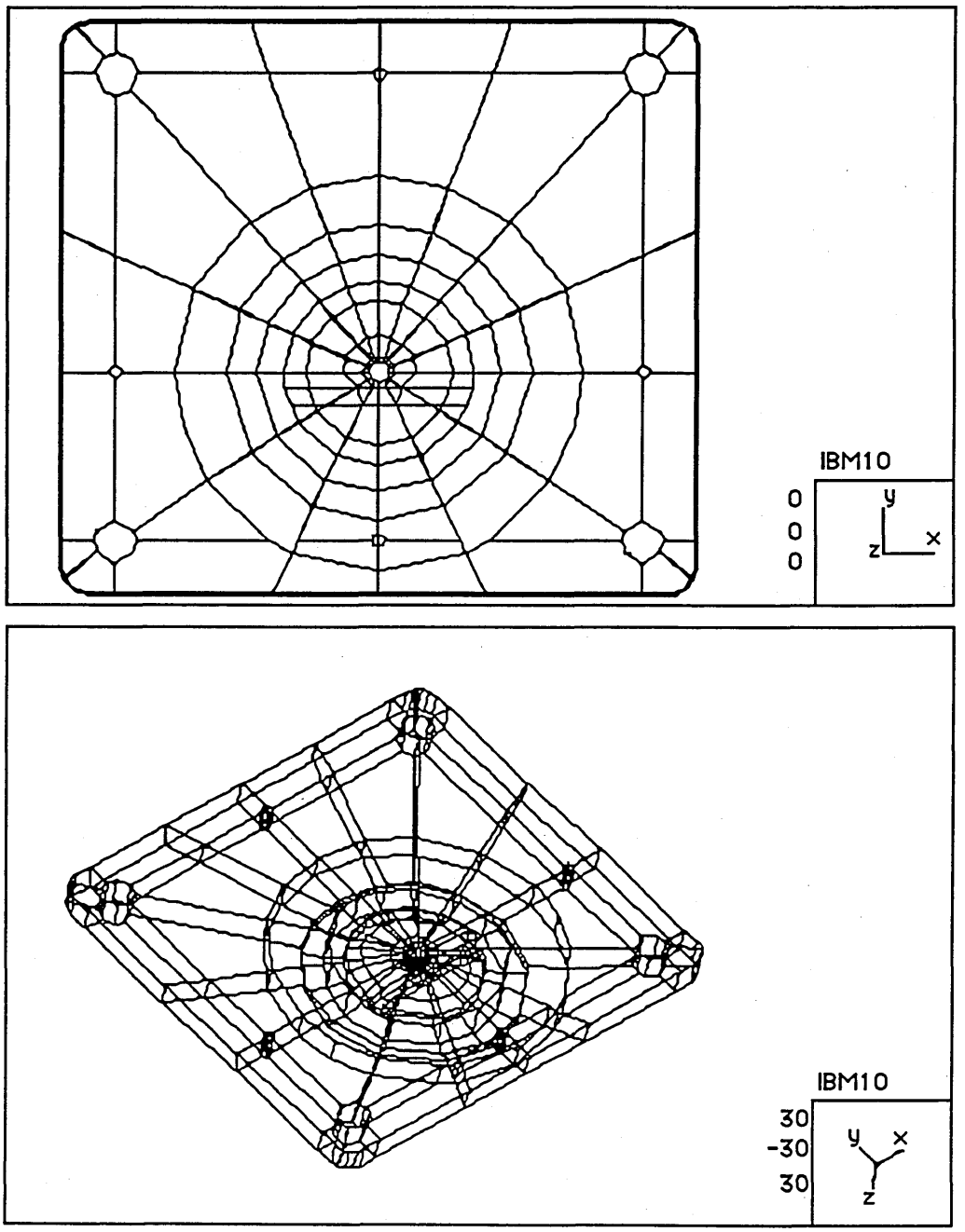

Fig. 7.3.2. Two views of the surface model of the geometry. (They are directly transferred through a CASIM subroutine based on GHOST80)

After generating the geometry, the next step is to use the finite element mesh generator to break all the surfaces into triangle elements, as shown in Fig.7.3.3.

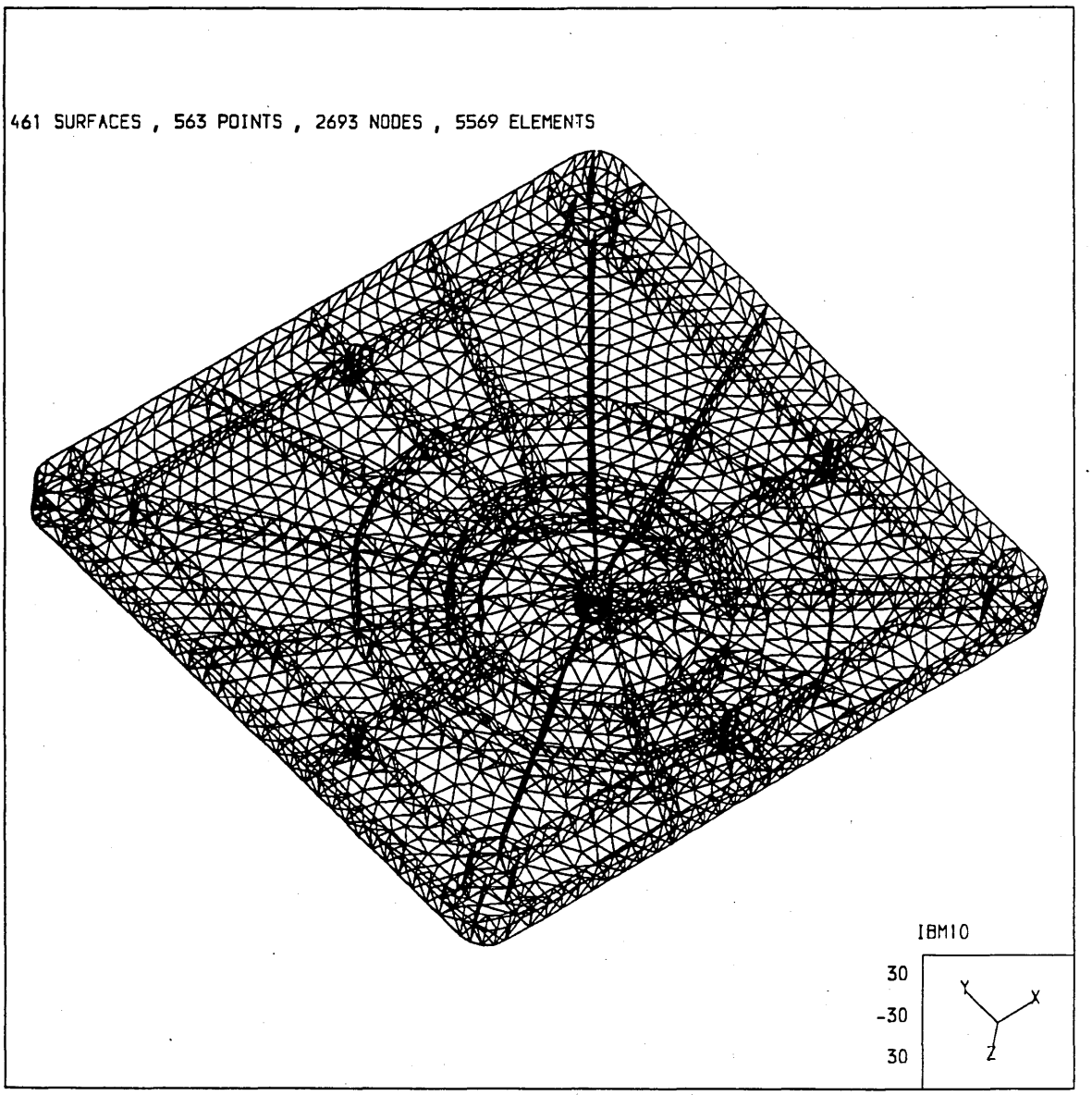

Fig.7.3.3 The mesh of the surface model. (This laser print-out is done through a PostScript file produced under GHOST80 environment)

7.3.3 Results of Moulding with H550

Having chosen the particular PVC to be used and generated the mesh of the geometry, we start to scan the processing conditions through 2D analysis. This method, as mentioned before, is the divided flow path approach which gives a quick and rough range of the processing parameters. However, since the geometry of this fitting is very complicated, and the 3D finite element calculation can be always used for more accurate analysis, it is not worth dividing the part into several branches and analyse them separately. The "autofile" choice is used since the maximum length

and the average thickness can be given for this scanning. The result of the scanning is listed as follow:

Table 7.3.3
MOLD TEMP 20.00 deg C MELT TEMP 195.00 deg C

TIME sec	PRESSURE MPa	STRESS @ START	STRESS @ END	TEMP @ END
0.20	9.5	131671.	45863.	200.
0.30	8.3	112700.	41359.	199.
0.50	7.0	92838.	36828.	196.
0.70	6.3	81842.	34620.	195.
1.00	5.7	71733.	33068.	192.
1.50	5.2	61924.	32532.	189.
2.00	4.9	55920.	33208.	185.
2.50	4.7	51752.	34566.	182.
3.00	4.7	48641.	36402.	179.
4.00	4.7	44232.	41189.	173.
5.00	4.8	41207.	47272.	167.
7.00	5.3	37255.	63276.	157.
10.00	6.5	33824.	98567.	143.
15.00	10.7	30844.	215830.	125.

* PLASTIC FROZEN RUN ABORTED *

From this table it can be seen that the time for filling stage can be chosen in a relatively big range, among which 0.7 second may be the best because the ending temperature is kept 195 °C. In fact, the other parameters can also be selected in a big range so that a relative large processing window can be found for this moulding. The resulting flow fields of above set of processing conditions are given as follows. From the filling pattern it can be easily seen that the flow front moves radially from the gate at first stage, when it hits side walls (it reaches the lower wall first since the complicated unsymmetrical character, though the gate is located slightly higher than the centre of the rectangle), the melt is then moving into corners. The thin ribs far from the gate is filled later than the thick plate. The temperature distribution is quite uniform, all falls into 6 °C difference. Low temperatures happen up in the top of the ribs since the thin thickness, which are also

responsible to late arrival of the melt into the ribs far from the gate. The max-min temperature difference after the filling is only 18 °C.

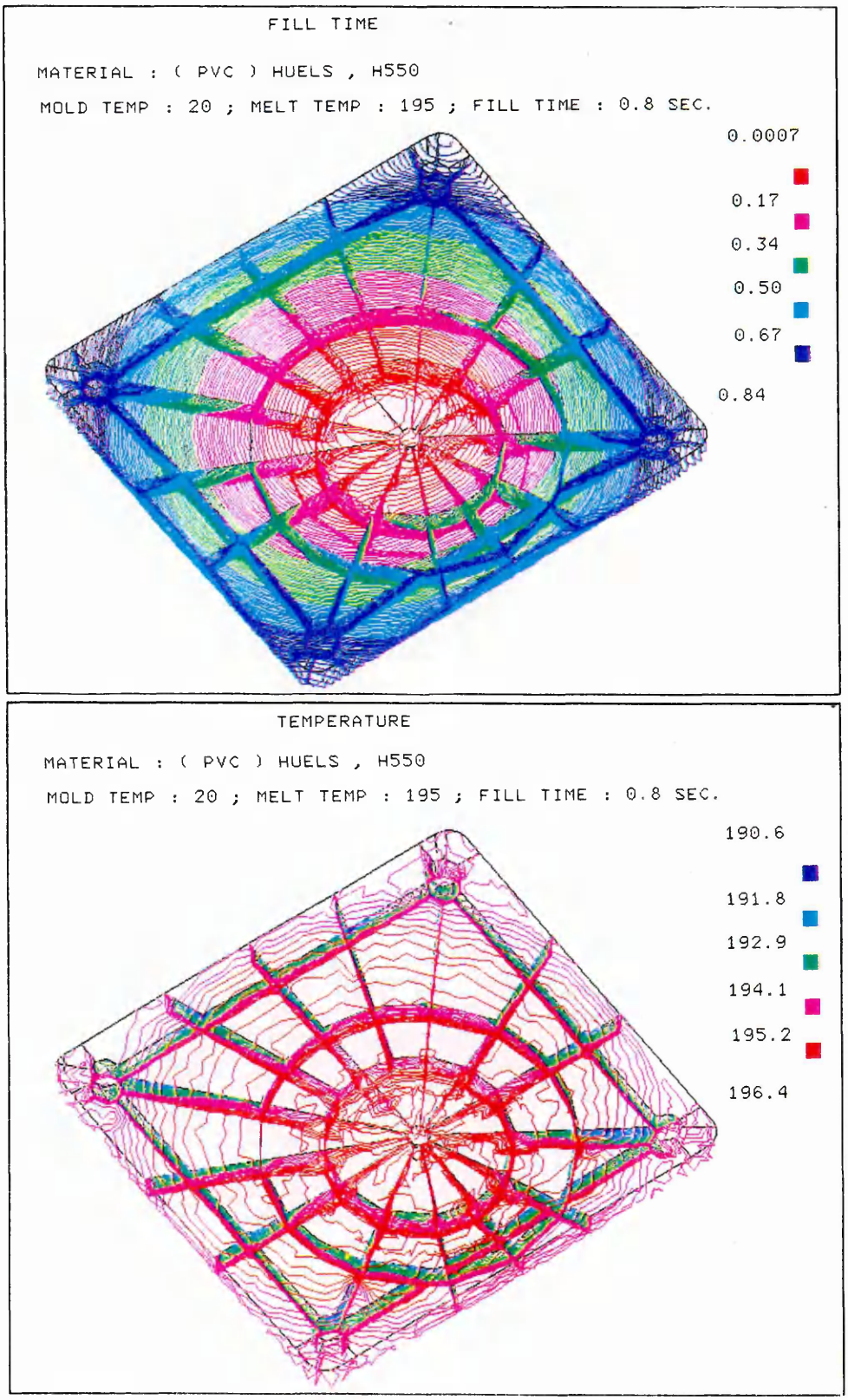

Fig.7.3.4. Filling pattern and temperature field.(Original colour pictures)

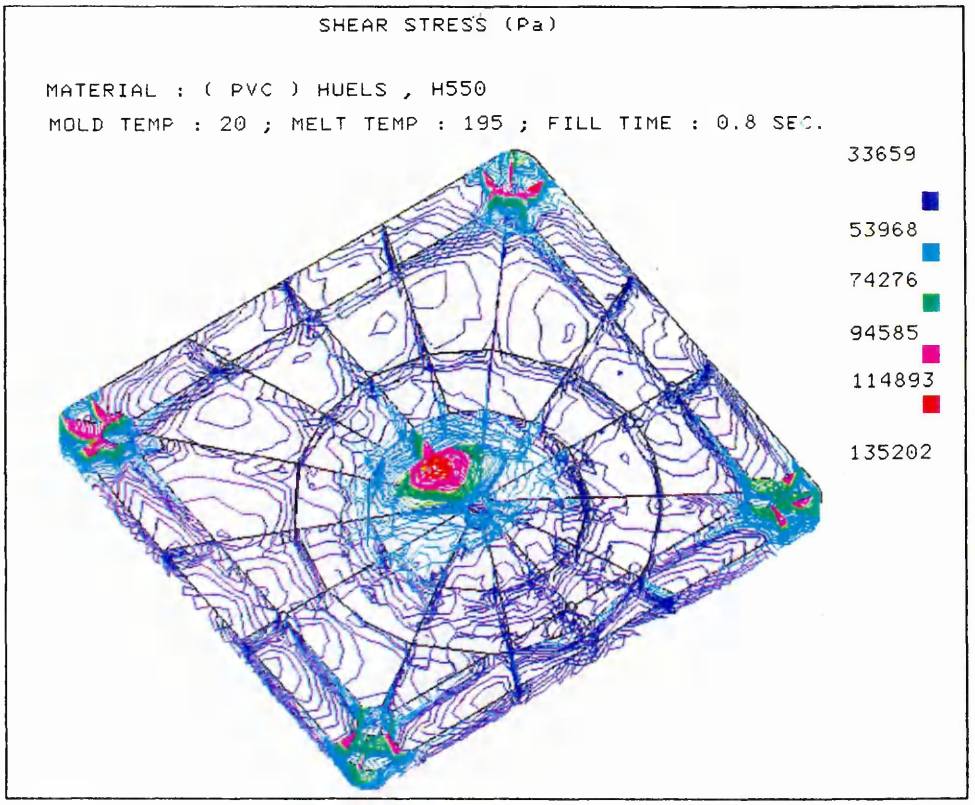

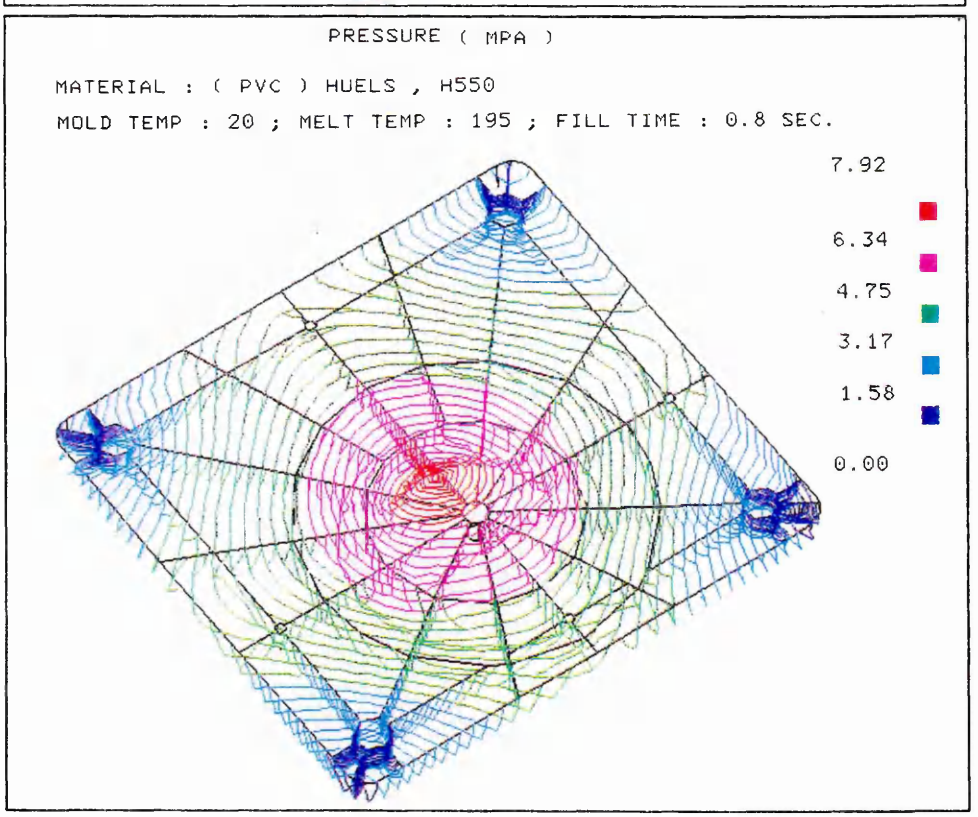

Fig. 7.3.5. Shear stress and pressure distribution
(Original colour pictures)

All the stress is less than the limit given above (150,000 pa). Clearly the four corners and the gate area are the high shear stress regions. The high

stressed ribs are not very important for this moulding, and the high stress in the gate area will quickly disappear after the packing stage starts. Two reasons contribute to the high stressed corner regions: the first one is the higher viscosity caused by the cooler melt flow through the longer paths than elsewhere; the other is the geometrical complexity in the corners which results in already cooler melt flowing at higher shear-rate than elsewhere. The pressure field at the end of filling indicates the gate position is quite ideal for uniform filling, as the four corners have been reached at the same time. This position is the result of previous trials since the original gate position caused uneven filling and higher stresses in the top corners, though it was in the centre of the rectangle.

7.3.4 Results of Moulding with EV103

The processing conditions for moulding material EV103 are much more difficult to find, though the shear stress limit is 50,000 higher than that of H550. The result from 2D scanning for processing conditions are listed below:

Table 7.3.4

MOLD TEMP 20.00 deg C MELT TEMP 205.00 deg C

TIME sec	PRESSURE MPa	STRESS @ START	STRESS @ END	TEMP @ END
0.20	27.9	371287.	132044.	217.
0.30	25.2	339837.	119224.	215.
0.50	21.9	299011.	104457.	212.
0.70	19.9	272165.	95888.	210.
1.00	17.9	244333.	88104.	208.
1.50	15.8	214044.	81288.	204.
2.00	14.4	193718.	78100.	201.
2.50	13.5	178736.	76809.	197.
3.00	12.9	167051.	76692.	194.
4.00	12.0	149695.	78702.	189.
5.00	11.5	137189.	82734.	184.
7.00	11.2	119969.	95111.	174.
10.00	11.5	103910.	123441.	161.
15.00	14.4	88413.	222962.	143.

* PLASTIC FROZEN RUN ABORTED *

From this table it can be seen that the only possible filling time is range from 2.0 to 5.0 seconds. This is only rough estimate because the average thickness given is 3.5 mm, and there are much thinner ribs which could give less ending temperature and/or higher starting and ending shear stresses. If the melt temperatures were less than 205 °C, there would be almost no choice for "fill time". 205 °C is the highest starting melt temperature available for rigid PVC, and in the barrel, the temperature must be less than 200 °C because the material may stay there for several machine cycles, the temperature higher than that for such a long time would result in PVC degrading. However, raising the melt temperature, according to the property of the PVC in table 7.3.2, can significantly reduce the viscosity, and subsequently reduce the stress level. One philosophy of MOLDFLOW is to use carefully designed feed system for frictional heating to give the same effect for lowering the stresses without degradation of the material. This philosophy is adopted here to raise the melt temperature up 13 °C through a deliberately designed sprue to reduce the stress level inside the cavity. The other cause for shear stress is the shear-rate which can be reduced by slowing down the filling rate when the filling is near the end. The viscosity is also a shear-rate dependent parameter, thus too low a shear-rate would also cause the increase of the stress level. Based on a compromised consideration, the filling rate profiling control technique is used. In general this control can also be regarded as a part of the ram position control in the whole cycle. MOLDFLOW supplies the filling rate profiling as is required for more practical flow analysis. In fact, near the end of filling, the melt will be squeezed into the corner extremities as shown schematically in Fig.7.3.6: the front speed would be accelerated anyway. If the original filling rate were maintained, the shear-rate in the

Table 7.3.5

Mold Temp: 20 °C	Volume%	% of Max Rate
Barrel Temp: 192 °C	80	95
Fill Time: 3.0 sec	85	88
Sprue Runner Size:	90	80
8x4x60 (mm)	95	70
Fill Rate Profile	97	65
	100	60

corners would be increased very quickly, and moreover, the temperature of the melt, after passing the longest flow path, might be lower than

elsewhere. The increase of viscosity caused by lower temperature with local increase of the shear-rate exaggerates the local shear stress level. Therefore the filling rate profile has to be carefully selected. After several simulation trials, the optimised processing condition is finally obtained as shown in table 7.3.5.

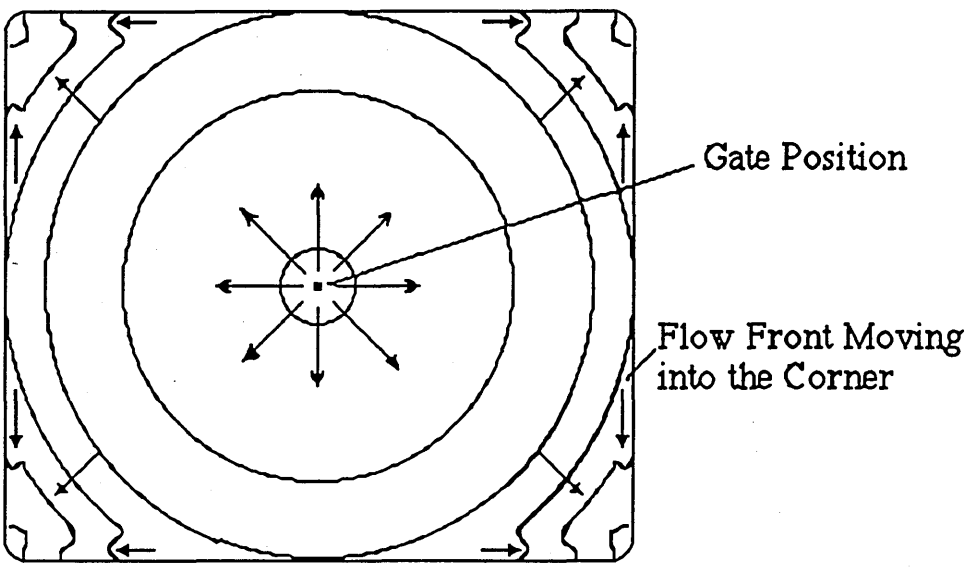

Fig. 7.3.6 The melt squeezing into corners

Under this set of conditions, the flow fronts as shown in Fig.7.3.7, by comparison with Fig.7.3.4, slow down when they reach the corners as they can be recognised by the density of the dark blue front lines. All the temperature is within 20 °C difference, and well distributed in the plate. The four corners are a few degrees lower because of the long distance from the gate. On the top of some ribs, it can be seen that the lowest temperature occurs, with danger of premature freezing and short shot if the melt temperature were not high enough. A few weld lines up in the top of some ribs can be detected by careful observation of the flow pattern. These weld lines are caused by the thickness difference between the plate and the ribs. The melt actually moves faster within the thick plate than it does in the thin ribs, and comes back to meet the slow-moving flow front in the thin ribs after it hits the side edges. The short-shot marks and weld lines can be seen clearly in the practical product (shown in Fig.7.3.1a). These weld lines or short shots would severely reduce the functions of the ribs which were designed to strengthen the plate. In fact, the thickness of the ribs has been thickened 0.75mm in the drawing (the original thickness was 1mm in the product), the effects should therefore not be so negative now. Thickening the ribs is a better and economic way to mitigate (or even eliminate) the

defects. The computer simulation here clearly demonstrates the capacity of prediction of the possible defects.

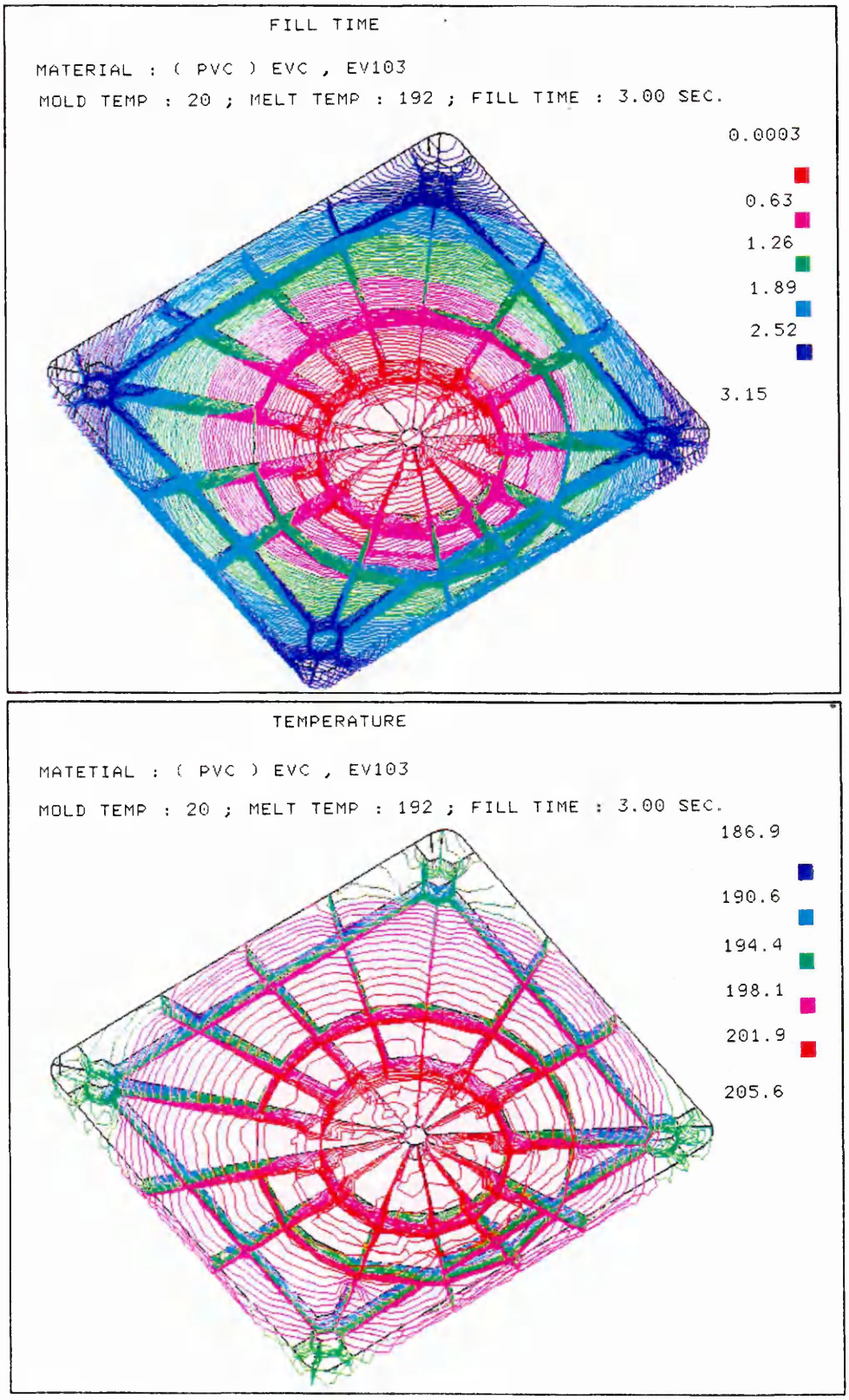

Fig.7.3.7. The filling pattern and temperature distribution. (Colour)

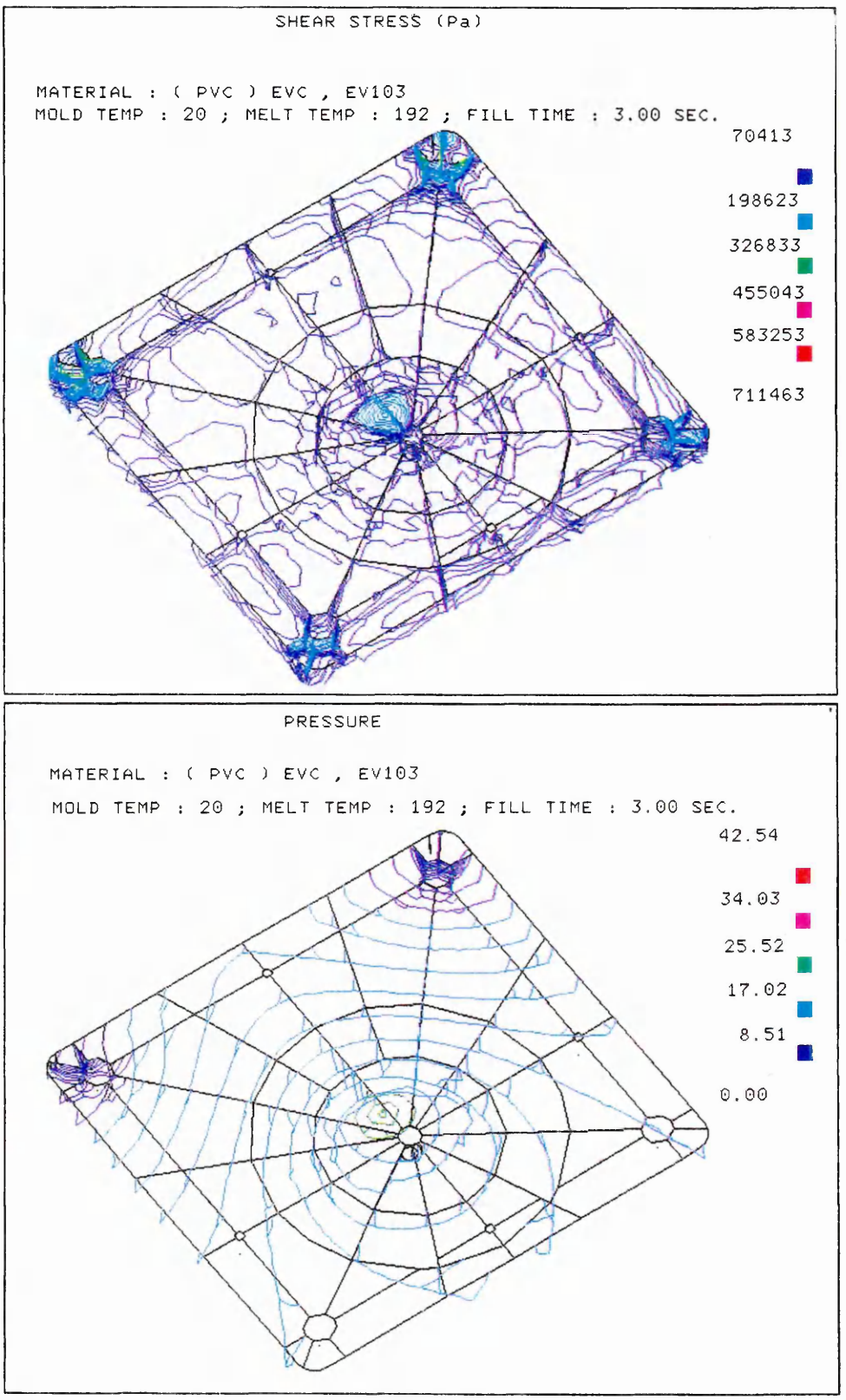

Fig.7.3.8. Shear stress and pressure distributions of part one.
(Original colour pictures)

From shear stress figures shown in the right column in Fig.7.3.8, it can be seen that the maximum shear stress is much higher than the limit

(200,000 pa), but most of the high stress area occurs inside the sprue runner in which the shear energy produced by the shear strain and stress has been contributed to the temperature increase, and the sprue runner will be cut off anyway since it is not part of the product. Except for the gate area and on the top of corner ribs, the stresses in the rest area are lower than the limit. The high stressed corner ribs will not cause much trouble if the temperatures there are high enough to ensure the flow into the extremities. The pressure distribution indicates the high pressure drop within the sprue runner, and the last bit to fill.

There are two other means which allow the processing control of this PVC moulding. One of them is to use hot-runner technology. This technology, which keeps the polymer heated throughout its passage from the barrel to the mould cavity, has been successfully employed with most polymers. However, temperature control problems and other restrictions like flow path blocking, along with high cost have made it difficult to apply the hot-runner technology to PVC mouldings. In recent years, significant developments have been made, and in many cases the difficulties mentioned above have been minimised or avoided entirely. Among them, the use of a titanium insert at the gate makes for a hotter gate and eliminates the need for polymer insulation and the possibility of degradation. Others include a variety of cartridge-, and band-, or coil-heated machine nozzles, sprue bushings, manifolds, and probes, heat pipes gate shut-off devices and electronic controllers for these heating elements. With these new developments, it is possible to control the melt under precise temperatures needed until it reaches the gate area. The rest of the cavity filling is the exactly the same as the results of starting with a melt temperature at 205 °C.

The other method to give better controls over the temperature and shear stress level is to re-profile the wall thickness of the plate. The approach will be explained in Chapter Eight.

7.4 Simulation on a Computer Part with Polycarbonate

A second example is the pivot plate which is used on the plate base underneath the monitor shown in Fig. 7.3.1b. The material indicated for this part is medium grade (or high grade) polycarbonate (PC), and it must be UV stabilised.

7.4.1 Material Aspect

Polycarbonate is based on bisphenol A and has an aromatic structure. It is this structure that is responsible for the high softening temperature, broad temperature usage, rigidity complemented by toughness, and the most important property, especially for this moulding, is its resistance to creep when under the design loads for a long time. It may be fabricated with a very smooth surface, but it has limited scratch and abrasion resistance. This problem is compounded by moisture and ultraviolet light so that UV resistance material required for this part. The most critical property of polycarbonate in the injection moulding process is the hydrolysis. At processing temperature, moisture promotes a hydrolytic attack on polycarbonate, resulting in a degradation of the polymer. The effects of this degradation can be visualised as streaks on the surface, and some small bubbles in the body which is a result of the generation of a gaseous degradation by-product, carbon dioxide.

Polycarbonates that are suitable for injection moulding generally fall into the average molecular weight range of 26,000 to 35,000. Molecular weights higher than the upper limit of this range tend to be difficult to process because of high melt viscosity. Since the viscosity increases as molecular weight increases, the medium grade of the molecular weight is chosen to simulate this moulding. Because of its high viscosity, polycarbonate is usually processed at a high temperature in order to obtain a less viscous melt. This requires both high barrel temperature and high injection force capabilities. In MOLDFLOW's guide menu, the material data for processing polycarbonate are 280-320 °C for barrel temperature, 60 °C for mould temperature, 500,000 Pa for the shear stress limitation, and the maximum shear-rate not higher than 40,000 1/s. Table 7.4.1 lists the properties of the material chosen from MATDB.

Table 7.4.1
ENICHEM
Material Grade Description

E107 PC SINVET 253-253\R ENICHEM MED VIS UV RESIS.1&2DATA MAY84
Material Grade Data

CONDUCTIVITY	J/(m.sec.degC)	==>	0.105
SPECIFIC HEAT	J/(kg.degC)	==>	1531.
DENSITY	kg/cu.m	==>	1040.
FREEZE TEMPERATURE	degC	==>	160.0
NO-FLOW TEMPERATURE	degC	==>	200.0

(continued in next page)

VISCOSITY

TEMPERATURE degC	SHEAR RATE 1/sec	VISCOSITY Pa.sec
280.0	1000.	496.9
300.0	100.0	495.5
300.0	1000.	324.3
300.0	1.000E+04	101.0
320.0	100.0	219.9
320.0	1000.	186.2

7.4.2 Geometric Aspect

The surface model generation of the geometry of this part is beyond the capacity of MOLDFLOW's pre-processor. The main difficulties are to generate the spherical surface piece accurately, and to give its intersection

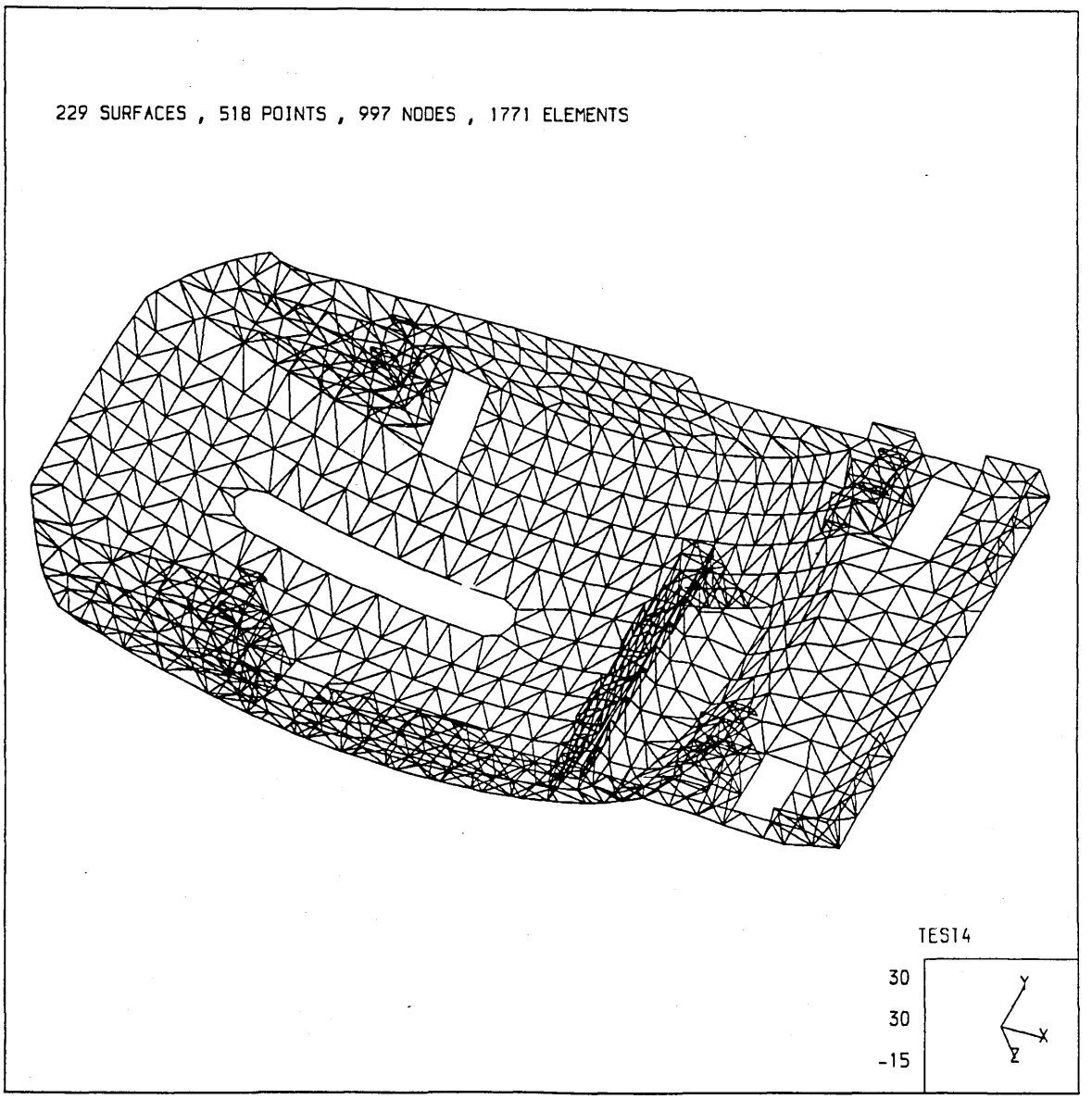

7.4.1 Finite element mesh of the geometry

curves with other surfaces. In order to compensate the capacity, some functions are established in CASIM's pre-processor, which can provide a piece of spherical surface as detail as possible, and produce any spatial curves formed by two intersected spatial surfaces. Detail of the method is introduced in next chapter.

The piece of spherical surface is cut off from a sphere by five planes, then eleven other planes are used to give the locations of holes on the spherical surface. With the rest surfaces being connected, the surface model of the geometry is completed as shown in Fig.7.4.1.

7.4.3 Processing Conditions

The rough processing conditions can be found in the same way as introduced in the last section. The "autofile" is used again to give a window of the conditions. The upper bounds of both mould and melt temperatures are chosen for the filling time scanning, and the lower bond of the filling time is 2.4 seconds. This lower bond has to be further confirmed by using 3D finite element analysis.

7.4.4 Result analysis

The gate is positioned near the centre by one end of the guide slot as shown in Fig.7.4.2. The longest flow path is to the down-right corner. From the flow pattern diagram it can be seen that some weld lines are formed by meetings of fronts enclosing holes. However, the biggest weld line is behind the big insert where the flow is slowed down by the thinner and more complicated path. Two flow streams surrounding the insert from both sides and the stream passing through the insert area join together just in the middle behind the insert. This weld line can be seen clearly from the practical product shown in Fig.7.3.1b. This proves the correct prediction by the simulation. The temperatures at these weld lines' areas shown in the lower half of Fig.7.4.2 are high enough for the fronts to "weld" together. Although the strength of the weld lines is never as high as the strength of the rest area, as mentioned in Chapter One, the positions of the weld lines do not harm much of the structure. The only potential crack may happen in the weld line on the other end of the guide slot, as the stress concentration there may reach a figure higher than the strength limitation of the weld line.

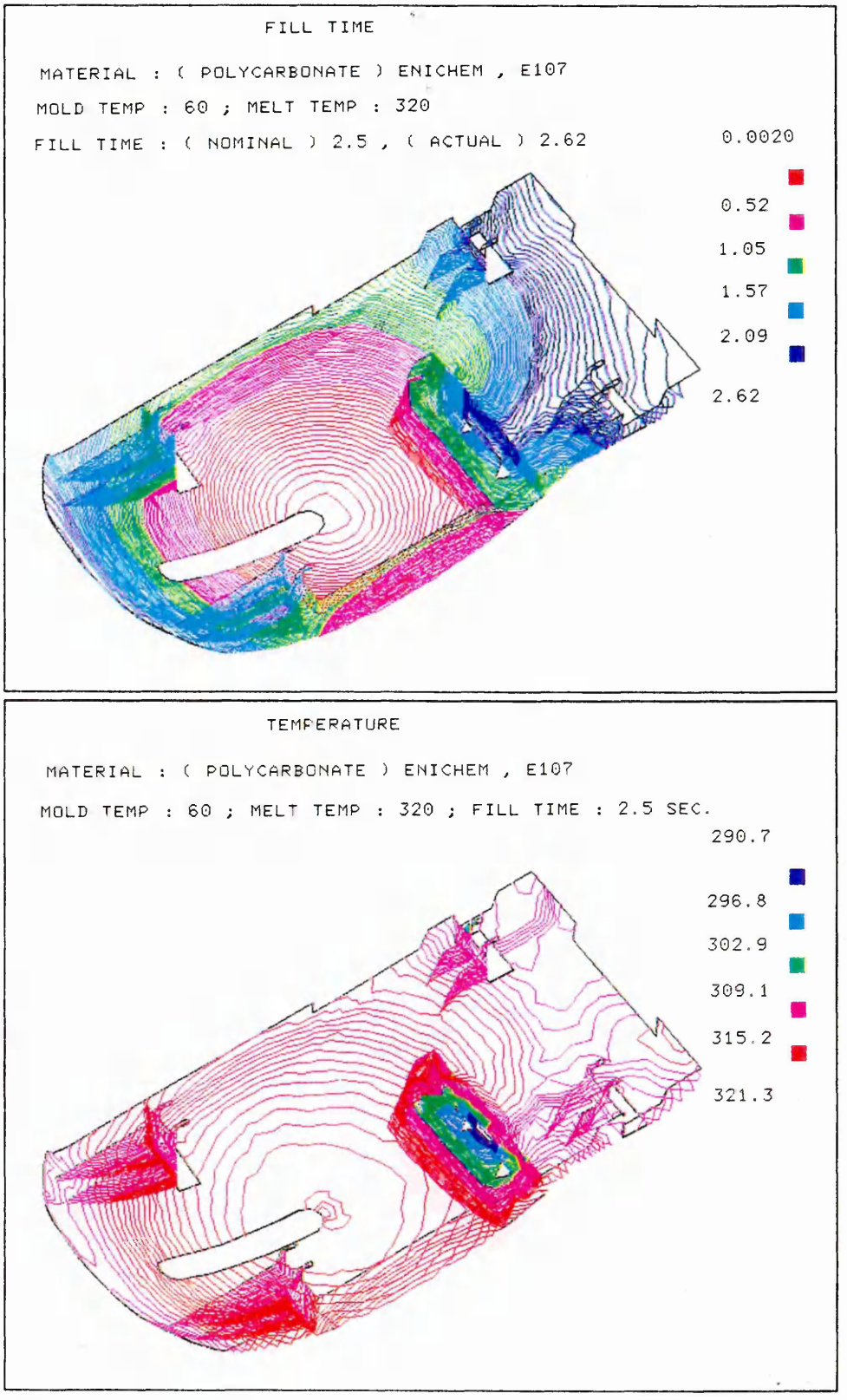

Fig.7.4.2. The flow pattern and temperature distribution.
(Original colour pictures)

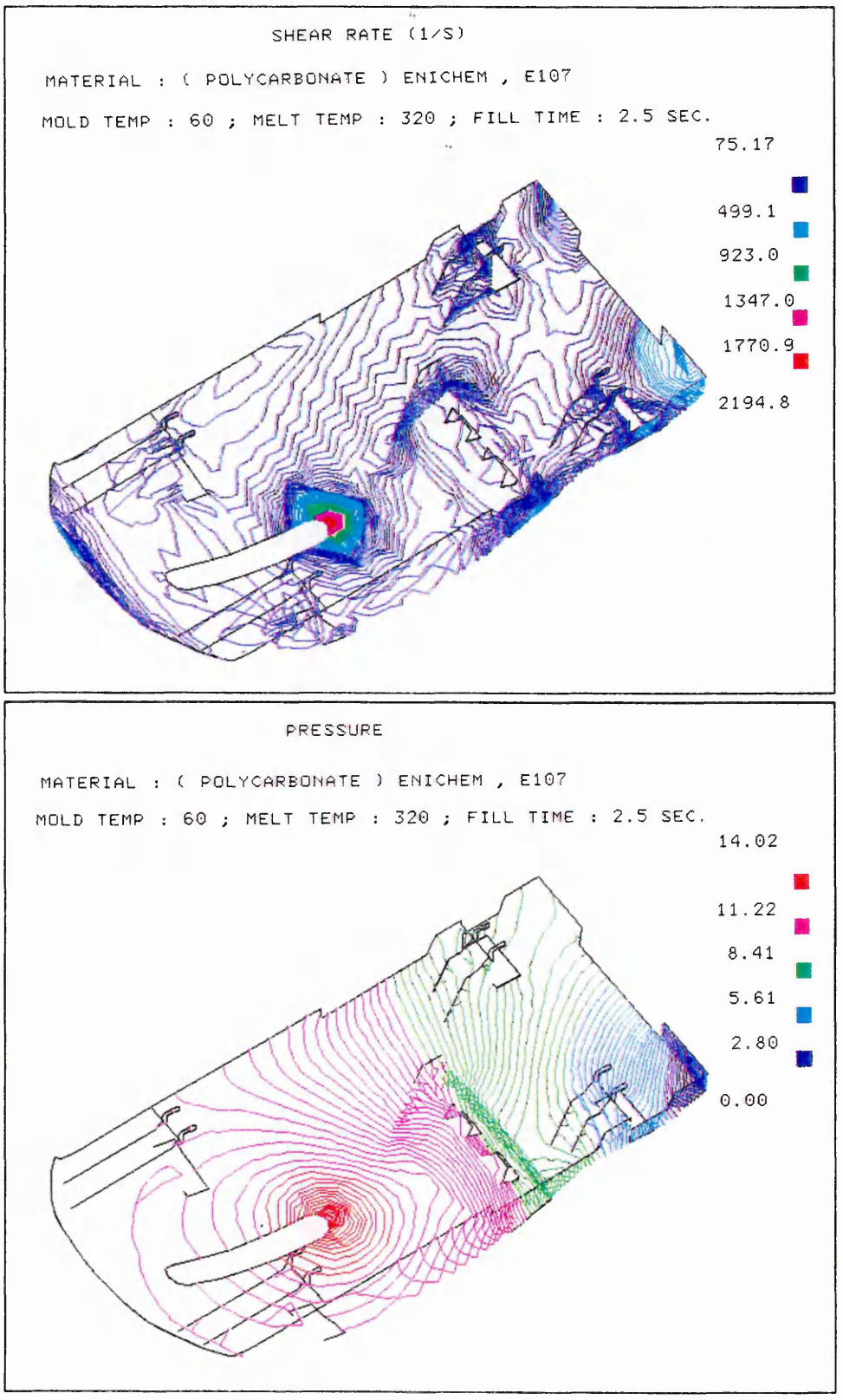

Fig.7.4.3 The shear strain rate and pressure distributions.
(Original colour pictures)

The lowest temperature is in the thin insert area in the centre, since the slow-moving of the flow and quick-cooling from both sides. It could be

potential area of hesitation effect if the thickness was designed thinner. The temperature falls into the range between 302.8 and 320.4 °C in the front during the filling stage, 290.7 and 321.3 in the cavity just after the filling finishes. These can be regarded as desirable ranges.

All the shear stress and shear strain rate are less than the limitation in the component. Because they have very similar distribution in the cavity, only the colour graph of shear strain rate is shown here. The laser-printed shear stress distribution by contour lines is shown in Fig.7.4.4. The high stressed area near the gate is caused by the high shear-rate as the material deforms the most at the area just under the gate. Because the high stressed area is only a tiny part of the whole component, and it can be soon reduced in the packing stage, it is harmless at all.

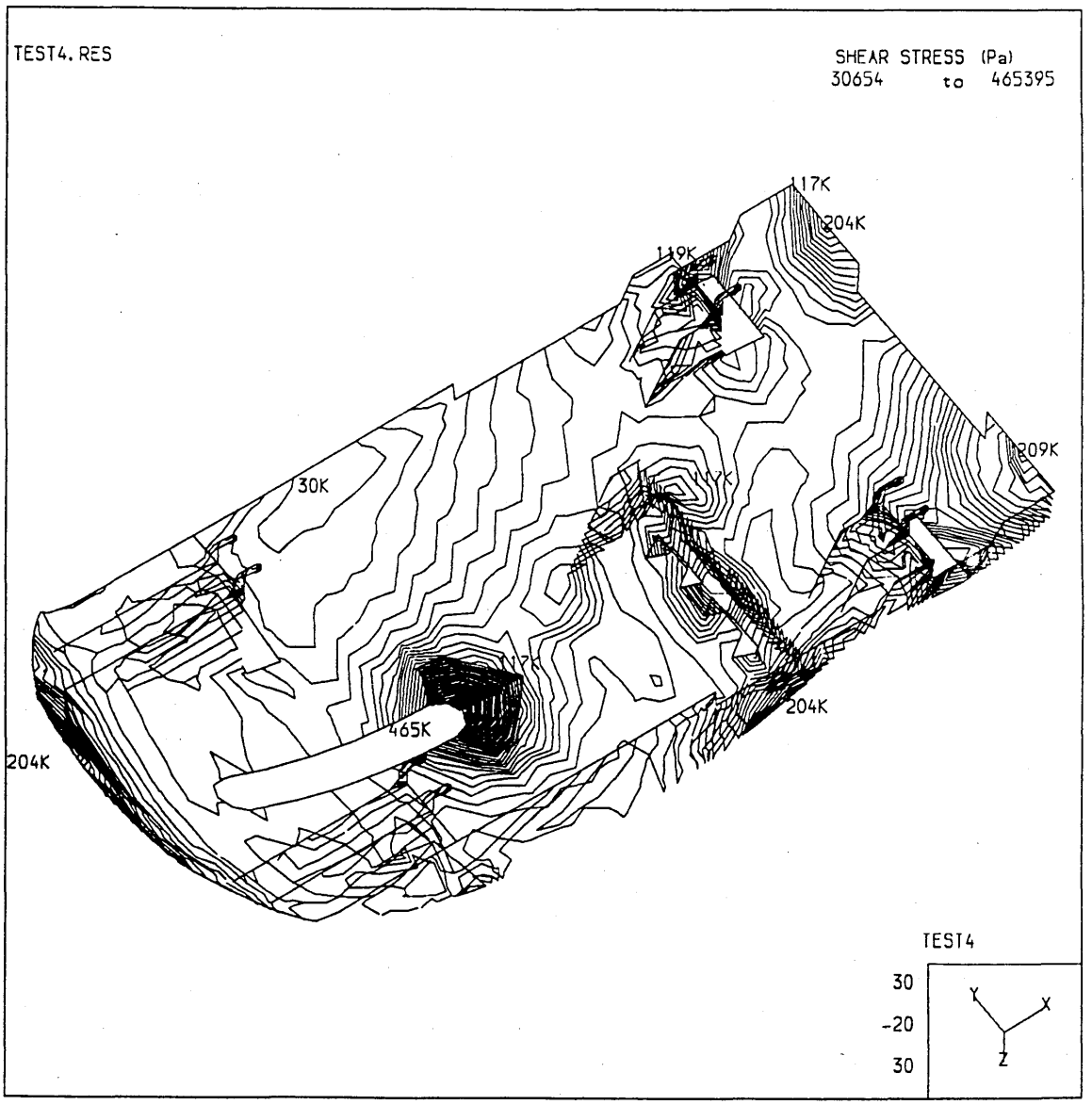

Fig.7.4.4. The shear stress distribution of part two.(PostScript picture)

7.5 Balancing a Feed System for a Set of Computer Parts

7.5.1 Introduction to balancing a feed system

Balancing a feed system means that by adjusting the dimensions of a feed system the plastic melt is ensured to reach each extremities at the same time so that all the impressions will be filled uniformly and evenly. However, balancing a feed system is very difficult for some family moulds. In general practice the majority of the feed systems are naturally balanced. Designers always try to avoid artificially balancing the feed systems for multi-cavity layouts. Fig.7.5.1 shows some examples of balanced runner systems for multi-impression mould. It is easy to situate the impressions on a pitch circle diameter and feed each impression directly from the sprue via a runner system.

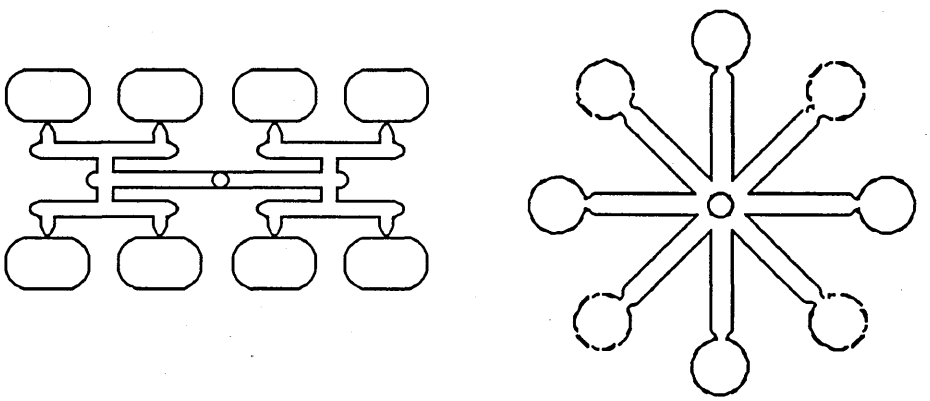

Fig.7.5.1. Naturally balanced feed systems

For tooling and economic reasons, sometimes partially balanced runner systems are used for multi-impression mould like those shown in Fig. 7.5.2 which need artificial balancing for the main runner or the sub-runner systems.

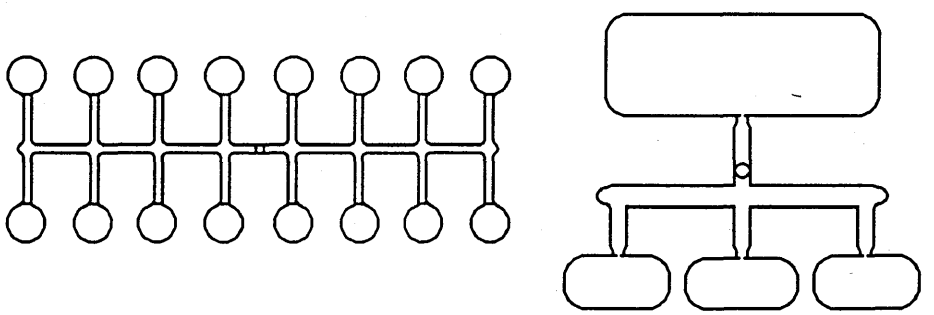

Fig.7.5.2 Partially balanced feed system

However, it is mandatory to balance some family moulds like the one to be shown in this section, and it is worth doing it because such a kind of complete set is better to be manufactured locally in a family mould rather than to be made separately in different moulds or even in different factories. From the moulding point of view, it is better to use the same moulding conditions, the same colour of the material in a set of moulds for a family of components which will be used together. If the balancing problem can be easily resolved, such family mouldings can obviously bring economic advantages.

Normally, conventional feed system balancing is often on-line and a matter of trial and error, and in most of the cases the balancing can only be achieved by varying the gate dimensions. It becomes possible when high efficient computer software systems are introduced to simulate the injection moulding processing. According to the MOLDFLOW philosophy[6] the runner dimensions are better to be chosen to balance the feed system instead of the gate dimensions because of four reasons:

a) The pressure drop over the gate can be heat-transfer dominated, so any small change in moulding conditions gives a large change in filling pattern.

b) Gates are very prone to hesitation effects.

c) Entrance and exit losses, which tend to be very unstable, form a high proportion of the total pressure drop.

d) Machining errors or wear have a major effect on pressure drops.

The size of a runner system is much larger than that of a gate, thus less sensitive to the hesitation and thermal effects, more stable and easier to machine accurately. Often there are two major variables to vary for the balancing (i) by varying the length and (ii) by varying the cross section. However, these can be generalised as the dimensional changings. There could be shape variations of a runner system. No matter which variable of the runner geometry varies, the aim is to balance within certain restrictions. Therefore a principle and some concepts should be introduced.

7.5.2 Balancing Principle and Some Criteria

Principle:

Under the same conditions, a balanced system must have the minimum energy lost.

This is generalised energy principle which can be used in balancing runner system as well as gating design. For balancing a runner system, one can deducte this principle as a more practical one: **Under the same processing conditions, for the case of varying a single variable of a runner system, the correspondent pressure at any point of an unchanged section is a single smooth valley function of the variable.**

This deduction gives an easy way to find out a balanced system by varying only one variable of the geometry. Fortunately, there are many methods for searching for the valley position of the function, so the problem is which way to choose for such a time-consuming calculation or expensive on-line trials.

If the form of the function could be found out, then it would be a simple calculation. Yet the function depends on the geometry of the feed system and cavities, on the properties of the plastic material to be used and on the processing conditions, and it is a high non-linear function of the variable.

This is, however, not sufficient to find out a best balanced runner system for a moulding because the geometry of a runner system can be any form and some other criteria must be given.

a) The cost of the material in the runner system should be as low as possible.

b) The cooling time for the runner system, if it dominates the cycle time (which is often the case), must be as short as possible.

c) In order to make use of the runner system to control the moulding process, i.e. the flow pattern, frictional heating and thermal shut off, the pressure drop along the runner system must be high enough. It is suggested that the total pressure drop, (cavity plus runners), is 70% of the maximum available injection pressure.

d) The processing window of moulding conditions should be large enough to bear the possible slight off-setting. This means that the valley point of the function will not move for a slight change of the processing conditions.

e) The way of ejecting the parts and runners must be taken into account.

7.5.3 Material and geometrical aspects of the parts

The parts for the feed system balancing analysis in the following sections are two housing components of an eight inch disc drive (Part No. 23F2210

and 23F2220) as shown in Fig.7.5.4-5. Although both components are geometrically complicated, for economic, appearance and other reasons, they are supposed to be moulded in a family mould. Therefore not only the optimised processing conditions for the moulding but also a balanced feed system have to be found.

The material indicated for them can be either BAYBLEND 1439 or BAYBLEND 1441 (B1439, B1441 for short in the following). These ABS/PC blend materials have characteristics intermediate between ABS and Polycarbonate. The principal advantageous characteristics include:

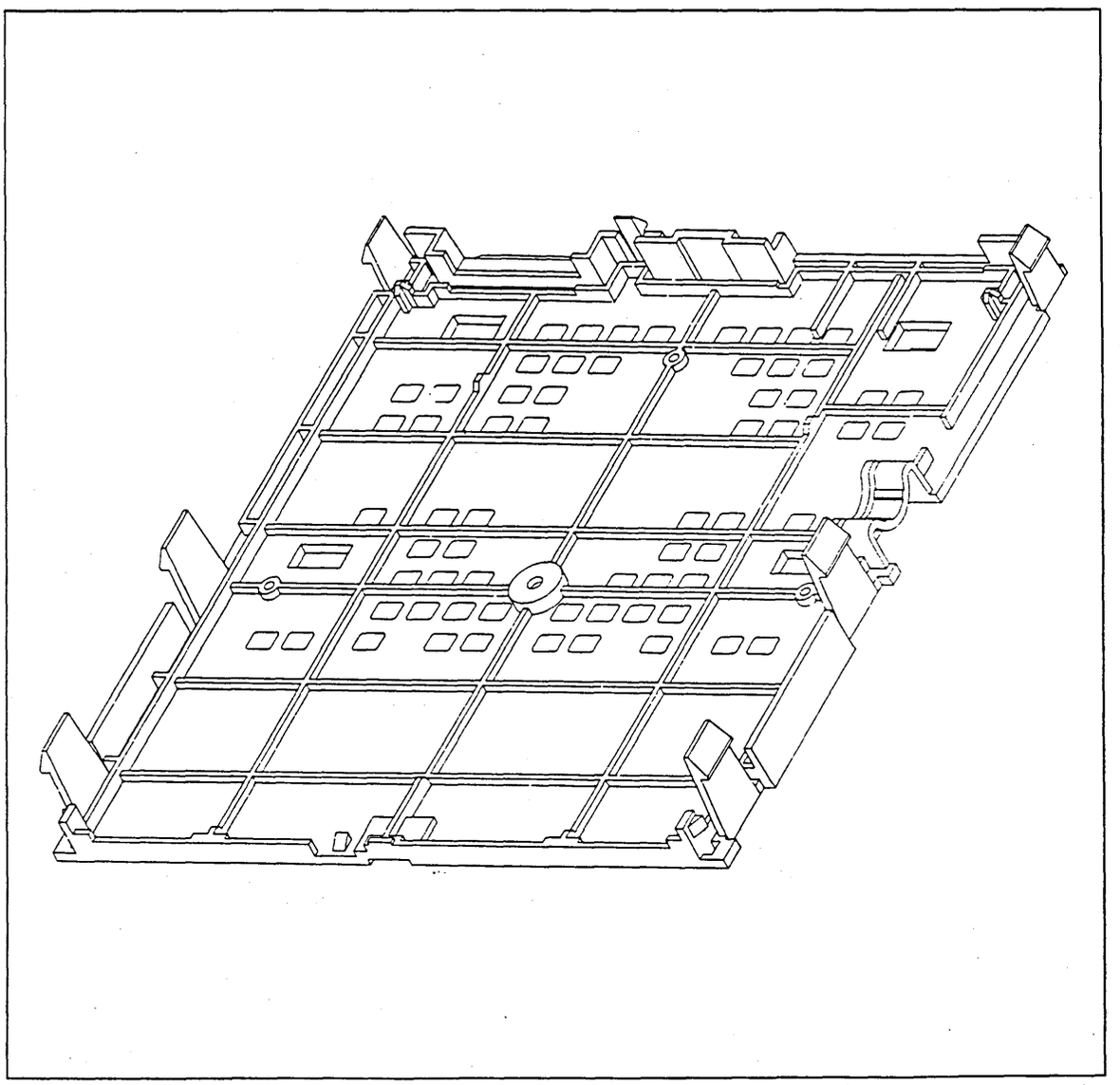

Fig.7.5.4. The geometry of Part One

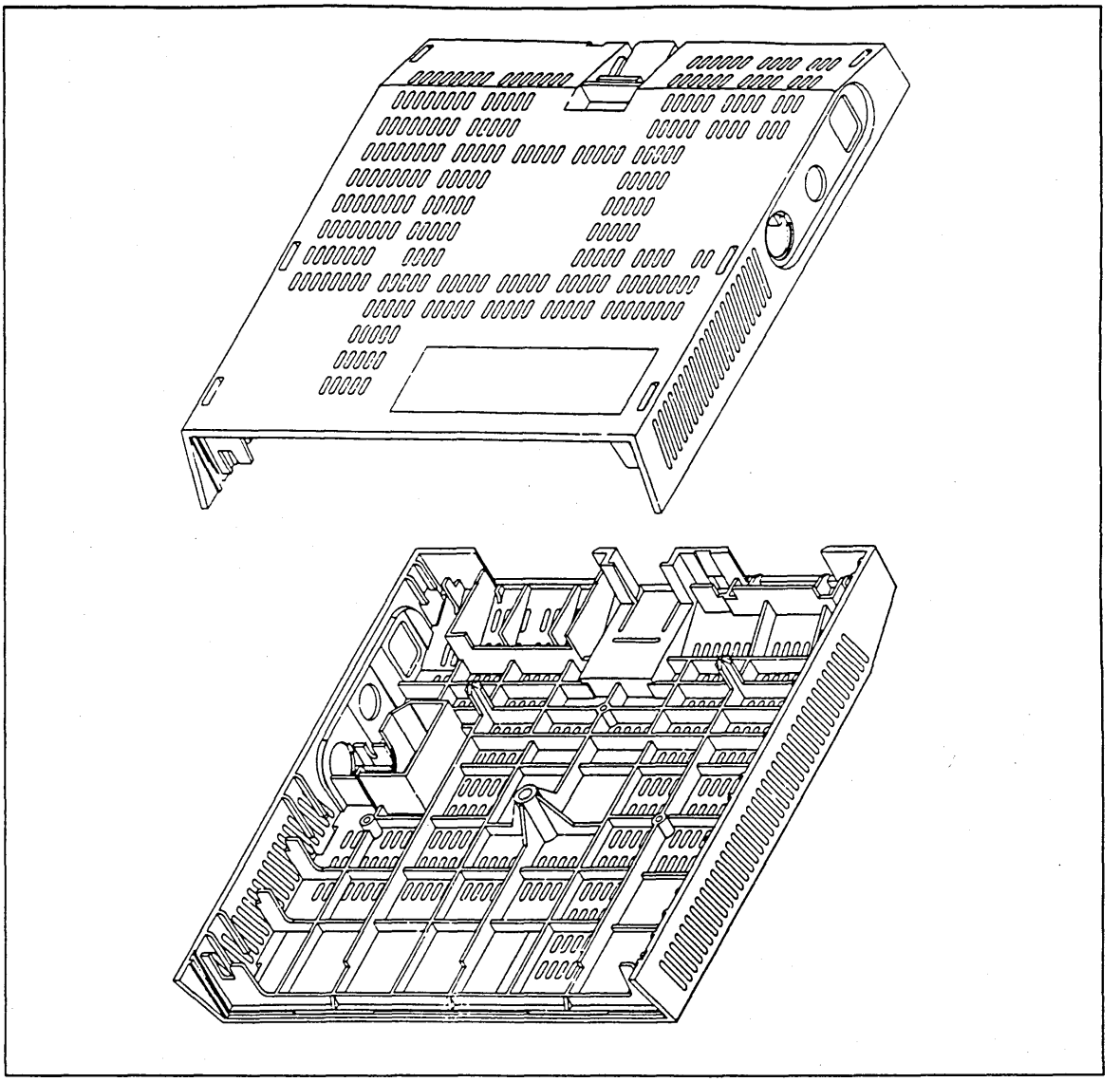

Fig. 7.5.5 The geometry of Part Two

*High impact strength and hardness
*Improved heat distortion temperature compared to ABS
*Dimensional stability
*Electrical properties independent of moisture and temperature.

However, these properties can be affected by different processing conditions. In some situations the effects can be considerable. Therefore it is just as important to choose the correct moulding conditions as it is to pick the right material; both are critical in determining the part mechanical properties. The moulding related properties of both B1439 and B1441 are given as follows:

Table 7.5.1. Moulding Properties of BAYBLEND 1439 & 1441

Major properties:

Property	Units	ABS/PC
Conductivity	J/m/sec/DegC	0.16
Specific Heat	J/kg/DegC	1730
Density	kg / cu.m	981.0
Freeze Temp	DegC	154.0
No-flow Temp	DegC	188.0
Barrel Temp	DegC	220-260
Mold Temp	DegC	30-60
Max Process Temp	DegC	280
Max Shear Stress	k.pa	300
Max Shear Rate	1 / sec	5000

Viscosity:

	Temp(C)	Shear Rate(1/s)	Viscosity
1439	240	1000.	203.3
	260	100.	348.0
	260	1000.	134.6
	260	10000.	37.09
	280	100.	216.9
	280	1000.	98.0
1441	240	1000.	342.2
	260	100.	692.4
	260	1000.	232.5
	260	10000.	61.35
	280	100.	458.7
	280	1000.	159.9

The major difference between B1439 and B1441 is between their viscosities. Since the viscosity of B1441 is much higher than that of B1439, and high shear stress is hardly avoided for this complicated geometry, it would be much more difficult to process the injection moulding with B1441. The high stressed areas can detract from the strength by a considerable amount (at least 10% to 20%), and it is obvious that for the first component, the corner snap-hooks are designed to bear high bending stresses. Yet they are the longest paths from the gate which must cause considerable high stress when the melt reaches these corner snap-hooks. What is worse, the cooling holes are designed on the ways to these extremities which make the paths even more tortuous. Therefore, high shear stresses are inevitable in these corner hooks. From material selection point of view, B1439 must be chosen as the material for these two mouldings, because its lower viscosity can lessen the high stressed situation.

The table also gives a window of melt (or barrel) temperature and mould temperature. However, the practical processing conditions have to be determined by the filling analysis because of the geometrical complexity. The key point can be found from this table for the mouldings, which is also one of the general characteristics of the polymer viscosity: the higher the temperature and the shear rate, the less the viscosity will be.

From geometrical point of view, it can be seen that the length of the path from machine nozzle to the extreme "out" position of the cavities is quite long, thus it demands a mould temperature at the upper bound of the range. Because of many holes in both parts there must be weld lines formed by the

meeting of fronts surrounding each hole. A higher mould temperature will give stronger weld lines, lower stress levels as well as glossier appearance. From above table it can be seen that the mould temperature can be fixed at 60 °C.

After setting down the mould temperature, the melt temperature and filling time can be roughly found out by 2D analysis in MOLDFLOW. (Although there is a function to balance a feed system in 2D analysis program, for these two complicated geometry, the function can not give accurate dimensions of the feed system.) A tiny error in dimensions of the feed system could result in the family moulding unbalance. Because of these reasons, before starting to design and balance the feed system, each part is analysed first separately, and the processing window is tested individually. The common section of the two processing windows can then be used as the initial processing conditions for the family moulding. The lists below show that the processing window for the first part can be in a small range from 260 °C to 280 °C in melt temperature and 1.5 to 3.0 seconds in filling time.

Table 7.5.2

MOLD TEMP 60.00 deg C MELT TEMP 280.00 deg C

TIME sec	PRESSURE MPa	STRESS @ START	STRESS @ END	TEMP @ END
0.20	22.2	193467.	127651.	291.
0.30	18.1	155832.	104310.	287.
0.50	14.0	117272.	81426.	283.
0.70	11.9	96628.	69856.	279.
1.00	10.0	78339.	60406.	275.
1.50	8.4	61468.	53175.	269.
2.00	7.5	51693.	50538.	264.
2.50	7.1	45216.	50523.	259.
3.00	6.9	40571.	51472.	254.
4.00	6.8	34312.	57338.	245.
5.00	7.2	30275.	67266.	236.
7.00	8.9	25393.	101126.	221.
10.00	15.1	21649.	208705.	203.

* PLASTIC FROZEN RUN ABORTED *

Table 7.5.3
MOLD TEMP 60.00 deg C MELT TEMP 260.00 deg C

TIME sec	PRESSURE MPa	STRESS @ START	STRESS @ END	TEMP @ END
0.20	28.3	260561.	158376.	275.
0.30	23.9	215757.	134415.	271.
0.50	19.3	168155.	110185.	266.
0.70	16.8	141813.	97701.	263.
1.00	14.6	117870.	87543.	259.
1.50	12.6	95176.	80260.	253.
2.00	11.7	81716.	78465.	248.
2.50	11.2	72652.	79647.	243.
3.00	11.1	66075.	82880.	239.
4.00	11.3	57110.	94210.	231.
5.00	12.1	51270.	111577.	223.
7.00	15.5	44171.	167168.	210.
10.00	29.7	38790.	290572.	199.

* PLASTIC FROZEN RUN ABORTED *

Because of the complexity of the dimension, the shear stress during injection moulding can be higher inside sharp transitions in cross sections, and in the four snap-hooks in the corners. Therefore the 2D analysis is not enough to give reasonable accurate processing conditions, 3D finite element analysis is needed for more accurate results.

7.5.4 Result Analysis on Each Part

(a) Part One (23F2210)

The geometry of this part is quite complicated, there are cooling holes and ribs across the part so that the mesh has to be fine enough to calculate it accurately, especially in some areas as shown in Fig. 7.5.5. The most difficult areas to mould, from the flow pattern analysis, are the four corner hooks. They are extremities, their thicknesses are thinner and they will be subject to bending.

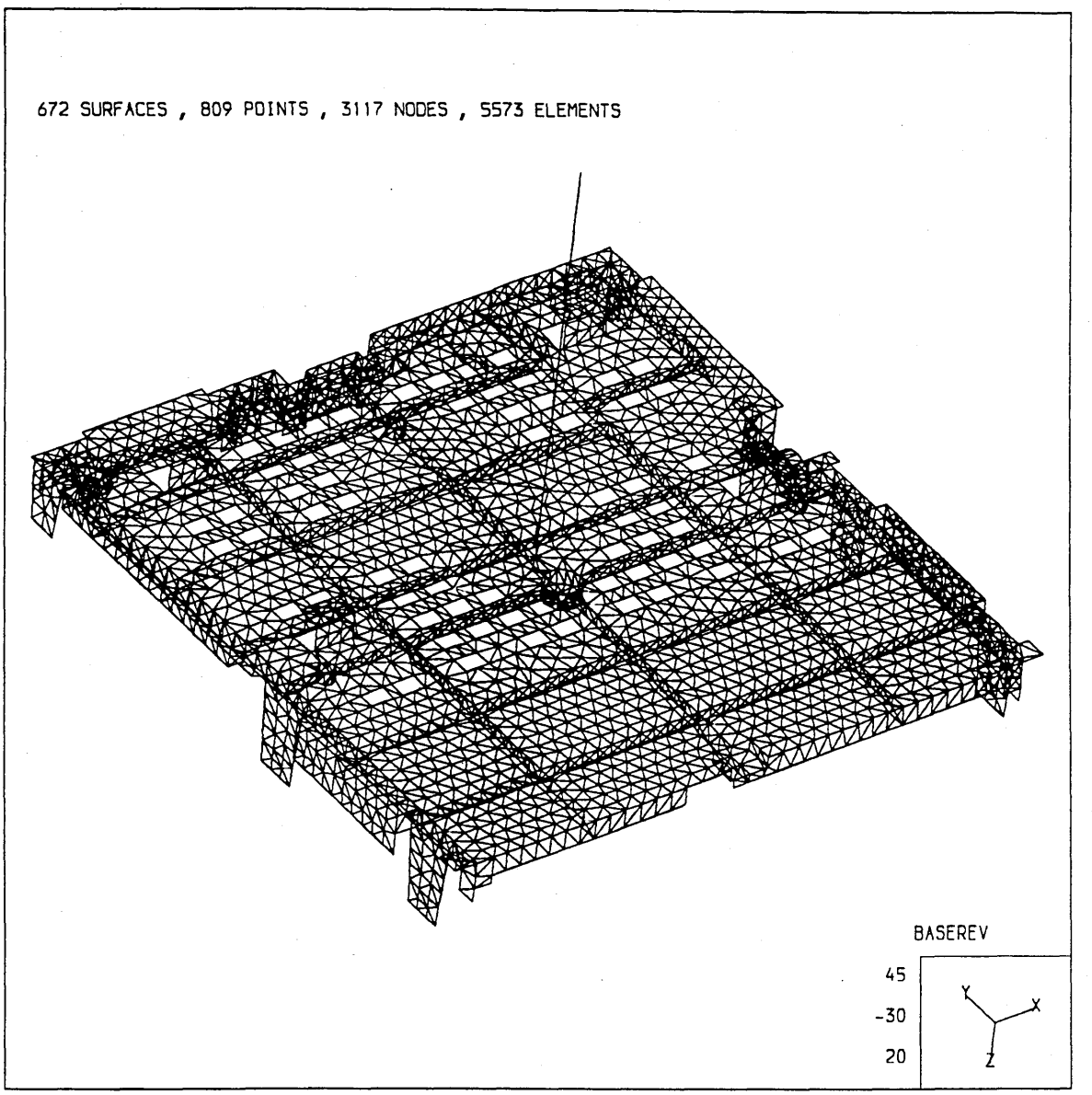

Fig. 7.5.5 The mesh of part one

The major factors which affect the temperature and the shear stress distributions are fill-time, melt temperature and flow rate profile. The profile of the flow rate, however, since it is assumed, cannot simulate the true processing situation but give an approximation result. The practical situation is that when the cavity has almost been filled, the flow rate begin to slow down. Therefore the flow rate profile is assumed as shown in Fig. 7.5.6 that the pressure inside the cavity is kept increasing and the ending flow rate is about 75% of the nominal flow rate.

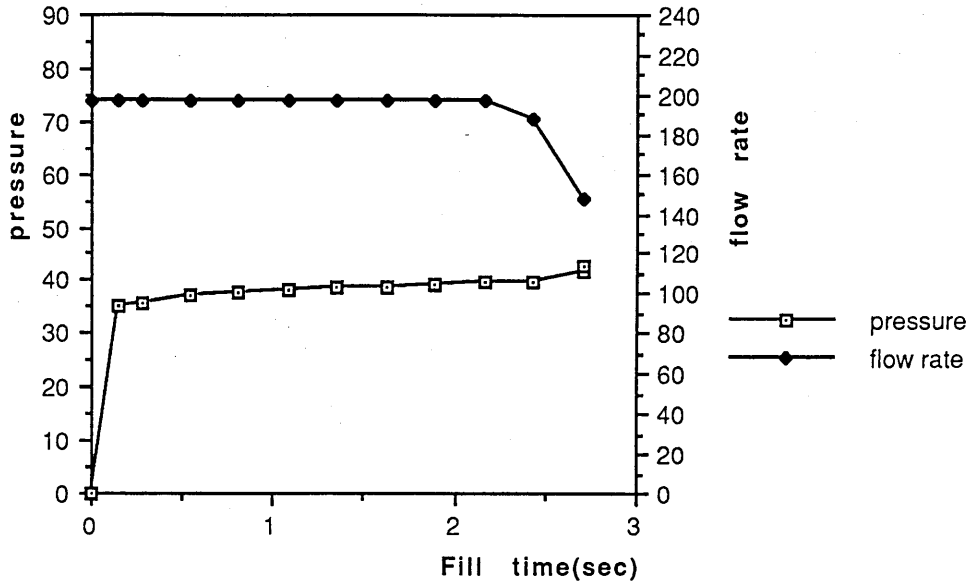

Fig.7.5.6 The flow rate profile and the corresponding pressure

The temperature and filling time effects on temperature range and maximum shear stress are given as shown in Fig. 7.5.7 and Fig. 7.5.8:

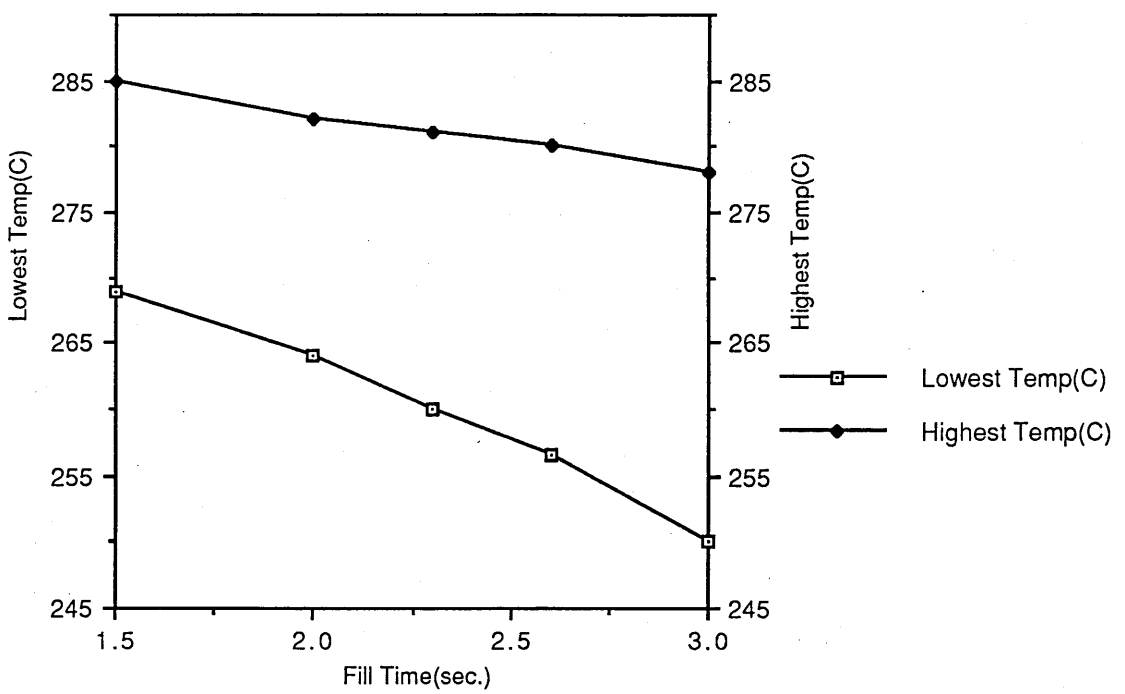

Fig. 7.5.7 Temperature range changes with the filling time

It can be seen that the shorter the filling time the smaller the temperature difference will be, but the maximum shear stress trend is a valley function, hence the processing window can be obviously chosen from the figures.

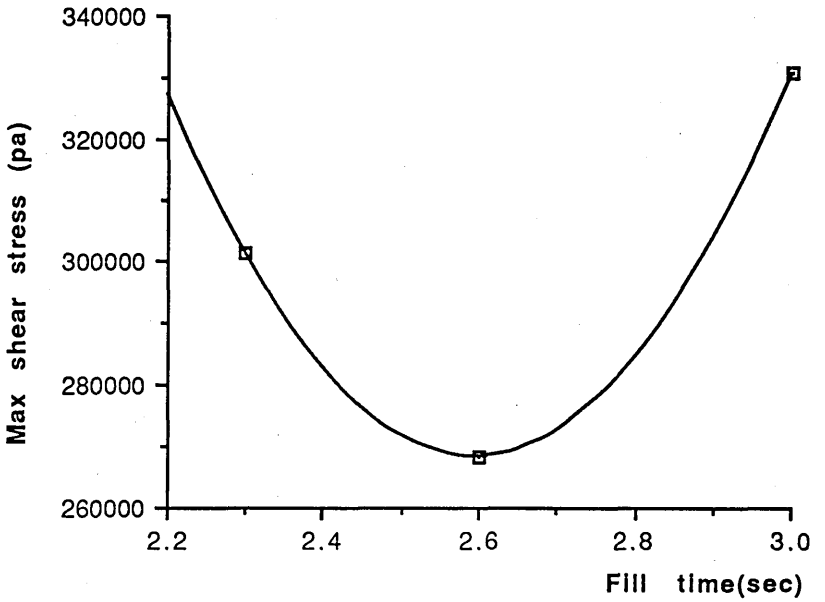

Fig. 7.5.8 The maximum shear stress changes with the filling time

The pictures shown in Fig.5.7.9-10 are the results of the moulding under the conditions as follows:

BARREL TEMPERATURE: 260 °C
MOULD TEMPERATURE: 60 °C
FILLING TIME: 2.6 SECOND

At first, it was found out that the maximum pressure needed for filling the part was only about 11Mpa. This means that the cavity pressure is not high, a runner system can be designed such that it can bear high pressure drop to control the flow. Thus a sprue runner is added to the cavity, its function is not only transfer the melt into the cavity but also control the flow. According to MOLDFLOW philosophy[6] that simply raising the barrel temperature will reduce stress levels, but will also give severe degradation problems because the plastic is then subject to a high temperature in the barrel for several machine cycles, a time measured in minutes. Using the frictional heating in the runner will give the same effect of lower stresses, but without risking degradation of the material, since the plastic is only subject to the higher melt temperature from the time it enters the runner system, until it starts to cool, a time measured in seconds.

The temperature is then within the range of 20 degrees except for the gate position. This is quite uniform distribution and satisfies the temperature requirements.

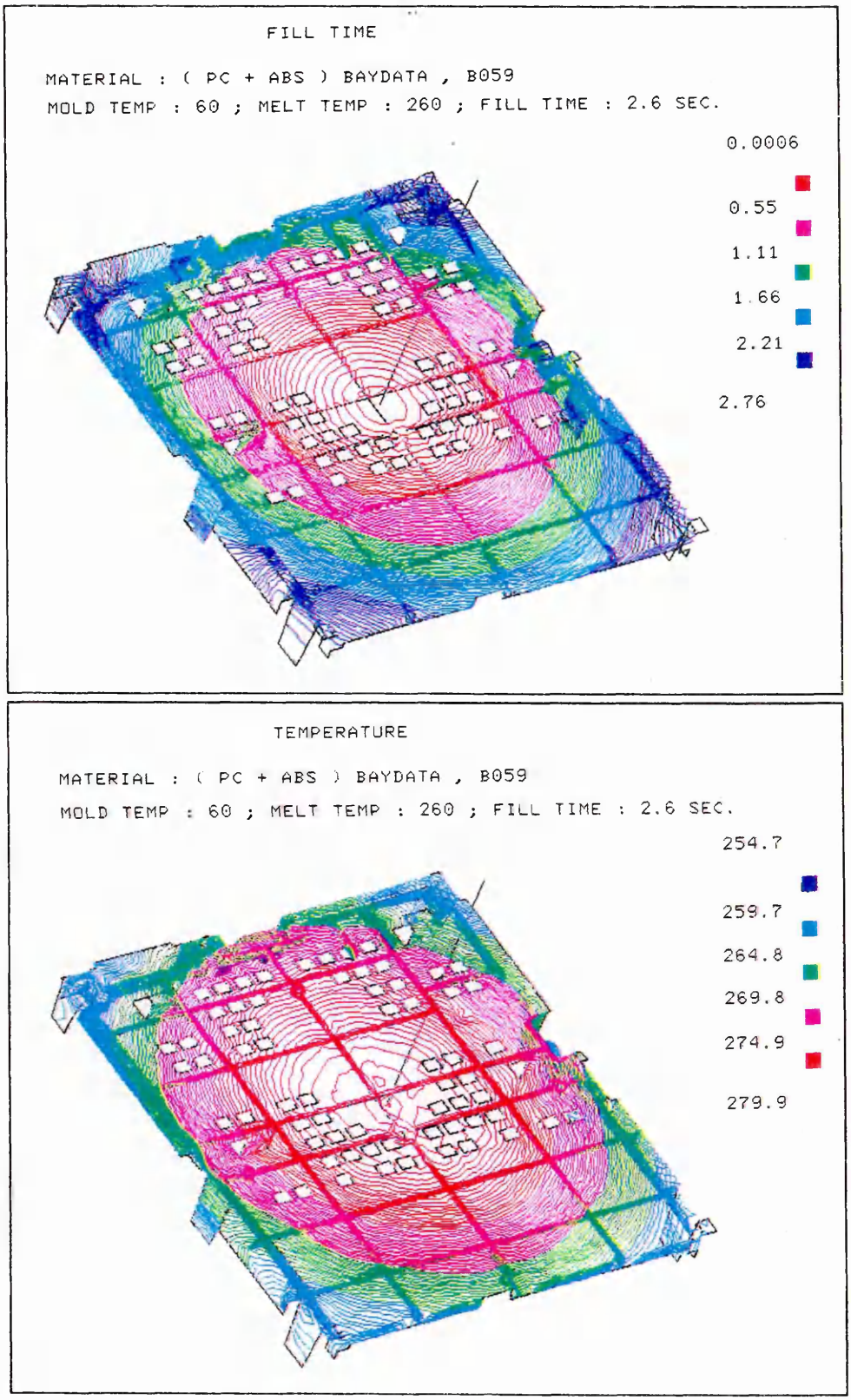

Fig.7.5.9. The flow pattern and temperature distribution.
(Original colour pictures)

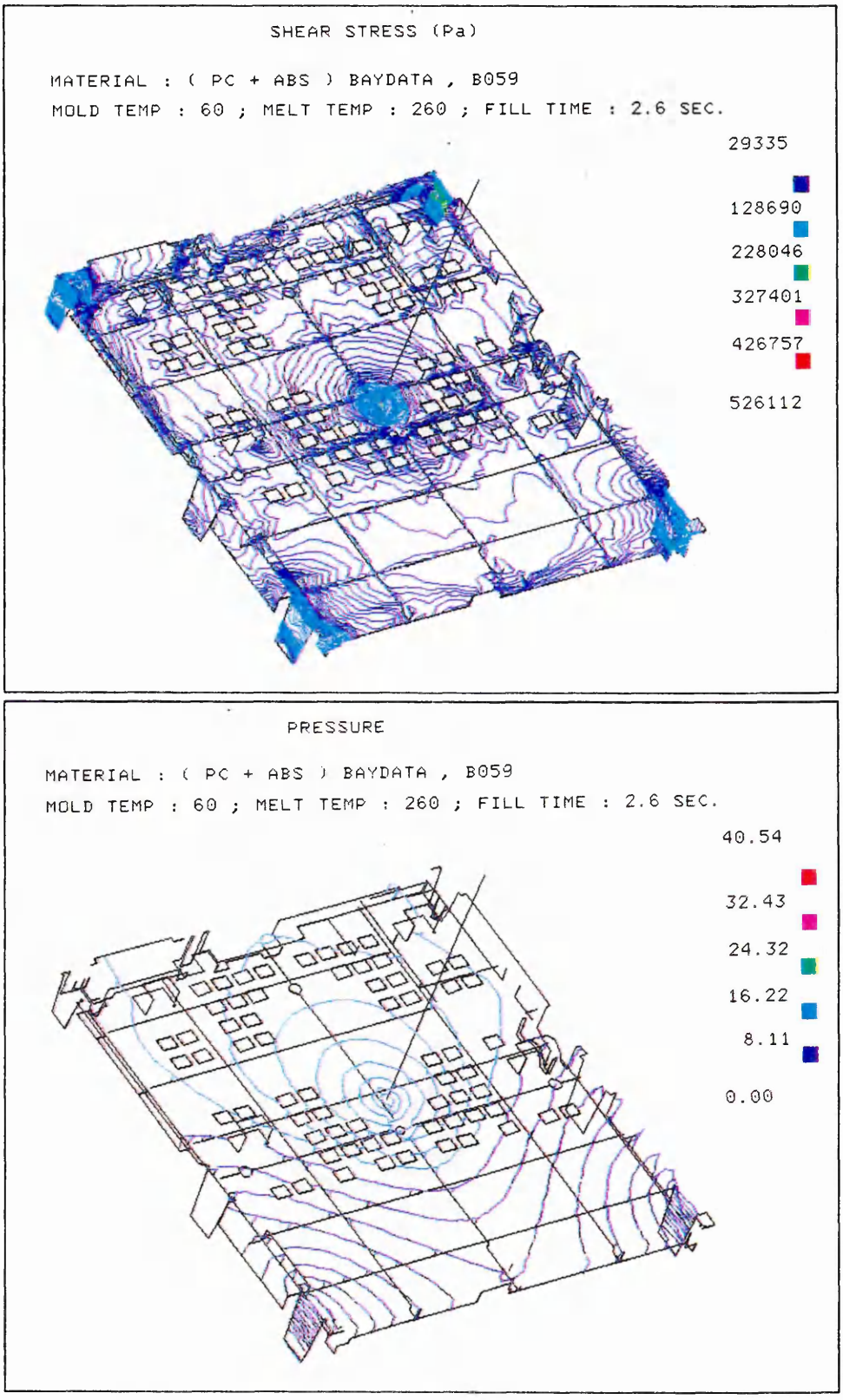

Fig. 7.5.10. The shear stress and pressure distributions.
(Original colour pictures)

The shear stress distribution is satisfactory as well. Because the longest flow path from the gate, and the sharp transition of cross section from

3.2mm to 2.5mm or 2.0mm in the hooks, the stresses there are relatively high comparing with the rest of the component, but the highest shear stress is only 268kpa in the upper corners.

If the flow rate is increased, that is , the filling time is decreased, a group of good results can also be obtained:

BARREL TEMPERATURE: 260 °C
MOULD TEMPERATURE: 60 °C
FILLING TIME: 2.3 SECOND

The results show that the temperature is still within 20 °C and the highest stress is about 301kpa. From the temperature result it can be seen that the melt temperature is increased about 20 °C during its passing through the runner. Then the shear stress is still under the limit although the flow rate increases and the material viscosity characteristics mentioned above are used here, a small but comprehensive report is given below:

Table 7.5.4

```
**************************************************************
*                                                            *
*                  REPORT FROM THE RESULT FILE               *
*                                                            *
* NUMBER OF NODES:      3117      NUMBER OF ELEMENTS:      5573 *
*                                                            *
* MAX   PRESSURE:       42.40          AT NODE NUMBER:     3115 *
* MAX FRONT TEMP:       280.80         MIN FRONT TEMP:     259.60 *
* MAX  END  TEMP:  279.5437            MIN  END TEMP: 235.1723 *
* MAX SHEAR RATE:  3028.190            AT ELEMENT NO.:     3911 *
* MAX SHR STRESS:   301221.            AT ELEMENT NO.:      388 *
* MAX  COOL TIME:       18.140         AT ELEMENT NO.:      158 *
* MAX CLAMP TONNAGE DURING CYCLE                41. Tonnes     *
* TOTAL VOLUME              .21E-03 cu.m              207.77     *
* NOMINAL FLOW RATE         .90E-04 cu.m/sec          90.33      *
* MOLD TEMP       60.0                                         *
* MELT TEMP      260.0                                         *
* B059  PC+ABS   BAYBLEND  FR  1439  V-0   BAYER   Co.         *
* ACTUAL INJECTION TIME: 2.3227                                *
*                                                            *
**************************************************************
```

A third set of conditions is given for offering the lower limit of the barrel temperature, and compose a processing window with the above two sets of the conditions as shown in Fig. 7.5.11:

BARREL TEMPERATURE: 256 °C
MOULD TEMPERATURE: 60 °C
FILLING TIME: 2.4 SECOND

Table 7.5.5

```
**********************************************************
*                                                        *
*              REPORT FROM THE RESULT FILE               *
*                                                        *
* NUMBER OF NODES:    3117     NUMBER OF ELEMENTS:   5573 *
*                                                        *
* MAX  PRESSURE:     43.90      AT NODE NUMBER:     3115 *
* MAX FRONT TEMP:   277.10      MIN FRONT TEMP:   255.50 *
* MAX  END  TEMP: 274.8716      MIN  END TEMP: 227.5912 *
* MAX SHEAR RATE: 2802.080      AT ELEMENT NO.:     3911 *
* MAX SHR STRESS:  305855.      AT ELEMENT NO.:      388 *
* MAX  COOL TIME:   17.580      AT ELEMENT NO.:      158 *
* MAX CLAMP TONNAGE DURING CYCLE          43. Tonnes     *
* TOTAL VOLUME          .21E-03 cu.m        207.77       *
* NOMINAL FLOW RATE     .83E-04 cu.m/sec     83.11       *
* MOLD TEMP     60.0                                     *
* MELT TEMP    256.0                                     *
* B059  PC+ABS  BAYBLEND FR 1439 V-0  BAYER  Co.         *
* ACTUAL INJECTION TIME: 2.4246                          *
*                                                        *
**********************************************************
```

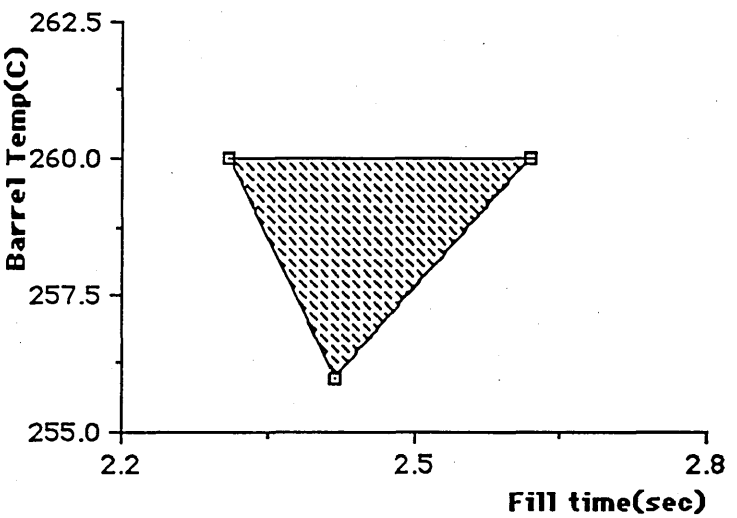

Fig.7.5.11. Processing window of part one

Other results indicate that if the processing conditions are a little bit outside the window determined by above results, either temperature or the shear stress will be beyond the requirements. Further improvements can be made either by a considerable arrangement of the cooling channels to cool down the material evenly to compensate the temperature distribution or by adjusting the flow rate profile making the ending flow rate less than 75%. Far too less of the ending flow rate may result in a short period of decreasing of pressure near the end of filling, and subsequently result in a little bit back flow or molecular orientation problem. These results are fully discussed in a student report[159] whose work was guided by the author.

(b)Part Two (23F2220)

The geometry of this part is more complicated than part one. There are groups of slots in grille, higher standing ribs and some small thin ribs and holes for interlocking the other part. The large number of equally sized and spaced grille makes the modelling difficult. Since the MOLDFLOW flow equations are based on an assumption of "slab flow" throughout the component — a valid assumption for a given flow which width is much greater than its thickness, the grille areas are clearly not the case. Therefore the presence of the grille requires a special consideration for the modelling. The major concern is the significant effects of the edges of a rectangular duct in respect of both the resistance of flow and heat transfer through them. There are two ways to account for the effects. One is that the thickness of the surfaces in the grille detail can be decreased to give an increased resistance to flow which will give a more accurate prediction of the pressure requirements and, due to the reduction in thickness, the heat transfer rate will be increased as well. However, it is difficult to quantify the thickness for both effects, normally only for an isothermal flow of which the equivalent pressure can be calculated by using a frictional factor to revise the thickness. An alternative way would be to use a runner element with an equivalent resistance to flow to model the grille element, in this way the program would allow for the heat transfer all the way round the perimeter of the element. In this case the same factor is used for calculating the radius of the runner element. The formulae for the factor, the revised thickness and the radius are given in reference [160].

The sprue runner is added on, and the whole finite element mesh is shown in Fig.7.5.12 in next page.

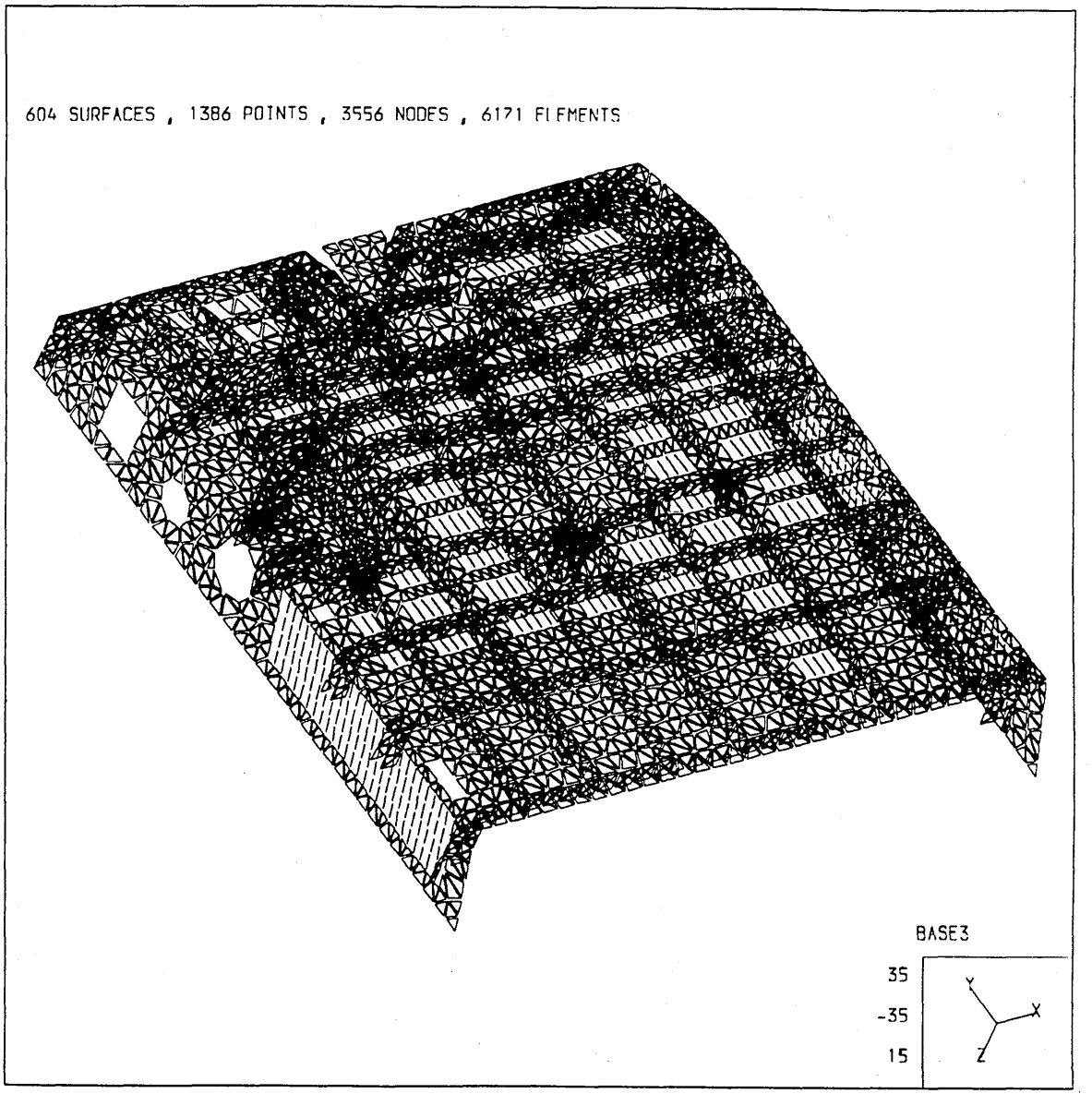

Fig.7.5.12. The finite element mesh of part two.

The small thin ribs in the corners have the same problem as part one does. However, the high stresses there are not so important as they occur in the hooks in part one. The moulding conditions are as follows:

BARREL TEMPERATURE: 260 °C
MOULD TEMPERATURE: 60 °C
FILLING TIME: 3.0 SECOND

The result pictures of the finite element analysis are shown in Fig.7.5.13 in solid mode. It can be seen that the resolution of the pictures is higher than those contour plots presented before and thirty two colours are used to represent different values in the three dimensional geometry.

A.(right) The flow pattern during the filling stage.

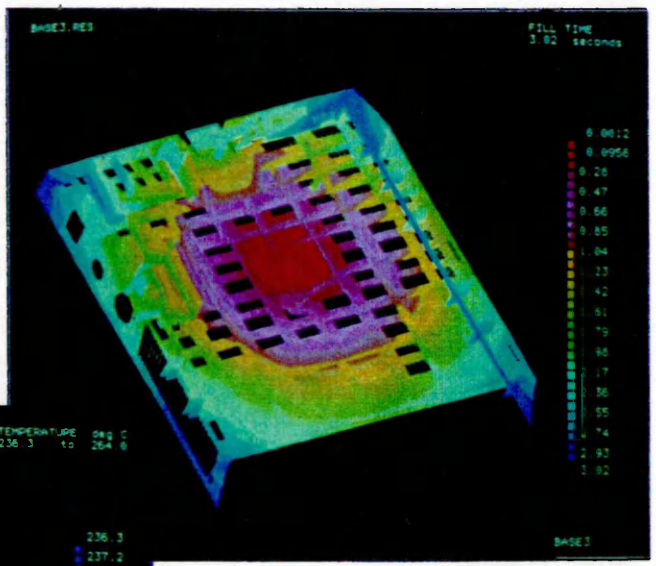

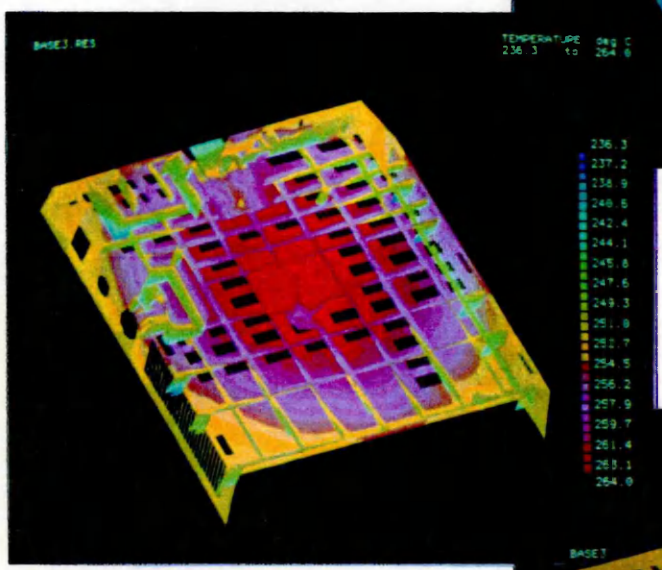

B.(left) The temperature distribution just after the filling.

C.(right) The pressure field just after the filling.

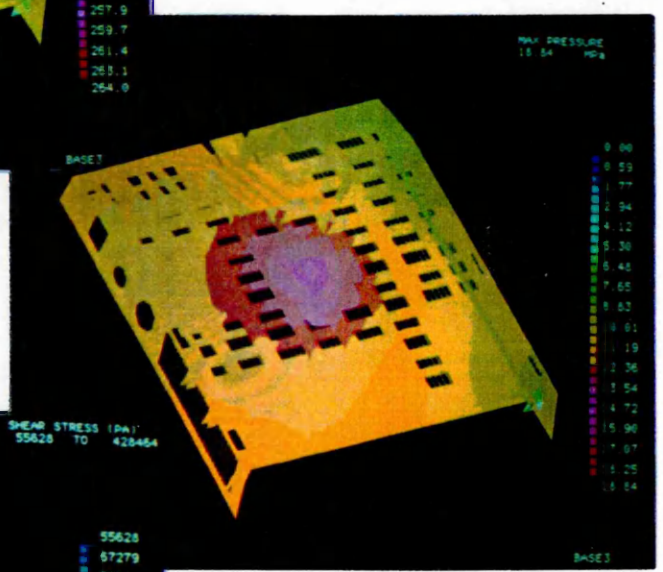

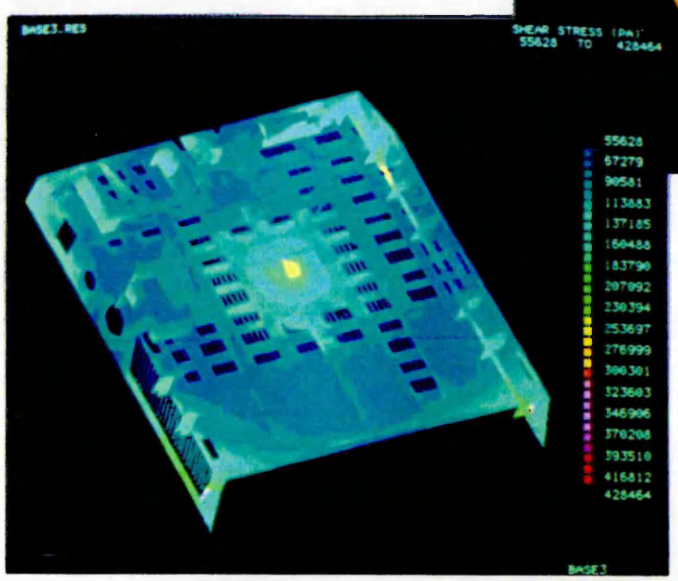

D.(right) The shear stress field at end of filling.

Fig.7.5.13. The result pictures represented in solid colours.

Because of the unsymmetrical feature of the geometry and so many slots to make the flow paths zigzagged, the flow pattern is quite complicated. The last area to fill can be determined from both the flow pattern and the pressure field which is up in the rib near the down-right corner (of part in the graphs). Two apparent weld lines can be observed in a enlarged flow pattern graph. Both the stress and the temperature are satisfactory. The highest stress occurs also up in that rib, and other high stressed areas are in the centre and up in the right wing close to the top-right corner. It would be suggested that the corner ribs be thickened up a little bit and the two grille elements in the middle of the right wing be merged into one, the result could be improved for above problems.

Since the processing window for this part is obviously larger than the window for part one, it is not necessary to simulate the moulding processing under other processing conditions. The common processing window should then be determined as the one for part one. The actual processing window must be checked through the finite element analysis.

7.5.5 Runner system design

a). Initial design

The criteria for this runner system design have been mentioned in section 7.5.2. In order to make use of the runner system to control the moulding processing, the pressure drop along the runners must be high enough to allow the passing melt in the runner to produce the frictional heating. This frictional heating plays an important role in reducing the shear stress level inside the cavities, because of the temperature increasing can dramatically reduce the viscosity of the melt, as mentioned before. Another important aspect of controlling the moulding processing is that the runner had better to be designed as a thermal shut-off, which can be frozen off first to protect the possible back flow from the cavities when the pressure decreases during the cooling stage. The ideal runner system is to pass the melt into the cavities, and transfer the pressure for holding for the minimum length of time to avoid sink marks, then to be frozen off, preventing flowing along the runner. However, it cannot always be designed as such, especially when relatively large amount of melt has to be injected into the cavities. On the other hand, the way of ejecting the mouldings and runners have to be taken into account.

The narrow parts of the runners to two cavities have both thermal off function and ejection function, since the narrow parts can be broken off naturally when the moulds are open, and taking the upper part out of the upper mould. The remaining parts on the components can be cut off. The initial size of the runners can be roughly calculated by a formula supplied below[161]:

$$D = \frac{\sqrt{W}\sqrt[4]{L}}{3.7} \qquad (7.5.1)$$

where W is the weight of the part, L is the length of the runner and D is the diameter. The factor 3.7 is for metric system.

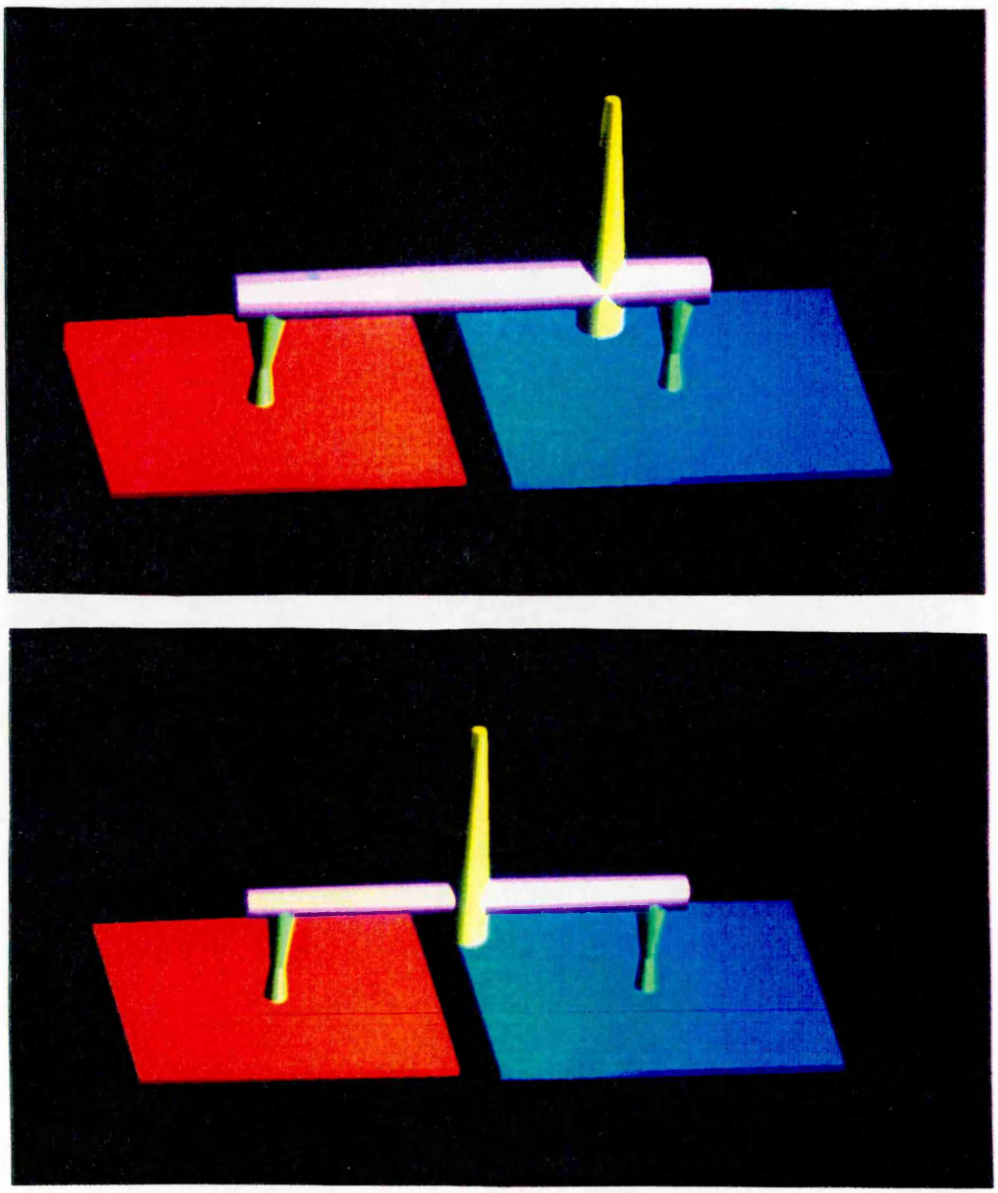

Fig.7.5.14. Two layouts of the runner system. Above: the same diameter but different lengths. Below: the same length but different diameters.

From this formula the size of each runner can be calculated separately. However, the layout of the cavities and the manufacturing cost must be taken into account, since either the length or the diameter can be varied for each cavity. The size of the sprue depends on the sizes of both runners following another formula for its tapered shape. From manufacturing point of view, it is better to locate the sprue in the centre of the upper plate. This means to balance the runners by adjusting the diameters. Nevertheless, the lengths of the runners are much less sensitive to a tiny error in tolerance. The two possible layouts are shown in Fig.7.5.14.

After the layout design, the two parts are put together, and broken into triangles as shown in Fig. 7.5.15.

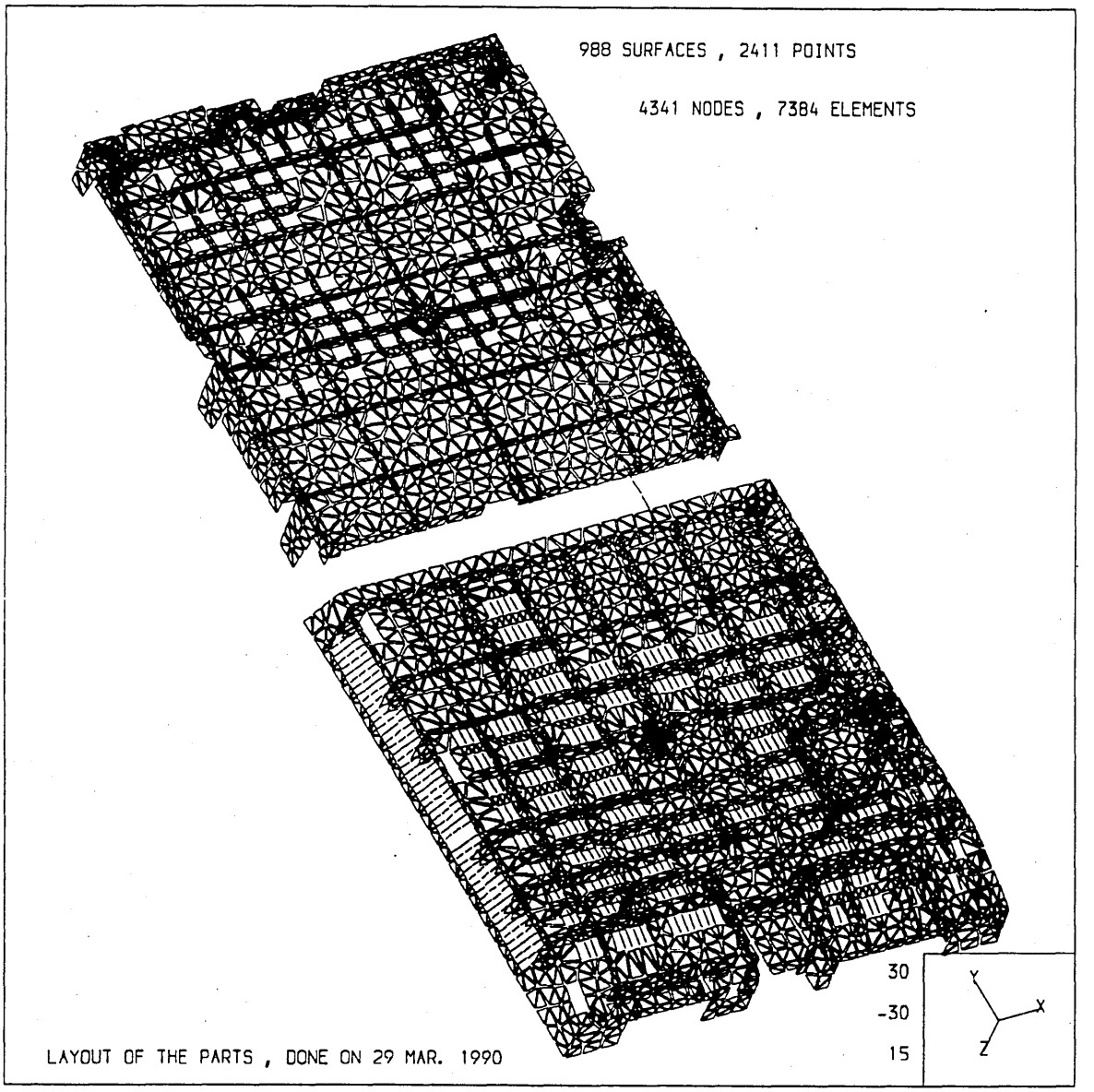

Fig.7.5.15 The mesh of the two components together.

b). Balancing of the dimensions of the runner system

From the mesh shown in Fig.7.5.15 it can be seen that to balance the feed system for these two cavities by three dimensional finite element method is very time-consuming because there are over seven thousands elements involved in the calculation. Since the resistance during the whole filling stage depends mainly on the complicated geometry for a given material, the calculation has to be done by no further simplification than this 3D analysis. The focus then has to be put on the number of calculation times for the balancing, that is, to find a quick way to search the balance status for the system. Fortunately, the principle introduced in the section 7.5.2 was soon found, and it was proved by this example. At first, the single variable is chosen as the length of one of the runners. Since the whole length of two joined runners is fixed as 270mm, the variable is actually the position of the sprue between the two runners. The position can only be in the half section of the bigger cavity side as shown in Fig. 7.5.14. Within this section, a simple optimisation method can be used since the pressure function of the position is a concave one. The *0.618 method* is chosen for the optimisation. The optimum method is to seek for the optimal position by selecting some regular points in the section as shown in Fig.7.5.16.

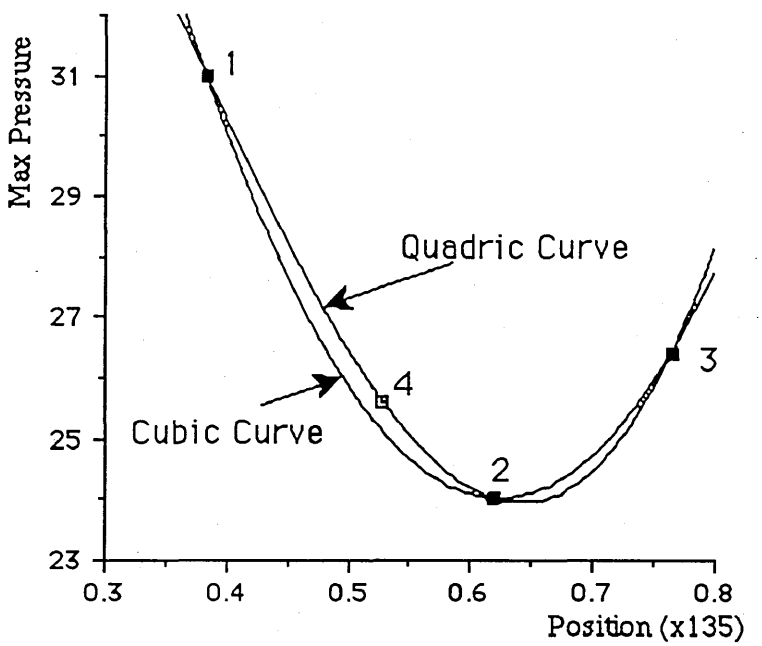

Fig. 7.5.16. *The 0.618 method* to seek for the balance position

The first trial is in the position of (1-0.618)xL, where L is assumed as the length of the section. And the second is in 0.618xL. By comparison of these two results, the optimal position must fall into the lower side, thus the

range for searching is reduced to 0.618xL, range from 0.382 to 1 of the length. Then repeating the same step, assuming L as the length of the new range, but only one trial is necessary since the other coincides with one of the previous trials. Following such way of searching until the error between the last two trials less than a pre-given small value, the optimal position can then be approached, as the fast convergence is obvious.

However, the number of trials can be further reduced by constructing a quadric or cubic curve by three or four trial points as shown in the graph. The zero point of the first derivative of the curve is very close the optimum position, and in order to reduce the calculation time, this position can be regarded as the final result though it is an approximation. For more precise result, a new narrower searching range can be formed by the lowest point of the trials and the zero point of the derivative multiplying a factor of 1/0.618, then to carry out the searching by *the 0.618 method* in this new range.

The method looks simple, and it is proved efficient. The important thing is its fundamental, the principle which the method is based on. Unfortunately, the method cannot be coded into the MOLDFLOW package, so all the optimisation scheme is carried out by hand. Finally, three groups of results of two types of balancing with different processing conditions are obtained as follow:

Table 7.5.6

Variable	Design	Runner 1	Runner 2	Processing Conditions
Diameter	1	15	15	Fill Time: 3.4 sec. Melt Temp: 260° C
Length	1	50	220	
Diameter	2	12	10.25	Fill Time: 4.3 sec. Melt Temp: 268° C
Length	2	135	135	
Diameter	3	11.55	10	Fill Time: 2.6 sec. Melt Temp: 260° C
Length	3	135	135	

The results of the finite element analysis of the balanced two mouldings under the first layout are given as following group of graphs in Fig. 7.5.17 (a-b, d-e).

A.(right) The flow pattern during the filling stage.

The flow patterns of the two parts are slightly different, though the the flows are from the centres of them. The thin grille certainly help the flow passing the hole areas in the second part; the high standing ribs take more part of the flow away from the main stream in the plate than the first one. The red centre in the second part indicates the arrival difference.

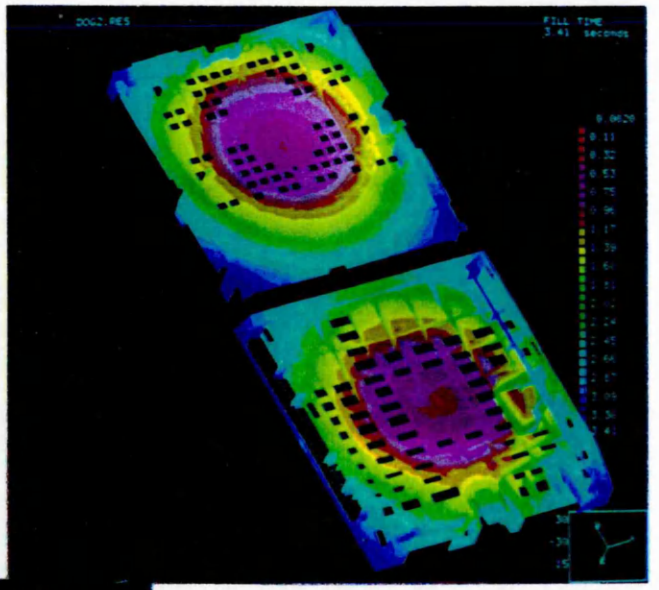

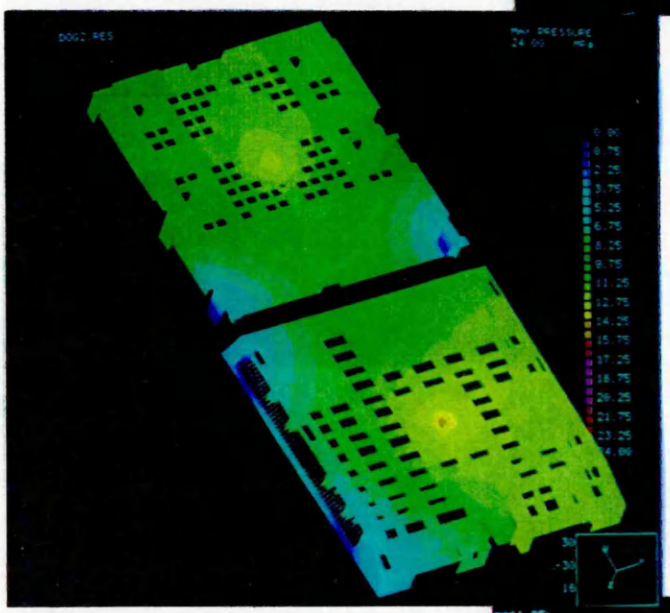

B.(left) The pressrue field just after the filling.

The blue colour indicates the last parts to fill which are the down corners of the first part and the rib in top-left corner. The brown and yellow colours in the centre of the second part indicate the pressure difference for filling the bigger volume. The higher pressures (pink and red colours) occur in the feed system.

C.(right) The pressure field of an unbalanced trial.

By comparison, this graph clearly indicates that the second half has been filled first and the pressure is built up inside the cavity, also the reading of the highest pressure is higher than that in the balanced pressure field shown above.

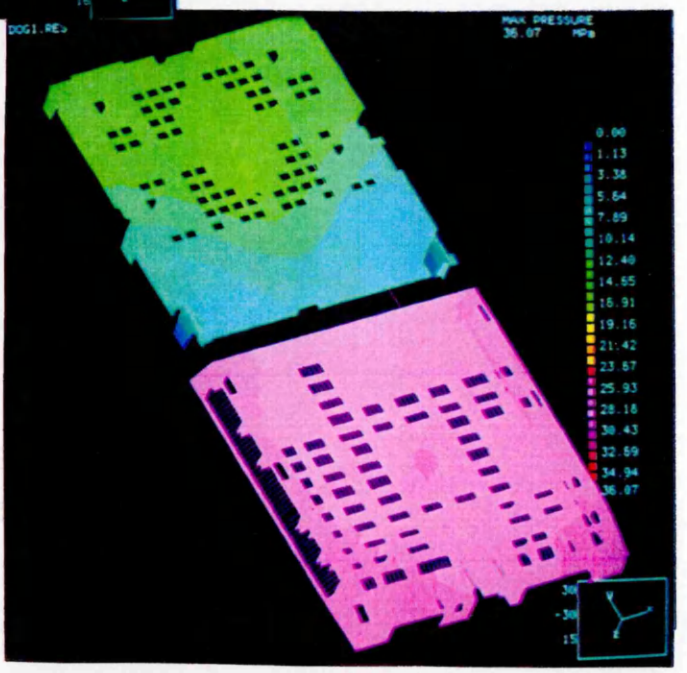

(Continued)

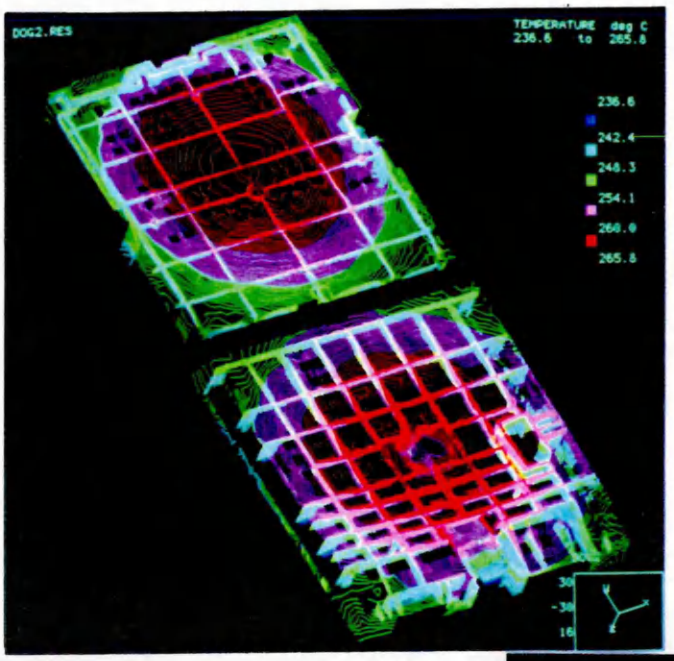

D.(left) The temperature field in contours.

The temperature plot in solid mode is just beyond the capacity of the program due to so many elements. Anyway, the blue colour can only be seen in the top of some small high standing ribs in the second part, most of the area is covered by the contours in green, pink and red colours, which indicate the difference of the temperature is suitable.

E.(right) The shear stress field at the end of filling.

The high stressed areas are in the lower corners of the first part, the corner ribs of the second part. A few red spots can be seen in the ribs of part two which are higher than the limit required, but they are not important in the moulding.

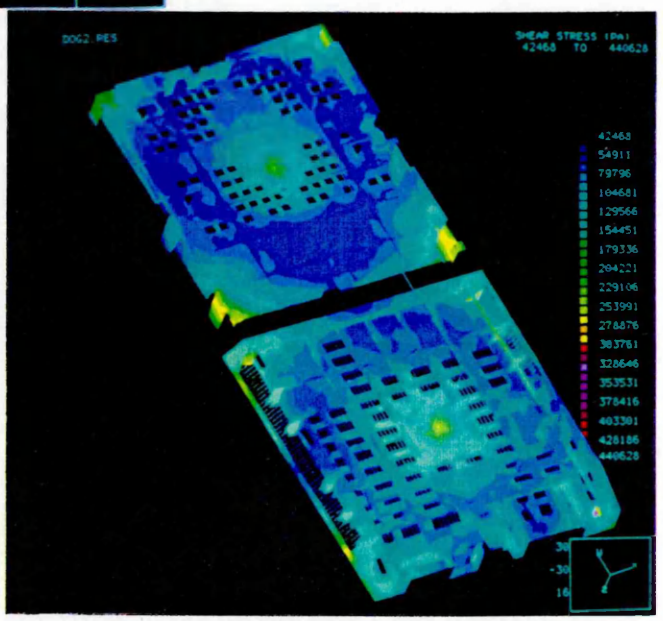

Fig.7.5.17. The result of the balanced family moulding. (Original colour pictures)

c). The stability of the balanced results

An artificially balanced runner system can only work over a certain range of moulding conditions. According to MOLDFLOW philosophy, the width of this range of the moulding conditions determines the stability of the moulding. Because the runner system is sensitive to a tiny change of diameters, some more calculations have been carried out for the stability of the last two designs. Fig. 7.5.18 shows the processing window of the second

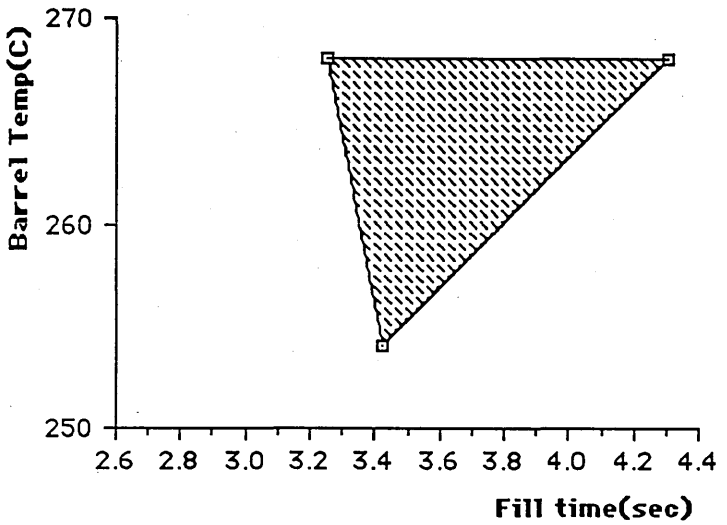

Fig. 7.5.18. The processing window for the second design

design, in which the stability has been proved. The third design allows much smaller range of change in the processing conditions. Three reports are given for its stability.

Table 7.5.7

```
**********************************************************
*                                                        *
*              REPORT FROM THE RESULT FILE               *
*                                                        *
* NUMBER OF NODES:     4341      NUMBER OF ELEMENTS:     7384 *
*                                                        *
* MAX   PRESSURE:      45.80       AT NODE NUMBER:      4327 *
* MAX FRONT TEMP:     278.80       MIN FRONT TEMP:     256.60 *
* MAX  END  TEMP:  278.5503        MIN  END TEMP:  232.0505 *
* MAX SHEAR RATE:  4059.730        AT ELEMENT NO.:      2270 *
* MAX SHR STRESS:   383997.        AT ELEMENT NO.:      5967 *
* MAX  COOL TIME:    25.190        AT ELEMENT NO.:       337 *
* MAX CLAMP TONNAGE DURING CYCLE          111.Tonnes       *
* TOTAL VOLUME            .52E-03 cu.m          524.52     *
* NOMINAL FLOW RATE       .22E-03 cu.m/sec      218.55     *
* MOLD TEMP      60.0                                      *
* MELT TEMP     257.0                                      *
* B059  PC+ABS   BAYBLEND FR 1439 V-0   BAYER  Co.         *
* ACTUAL INJECTION TIME:  2.4042                           *
*                                                        *
**********************************************************
```

```
**********************************************************
*                                                        *
*              REPORT FROM THE RESULT FILE               *
*                                                        *
* NUMBER OF NODES:     4341      NUMBER OF ELEMENTS:     7384 *
*                                                        *
* MAX   PRESSURE:      43.00     AT NODE NUMBER:         4327 *
* MAX FRONT TEMP:      280.30    MIN FRONT TEMP:       255.80 *
* MAX  END  TEMP:  279.9326      MIN  END  TEMP:   229.9779 *
* MAX SHEAR RATE: 3724.730       AT ELEMENT NO.:         2270 *
* MAX SHR STRESS:  383997.       AT ELEMENT NO.:         5967 *
* MAX  COOL TIME:    25.190      MIN  COOL TIME:        3.390 *
* MAX CLAMP TONNAGE DURING CYCLE          106.Tonnes        *
* TOTAL VOLUME          .52E-03 cu.m          524.52        *
* NOMINAL FLOW RATE     .20E-03 cu.m/sec      201.74        *
* MOLD TEMP      60.0                                      *
* MELT TEMP     260.0                                      *
* B059  PC+ABS   BAYBLEND FR 1439 V-0   BAYER  Co.         *
* ACTUAL INJECTION TIME:  2.6049                           *
*                                                        *
**********************************************************
**********************************************************
*                                                        *
*              REPORT FROM THE RESULT FILE               *
*                                                        *
* NUMBER OF NODES:     4341      NUMBER OF ELEMENTS:     7384 *
*                                                        *
* MAX   PRESSURE:      42.90     AT NODE NUMBER:         4327 *
* MAX FRONT TEMP:      280.00    MIN FRONT TEMP:       254.50 *
* MAX  END  TEMP:  279.5129      MIN  END  TEMP:   227.9691 *
* MAX SHEAR RATE: 3585.910       AT ELEMENT NO.:         2270 *
* MAX SHR STRESS:  399487.       AT ELEMENT NO.:         5967 *
* MAX  COOL TIME:    25.190      MIN  COOL TIME:        3.340 *
* MAX CLAMP TONNAGE DURING CYCLE          112.Tonnes        *
* TOTAL VOLUME          .52E-03 cu.m          524.52        *
* NOMINAL FLOW RATE     .19E-03 cu.m/sec      194.27        *
* MOLD TEMP      60.0                                      *
* MELT TEMP     260.0                                      *
* B059  PC+ABS   BAYBLEND FR 1439 V-0   BAYER  Co.         *
* ACTUAL INJECTION TIME:  2.7051                           *
*                                                        *
**********************************************************
```

7.5.6 Geometrical modification on the first component

There is not big difference between designing with plastics and designing with other materials like wood, concrete, and some metals. Of course, all the design information is based on properties of the material, structural response, performance characteristics, part geometry, process variables, and economics. However, sometimes the particular characteristics in injection moulding process are ignored in part design which could result in some effects on the design. A very bad flow pattern could be caused by the geometrical shape, and it subsequently results in somewhere overpack, different cooling and shrink rate, and finally a warp product. These characteristics, which other materials may not have, are the flow effects and thermal effects on the melt during the injection moulding process. For example, the geometrical design of part one (23F2210) may not be considered as a good one from the moulding processing point of view. As mentioned in the analysis, the corner hooks are designed to bear possible fatigue bending, but there are three geometrical factors to increase the flow stresses there: the longest path from the gate; the sharp transaction of the thickness; and the holes jamming the way of the flows reaching the corners. Since the holes and ribs in the part play the cooling and structuring roles of the part, rearrangement of them does not affect the appearances and functions. This rearrangement should be under the consideration of the geometrical effects on the moulding. Fig.7.5.19 shows the mesh of the modification of the component. This arrangement of the holes and ribs can give much better flow pattern as shown in the fill time picture below. The holes, which still play the cooling roles of the part, are now put on the direct way of the flow to the edges, while the rids are put in diagonals to encourage the flows to the corners, and more important, they can also strengthen the part because biggest bending occurs in diagonals rather than in longitudinal or latitudinal directions. As shown in contour pictures below, this geometrical design can improve the high stress level in the corner hooks, and give a better temperature distribution, and the better flow pattern which decreases the possibility of warpage that original design may have. The only possible remaining defect is the weld lines created by the holes, which can be solved by increasing the mould and melt temperatures to assure that the temperatures at meeting fronts are high enough.

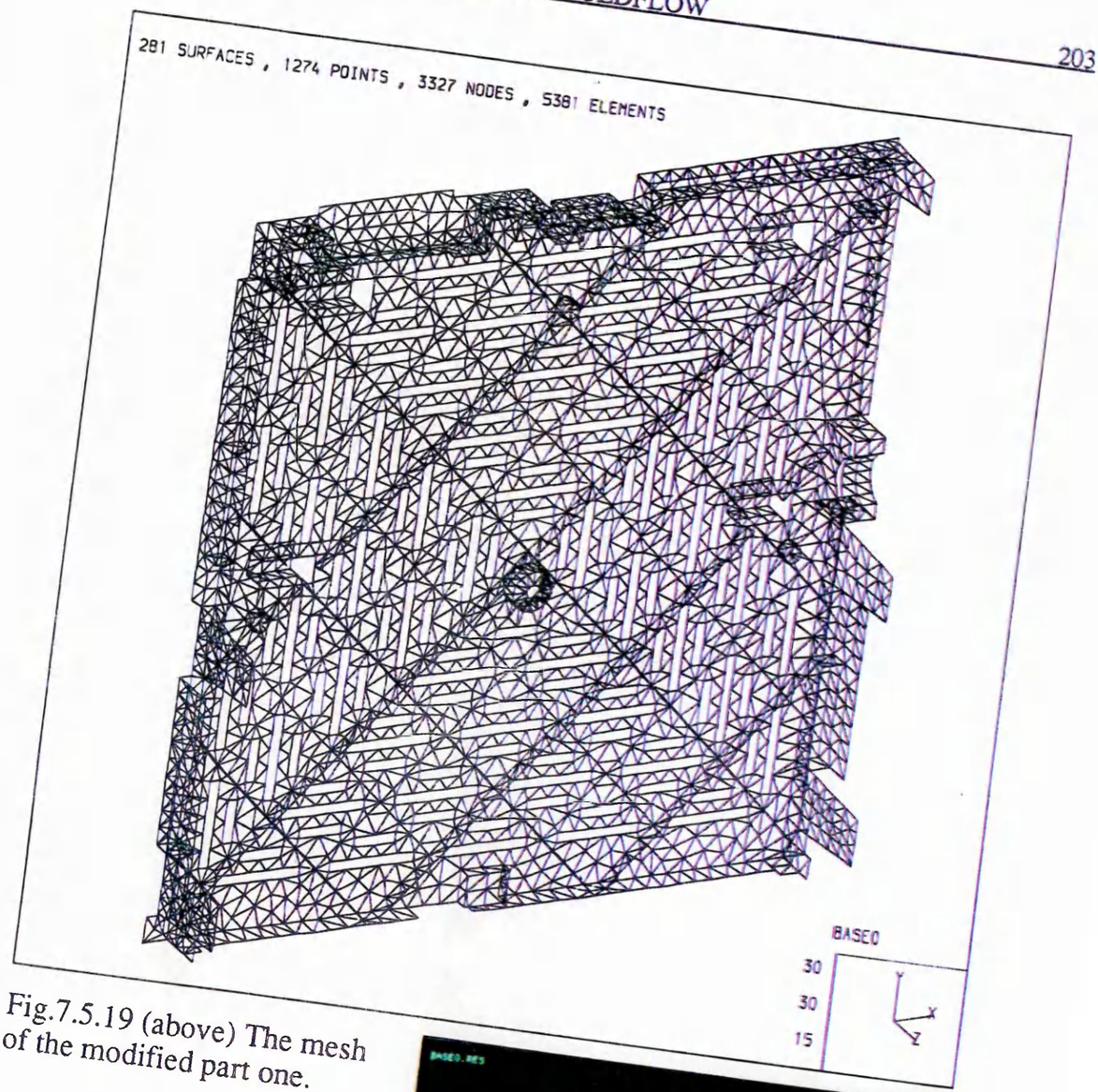

Fig.7.5.19 (above) The mesh of the modified part one.

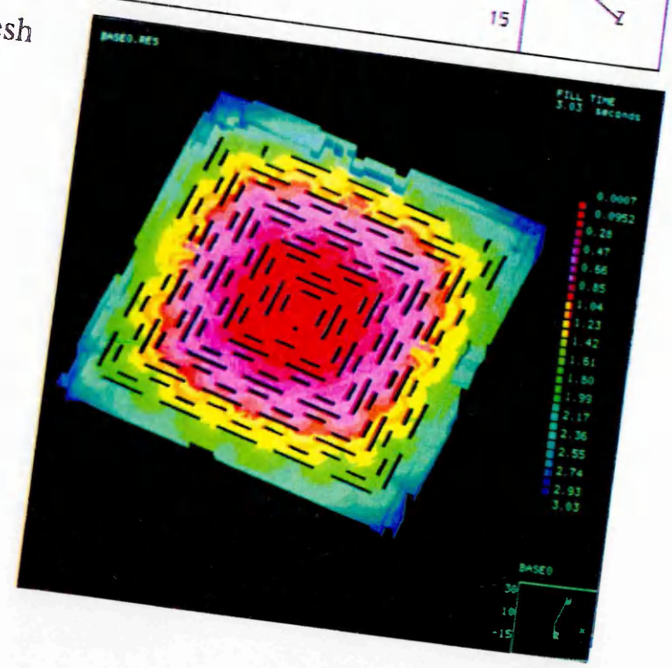

Fig.7.5.20 (right) The flow pattern of the modified part one. The front is close to a rectangular shape. (Original colour picture)

A.(right) The pressure field.

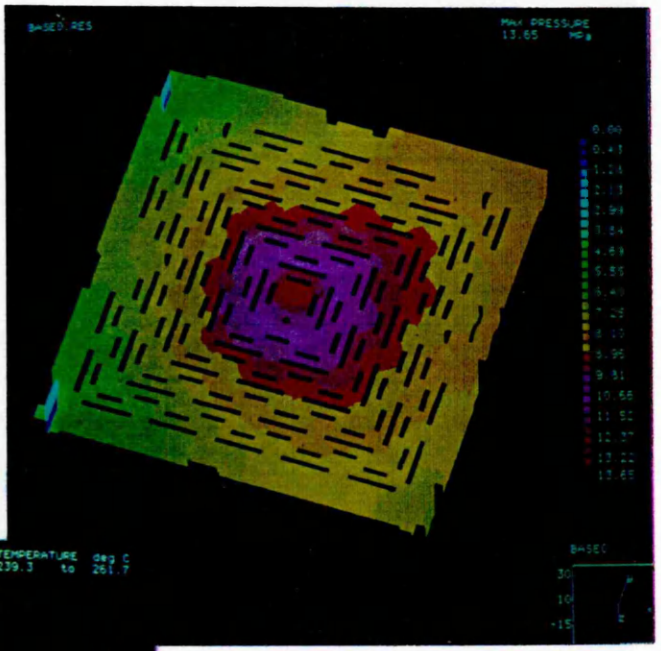

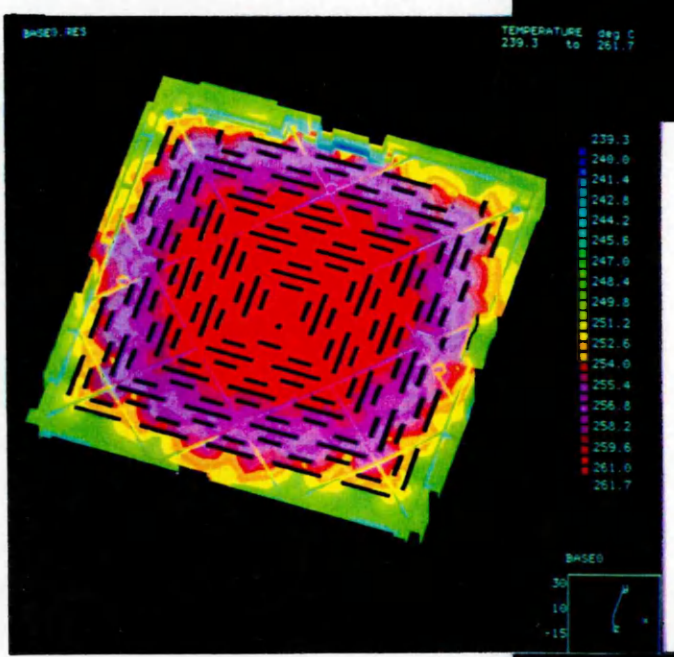

B.(left) The temperature field. The distribution is close to a rectangular shape.

C.(right) The shear stress distribution.

The highest shear stress occurs at the centre instead of corner hooks.

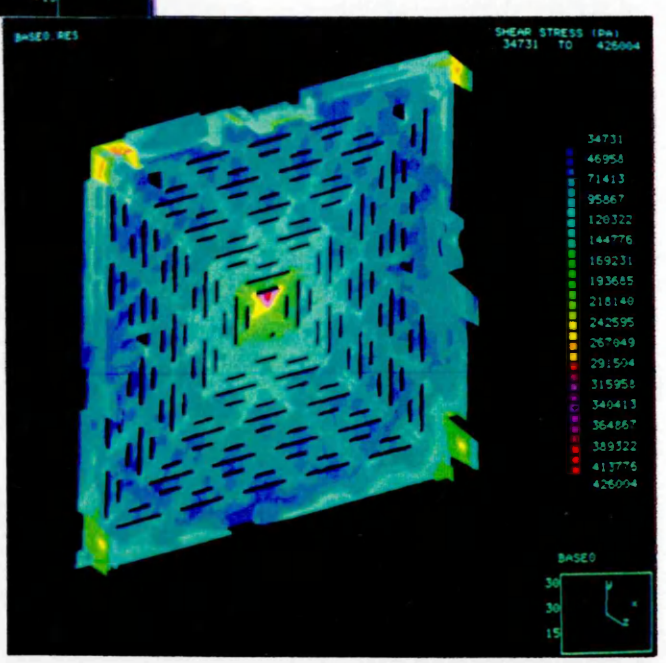

Fig.7.5.21. The result pictures of the modified part one.

7.6 Conclusions

This chapter has introduced MOLDFLOW and given analyses of several practical processing examples of IBM's components. Each example has its own features and complexities in both material and geometrical aspects. The package has shown its powerful functions in solving those difficulties. All the above results have been appraised and assented by IBM's plastic processing experts. There are a few more examples which have many similarities to the above, and also some different treatments from the above calculations, such as multigate moulding exercises. They are not selected in this paper because of unnecessary lengthy.

The whole philosophy of MOLDFLOW and design ideas as well as its shortcomings give us a broader horizon to consider the simulation, especially in mathematical modelling aspect and geometrical treatment. It should be admitted that some of the modelling in previous chapters are based on the inspirations from the use of this package; and some of the functions in next chapter are actually supplements or replacements of this package. It should also be pointed out that the package has its vital defect — no velocity vector outputs which are crucial in simulating the orientations of particles or fibres in some plastic components, though the designers are trying to improve the modelling to give these functions, as the author knows. These functions, as mentioned in the first chapter and shown in other previous chapters, are better to be fulfilled in such a model that the Lagrangian viewpoint is adopted, and the velocity components are part of the basic variables to be solved in the equations.

Chapter Eight

CASIM Program Design

8.1 Introduction

CASIM are the five initials of Computer Aided Simulation of Injection Moulding. The idea to design such a program to simulate the injection moulding process had occurred to the author before MOLDFLOW arrived when no other packages had been available for the analyses. The idea contains two points: the first one is just like most of the present CAE packages, to bring both suitable numerical methods and graphically enhanced pre- and post-processing techniques or CAD techniques together; and the second is to address the shortcomings of commercialised packages in which the numerical models cannot be changed if they are not well suited for a type of problem. The past experiences of dealing with packages give the author some lessons in his research; the main problem is always the lack of flexibility of changing models, or the inability to put ones own ideas into packages. It is obvious that ABAQUS[162] cannot solve most of the injection moulding problems in which not only the constitutive models have to be changed, but also the basic variables have to be changed from displacement to velocity. What is more, if one wants to replace the finite element model by a boundary element model, all the FE packages like ABAQUS appear to be inadequate. Therefore for some research, fundamental changes must be implemented and this can only be done by designing ones own program.

After MOLDFLOW's arrival, CASIM has been extended to assist some of the pre- and post-processing functions which MOLDFLOW appears to be lacking. Similarly some functions of MOLDFLOW which are not necessary to be designed again are used with CASIM. This is not to say that CASIM is becoming a complementary package of MOLDFLOW because it has its own kernel — the boundary element models, equation solver, and pre- and post-processors. These functions can give CASIM an independent position without any doubt.

However, to code a new viable package is a challenging task. Software engineering is a huge subject, and it requires a great deal of knowledge including establishing mathematical models, mastering computer environments, languages, data structures, modular programming skills, and so on.

For a large program, the coding is often carried out by a few persons co-operating together for a few years. Because of replanting reasons, the most important thing may be the experience of coding in various computers, and one has to think about designing a software which depends on hardwares as little as possible. The need for hardware independence relates not only to computer languages like standardised FORTRAN, PASCAL or even C which are widely used in engineering and science research, but also to operating systems and graphical supporting systems like UNIX and its progeny, and GKS[163] and its compatible systems.

The design of CASIM program is mainly, from the software engineering point of view, based on the software shielded idea. There are some good graphical bases available in IBM3090, the main frame of the University of Glasgow, such as CATIA[164], IAX[165], or some good packages in the VAXes, such as I-DEAS[166], PATRAN[167], UNIRAS[168]. However, since CASIM may be used in other systems in future, the best environment for it here is the international standardised graphical supporting system supplied, such as PHIGS[169], GKS, and widely used handy GHOST-80[170] which can produce a PostScript file which subsequently can be transferred to other facilities. The language used is mainly FORTRAN 77 which has been long and widely used and well developed for engineering and science applications and is hardware independent. The hardware environments are the IBM5080 series and PC graphical terminals connecting with the main frame IBM3090 in which the current operation system is VM/XA, and other graphical facilities connected with the mainframe such as laser-printer, plotter and hard-copy machines.

CASIM has been coded in this structure such that a program library is created which can contains both the modules used for the elementary system functions like graphic and data input / output, and the modules for analysing the injection moulding processing. The latter modules contain programs based on boundary element methods, and even ones linking the MOLDFLOW library. After nearly three years endeavour, the skeleton of a big package has appeared, and some fundamental graphical functions in both two and three dimensional views have been coded and appear to be working well. The kernel — some boundary element numerical technique modules in two dimensional problems have been finished. The further development depends only on supports and time. The whole programming idea is mainly based on the reference[171].

8.2 General Construction and Objectives

The general construction of CASIM is designed as a tree structure. All the "limb" modules are connected to a general control level— execution command level which is the "trunk" or "root" of the tree. In next level, the corresponding "bough" programs are connected to each of the "limb" modules. Further more, the "branch" subroutines are connected to each of the programs, and more basic "twig" functions are called by those subroutines. Each module or sub-module in different levels has a clear function and a certain independence, allowing it to be connected through its interface. This so-called HIPO (Hierarchical Input Process Output) technique is one of the modular programming technologies, and it gives an explicit structure of the package. However, there is an implicit data structure which is used by all the modules except some exotic programs which are linked to the highest level. The explicit and implicit structures are shown in Fig.8.1.1. The detail functions of some main modules are given in the following sections.

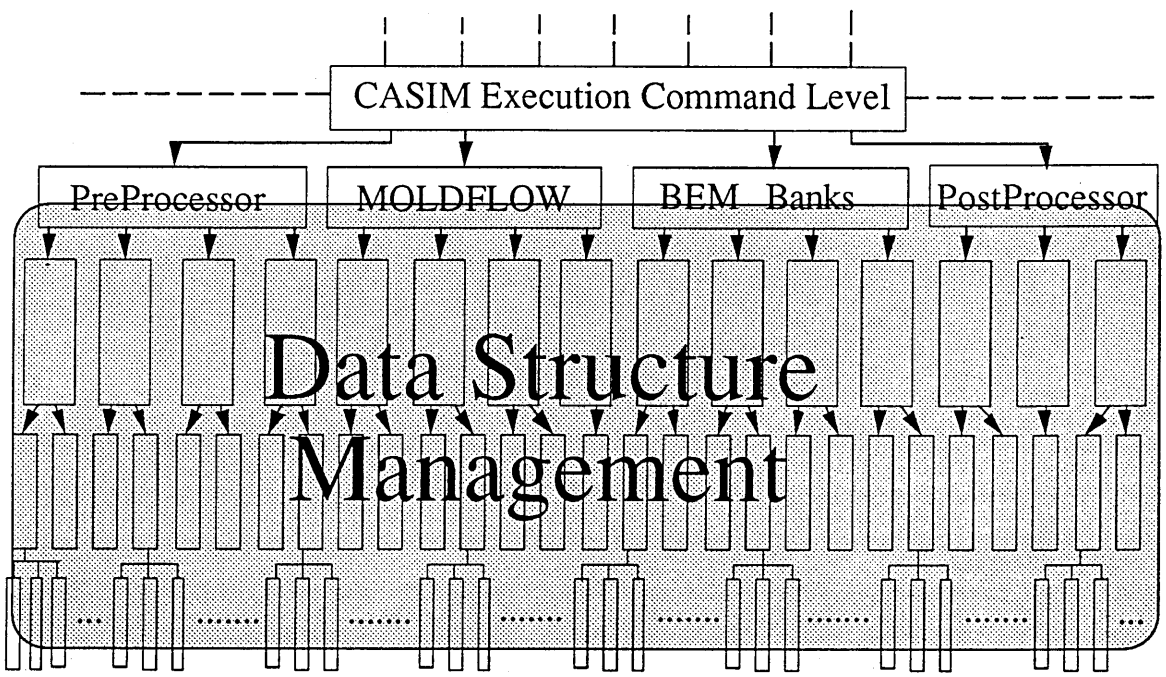

Fig. 8.1.1 The explicit structure and their base — data structure, dotted line means that some more modules can be connected.

The CASIM execution command level is coded in command statements, so that different modules coded in different languages or some executable modules like MOLDFLOW can be connected together, and each of the

"bough" modules can be designed to use the whole storage of the computer. This form of the structure can be used in the next level, if some of the "branch" modules need to use the whole storage. Since the execution level is coded in a sort of interpreted language, not like FORTRAN or some other high level computer languages, the source statements cannot be compiled or "hidden", only used in the form of highest level's structure.

The main programs of the first level modules are designed to use "cases". The option of next level's modules can be chosen either from the choice board from which the information into the program is an integer, or by command inputting which gives a string of characters into the program, or by some other means like locating the crosshair in a menu which is then "translated" into an integer to give to the program.

The design of CASIM must have the following objectives: It must

- be capable of solving various problems appeared in injection moulding process,
- be a clearly modularised program, easily expanded with more functions or models
- adopt the resources such as storage of a computer as efficiently as possible, especially for fitting small computers
- use graphical predominance in handling inputting and outputting
- allow easy replacement in constitutive models
- be stable and have fast kernel models and solver
- have easily interfacing with other packages

One of the major tasks of those objectives is to design a data structure.

8.3 Data structure

A programmer faces two major problems when he or she is coding a program: which model to use and which kind of data structure to adopt. Simply speaking, a combination of a mathematical model and a data structure is a program[172]. For most of the computational structural / fluid mechanics program designers, the biggest headache is how to efficiently use the limited computer resources such as the internal storage. Although FORTRAN is overwhelmingly adopted as the computer language in most of the engineering and science aspects, however, the functions of FORTRAN in data management is not satisfied since it has only a static, simple data

structure. Therefore, a dynamic data structure is designed for most of the modules. The idea stems from JINEGS system[171] but this one is simpler and easier to be adopted.

If the whole internal storage resource is assumed to be a large one dimensional array as shown in Fig.8.3.1, it can then be divided into three regions: director region, record region, and vacant region. Each record can also be divided in these three regions, and so on.

Fig. 8.3.1 The storage divisions

In director region, there are some pointers to give information about the record region and the vacant region. For example, the first number of the director region gives the total length of the array, the second is the length of the director region, and the third is the number of the records currently stored in the array. The rest of the elements in the director region are the positions of the records currently stored in the array. In this management system, the internal storage resource can also be used for much larger problems, because it stores the current records only for a module, not the whole records for the package. When the memory is nearly full, one pointer in the director region will give a sign for the program dumping some of the records which are not in use into disk space. When some other records are needed which are not in the memory, some of the pointers in the director region will change their status and ask to load in these records from the disk space into the vacant region. Therefore the whole internal memory is managed like a simple virtual memory management system within the package. Details about the idea can be found in the reference[171].

8.4 Input / Output

The external space is accessed by Input / Output interfaces. The disk files can be classified by their usage as the following five types:

- Input Data Files.
- Output Result Files.
- Files from other packages like MOLDFLOW.
- Intermediate Files for memory management.
- Specially formatted graphical Files.

From a programming point of view, they are just IO files. The input and output functions of these files are designed to be shielded within a few subroutines, because they are most likely to be dependent on the machines.

From the experience of using other finite element packages, the format and rules of input files are a real headache. A user has to search big manuals to find out the way of inputting data, and the error messages feedback from running the package are often confusing or misleading. Although boundary element methods have the obvious advantage in preparing data for some complicated problems, handy graphical pre-processing is the most intuitive way of giving the necessary information about the problem to a computer. Any error related to the geometry can be immediately detected from graphical output on screen. Therefore some subroutines have been designed for the surface drawing, boundary condition setting, and so on. After the processing, an input file is produced. Because of the time-dependent or iterative requirements, the input file can also be produced by the kernel programs during the calculation for re-starting a long job again.

Also, some of the input files may come from other packages like MOLDFLOW, or sometimes the MOLDFLOW input files are manipulated, improved through the pre-processing routines and transferred back to MOLDFLOW, or sometimes the initial input files are produced by the pre-processor then transferred to MOLDFLOW. The result files really need to be shared by both MOLDFLOW's post-processor and the CASIM post-processor, otherwise too much disk space would be involved in the file handling. All these require the IO interface to be designed predominantly using MOLDFLOW file formats, though they are not ideal. Easily, the interface can be extended to standardised graphical formats like IGES (Initial Graphics Exchange Specification, American National Standard, also adopted by several other countries) to handle geometrical information exchange with some CAD/CAM software systems, or other formats to communicate with other FE packages like ABAQUS.

The result files are produced in order, distinguished by a name with a number. The name represents the problem type, and the number corresponds to an intermediate result at a predetermined time. Anyone of the result files can be read and transferred into a graphical form. Pictures are the language of engineering. If there is a picture for the same result of a print-out, nobody would like to read the lengthy numbers.

The graphical information can be stored, transferred in a few different forms. For space saving, the graphical information can be packed. For animation use, the graphical information at different time steps must be stored in the form of pictures in order to increase the speed of showing. For laser-printing-out, the graphical data have to be transferred through GHOST-80 environment to PostScript files. Some programs with special functions have been designed for these requirements. Fig.8.4.1 shows the IO layout of CASIM.

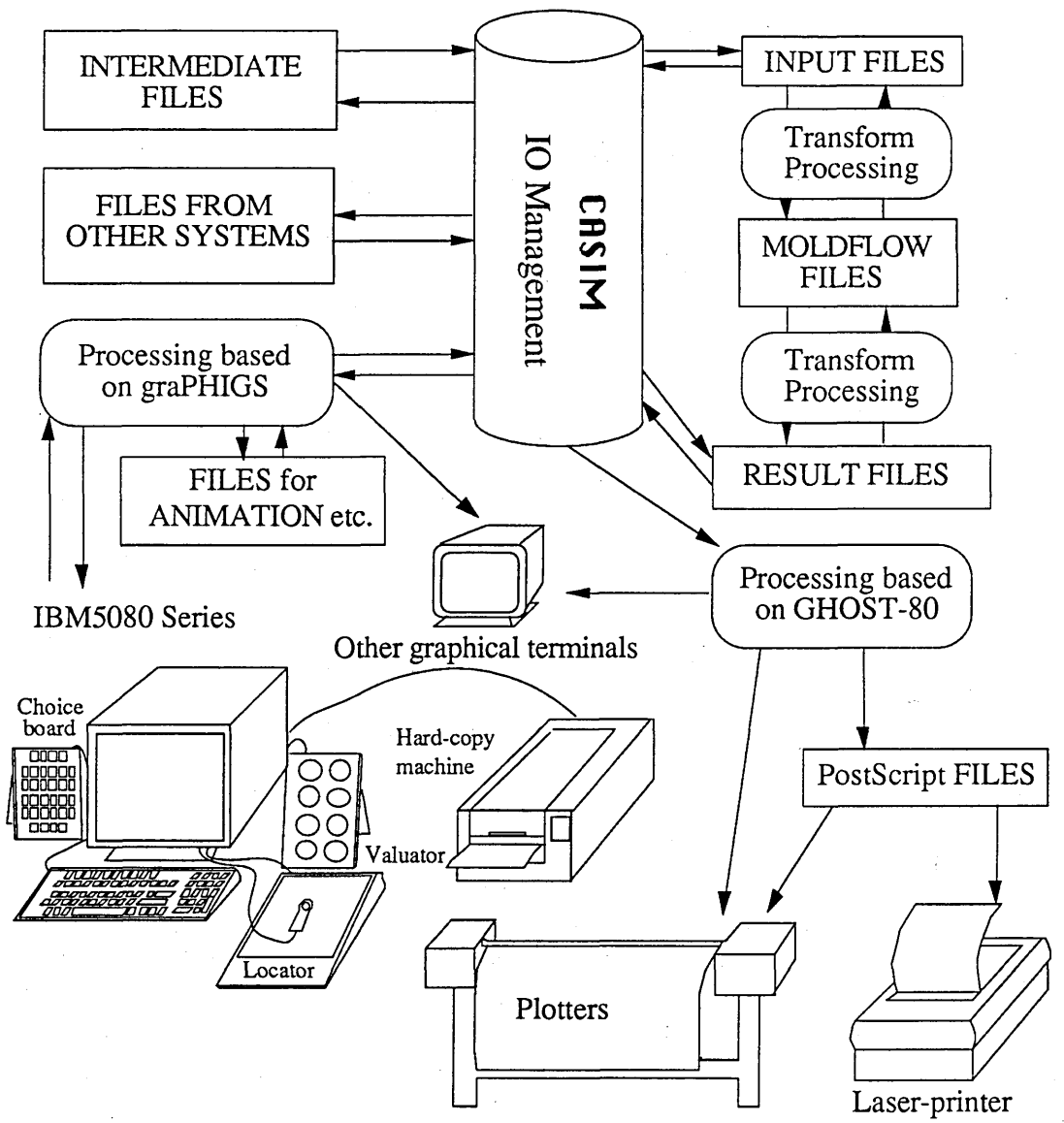

Fig.8.4.1 The Input / Output layout.

8.5 Modules in Pre-Processor

8.5.1 Introduction

The pre-processor contains some basic functions like surface generation, outline checking, etc. Some of the functions are designed to give geometrical information for two dimensional boundary element analysis, others are specially designed to compensate MOLDFLOW's pre-processor SMOD since it is not good enough for giving various geometrical information to the program. A new user may have to spend a few weeks using SMOD to input a complicated geometry. Some kinds of geometry cannot be easily inputted, though theoretically a shape may be just a piece of surface which can be expressed by a mathematical function. This pre-processor therefore supplies not only the necessary functions but also the potentials for the author to expand the capacity to handle any difficulty in generating a correct geometry, and simplify the procedures to make it more user friendly.

8.5.2 Surface Generation

Although the geometries in the injection moulding process are three dimensional, they are often composed of some shell elements for simplified mathematical models because the thickness dimension is much less than the other two dimensions. These shell elements are defined by surfaces and their thicknesses are contained in the information only in a digital form. In this case the surface model for generating a three dimensional geometry is preferable.

CASIM pre-processor is designed to use mathematical functions to handle different geometries. The information is then transferred into point coordinates and surfaces defined by these points. Two input files containing the point and surface information are subsequently produced in the same format as those produced from MOLDFLOW, so they can be transferred between these two packages and compensate each other's shortcomings.

Generating an intersection curve of two curved surfaces is one of the advantages of this pre-processor. In the second example of Chapter Seven, the geometry of the component has a piece of spherical surface which intersects with a series of planes, requires the generation of 14 intersection curves. In the following example which is a simpler pivot under an IBM

PC's terminal, there is also a piece of spherical surface and about 12 intersection curves on it. The geometry generation would take a long time with SMOD. The method used in generating the intersection curves is the same as the contour isoline generation which is introduced in section 8.6.3.

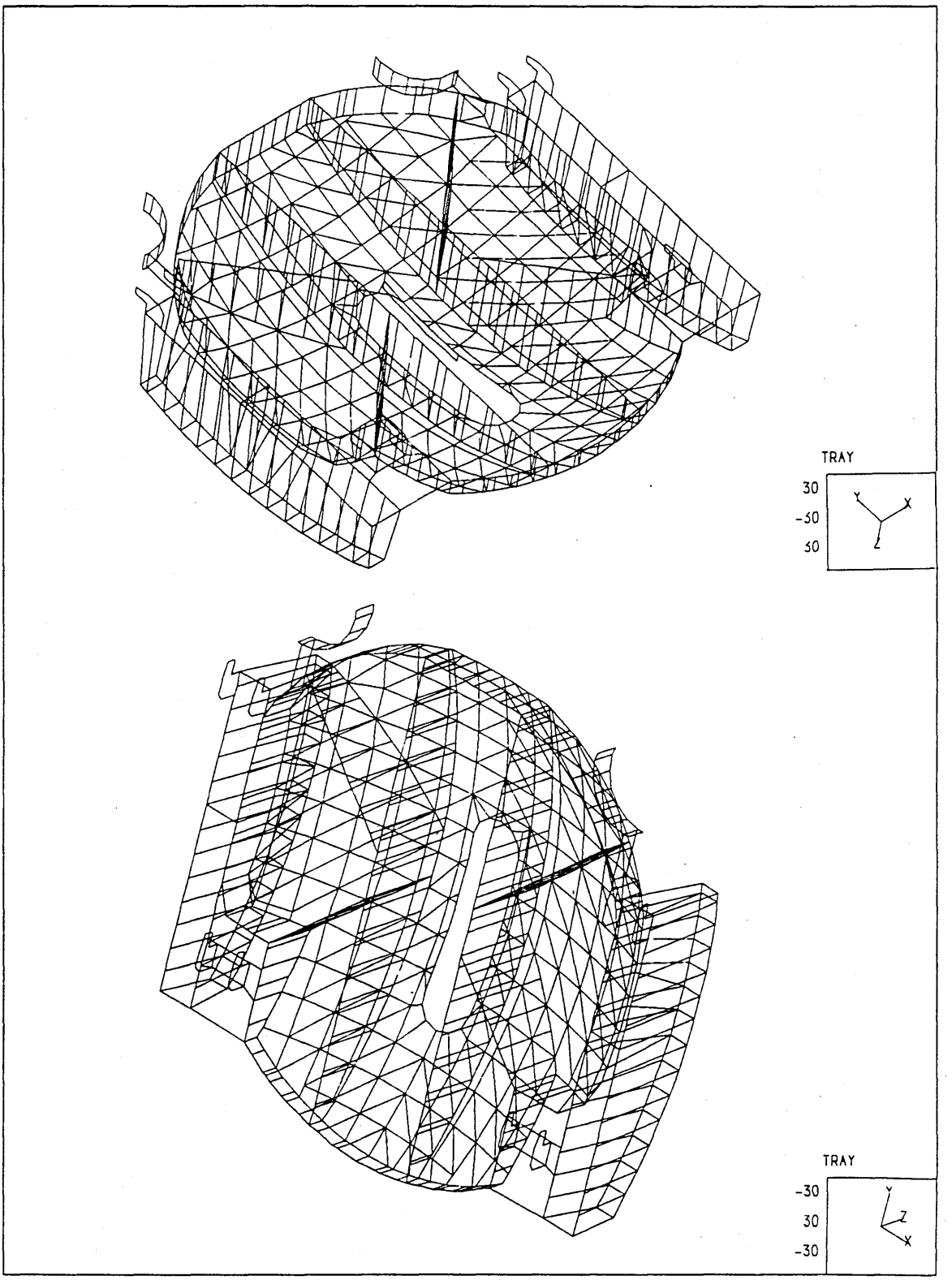

Fig.8.5.1.Two views of the surface generation of the IBM PC's pivot.

8.5.3 Outlining

It was surprising when it was found out that there was no such function in MOLDFLOW to check for lack of connectivity between two connecting surfaces — the problem very commonly encountered by new users. This kind of "crack" can result in completely wrong answer to the flow as shown in Fig.8.5.2. The mistake is caused by two separately defined surfaces not connecting properly each other.

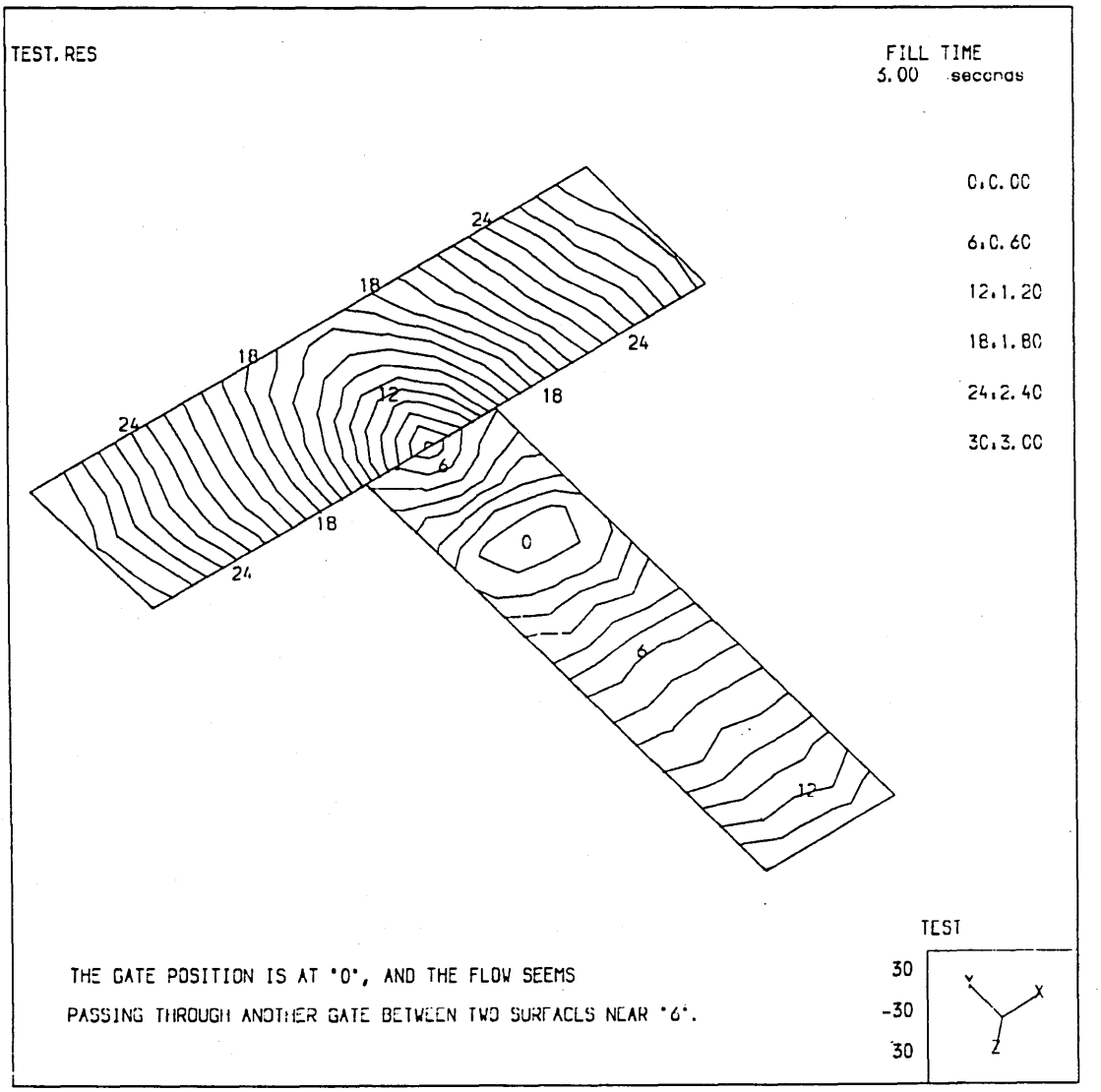

Fig.8.5.2. A "crack" line results in a wrong prediction.

For a simple geometry, this kind of mistake can be easily detected and rectified. Yet for a complicated geometry, when there are so many surfaces, it has to be checked out and shown clearly on screen by the computer. The method used here is very simple and straightforward.

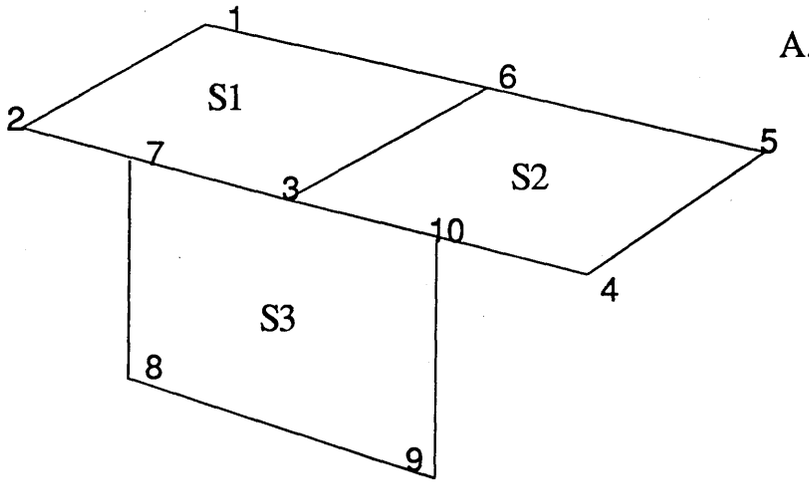

A. A part is defined by three surfaces:
S1: 1-2-3-6;
S2: 3-4-5-6;
S3: 7-8-9-10.

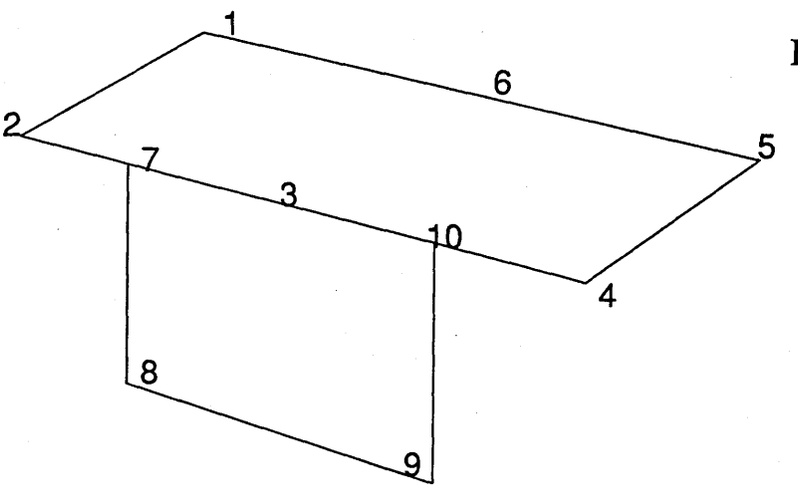

B. The line between points 3 and 6 is cancelled because it is shared by S1 and S2. A "crack" line mistake is created between points 7 and 10 because the lines 7-3, 3-10, and 7-10 are not shared by their neighbouring surfaces.

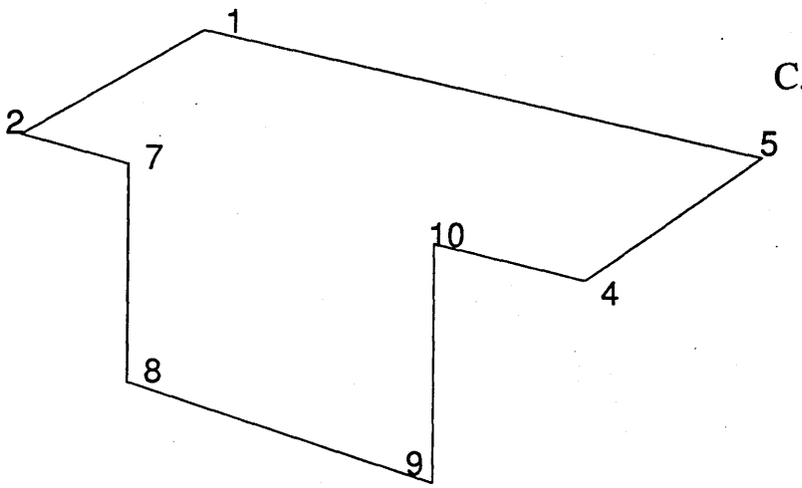

C. The outline of the part. The correct surfaces should be defined as:
S1: 1-2-7-3-6;
S2: 3-10-4-5-6;
S3: 7-8-9-10-3.

Fig.8.5.3. Schematic view of outline and a "crack" line mistake.

For any geometry defined by polygonal surfaces, the outline of the geometry is composed by the edges of some surfaces. Each of these edges belongs only to one surface. In other words, any line which bridges between two nodes more than once is not a section of the outline. The mistake of a

"crack" line appears when a common edge of two (even more) adjacent surfaces is defined by more than two nodes, and one (or more) of the nodes is not shared by the two adjacent surfaces. The lines which connect with this node (or these nodes) are therefore exposed as a part of the outline of the geometry, as is the line opposite it. Fig.8.5.3 shows the difference between a "crack" line and outline schematically. Following this principle, two subroutines have been designed. One of them is for checking each edge of all the surfaces, and shows on the screen those edges which belong to only one surface. The other is for checking each side of all the triangular elements, and shows those sides which belong to only one triangle. Obviously the former is much quicker because many less loops are required than the latter for the same purpose, while the latter can be used for more general cases. Fig.8.5.4 gives an example of checking for a "crack" line mistake in a complicated geometry.

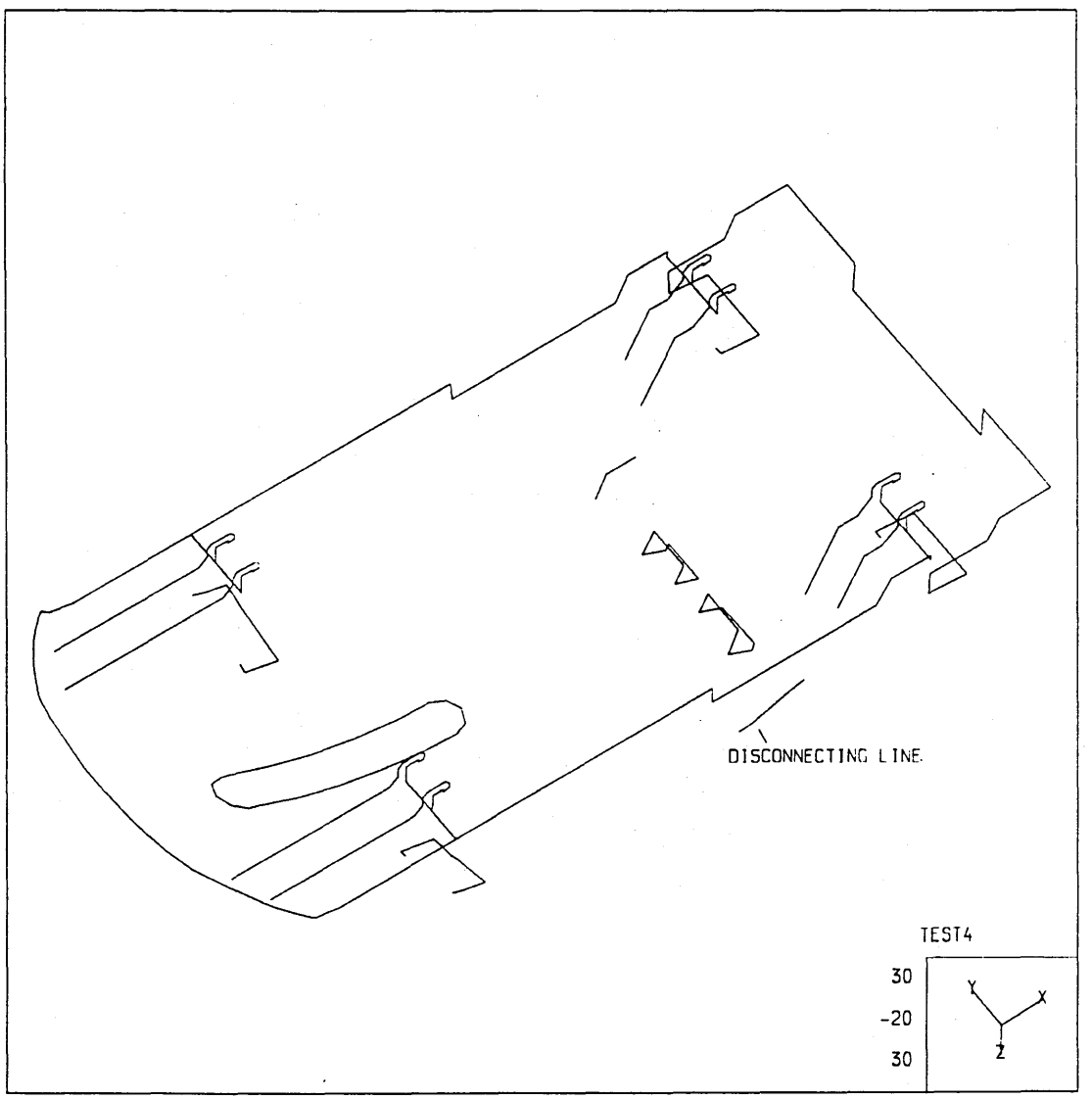

Fig.8.5.4. Checking a crack line mistake in a complicated geometry.

8.5.4 Re-profile the Wall

Only one thickness is defined to one surface in MOLDFLOW's pre-processor SMOD. However, for some problems the thickness may be required to assign to elements to re-profile the walls of a component in order to improve the flow pattern, temperature and shear stress distributions as it is mentioned in Chapter Seven.

The function of changing element's thickness is designed in CASIM pre-processor. After displaying the finite element mesh on the screen, one can use the locator (mouse) to click the element if the thickness of which is considered not suitable for the injection moulding. A new thickness can then be inputted to replace the original, and a colour representing the thickness appears on the element to distinguish it from other elements with different thicknesses. Although the re-profiling of the wall thickness is done in this manual way, the wall profile can be intuitively seen by the representative colours, and subtle changes in element scale can be made.

Hereafter is the re-profiling of the first example in Chapter Seven. The aim of re-profiling this part is to improve the flow pattern in such a way that the original radial moving fronts are changed to those very close to a rectangular shape with round corners as shown in Fig.8.5.6. This flow pattern is realised by thickening up the diagonal paths to the corners and thinning out the paths to the four sides as shown schematically as follow:

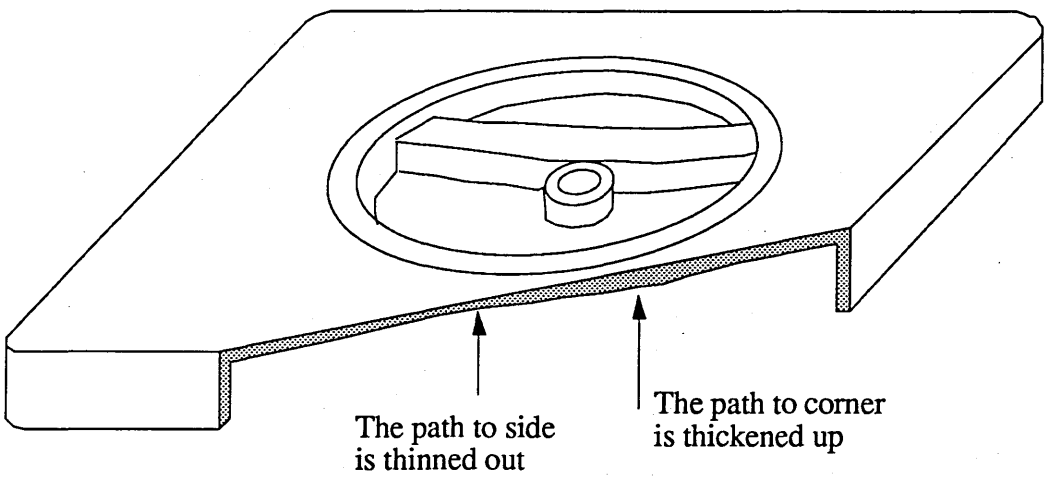

Fig.8.5.5. Schematic view of the wall profiling.

These thickness changes can be done, not necessary but the strength of the structure being ensured, within the tolerance, and only in the back side of the plate.

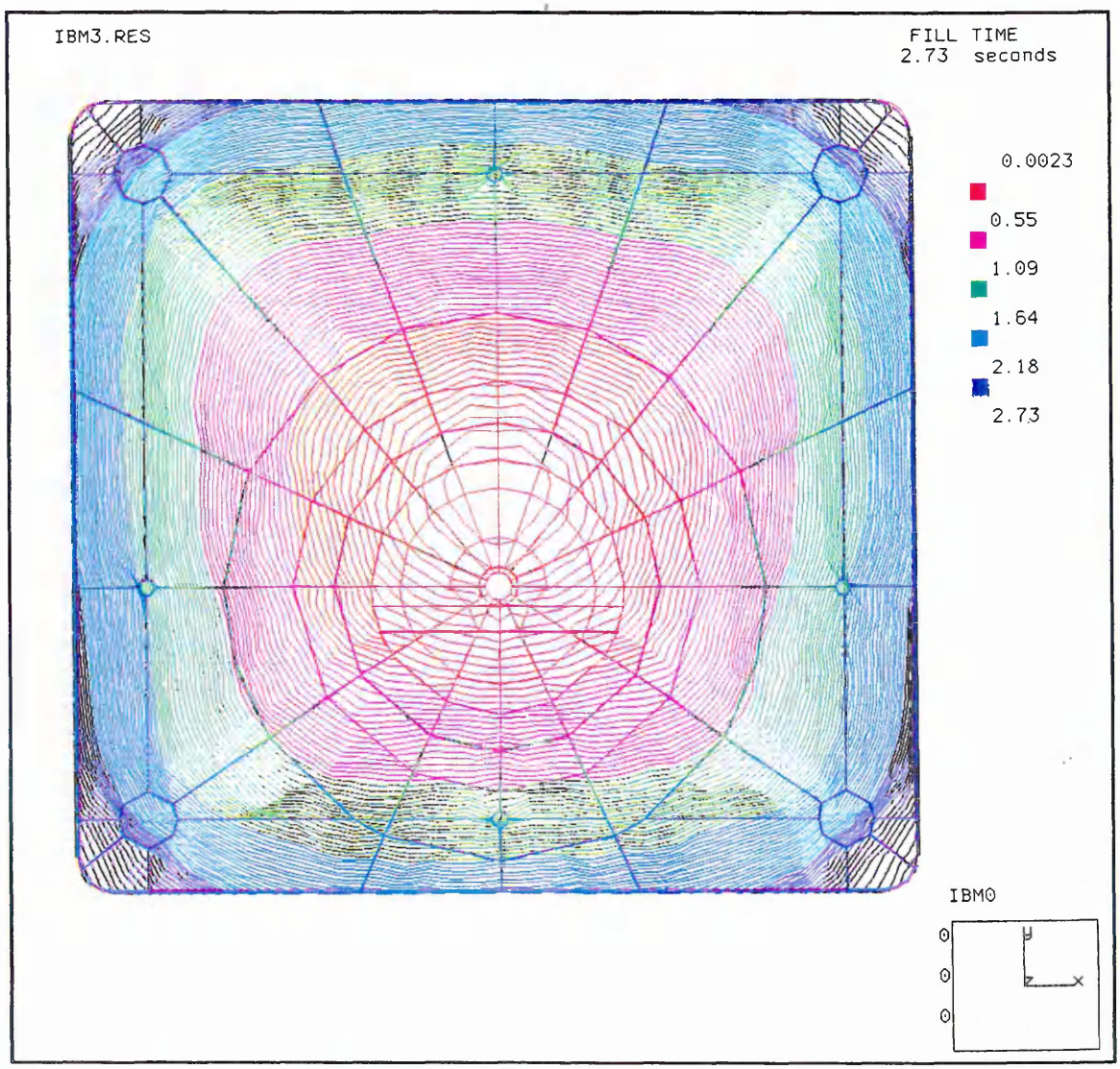

Fig.8.5.6 The flow pattern after reprofiling the wall.

This re-profiling results in the hotter melt flowing through the thicker paths to the corners, arriving there almost at the same time as it reaches the sides, and subsequently reducing the shear stress there. However, this re-profiling is just done by using the function of changing thickness element by element on the screen, and there is no rule to follow but trial and errors. Also there are some other aspects to be taken into account, for example, whether or not it would improve the shrinkage and warpage effects, and mould machining feasibility, etc. Therefore it should be expected to have a sounder research on this wall-profiling work.

The temperature and shear stress distributions after re-profiling the wall in this way are given in the next page. The material used here is ABS, thus the temperature and shear stress ranges are different from those shown in Chapter Seven.

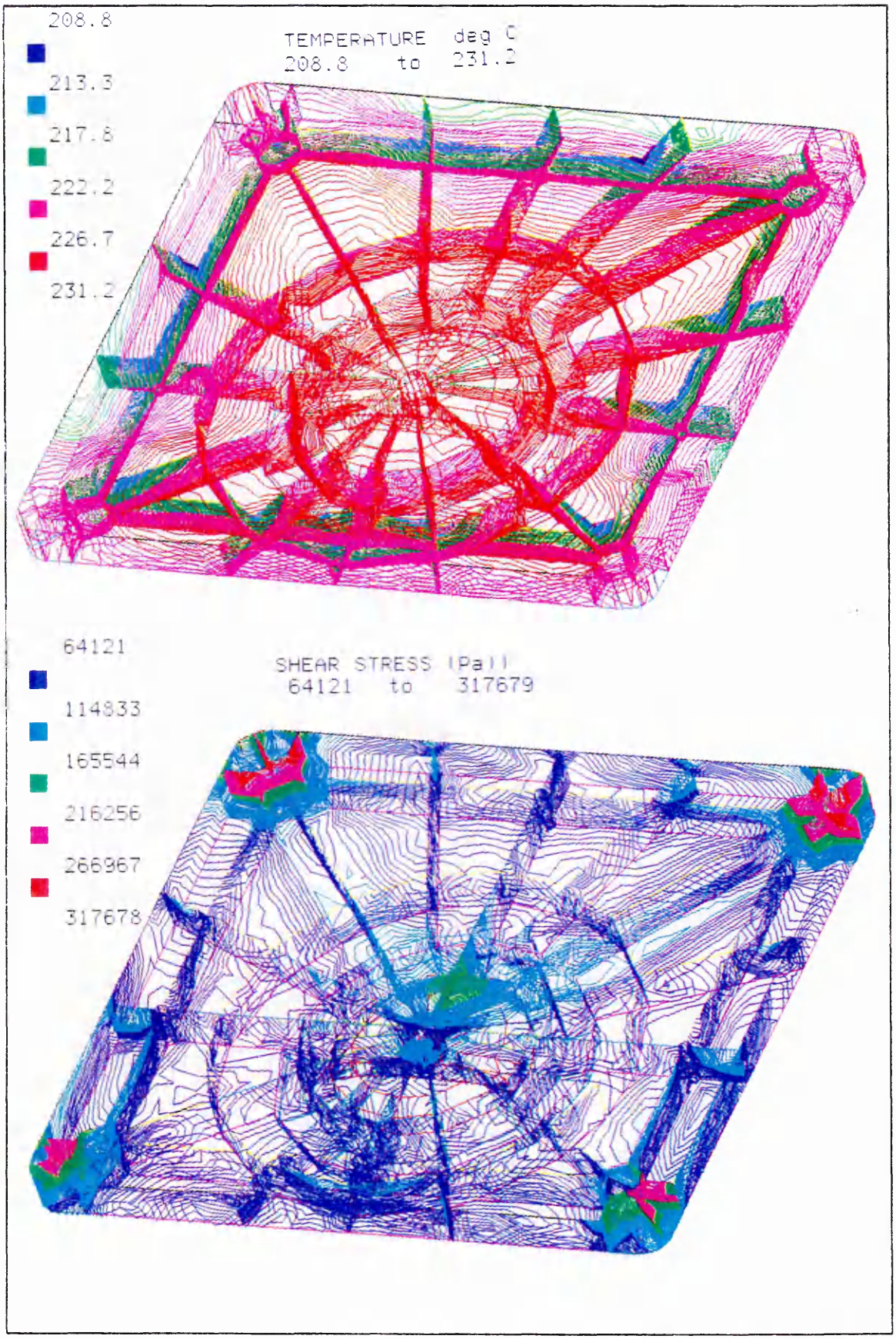

Fig.8.5.8. The temperature and shear stress distributions after re-profiling the wall.

8.6 Modules in Post-Processor

8.6.1 Introduction

The post-processor is designed separately from the pre-processor. The object to be processed is directly put into a three dimensional space which can be translated, rotated, and scaled. In this way, the object can be easily viewed in detail in any direction, from any side, and at any part freely by simply turning different valuators (which DRES, MOLDFLOW's post-processor, cannot do). Besides these basic functions, some other functions are designed such as displaying mesh result and thickness distribution, contouring the physical values for a three dimensional object, displaying moving pictures, plotting a vector picture, and so on.

8.6.2 Displaying Mesh and Thickness

Based on the IO interface and data structure, the plotting functions are simply to transfer the element and node information onto the screen in three dimensions. The reading and outputting of the data are much quicker than corresponding functions of MOLDFLOW's post-processor DRES since not much transformation need to be done in this module. With functions of turning valuators, the three dimensional object is just like an object in the hand, one can view it freely. The lower-right corner box shows a coordinate base axes for a clear indication of the view angle, the position of origin and the scale of the picture. Command "plot1" gives a colour picture in which different colour gives different thickness, and "plot0" gives a monochromatic picture using a default colour otherwise defined before-hand. Command "dispnum" can display the node numbers on each node with a reasonable size which will not be enlarged when the picture is being enlarged. A prompt will appear after the command to let the user give the range of the numbers to display. If "fill" command is used, the object is then filled with a previous defined colour as shown in Fig.8.6.1.

The output on other graphical facilities is based on a two dimensional information. For instance, in GHOST-80 environment the three dimensional coordinate data have to transformed into an X-Y only coordinates, then the graphical output is possible. In fact, all the laser-printed plots shown in this thesis are through this transformation.

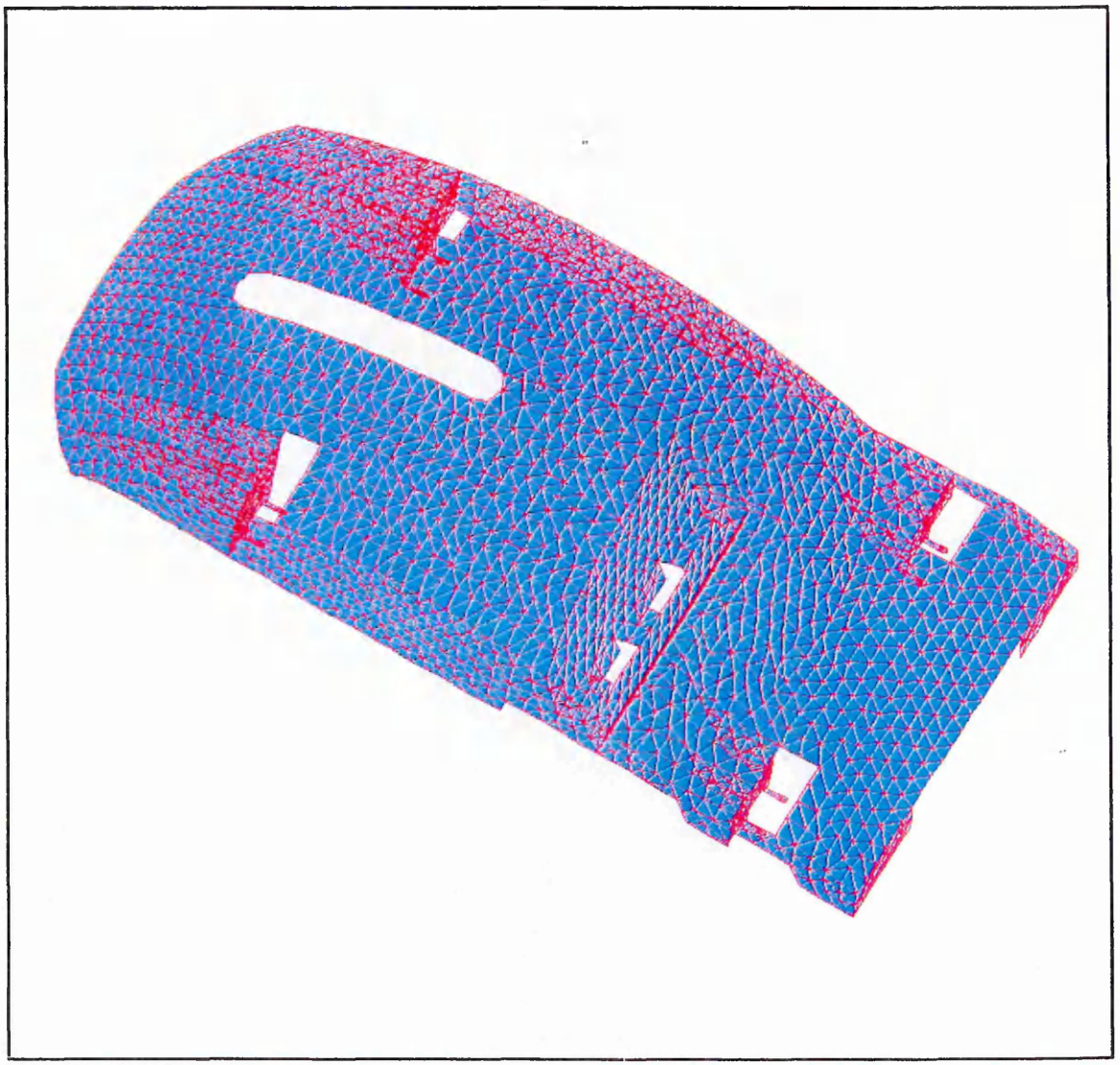

Fig.8.6.1 The objective filled with a colour.

8.6.3 Contouring physical values in a three dimensional object

Contour plotting (or isoline plotting) is normally a wide-adopted technique for representing a scalar function of two variables. The technique is actually to cut a three dimensional curve surface with a series of parallel planes, so that the scar curves left are the contour lines needed. However, for contouring on three dimensional surfaces of virtually no thickness, the technique can no longer be interpreted in an intuitive geometrical way since it is hard to imagine a four dimensional problem in a three dimensional space. For instance, a four dimensional function is expressed as follow:

$$Ax + By + Cz + Df(x, y, z) + E = 0 \qquad (8.6.1)$$

where A, B, C, D and E are constants, and f(x,y,z) is the scalar function to be contoured. The task is to use a series of f planes in four dimensional space (like f(x,y,z) = constants) to cut the curved surface. The scar curves left on the three dimensional object by the cuttings should then be the contour lines wanted. For more general cases the planes are four dimensional space planes. For a single element, the technique is interpreted in the following steps:

1).Calculate all the distances between node i (i=1,2,3) and the plane with the following equation:

$$D_i = \frac{(Ax_i + By_i + Cz_i + Df_i + E)}{\sqrt{A^2 + B^2 + C^2 + D^2}}; \quad (i = 1, 2, 3) \qquad (8.6.2)$$

2).Check if there is an crossed point between the plane and each side line of the element by the following condition:

$$D_i * D_j \leq 0; \qquad (i, j = 1, 2, 3; i \neq j) \qquad (8.6.3)$$

3).If equation (8.6.3) is satisfied, calculate the coordinates of the crossed point between the ith and jth node by

$$\left.\begin{aligned} x &= x_i + \frac{(Ax_i + By_i + Cz_i + Df_i + E)(x_i - x_j)}{\sqrt{A*(x_i - x_j) + B(y_i - y_j) + C(z_i - z_j) + D(f_i - f_j)}} \\ y &= y_i + \frac{(Ax_i + By_i + Cz_i + Df_i + E)(y_i - y_j)}{\sqrt{A*(x_i - x_j) + B(y_i - y_j) + C(z_i - z_j) + D(f_i - f_j)}} \\ z &= z_i + \frac{(Ax_i + By_i + Cz_i + Df_i + E)(z_i - z_j)}{\sqrt{A*(x_i - x_j) + B(y_i - y_j) + C(z_i - z_j) + D(f_i - f_j)}} \end{aligned}\right\} \qquad (8.6.4)$$

(i≠j, i,j=1,2,3)

4).The number of the crossed points in an element must be even, so check if there are crossed points on adjacent sides, or otherwise on the opposite sides, connecting them in pairs with a line.

If all these four steps are done for all the elements, all the segment lines will assemble a curve which is the scar curve left by the cutting plane. If the same steps are done for all the elements by a series of parallel planes of f(x,y,z) = constants, all the scar curves left by the these parallel planes are the contours wanted.

The subroutines for this function are PROFILE, DISTANCE, CROSS.

8.6.4 Vector an Fibre Plotting

One of the basic requirements for post-processing of a numerical analysis of a flow problem is the vector plotting. To the author's surprise, the MOLDFLOW version 5.4.2 here doesn't have the function to plot vectors. In fact, the result file produced by the MOLDFLOW doesn't even have the information of the velocity field since the basic variables are not velocity components. Therefore it cannot be used for studying either the velocity distribution across the part geometry, or the fibre-orientation. Only by writing one's own program, can these phenomena be studied and displayed.

The basic variables designed in CASIM include the velocity, therefore a vector display function for the velocity field is designed. Since the mathematical base behind this function is very simple, it is not necessary to mention it here. The subroutines for this function are VECTOR and ARROW. The vector pictures for this thesis have already shown in Chapters Five and Six.

The fibre plotting is based on the information of the fibre position and its orientation angle. Because of the assumptions used in the fibre orientation calculation in Chapter Five, the length of a fibre is not important (only for short fibres). Therefore it is just an input parameter here.

8.6.5 Representation of Shaded Objects or Functions and Images

The representation of shaded objects or functions and images is quite important in modern CAE techniques. Although a screen is a two-dimensional medium, a user can have an intuitive perception of a three dimensional object or function by using this technique. It is also one of the author's own interests to design the function into his own package.

IBM5080 has the capacity to display an image of 1024x1024 pixels with 256 colours or grey degrees. In the graPHIGS disk of the main frame there is a module called WINSOM which can produce an image file. The data

required for this module is typically a solid model of a geometry, which needs the resolution, light positions, rotation angles, scale, and the positions and sizes of some primitive solids, such as cube, sphere, cylinder, cone, and so on (as shown in Fig.8.6.2). These primitives are combined through the use of Boolean operations of union, intersection, and difference to construct complex shapes. Any shape produced by this operation is then transformed from a vector-oriented form to a raster-oriented (or dot-matrix) one with 256 levels of colour shading. This function is also one of the objectives for extending PHIGS, which will be included in PHIGS(++)[173], therefore the author does not need to code his own module to replace WINSOM.

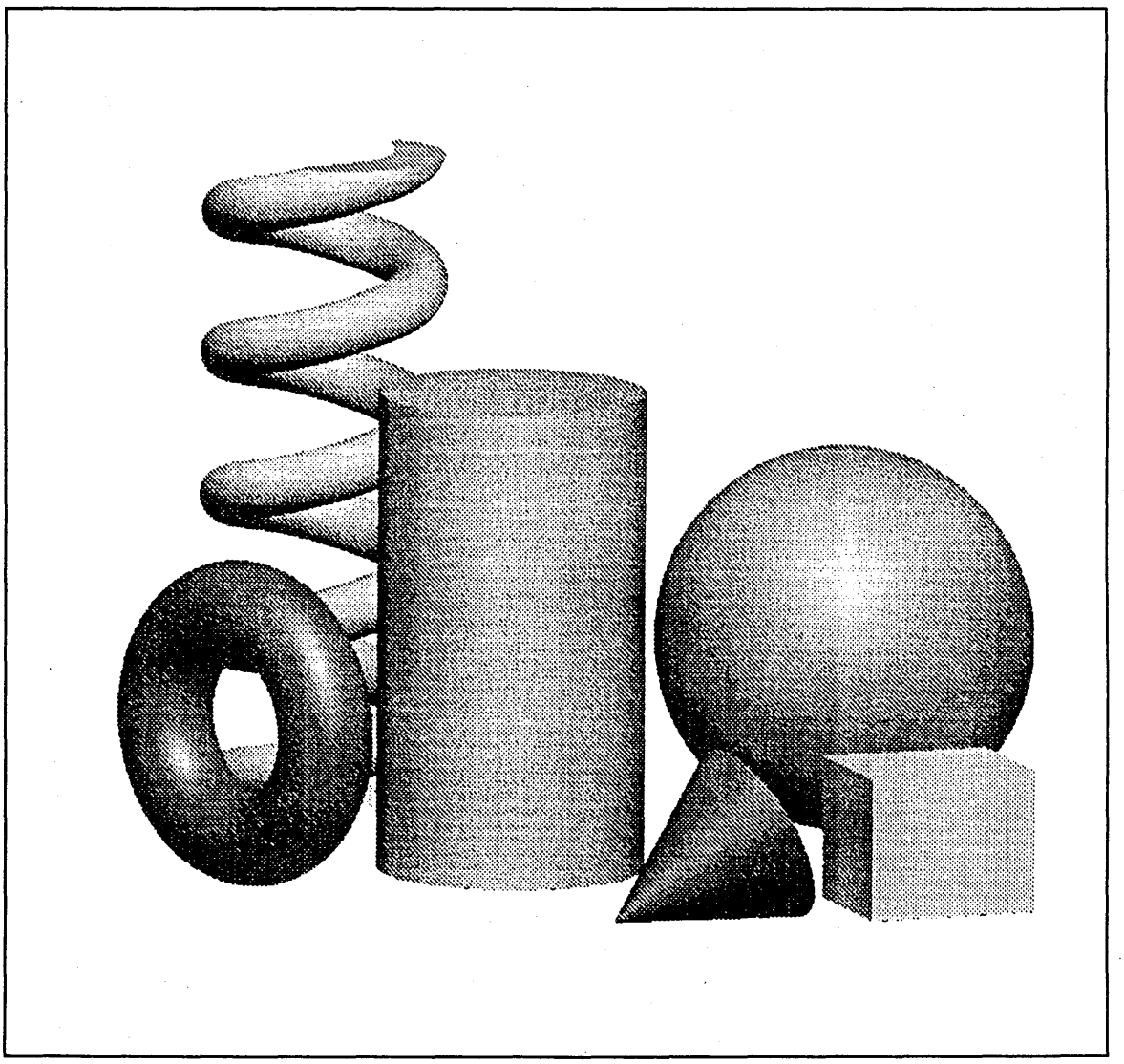

Fig.8.6.2 The geometrical primitives for constructing a geometry

The format of the image file is a square matrix which consists of $2^n x 2^n$ (n=1,10) EBCDIC codes to represent the pixels. Each of the codes represents a colour or a grey degree of the pixel. Since EBCDIC codes represent 256 different characters, the basic requirements for a subroutine to display the image is to load in the image file and to translate the codes into the corresponding colour numbers, and then send the pixels onto the corresponding positions of the screen. The colour pictures of the runner system in Fig.7.5.14 (page 194) are the examples of the images.

Another task for the image representation is to construct a PostScript file of the image which subsequently can be transferred through the computer network to other systems. For instance laser-printing of an image requires a PostScript file to describe the pixels.

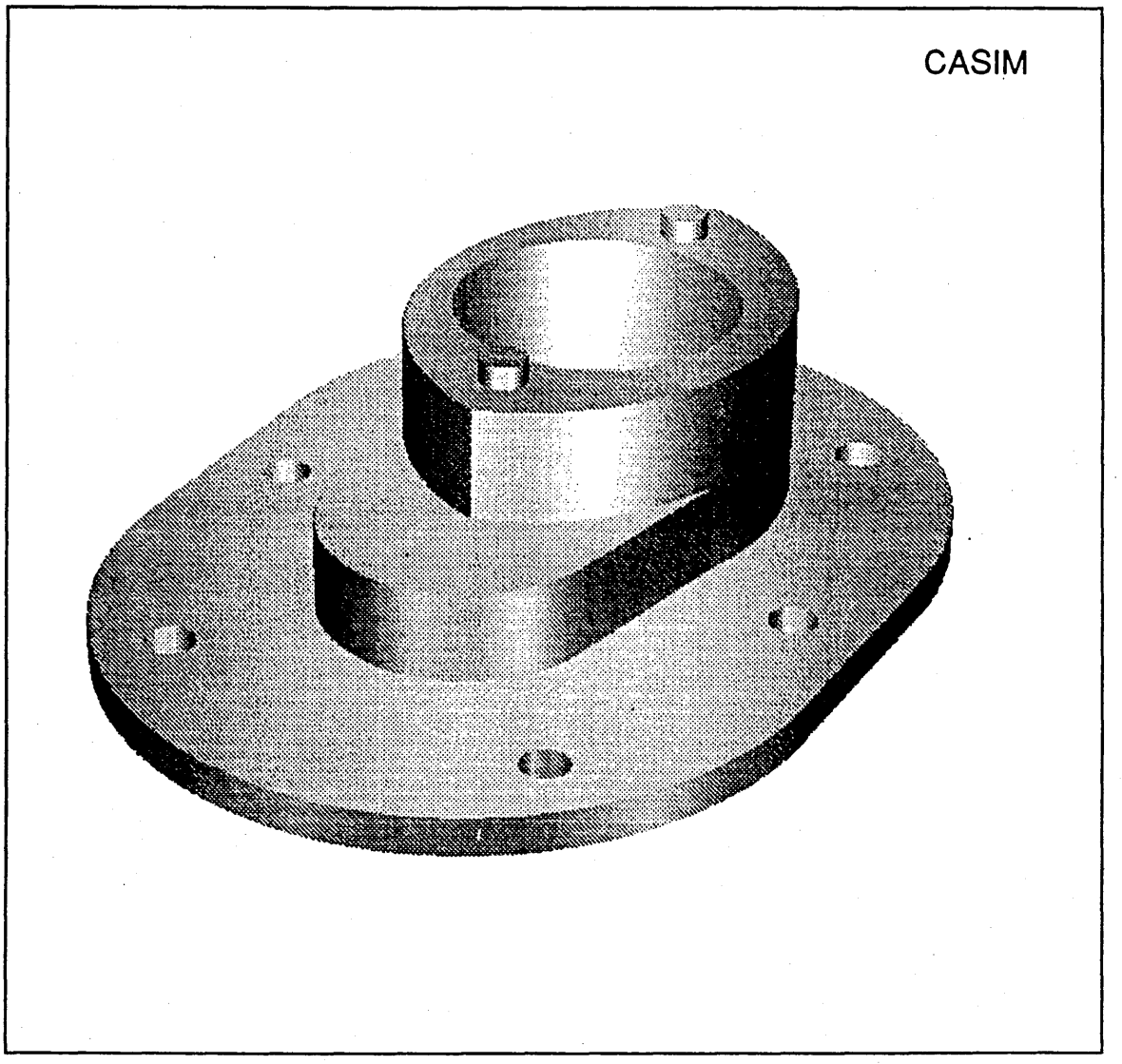

Fig.8.6.3 A three dimensional image of a part geometry

Since the version of graPHIGS here can only display 64 colours or greys onto the screen at the same time, and the laser-printer can only accept 16 greys, another function is to reduce the image grade down. Although the images have lost their nice colours and greys by such downgrading, the print-outs of them through laser-printing are still quite impressive. Hereafter there are some images printed from laser-printer 3820.

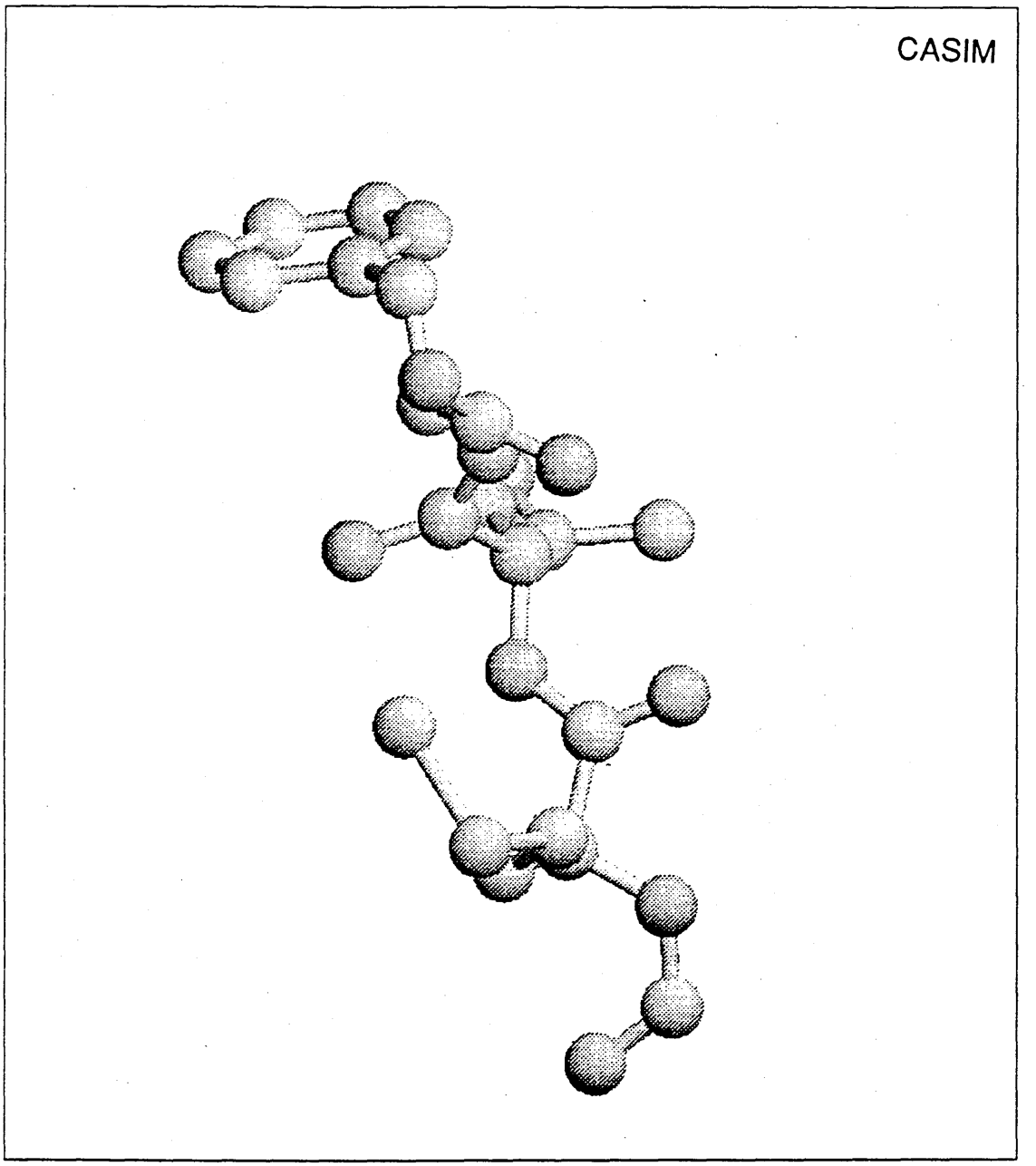

Fig. 8.6.4 A three dimensional image of a section of a large molecule

8.6.6 Animation

For studying a time-dependent problem, one task for post-processing is to be able to display animation which demonstrate the physical phenomena changing with time. CASIM is designed to show such kind of movie-like pictures. Since there are a large amount of data to handle, CASIM is designed to give users two choices in using this function. The first choice is to store all the information needed throughout the time period by relatively permanent result files, each of the files representing the physical fields at a time step. The digital result files have to be transferred sequentially into graphical files first and be stored in the disk, before all the graphical files can be displayed at a speed which can give the impression of a movie. Details of any individual time step can be chosen to be displayed again. The second choice is to connect the post-processing with the kernel computing, that is, to display the flow fields at the end of each time step of BE computation. Obviously, the first choice requires a very large disk space, but the animation can give a relatively fast speed and all the information of the result files is retained to be re-displayed without the computation again. On the contrary, the second choice requires only the necessary disk space to carry out the computation, but the animation is relatively slow, and the information has to be retained by auxiliary equipment like a video camera with a time-setting function.

8.7 BEM Modules

8.7.1 Introduction

In previous chapters (Three, Four, Five and Six), the mathematical developments for different boundary integral equations describing different problems in injection moulding and the numerical examples have been given in detail. The implementations of these models yield the following four BEM (Boundary Element Methods) modules which become the kernel of CASIM. Although there are quite big differences between Laplace and Stokes equations, and between steady and unsteady problems, the layouts of the flow charts for these modules appear to have many similarities, and are even identical in a more general view.

Simply speaking, these similarities stem from the basic principle behind the boundary integral equation method. It can be seen that the common

features of these four boundary element approximations are similar to those in the finite element methods which include evaluation of a local stiffness matrix for each boundary element, assemblage of the local stiffness matrices into a global stiffness matrix and the known boundary conditions into a vector to form simultaneous algebra equations, and finally the solution to the equations.

The differences come from the intrinsic properties in each of the governing equations. An unknown vector field requires double or triple the calculations of a scalar field in the evaluations and assemblages for the same number of elements; Time-dependent problems require a domain integral to be evaluated. The most essential difference is from the fundamental solution corresponding to each of the controlling equations.

From a viewpoint of reducing the whole program length to save the computer resources, the similarities might be used in the program structure design, that is, the same subroutines could be called for the same purpose in a different module, and the differences could be made by the interfacial arguments of the subroutines. Nevertheless, this kind of programming should be used only in some cases with extreme care because it breaks the rule of a "tree structure" — a module cannot be called by two or more modules in higher level. In fact, the predominant computer resource is the internal storage, which can be saved by separately using each of the modules. Therefore each of the modules is designed to reside in the internal storage temporarily by its own. However, the similarities can be certainly used for drawing flow charts for saving the pages here, and the differences are then explained later.

8.7.2 Flow Charts

Here is the flow chart (shown in Fig.8.7.1) for the simplest boundary element model — potential problem controlled by a Laplace equation. The basic structure of other boundary element models will not have much difference in terms of the boundary integrations. It is assumed that the pre-processing has been done so that all the boundaries have been broken into elements and the input files contain all the necessary information and the corrections have been checked.

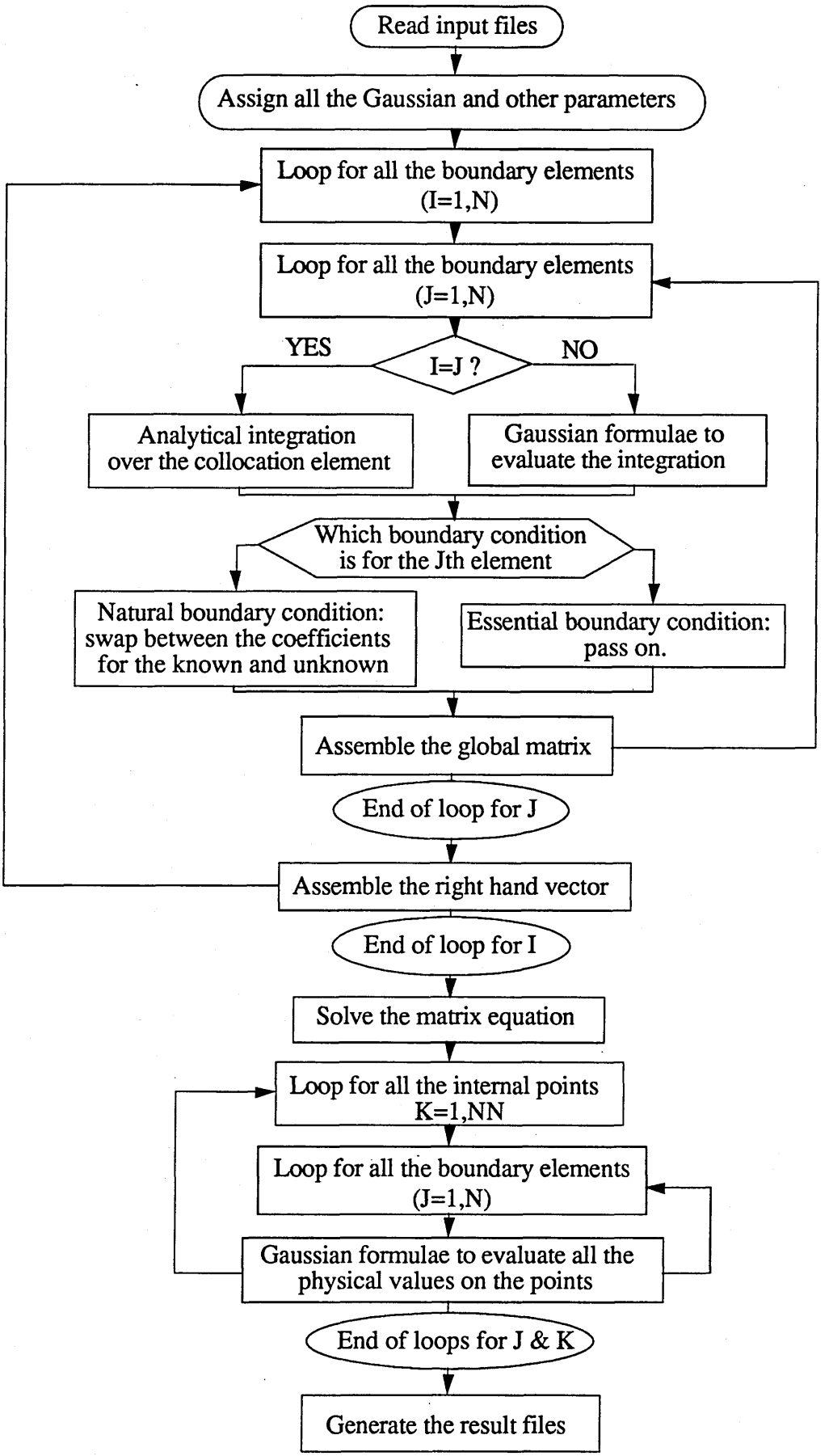

Figure 8.7.1 The flow chart of a boundary element program.

From this flow chart it can be seen that some modules can be drawn in terms of distinguished functions. For example, the first box can be written in a module called "INPUT", and the second called "GAUSS" for short. The function in the double loops after GAUSS is to form the coefficients of the matrix equation. Thus the module for the whole double loops is called "FMAT" for short. The module for solving the equations is obviously called "SOLVER" and the standard Gaussian elimination method is used in it because the matrix is a fully populated positive unsymmetrical one. The physical values on all the internal points are produced in module called "INTER" which differs from a lower level module called "INTE". This module is called by FMAT and INTER to perform the Gaussian formulae for evaluating the boundary integration, and the analytical integration over a collocation element is carried out by "INLO" module. The result files are produced by "OUTPUT" and "PLOT" modules for printing-out and graphical display, respectively.

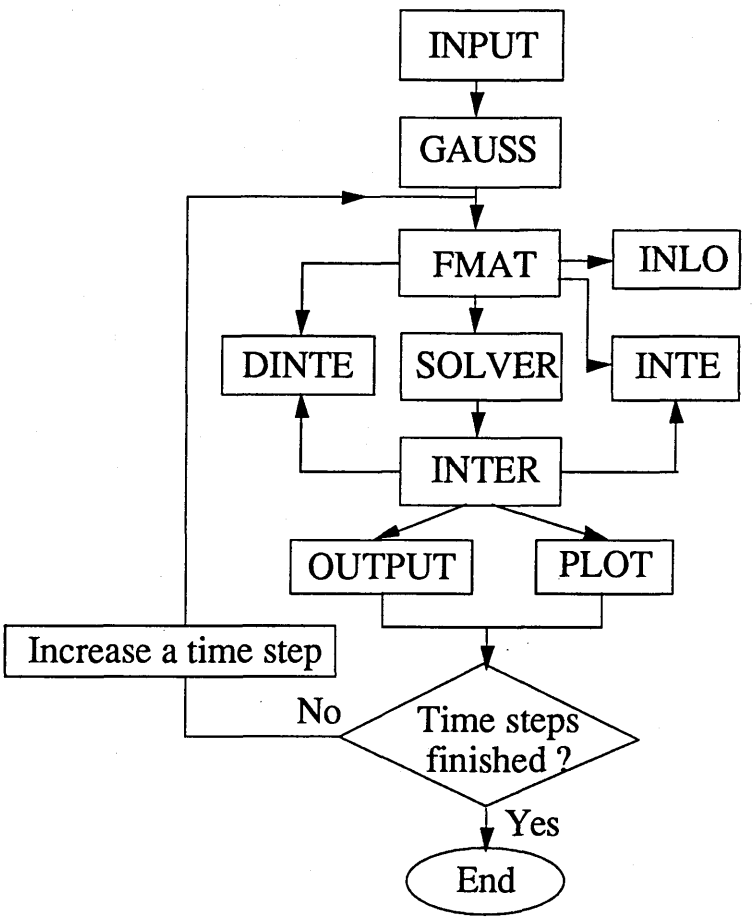

Figure 8.7.2 A flow chart composed of modules

In fact, all the boundary element models in this thesis involve a time-marching scheme. Thus a bigger loop for the time steps begins from FMAT and it goes through the rest of the flow chart until the physical fields at the moment are saved in the result files. For real time-dependent problems like transient heat conduction in Chapter Four and unsteady viscous flow in Chapter Six, a domain integral has to be evaluated. The module for evaluating the domain integral is called "DINTE" which is used within INTER and FMAT modules. For the transient heat conduction model, the coefficients of the matrix are the same in each time step, but those in the right hand side vector alter with time. A flow chart composed of the modules explains the procedure schematically in Fig.8.7.2.

Two more modules are added in the flow chart for the boundary element programs in Chapters Three, Five and Six. They are called "MOVEP" and "ADDPT". The main function of MOVEP is to move the nodes on the boundaries and / or internal points at their own speeds. From the examples given in these chapters it can be seen that there are the following cases. In some examples only the boundary nodes are moved with time to give a flow pattern of the front positions. For the problems in a frame of moving reference only the internal points are repositioned at each step to demonstrate the particle orientations. For a purely Lagrangian type flow both boundary nodes and internal points have to be updated to allow progression to the next step. Therefore at the interface of MOVEP an argument is passed indicating which group of points to move. Only those which are permitted to move in a specific direction (or directions) can move, and once they meet the wall, the conditions on them will be changed so that next time they cannot move so freely again. The functions of module ADDPT are to add and/or delete a node on the boundary. If the length of a boundary element is longer than a critical length (which is 1.2~1.5 times of the average length of all the elements in the programs), the module will automatically perform the "adding" function to insert a node between the two nodes defining the element. Then the boundary conditions and the physical values will be assigned to the new node and element. If the opposite case happens a node will be take away and the two adjacent elements will be joined together. Owing to the data structure, the insertion and deletion cause only the numbering system a little change, and the cells which other nodes have occupied for their information will not be repositioned. A block flow chart is shown below for this type of moving boundary problems.

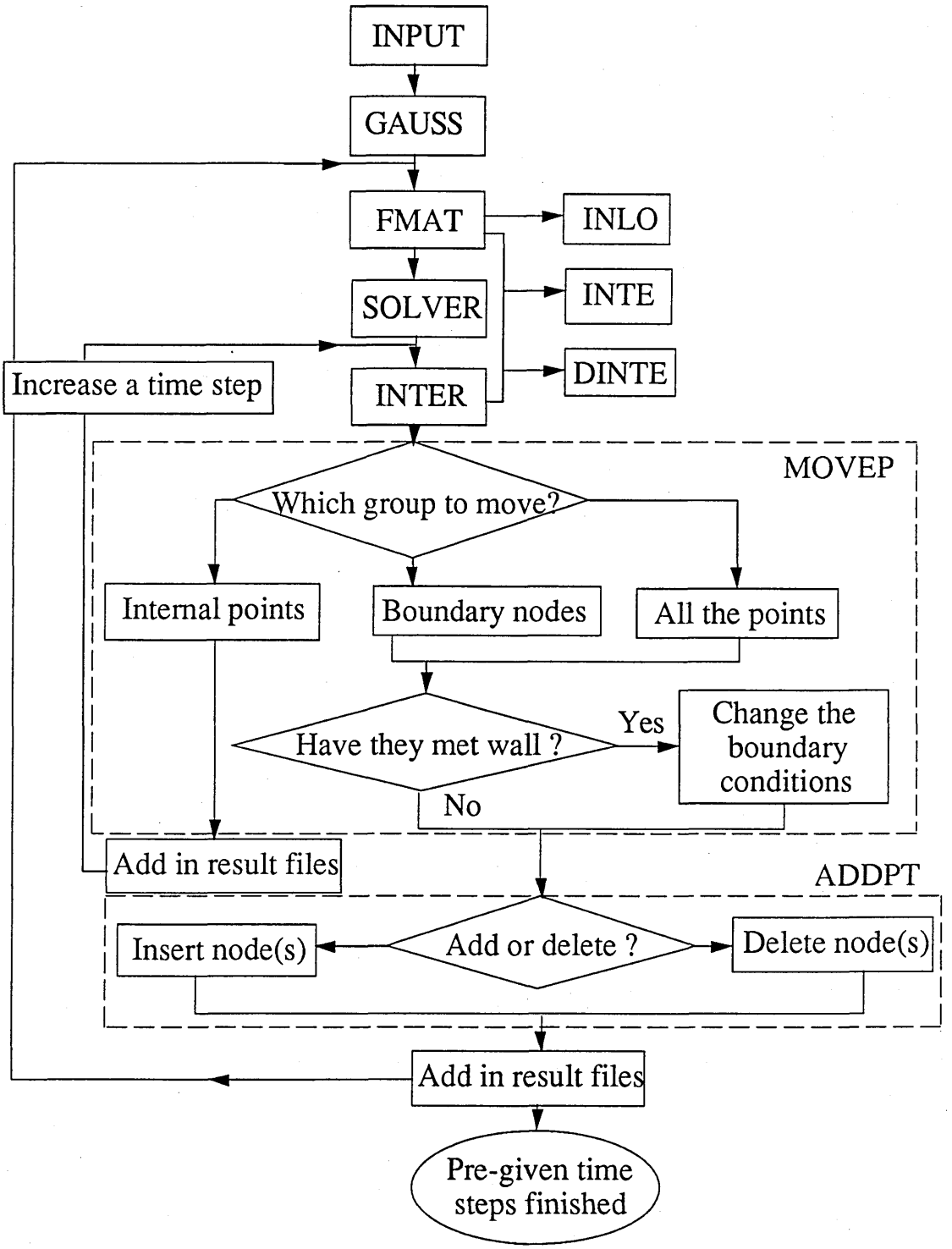

Figure 8.7.4 A block flow chart for moving boundary problems.

8.7.3 The differences

The lower level modules INTE, INLO and DINTE are coded for carrying out the integrations involving the fundamental solutions. Thus the basic difference in these four fundamental solutions appear to be included in

these three modules. There are some other differences which are explained in modular blocks below.

BEMST

Boundary Element Method for Steady Temperature or Potential Flow problems. The basic unknown for the matrix equation is a potential or a temperature field. If it is for a velocity potential, the unknown velocity components can be worked out in an explicit evaluation. These values on the internal points can be evaluated, in the same way as the potential values in INTER, by calling a lower level subroutine called INTEV. Yet the values of them on the boundaries have to be approximated by using equations (3.3.4) which use the flux values on the boundary. The calculation of the boundary values is coded in a lower module called BOUNV.
A time-marching scheme is needed only for a moving boundary problem, like the examples shown in Chapter Three.
BEMST can be easily extended for solving a Poisson equation which needs a domain integral to be evaluated.

BEMTR

Boundary Element Method for Transient Heat Transfer problems. The basic unknown for the matrix equation is a temperature field. A time marching scheme is needed, because the boundary never moves, the coefficients of the matrix will not be calculated again except the right hand side vector. A domain integral is needed for the base of forward time-marching.
For a multimedium heat transfer problem, all the geometrical and physical data group in terms of different media. FMAT is coded to handle the interfacial elements when their corresponding coefficients are put into the proper positions in the global matrix and right hand side vector.
In order to reduce the size of the matrix, a trial program of the model without the interfacial elements is coded. The difference is in the calculation of the distance inside the module INTE.

BEMSV

Boundary Element Method for Steady Viscous Flows. The basic unknowns for the matrix equation is the velocity components of a fluid flow field. The storage and calculations then doubled for a two dimensional problem. A time marching scheme is needed only for a moving surface problem in which case all the coefficients of the matrix have to be calculated again. A domain integral is needed for moderate or higher Renolds numbers' problems which are not the common case of injection moulding process.
The pressure, strain rate on the internal points can be worked out in a explicit form, and the formulas for the pressure, strain rates are coded in lower level modules called INTEP & INTES, respectively. For the pressure, strain rate values on the boundary nodes, another module called BOUNPS covers the calculation which uses the formulas given in Appendix C and avoids the singularities.

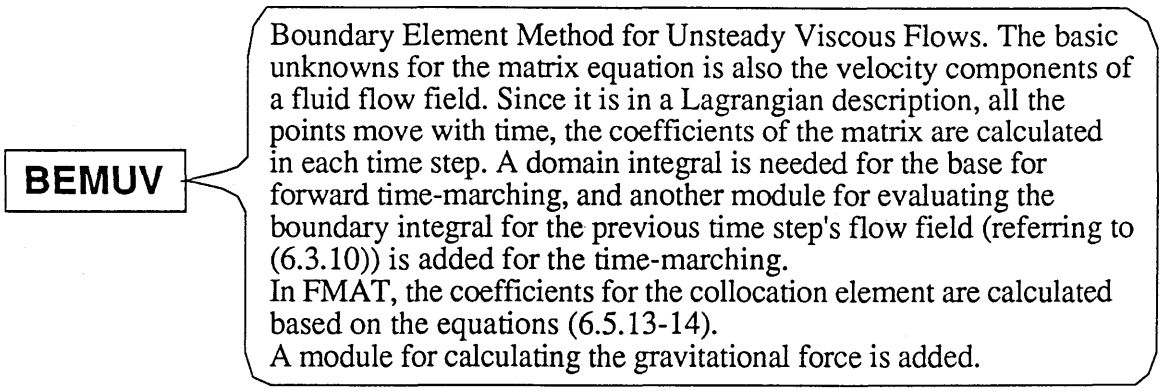

8.8 Miscellaneous

There are some other functions of CASIM which are not introduced in the previous sections because of less important and unnecessary lengthy. Some of them are mentioned briefly hereafter.

Two-dimensional geometry inputting by using the locator: One can put a two dimensional graph on the locator-board and use the locator to follow the boundaries / curves to input the information into the program. It appears on the screen and all the coordinates can be saved.

Displaying the functional keys of the choice board: when one puzzles how to use the function keys in the choice board, press one of the keys to display the all the menu immediately.

Palette: one of the functions is to set up the colour table. Theoretically, IBM5080 graphical terminal can display 32,767 colours. All one should do under CASIM status is to use the palette function, and click a colour, use three of the valuators to give the percentages of RGB (Red, Green, and Blue) to reset it.

Setting-up the boundary conditions: for a two dimensional problem, the boundary conditions can be setup by clicking each of the boundaries and give a sign for the correct condition. All the signs can be visualised on the screen so that they can be checked directly.

Chapter Nine

Concluding Remarks

In the previous chapters the mathematical models for computer simulation of injection moulding have been presented. Although the practical computer simulation work of some IBM's computer parts is based on a finite element package — MOLDFLOW, the development of boundary element techniques is the emphasis of the thesis. The obvious benefits in using the boundary element techniques have been shown through the examples, as the system equations are expressed exclusively in terms of unknowns at boundary nodes. The methods are especially attractive in moving free surface problems which usually require mesh generation at various stages of the analysis. Based on the theoretical developments, these models can be implemented for a three dimensional case. Although some form of domain integration is required when analysing the viscous flow problem, or the time-dependent heat transfer problem, the corresponding discretisation effort is relatively minor in contrast to what is involved in generating a full finite element mesh. However, it is precisely because of the domain integral involvement that the boundary-only scheme is considered to be limited in the case of material and geometric linear problems. From Chapter Two to Chapter Six it can be seen that the further work on these topics will unavoidably encounter a domain integral evaluation. In the last section of Chapter Two, a dual reciprocity method is introduced for overcoming the barrier, and in Chapter Four, the method is proposed again by the formulation for transforming the domain integral into boundary integral series which involves the temperature field at the previous time step. As long as the method works, some more developments can be easily done. Therefore the immediate work and the next step should be the implementation and examination of the dual reciprocity method.

Yet this is not the only problem occurring in the development and application of a boundary element method. From some references it can be seen that the method is better suited in a convex domain, otherwise the domain should be divided into convex sub-domains. This kind of division, however, may not be known beforehand if the domain has a moving boundary, such as the melt flow during the filling stage. For the cooling stage, a complicated geometric part may require a great number of

interfacial elements for multi-medium heat transfer analysis. Thus the potentials in further reducing the size of this type of problem are conceived in the discussions in Chapter Four.

If domain integral involvement and a concave domain are no longer of worry in the application of a boundary element method, the development of the integral equations for the temperature and pressure in Chapter Three can then be easily implemented. The whole physical phenomena of the melt flow in a thin cavity with an uniform thickness will then be worked out with much less computing effort. The problems mentioned in the discussion section of Chapter Three are still to be solved.

The generalised Newtonian flow models used in Chapters Two and Three should not be difficult to use in the formulations of the boundary integral equations in Chapters Five and Six. In fact, the creeping motion models are not limited to Newtonian flow. Starting from the creeping motion models, the boundary element techniques can be theoretically extended for studying flows with any kind of constitutive model. Tran-Cong and Phan-Thien[133] suggested a way to handle the non-Newtonian model within the Navier-Stokes equations, the parts of the extra stress tensor representing the non-Newtonian effects being put in a domain integral. Tosaka and Kakuda[151] also proposed that the Newtonian part and the time dependent part are separated from the extra stress tensor, and the remaining part joins the forcing vector on the right hand side. In this way the resulting equations can be transferred into a group of boundary integral equations. Apart from a domain integral which arise from the treatments of a non-Newtonian model, there is another difficulty troubling us — the convergence of the iteration with the domain integral. Nevertheless, complicated constitutive models are not advised in computer simulation of the melt flow in injection moulding process, because nowadays only the dominant characteristics need to be efficiently worked out. The further development of creeping motion models should include the temperature and shear-rate dependence of the viscosity, which means the energy equation must be taken into account.

It should be realised that the inherent limitation of the boundary element method is that it is based on the direct utilisation of a weight function — preferably the fundamental solution for the governing equations. What has been done in this thesis are the developments and applications of those equations for which the fundamental solutions are well known or can be worked out. In more complicated cases, for example, the compressible fluid

flow model which should be used in compression stage of the injection moulding, the fundamental solution(s) may not be obtained.

Using an existing package is very convenient for analysing physical phenomena appearing from a problem. Yet it has to said that for research, the creative ability may be limited within the capacity of the package. One can never do anything beyond what the package designers have coded. Of course nowadays computer packages are designed more and more flexibly and source statements are accessible by a user. This should be included as one of the basic requirements for CASIM program design.

Finally, it is well known that the topics in computer simulation of injection moulding include not only those which have been appeared in this thesis, but also many others. There is still a long way to go in the research on this work. This means that the research should never be limited to computer simulation, it must combine the theoretical and computational studies with the corresponding experimental ones.

REFERENCES

[1]Rosato, D.V.,"The Complete Injection Molding Operation", Chapter 1, *Injection Molding Handbook* (Ed. Dominick V. Rosato, Donald V. Rosato) 1986 Van Nostrand Reinhold, New York.

[2]German Patent DRP 485362.

[3]Laeis, M. E., *Der Spritzguß thermoplastischer Massen.* Carl Hanser Verlag, Munich, 1959.

[4]U.S. patent 2,734,226, February 14, 1956

[5]Johannabes, F. *Injection Molding Machines: A User's Guide*, Munchen; Wien: Hanser, 1983.

[6]"The MOLDFLOW Design Principles", Moldflow Pyt Ltd.

[7]Powell, P., "Basic Considerations: Processing — The Essential Rules", *Moulding Plastics to Tolerance*, Seminar on 19 Nov. 1987 in Solihull

[8]Thomas, R. and McCaffery, "The Prediction of Real Product Shrinkages, Calculated from a Simulation of the Injection Molding Process", Conference Proceedings of *SPE 47th ANTEC'89* , p371-375, 1989.

[9]Oda, K., White, J. L. and Clark, E. S., "Jetting Phenomena in Injection Mold Filling", *Polymer Engineering and Science*, Vol.16, No. 8, p585-592, 1976.

[10]Austin, C., "Flow of Plastics into a Mold", p349-358, "Process Analysis Tools for Plastics Processing", Chapter 13, *Injection Molding Handbook* (Ed. Dominick V. Rosato, Donald V. Rosato) 1986 Van Nostrand Reinhold, New York.

[11]Wang, K.K. *et al.* "Cornell Injection Molding Project", Progress Report #11, College of Engineering, Cornell University, Ithaca, NY, 1985

[12]Wang, K.K. "Computer-Aided Engineering (CAE) for Injection Molding of Plastics", *AIChE Symposium Series*, No.260 Vol. 84, p37-51, 1988

[13]Richardson, S., "Hele Shaw Flows with a Free Boundary Produced by the Injection of Fluid into a Narrow Channel", *Journal of Fluid Mechanics*. Vol. 56, part 4, p609-618, 1972.

[14]Wang, K.K., Shen, S.F., Hieber, C.A., and Stevenson, J.F. in Proceedings of the International Conference on Polymer Processing, MIT, (Ed. Suh, N.P., Sung, N.H.) Cambridge, MA, 1977, p293

[15]Harry, D.H. and Parrott, R.G.,"Numerical Simulation of Injection Mold Filling", *Polymer Engineering and Science*, Vol. 10. No.4. p209-214,1970

[16]Basov, N.I. and Felipchuk, I. I.,"Nonisothermal Flow of a Polymer Melt Accompanied by Phase Transition of the First Kind", *Heat Transfer-Soviet Research*, Vol.4, No.2, p94-101, 1972.

[17]Kamal, M. R. and Kenig, S., "The Injection Molding of Thermoplastics Part I: Theoretical Model", *Polymer Engineering and Science*, Vol. 12, p294-301, 1972

[18]Berger, J.L. and Gogos, C. G., "A Numerical Simulation of the Cavity Filling Process with PVC in Injection Molding", *Polymer Engineering and Science*, Vol. 13, p102-112,1973

[19]Broyer, E. Gutfinger, C. and Tadmor, Z. "A Theoretical Model for the Cavity Filling Process in Injection Modling", *Trans. Soc. Rheology*, Vol.19:3, p423-444 ,1975

[20]Kamal, M.R., Kuo, Y. and Doan, P.H., "The Injection Molding Behavior of Thermoplastics in Thin Rectangular Cavities", *Polymer Engineering and Science*, 15, p863-868,1975

[21]Kuo, Y. and Kamal, M.R., "The Fluid Mechanics and Heat Transfer of Injection Mold Filling of Thermoplastic Materials", *AIChE Journal*, Vol. 22, No. 4, p661-669, July, 1976

[22]White, James L., "Fluid Mechanical Analysis of Injection Mold Filling", *Polymer Engineering and Science*, Vol. 15, p44-50, 1975

[23]Hieber, C.A. and Shen, S.F., "A Finite-Element/Finite-Difference Simulation of the Injection-Molding Filling Process", *Journal of non-Newtonian Fluid Mechanics*, Vol. 7, 1-32, 1980

[24]Shen, S.F., "Simulation of Non-isothermal Polymeric Flows in the Injection Molding Process", *Finite Element Flow Analysis*, (Ed. T. Kawai), Proc. 4th Int. Symp. on Finite Element Methods in Flow Problems, University of Tokyo Press, 1982.

[25]Shen, S.F., "Simulation of Polymer Flows in the Injection Moulding Process", *Int. Journal for Numerical Method in Fluids*, Vol. 4, p171-183, 1984.

[26]Kwon, T.H., "Application of the Boundary Integral Method to the Non-isothermal Flow of a Polymeric Fluid Advancing in a Thin Cavity of Arbitrary Shape", M.S. Thesis, Cornell University, 1982.

[27]Jin, H., Samuelsson, A. and Tullberg, O., "Boundary Element Method for the Injection-Moulding Filling Process of Thin Cavities", *Engineering Analysis*, Vol. 2, No. 1, p9-15, 1985.

[28]Kamal, M.R., and Lafleur, P.G.,"Computer Simulation of Injection Molding", *Polymer Engineering and Science*, Vol. 22, No. 17, p1066-1074, 1982.

[29]Dietz, W.,"A Cooling Time Model for Plastic Processing Operations", *Polymer Engineering and Science*, Vol. 18, p1030-1036, 1978.

[30]Tadmor, Z., "Molecular Orientation in Injection Molding", *Journal of Applied Polymer Science* Vol. 18, p1753-1772, 1974.

[31]Bhattacharji, S. and Savic, P., *Proc. Heat Transfer Fluid Mech. Inst.* p248-, 1965.

[32]Castro, J.W. and Macosko, C.W., "Studies of Mold Filling and Curing in the Reaction Injection Molding Process", *AIChE Journal,* Vol. 28, No. 2, p250-260, March, 1982.

[33]Bigg, D.M., SPE ANTEC Tech. Papers, Vol. 21, p301-,1975.

[34]Huang, C.F., "Simulations of the Cavity Filling Process with the Marker-and-Cell Method in Injection Molding", Ph.D. thesis, Stevens Institute of Technology, Hoboken, N.J., 1978.

[35]Lafleur, P.G., and Kamal, M.R., "A Structure-Oriented Computer Simulation of the Injection Molding of Viscoelastic Crystalline Polymers Part I: Model with Fountain Flow, Packing, Solidification", *Polymer Engineering and Science*, Vol.26, p92-102,1986.

[36]Kamal, M.R. and Lafleur, P.G., "A Structure-Oriented Computer Simulation of the Injection Molding of Viscoelastic Crystalline Polymers Part II: Model Predictions and Experimental Results",*Polymer Engineering and Science*, Vol.26, p103-110, 1986.

[37]Welch,J.E.; Harlow,F.H.; Shannon,J.P.; Daly,B.J., "The MAC Method — A Computing Technique for Solving Viscous Incompressible Transient Fluid-Flow Problems Involving Free Surfaces", LA-3425, Nov. 1965.

[38]Mavridis, H., Hrymak, A.N. and Vlachopoulos, J., "Finite Element Simulation of Foutain Flow in Injection Molding", *J. Polymer Engineering and Science*, Vol. 26, No.7, p449-454, 1986.

[39]Mavridis, H., Hrymak, A.N. and Vlachopoulos, J., "Deformation and Orientation of Fluid Elements Behind an Advancing Flow Front", *J. Rheology*. Vol.30, No.3, p555-563, 1986.

[40]Tucker III, C.L., "Computer Modeling for Polymer Processing — Fundamentals", *Computer Aided Engineering for Polymer Processing*

(Series Editor: Bernhardt, E. C.) Vol. 2, Hanser Publishers, Munich-Vienna-New York, 1989

[41]Austin, C., "Mold Cooling", Soc. of Plastics Engrs. Tech. Papers, Vol.31, p764-766, 1985.

[42]Sing, K.J., "Design of Mold Cooling System", in *Injection Molding Fundamentals* (Ed. Isayev, A.I.), p567-606, Mercel Dekker, New York, 1987.

[43]Schauer, K.R., "Mold Cool Analysis", p358-381, "Process Analysis Tools for Plastics Processing", Chapter 13, *Injection Molding Handbook* (Ed. Dominick V. Rosato, Donald V. Rosato) Van Nostrand Reinhold, New York, 1986.

[44]Srinivasan, K. and Devries (Eds.) "Computer-Aided Design and Manufacture of Dies and Molds", *ASME*, 1988.

[45]Himasekhar, K. and Wang, K.K., "Mold-Cooling Simulation in Injection Molding of Three-Dimensional Thin Plastic Parts", 1989 National Heat Transfer Conference, HTD Vol. 110, *Numerical Heat Transfer With Personal Computers and SuperComputing*, p129-136, 1989.

[46]Manzione, L. T., "Applications of Computer Aided Engineering in Injection Molding", *Computer Aided Engineering for Polymer Processing* (Series Editor: Bernhardt, E. C.) Vol. 1, Hanser Publishers, Munich-Vienna-New York, 1987.

[47]Tseng, A.A., Sun, P.F. and Kolluri, S.P., "Computer-Aided Modeling of Polymer Processing: A Review", Conference Proceedings of *SPE 47th ANTEC'89* , p267-270, 1989.

[48]Crombie, A., A Seminar Report on Computer Simulation of Injection Moulding, 1989.

[49]Reddy, K. H., "The Development/Implementation of ACTFLOW, a CAE Environment Designed for Polymer Flow Analysis", Conference Proceedings of *SPE 47th ANTEC'89* , p1766-1768, 1989.

[50]Gosztyla, J. "CAD/CAM for Plastic Part and Mold Design", Chapter 12, *Injection Molding Handbook* (Ed. Dominick V. Rosato, Donald V. Rosato) Van Nostrand Reinhold, New York. 1986.

[51]Astarita, G., Marrucci, G., *Principles of Non-Newtonian Fluid Mechanics* McGraw-Hill, London, 1974.

[52]Schowalter, W. R., *Mechanics of Non-Newtonian Fluids*, Oxford: Pergamon, 1978.

[53]Bird, R. B., Armstrong, R. C., Hassager, O., *Dynamics of Polymeric Liquids* Vol. 1: Fluid Mechanics, John Willey & Sons, Inc. printed in U.S.A., 1987.

[54]Bird, R. B., *Dynamics of Polymeric Liquids* Vol. 2: Kinetic Theory, John Willey & Sons, Inc. printed in U.S.A., 1987.

[55]Tanner, R.I., *Engineering Rheology*, Oxford Engineering Science Series 14, Oxford Science Publications, 1988.

[56]Kamal, M. R. and Ryan, M.E., "Rheological Aspects in the Modeling of Plastic Processing", *Advances in Rheology*, Vol. 1: Theory (Ed. Baltasar Mena, Andres Garcia-Rejon and Carlos Rangel-Nafaile) Proc. IX Int. Congress on Rheology, Mexico, p67-127, 1984.

[57]Crochet, M. J. and Walters, K. "Numerical methods in non-Newtonian fluid mechanics", *Annual Review of Fluid Mechanics* ,Vol. 15, p241-260, 1983.

[58]Casewell, B., "Lagrangian Concepts for the Numerical Analysis of Viscoelastic Flow", *Amorphous Polymers and Non-Newtonian Fluids* — The IMA Volumes in Mathematics and Its Applications Vol. 6, (Ed. Dafermos, C.; Ericksen, J. L.; Kinderlehrer, D.) Springer-Verlag, p21-32, 1987.

[59]von Neumann, J. and Richtmyer, R.D., "A Method for the Numerical Calculations of Hydrodynamics shocks", *Journal of Application in Physics*, Vol. 21, p232-237, 1950.

[60]Kolsky, H.G., "A Method for the Numerical Solution of Transient Hydrodynamic Shock Problems in Two space Dimensions", Report LA-TR-73-3, Los Alamos Scientific Laboratory, 1955.

[61]Wilkins, M.L., "Claculation of Elastic-Plastic Flow", Report UCRL-7322, Rev. 1, Lawrence Livermore National Laboratory, 1969.

[62]Goudreau, G.L. and Hallquist, J.O., "Synthesis of Hydrocode and Finite Element Technology for Large Deformation Lagrangian Computation", *Computational Aspects of the Finite Element Method*, CAFEM-5, (Ed. Claudeman, J.F. and Rosanoff, R.A.), West Berlin, Germany, 1979.

[63]Huffenus, JP. and Khaletzky, D., "The Lagrangian Aproach of Advective Term Treatment and Its Application to the Solution of Navier-Stokes Equations", *Int. Journal for Numerical Methods in Fluids*, Vol. 1, p365-387, 1981.

[64]Hasseger, O. and Bisgaard, C. "A Lagrangian Finite Element Method for the Flow of Non-Newtonian Liquids", *Journal of Non-Newtonian Fluid Mechanics*, Vol. 12, p153-164, 1983.

[65]Bach, P. and Hassager, O.,"An Algorithm for the Use of the Lagrangian Specification in Newtonian Fluid Mechanics and Applications to Free-Surface Flow", *Journal of Fluid Mechanics*, Vol. 152, p173-190, 1985.

[66]Ramaswamy, B. Kawahara, M. and Nakayama, T.,"Lagrangian Finite Element Method for the Analysis of Two-Dimensional Sloshing Problems", *Int. Journal of Numerical Methods in Fluids*, Vol. 6 p659-670, 1986.

[67]Ramaswamy, B. and Kawahara, M.,"Lagrangian Finite Analysis Applied to Viscous Free Surface Fluid Flow", *Int. Journal of Numerical Methods in Fluids* Vol. 7, p953-984, 1987.

[68]Harlow, F. H., "The Particle-In-Cell Computing Method for Fluid Dynamics", *Methods in Computational Physics*, Vol. 3, Alder, Fernbach, and Rotenberg, Eds., Academic Press, New York and London, p319. 1964.

[69]Harlow, F. H. "PIC and Its Progeny", LA-UR-87-1862, 1987.

[70]Amsden, A. A.; Hirt, C. W., "YAQUI: An Arbitrary Lagragian-Eulerian Computer Program for Fluid Flow at All Speed", LA-5100, Mar. 1973.

[71]Peric, M., "A Finite Volume Method for the Prediction of Three-Dimensional Fluid Flow in Complex Ducts", Ph.D. Thesis, University of London, 1985.

[72]Wang, Z. and Li, H., "Free Lagrange Method with Slide Interfaces", p451-456, Computational Physics (Ed. Li De Yuan, Feng Da Hsuan), Proceedings of ICCP, World Scientific, 1988.

[73]Fredholm, I., "Sur une classe d'equations fonctionelles", *Acta Math.* Vol. 27, p365-390, 1903.

[74]Jaswon, M. A., "A Review of the Theory", Chapter 1, *Topics in Boundary Element Research* Vol. 1: Basic Principles and Applications, (Ed. Brebbia, C.A.), Springer-Verlag, Berlin Heidelberg New York Tokyo, 1984.

[75]Brebbia, C. A., *The Boundary Element Method for Engineers*, Pentech Press, London 1978.

[76]Nardini, D. and Brebbia, C. A.,"Boundary Element Integral Formulation of Mass Matrices for Dynamic Analysis", Chapter 7, *Topics in Boundary Element Research*, (Ed. Brebbia, C.A.), Vol.2, p192-207, Springer-Verlag, Berlin and New York, 1985.

[77]Wrobel, L.C., Brebbia, C.A. and Nardini, D., "The Dual Reciprocity Boundary Element Formulation for Transient Heat Conduction", *Finite*

Elements in Water Resources VI, (Eds. Sa da Costa, C.A., Melo Baptiste, A., Gray, W.G., Brebbia, C.A. and Pinder, G.F.) Springer, Berlin, 1986.

[78]Wrobel, L.C."On the use of Time-Dependant Fundamental Solutions for the Boundary Element Formulation of Diffusion Problems", *Boundary Elements X*, Vol.2 (Ed. Brebbia,C.A.) p1-13, 1988.

[79]Nowak, A. J. and Brebbia, C.A.,"The Multiple-Reciprocity Method. A New Approach for Transforming B.E.M. Domain Integrals to the Boundary",*Engineering Analysis with Boundary Elements*, No.3, Vol.6, p164-168, 1989.

[80]Nowak, A. J. and Brebbia, C.A., "Solving Helmholtz Equation by Multiple Reciprocity Method", *Computer and Experiments in Fluid Flow*, Ed. Carlomagno; G.M. and Brebbia; C.A., Computational Mechanics Publication, Southampton, p265-270, 1989.

[81]Nowak, A. J. and Brebbia, C.A., "The Multiple Reciprocity Boundary Method in Elasticity: A New Approach for Transforming Domain Integrals to the Boundary", *International Journal for Numerical Methods in Engineering*, No. 31, Vol. 4, p709-727, 1991.

[82]Neves, A. C. and Brebbia, C.A., "The Multiple Reciprocity Method Applied to Thermoelastic Problems with Concentrated and Distributed Heat Sources", *Boundary Element Technology VI*, (Ed. Brebbia, C.A.) p201-214, 1991.

[83]Trefftz, E. " Über die Kontraktion kreisförmiger Flüssigkeitsstrahlen" *Z. Math. Phys.*, 64, 34, 1917.

[84]Oseen, C. W., *Neuere Methoden und Ergebnisse in der Hydrodynamik*, Akad. Verlagsgesellschaft, Leipzig, 1927.

[85]Hess, J. L. and Smith, A. M. O.,"Calculation of Potential Flow about arbitrary bodies", *Progress in Aeronautical Sciences*, Vol.8 (Ed. Kuchemann, D.) Pergamon Press, London 1967.

[86]Wu, J.C. and Thompson, J.F. "Numerical Solutions of Time-Dependent Incom-pressible Navier-Stokes equations using an Integro-Differential Formulation", *Computational Fluids* Vol.1 p197-215, 1973.

[87]Coleman, C.J., "A Contour Integral Formulation of Plane Creeping Newtonian Flow", *Q. J. Mech. appl. Math.*,Vol. XXXIV, Pt. 4, p453-464, 1981.

[88]Coleman, C.J., "On the Use of Boundary Integral Methods in the Analysis of Non-Newtonian Fluid Flow", *J. of Non-Newtonian Fluid Mechanics*, Vol.16, p347-355, 1984.

[89]Bush, M.B. and Tanner, R.I.,"Numerical Solution of Viscous Flows Using Integral Equation Methods", *Int. J. Numerical Methods in Fluids*, Vol.3, p71-92, 1983.

[90]Tosaka, N. and Onishi, K.,"Boundary Integral Equation Formulations for Steady Navier-Stokes Equations Using the Stokes Fundamental Solutions",*Engineering Analysis*, Vol..2, p128-132, 1985.

[91]Tosaka, N. and Onishi, K.,"Boundary Integral Equation Formulations for Unsteady Incompressible Viscous Fluid Flow by Time-differenc-ing",*Engineering Analysis*, Vol.3, p101-104, 1986.

[92]Kitagawa, K., Brebbia, C.A., Wrobel, L.C. and Tanaka, M.,"Boundary Element Analysis of Viscous Flow by Penalty Function Formulation", *Engineering Analysis*, Vol.3, p194-200, 1986.

[93]Kitagawa, K., Brebbia,C.A. and Tanaka, M.,"A Boundary Element Analysis of Natural Convection Problems by Penalty Function Formulation," *Boundary Elements X*, (Ed. Brebbia, C. A.), Vol.2, p323-341, Springer-Verlag, Berlin and New York, 1988.

[94]Banerjee, P.K., Morino, L.(Ed.),"Boundary Element Methods in Nonlinear Fluid Dynamics", *Developments in Boundary Element Methods* Vol.6, Elsevier Applied Science, London, New York, 1990.

[95]Brebbia,C.A.(Ed.), "Viscous Flow Applications", *Topics in Boundary Element Research* Vol.5, Springer-Verlag, Berlin, Heidelberg, 1989.

[96]Hebeker, F.K.,"On Lagrangian and Boundary Element Methods for Some Unsteady Isothermal Navier Stokes Flows", *Boundary Elements X*, (Ed. Brebbia, C.A.), p373-380, 1988.

[97]Denn, Morton M., "Pressure Drop-Flow Rate Equation for Adiabatic Capillary Flow with a Pressure- and Temperature-Dependent Viscosity", *Polymer Engineer-ing and Science*, Vol.21, No.2, p65-68, Mid-February, 1981.

[98]Richardson, S.M., "Choking of Liquid Flows", *Journal of Fluid Mechanics*, Vol. 199, p563-568, 1989.

[99]Happel and Brenner, "*Low Reynolds Number Hydrodynamics*", Prentice Hall Inc. London, Sydney, Toronto, Delihi, Tokyo, 1965.

[100]Hagan, G. Annual Physical Chemistry, Vol. 46, p423-442, 1839.

[101]Poiseuille, J. L. Comptes Rendus, Vol. 11, p961-1041, 1840; Vol.12, p112, 1842.

[102]Ostwald, W., *Kolloid-Z.*, Vol. 36, p36-117, 1925; de Waele, A. *Oil Color Chemical Assoc. J.* Vol. 6, p33-38, 1923.

[103]Dodge, D.W. and Metzner, A.B., *AIChE J.*, Vol. 5, p189-204, 1959.

[104]Kleindienst, U., Doctoral Dissertation, Universität Stuttgart, 1976.

[105]Penwell,R.C., Porter,R. S. and Middleman, S.,"Determination of the Pressure Coefficient and Pressure Effects in Capillary Flow", *Journal of Polymer Science*, Vol.9, p731-745, 1971.

[106]Kearsley,E.A.,"The Viscous Heating Correction for Viscometer Flows",*Trans. Soc. Rheol.* Vol. 6, p253-261, 1962.

[107]Bird, R.B., Stewart, W.E. and Lightfoot, E.N. *Transport Phenomena*, Wiley, New York, p307-308, 1960.

[108]Dinh, S.M. and Armstrong, R.C.,"Non-isothermal Channel Flow of Non-Newtonian Fluids with Viscous Heating", *AIChE Journal* Vol. 28, No.2, p294-301, 1982.

[109]Martin, B, "Some Analytical Soluions for Viscometric Flows of Power-Law Fluids with Heat Generation and Temperature Dependent Viscosity", *Int. J. Non-Linear Mechanics*, Vol. 2 p285-301, 1967.

[110]Richardson, S.M., "Injection Moulding of the Thermaoplastics: Freezing of variable-viscosity fluids, I Developing Flows with very high heat generation", *Rheologica Acta*, Vol. 25, p180-190, 1986.

[111]Richardson, S.M., "Injection Moulding of the Thermaoplastics: Freezing of variable-viscosity fluids, II Developing Flows with very low heat generation", *Rheologica Acta*, Vol. 25, p308-318, 1986.

[112]Richardson, S.M., "Injection Moulding of the Thermaoplastics: Freezing of variable-viscosity fluids, III Fully-developed Flows", *Rheologica Acta*, Vol. 25, p372-379, 1986.

[113]Richardson, S.M., "Flows of Variable-Viscosity Fluids in Ducts with Heated Walls", Journal of Non-Newtonian Fluid Mechanics, Vol. 25, p137-156, 1987.

[114]Middleman, S. "*Fundamentals of Polymre Processing*", McGraw-Hill, 1977.

[115]Brebbia, C.A., and Nardini, D., "Dynamic Analysis in Solid Mechanics by an Alternative Boundary Element Procedure", *International Journal of Soil Dynamics in Earthquake Engineering*, Vol.2, p228-233, 1983.

[116]Wrobel, L.C. and Brebbia, C.A., "The Dual Reciprocity Boundary Element Formulation for Nonlinear Diffusion Problems", *Computer Methods in Applied Mechanics and Engineering*, Vol.65, p147-164, 1987.

[117]Loeffler, C.F. and Mansur,W.J., "Dual Reciprocity Boundary Formulation for Potential Problems in Infinite Domains", *Boundary Elements* X, p155-163, 1988.

[118]Reynolds, O., "On the Theory of Lubrication and Its Application to Mr. Beauchamps Tower's Experiments", *Phil. Trans. Royal Society*, Vol. 177, p157-234, 1886.

[119]Beyer, C.E. and Spencer, R.S., "Rheology in Molding", in *Rheology:Theory and Applications*, (Ed. Eirich, F.R.), Vol. 3, Chapter 14, p505-551, Acamedic Press, 1960.

[120]Himasekhar,K., Hieber,C.A. and Wang,K.K., "Computer-Aided Design Software for Cooling System in Injection Molding", Conference Proceedings of *SPE 47th ANTEC'89* , p352-355, 1989

[121]Kenig, S., and Kamal, M. R. "Cooling Molded Parts - A Rigorous Analysis", *Soc. of Plastics Engineers Journal*, July, p50-57, 1970

[122]Boley, B.A., Weiner, J.H. *Theory of Thermal Stresses*, J. Wiley, 1960

[123]Chang, Y.P., Kang, C.S., Chen, D.J., "The use of fundamental Green's functions for the solution of problems of heat conduction in anisotropic media", *Int. J. Heat Mass Transfer*, 16, p1905-1918, 1973

[124]Shaw, R.P., "An Integral Approach to Diffusion", *International Journal of Heat and Mass Transfer*, Vol.17, p693-699, 1974

[125]Wrobel, L.C., "Potential and Viscous Flow Problems Using the Boundary Element method", PhD Thesis, Southampton, 1981

[126]Wrobel, L.C., Brebbia, C.A., "Time Dependent Potential Problems", Chapter 6 in *Progress in Boundary Element Methods*, Vol. 1 (Ed. C.A. Brebbia), Pentech Press, London, Halstead Press, USA, 1981

[127]Skerget, P., Brebbia, C.A., "Time Dependent Non-Linear Potential Problems", Chapter 3 in *Topics in Boundary Element Research* Vol. 2, (Ed. C.A. Brebbia) p63-86, Springer-Verlag, New York, 1984

[128]Pina, L.G. and Fernandes, J.L.M., "Application in Transient Heat Conduction", Chapter 2 in *Topics in Boundary Element Research* Vol. 1, (Ed. C.A. Brebbia) p41-58, Springer-Verlag, New York, 1984

[129]Vick, B., Golan II, L.P., "Computational Aspects of the Boundary Element Method Applied to Frictional Heating", *Boundary Elements XIII*, (Ed. Brebbia, C.A.), p330-344, 1991

[130]Pasquetti, R. and Caruso, A. "Boundary Element Approach for Transient and Nonlinear Thermal Diffusion", *Numerical Heat Transfer*, Part B, Vol. 17, p83-99, 1990

[131]Abramowitz, M., Stegun, I.A., *Handbook of mathematical functions*. Dover Publications, New York, 1965

[132]Tran-Cong, T. and Phan-Thien, N., "Three Dimensional Study of Extrusion Process by Boundary Element Method. Part I. An Implementation of High Order Elements and Some Newtonian Results", *Rheologica Acta*, Vol. 27, p21-30, 1988

[133]Tran-Cong, T. and Phan-Thien, N., "Three Dimensional Study of Extrusion Process by Boundary Element Method. Part II. Some Non-Newtonian Results", *Rheologica Acta*, Vol. 27, p639-648, 1988

[134]Lorentz, H.A., Abhandl, Theoretical Physics, Vol.1, p23-, 1906

[135]Schmidt, L.R."A Special Mold and Tracer Technique for Studying Shear and Extensional Flows in a Mold Cavity During Injection Molding", *Polymer Engineer-ing and Science*, Vol.14, p797-800, 1974

[136]Schmidt, L.R., "Experimental Studies of Injection-Mold Filling", in *Proceedings of the International Conference on Polymer Process*, MIT, (Eds: Suh, N.P. and Sung, N.H.) Cambridge, MA, p315-328, 1977.

[137]Schmidt, L.R., "Interrelationship of Flow, Structure, and Properties in Injection Molding", *the Proceedings of the 2nd World Congress of Chemical Engineering*, Montreal, Canada, Vol.VI, p516-518, Oct., 1981.

[138]Kamal, M. R., in *Applications of Computer Aided Engineering in Injection Molding*, (Ed. Manzione,L.T.), Hanser Publishers, Munich-Vienna-New York,1987

[139]Gogos, C. G., Huang, C.F. and Schmdit, L. R. "The Process of Cavity Filling Including the Fountain Flow in Injection Molding", *Polymer Engineering and Science,* Vol. 26, p1457-1466, 1986.

[140]Schmidt, L.R., Private Communication. 1992.

[141]Jeffery, G.B., "The Motion of Ellipsoidal Particles Immersed in a Viscous Fluid", *Proceedings of Royal Society*, A102, p161-179, 1923.

[142]Goldsmith, H.L. and Mason, S.G., "The Microrheology of Dispersions", in *Rheology:Theory and Applications*, (Ed. Eirich, F.R.), Vol. 4, Chapter 2, p85-250, Acamedic Press, 1967.

[143]Givler, R.C., Crochet, M.J., Byron Pipes, R. "Numerical Prediction of Fiber Orientation in Dilute Suspensions", *Journal of Composite Materials*, Vol. 17, p330-343, 1983.

[144]Durlofsky, L. and Brady, J. F., "Dynamic Simulation of Hydrodynamically Interacting Particles", *Journal of Fluid Mechanics*, Vol. 180, p21-49, 1987.

[145]Tran-Cong, T. and Phan-Thien, N., "Stokes Problems of Multiparticle Systems: A Numerical Method for Arbitrary Flows", *Physical Fluids* A 1(3), p453-461, 1989.

[146]Ingber, M. S., "Numerical Simulation of the Hydrodynamic Interaction Between a Sedimenting Particle and a Neutrally Buoyant

Particle", *International Journal for Numerical Methods in Fluids*, Vol. 9., p263-273, 1989.

[147]Ingber, M. S., Li, J., "A Boundary Element Study of the Motion of Rigid Particles in Internal Stokes Flow", *Boundary Elements* XIII, p149-160, 1991.

[148]Hörmander, L., "On the theory of general partial differential operators", Acta Mathematica, 94, p161- , 1955.

[149]Dargush, G.F. and Banerjee, P.K., "A Time-Dependent Incompressible Viscous BEM for Moderate Reynolds Numbers", Chapter 3 of reference [93].

[150]Piva, R. and Morino, L., "A Boundary Integral Formulation in Primitive Variables for Unsteady Viscous Flows", Chapter 4 of reference [93].

[151]Tosaka, N., and Kakuda, K., "Newtonian and Non-Newtonian Unsteady Flow Problems", Chapter 5 of reference [93].

[152]Lee, C.-C., Folgar, F. and Tucker, C.L., "Simulation of Compression Molding for Fiber-Reinforced Thermosetting Polymers", *Journal of Engineering for Industry*, Vol. 106, p114-125, 1984.

[153]Osswald, T. A. and Tucker, C. L., "A Boundary Element Simulation of Compression Mold Filling", *Polymer Engineering and Science,* Vol. 28, No. 7, p413-420, 1988.

[154]Barone, M.R. and Osswald, T.A., "Boundary Integral Equations for Analyzing the Flow of a Chopped Fiber Reinforced Polymer Compound in Compression Molding", *Journal of Non-Newtonian Fluid Mechanics*, Vol.26, p185-206, 1987.

[155]Barone, M.R. and Caulk, T.A., "A Model for the Flow of a Chopped Fiber Reinforced Polymer Compound in Compression Molding", ASME *Journal of Applied Mechanics*, Vol.53, p361-371, 1986.

[156]"CAD/CAE Interfaces to MOLDFLOW", Moldflow Pty Ltd.

[157]Austin, C.,"Go With the Flow",*World Plastics & Rubber Technology*, Cornhill Publications Limited, London, 1989.

[158]"MOLDFLOW manuals", Vol. I & II, Moldflow Pty Ltd.

[159]Ng, Chung-hang, "Computer Simulation of an Injection Moulding", Final Year (Hons) Project Report, Department of Mechanical Engineering, University of Glasgow, May, 1990.

[160]"Modelling of Grille Details for MOLDFLOW Flow Analysis", Moldflow Pty Ltd.

[161]Pye, R.G.W., "Injection Mould Design",Longman Scientific & Technical, 1989

[162]ABAQUS, Version 4.8, Hibbitt, Karlsson & Sorensen, Inc., 1989.

[163]GKS — Graphical Kernel System, ISO IS 7942, 1985

[164]CATIA Base, Version 3, Dassault Systems, March 1988

[165]IAX — Image Applications eXecutor, IBM IAX Image Processing System, First Edition, IBM United Kindom Scientific Centre, Aug. 1987.

[166]I-DEAS™ — Integrated Design Engineering Analysis Software, Level 4 SDRC — Structural Dynamics Research Corporation, 1988

[167]PATRAN, PDA Engineering, Basingstoke, U.K.

[168]UNIRAS, Version 6.1, UNIRAS A/S, SØBORG, Denmark, June 1989.

[169]PHIGS — Programmer's Hierarchical Interactive Graphics System, ISO IS 9592, 1985.

[170]Calderbank, V. J., Prior, W. A. J., The GHOST Graphical Output System, UKAEA, Culham Laboratory, 1977.

[171]Zhong, W., "*Programming on Computational Structural Mechanics in Micro-computer*", Hydroelectro-power Publication, Beijing, 1986.

[172]Wirth, N. "*Algorithm + Data Structure = Program*", Prentice-Hall, 1976

[173]Encarnacao, J.L.; Lindner, R.; Schlechtendahl,E.G. et al, "*Computer Aided Design, Fundamentals and System Architectures*", Second, Revised and Extended Edition, Springer-Verlag, Berlin Heidelberg New York London Paris Tokyo Hong Kong Barcelona, 1990

Appendix A

Integral Formulation For Heat Convection With Constant Velocity

The integral equation for this case can be easily derived by using the weighted residual method, as we use the fundamental solution as the weight function for equation (4.3.4) over the spatial and time domain $\Omega x[t,t_0]$

$$\int_{\Omega}\left(\alpha T_{,jj} - \bar{u}_1\delta_{1j}T_{,j} - \frac{\partial T}{\partial t'}\right)T^* d\Omega\, dt' = 0 \qquad (A.1)$$

Integrating it by parts it becomes

$$\int_{t_0}^{t}\left\{\int_{\Gamma}\left(\alpha T_{,j} - \bar{u}_1\delta_{1j}T\right)T^* n_j d\Gamma - \int_{\Omega}\left[\left(\alpha T_{,j} - \bar{u}_1\delta_{1j}T\right)T^*_{,j} + \frac{\partial T}{\partial t'}T^*\right]d\Omega\right\}dt' = 0 \qquad (A.2)$$

The first part of the second integral can be integrated again by parts:

$$\int_{t_0}^{t}\left[\int_{\Gamma}\left(\alpha T_{,j} - \bar{u}_1\delta_{1j}T\right)T^* n_j d\Gamma - \int_{\Gamma}\alpha T T^*_{,j} n_j d\Gamma\right]dt' +$$
$$\int_{t_0}^{t}\int_{\Omega} T\left(\alpha T^*_{,jj} + \bar{u}_1\delta_{1j}T^*_{,j} + \frac{\partial T^*}{\partial t'}\right)d\Omega dt' - \int_{t_0}^{t}\int_{\Omega}\left(T\frac{\partial T^*}{\partial t'} + T^*\frac{\partial T}{\partial t'}\right)d\Omega dt' = 0 \qquad (A.3)$$

The first domain integral disappears since the adjoint equation equals zero before time t, and we have the following equality from above derivation:

$$\int_{t_0}^{t}\left[\int_{\Gamma}\alpha T\frac{\partial T^*}{\partial n}d\Gamma - \int_{\Gamma}\left(\alpha\frac{\partial T}{\partial n} - \bar{u}_1 n_1 T\right)T^* d\Gamma\right]dt' + \int_{t_0}^{t}\int_{\Omega}\frac{\partial(TT^*)}{\partial t'}d\Omega dt' = 0 \qquad (A.4)$$

The last term of this expression can be modified by interchanging the order of integration, i.e.

$$\int_{t_0}^{t}\int_{\Omega}\frac{\partial(TT^*)}{\partial t'}d\Omega dt' = \int_{\Omega} TT^*\Big|_{t'=t} d\Omega - \int_{\Omega} TT^*\Big|_{t'=t_0} d\Omega \qquad (A.5)$$

The fundamental solution has the following property:

$$\lim_{t' \to t} T^* = \delta(x - x') \qquad (A.6)$$

so that the first integral relates directly to the value of the temperature at point x and at time t. Finally, we have the integration equation for the temperature distribution in the fluid field:

$$cT(x,t) = \int_{\Omega} TT^*\Big|_{t'=t_0} d\Omega + \int_{t_0}^{t}\left[\int_{\Gamma}\left(\alpha\frac{\partial T}{\partial n} - \tilde{u}_1 n_1 T\right)T^* d\Gamma - \int_{\Gamma}\alpha T\frac{\partial T^*}{\partial n}d\Gamma\right]dt' \qquad (A.7)$$

Appendix B

Exponential Integral Function and Its Approximations

The exponential integral function is defined by

$$E_1(x) = \int_x^{\infty} \frac{e^{-u}}{u}\, du \qquad \text{(B. 1)}$$

The series expansion of this function is

$$E_1(x) = -\gamma - \ln x - \sum_{n=1}^{\infty} \frac{(-1)^n x^n}{n\, n!} \qquad \text{(B. 2)}$$

where γ=.5772156649 . . . . is Euler's constant.

The polynomial and rational approximations of this function is given as follows:

$$\left.\begin{aligned} &E_1(x) = -\ln x + a_0 + a_1 x + a_2 x^2 + a_3 x^3 + a_4 x^4 + a_5 x^5 + \varepsilon(x) \\ &a_0 = -.57721566,\ a_1 = .99999193,\ a_2 = -.24991055, \\ &a_3 = .05519968,\ a_4 = -.00976004,\ a_5 = .00107857 \\ &0 \le x \le 1;\ |\varepsilon(x)| < 2 \times 10^{-7} \end{aligned}\right\} \qquad \text{(B. 3)}$$

$$\left.\begin{aligned} &E_1(x) = \frac{1}{xe^x} \frac{x^4 + b_1 x^3 + b_2 x^2 + b_3 x + b_4}{x^4 + c_1 x^3 + c_2 x^2 + c_3 x + c_4} + \varepsilon(x) \\ &b_1 = 8.5733287401,\ b_2 = 18.0590169730, \\ &b_3 = 8.6347608925,\ b_4 = .2477737343 \\ &c_1 = 9.5733223454,\ c_2 = 25.6329561486, \\ &c_3 = 21.0996530827,\ c_4 = 3.9584969228 \\ &1 \le x \le \infty;\ |\varepsilon(x)| < 2 \times 10^{-8} \end{aligned}\right\} \qquad \text{(B. 4)}$$

The integrations over the linear collocation element can be evaluated analytically:

$$I_1 = \int_0^R \left(1 - \frac{r}{R}\right) E_1(s)\,dr = \frac{R}{2}\left[3 - \gamma - \ln S - \sum_{n=1}^{\infty} \frac{(-1)^n S^n}{n(2n+1)(n+1)!}\right] \quad (B.5)$$

$$I_2 = \int_0^R \frac{r}{R} E_1(s)\,dr = \frac{R}{2}\left[1 - \gamma - \ln S - \sum_{n=1}^{\infty} \frac{(-1)^n S^n}{n(n+1)!}\right] \quad (B.6)$$

$$I_3 = \int_0^R \left(1 - \frac{r}{R}\right)^2 E_1(s)\,dr$$

$$= \frac{R}{3}\left[\frac{11}{3} - \gamma - \ln S - \sum_{n=1}^{\infty} \frac{3(-1)^n S^n}{n(2n+1)(2n+3)(n+1)!}\right] \quad (B.7)$$

$$I_4 = \int_0^R \frac{r^2}{R^2} E_1(s)\,dr = \frac{R}{3}\left[\frac{2}{3} - \gamma - \ln S - \sum_{n=1}^{\infty} \frac{3(-1)^n S^n}{n(2n+3)n!}\right] \quad (B.8)$$

where $s = \alpha r^2$ and $S = \alpha R^2$, α is a constant.

Each of the four infinite series is practically formed by the products in which the general terms are given as follows (superindex is corresponding to the order of the integrals):

$$S_1^1 = \frac{S}{6}; \quad S_n^1 = S_{n-1}^1 \frac{(2n-1)(1-n)}{(2n+1)(n+1)n} S \quad (B.9)$$

$$S_1^2 = \frac{S}{2}; \quad S_n^2 = S_{n-1}^2 \frac{(1-n)}{(n+1)n} S \quad (B.10)$$

$$S_1^3 = \frac{S}{30}; \quad S_n^3 = S_{n-1}^3 \frac{(2n-1)(1-n)}{(2n+3)(n+1)n} S \quad (B.11)$$

$$S_1^4 = \frac{S}{5}; \quad S_n^4 = S_{n-1}^4 \frac{(2n+1)(1-n)}{n(2n+3)n} S \quad (B.12)$$

Appendix C

Pressure, Stresses and Strain Rates on Boundary

At each boundary node, the pressure P, stresses and strain rates can be determined by solving the following relations simultaneously:

$$\sigma_{ji}(\zeta)n_j(\zeta) = N_\omega(\zeta)\tau_{i\omega} \qquad (C.1)$$

$$\sigma_{ji}(\zeta) + \delta_{ji}\,\mathrm{Re}P(\zeta) - U_{i,j}(\zeta) - U_{j,i}(\zeta) = 0 \qquad (C.2)$$

$$U_{i,j}(\zeta)\frac{\partial x_j}{\partial \zeta} = \frac{\partial N_\omega}{\partial \zeta}U_{i\omega} \qquad (C.3)$$

$$\mathrm{Re}P(\zeta) + \frac{1}{\delta_{ii}}\sigma_{ii}(\zeta) = 0 \qquad (C.4)$$

For two dimensional problems, there are nine equations from which nine unknowns are to be solved. Two further relations can be used:

$$\sigma_{xy} = \sigma_{yx} \qquad (C.5)$$

$$U_{xx} + U_{yy} = 0 \qquad (C.6)$$

Then equations (C.1) become

$$\left.\begin{aligned}\sigma_{xx}n_x + \sigma_{xy}n_y &= T_x\\ \sigma_{xy}n_x + \sigma_{yy}n_y &= T_y\end{aligned}\right\} \qquad (C.7)$$

Equation (C.2) become

$$\left.\begin{aligned}\sigma_{xx} + ReP - 2U_{xx} &= 0\\ \sigma_{yy} + ReP - 2U_{yy} &= 0\\ \sigma_{xy} - U_{xy} - U_{yx} &= 0\end{aligned}\right\} \qquad (C.8)$$

Equations (C.3) become

$$\left.\begin{aligned}U_{xx}x_{21} + U_{xy}y_{21} &= U_x^{21}\\ U_{yx}x_{21} - U_{xx}y_{21} &= U_y^{21}\end{aligned}\right\} \qquad (C.9)$$

and equation (C.4) becomes

$$ReP + \frac{1}{2}(\sigma_{xx} + \sigma_{yy}) = 0 \qquad (C.10)$$

In fact we can reduce the number of unknowns to four: P, U_{xx}, U_{xy}, U_{yx}.
(C.7a)xn_y plus (C.7b)xn_x gives

$$U_{xy} + U_{yx} - T_x n_y - T_y n_x = 2\,RePn_x n_y \qquad (C.11)$$

(C.7a)xn_x minus (C.7b)xn_y gives

$$2(2n_x^2 - 1)U_{xx} = (2n_x^2 - 1)ReP + T_x n_x - T_y n_y \qquad (C.12)$$

From equation (C.9) we can see that if y_{21}=0, then n_x=0, and

$$U_{xx} = \frac{U_x^{21}}{x_{21}};\ U_{yx} = \frac{U_y^{21}}{x_{21}};\ P = \frac{T_y n_y - 2U_x^{21}/x_{21}}{(1 - 2n_y^2)Re} \qquad (C.13)$$

if x_{21}=0, then n_y=0, and

$$U_{xx} = -\frac{U_y^{21}}{y_{21}};\ U_{xy} = \frac{U_x^{21}}{y_{21}};\ P = \frac{T_x n_x + 2U_y^{21}/y_{21}}{-Re} \qquad (C.14)$$

In other cases

$$P = \frac{\left[\left(\frac{y_{21}}{x_{21}} - \frac{x_{21}}{y_{21}}\right)\frac{(T_x n_x - T_y n_y)}{(2n_x^2 - 1)} + 2\left(T_x n_y + T_y n_x - \frac{U_x^{21}}{y_{21}} - \frac{U_y^{21}}{x_{21}}\right)\right]}{\left[\mathrm{Re}\left(\frac{y_{21}}{x_{21}}\frac{x_{21}}{y_{21}}\right) - 4\,\mathrm{Re}\, n_x n_y\right]} \qquad \text{(C. 15)}$$

$$U_{xx} = \frac{\left[2n_x n_y \frac{(T_x n_x - T_y n_y)}{(2n_x^2 - 1)} + T_x n_y + T_y n_x \frac{U_x^{21}}{y_{21}} - \frac{U_y^{21}}{x_{21}}\right]}{\left[\left(\frac{y_{21}}{x_{21}}\frac{x_{21}}{y_{21}}\right) - 4n_x n_y\right]} \qquad \text{(C 16)}$$

$$U_{yx} = U_{xx}\frac{y_{21}}{x_{21}} + \frac{U_y^{21}}{x_{21}};\ U_{xy} = \frac{U_x^{21}}{y_{21}} - U_{xx}\frac{x_{21}}{y_{21}} \qquad \text{(C. 17)}$$

Appendix D

Operator Matrix Approach for Rederivation of Oseenlet

Here the fundamental tensor solutions satisfying the following system (time dependent creeping motion equations) are rederived by resorting the Hörmander's operator matrix method

$$u^*_{ik,i} = 0 \tag{D.1}$$

$$\sigma^*_{ikj} = -\mathrm{Re}\,P^*_k\delta_{ij} + u^*_{ik,j} + u^*_{jk,i} \tag{D.2}$$

$$\sigma^*_{ikj,j} - \mathrm{Re}\frac{\partial u^*_{ik}}{\partial t} + b_{ik} = 0 \tag{D.3}$$

in which the tensor force can be defined as:

$$b_{ik} = -\delta_{ik}\delta(x - x')\delta(t - t') \tag{D.4}$$

Equations (D.1-D.4) imply a fictitious unsteady viscous flow field in which the velocity component in the i-direction at the observation point x at moment t is caused by a source of unit strength in the k-direction at point x' at moment t'.

Substituting Equations (D.1), (D.2) and (D.4) into Equation (D.3) yields:

$$-\mathrm{Re}P^*_{k,j}\delta_{ij} + u^*_{ik,jj} - \mathrm{Re}\frac{\partial u^*_{ik}}{\partial t} = \delta_{ik}\delta(x - x')\delta(t - t') \tag{D.5}$$

where Re is the Reynolds number.

This equation together with equation (D.1) can be summarized in a matrix form as follow:

$$\begin{bmatrix} \Delta - \mathrm{Re}\frac{\partial}{\partial t} & 0 & 0 & -\mathrm{Re}D_1 \\ 0 & \Delta - \mathrm{Re}\frac{\partial}{\partial t} & 0 & -\mathrm{Re}D_2 \\ 0 & 0 & \Delta - \mathrm{Re}\frac{\partial}{\partial t} & -\mathrm{Re}D_3 \\ D_1 & D_2 & D_3 & 0 \end{bmatrix} \begin{Bmatrix} u^*_{1k} \\ u^*_{2k} \\ u^*_{3k} \\ P^*_k \end{Bmatrix} = \begin{Bmatrix} \delta_{1k} \\ \delta_{2k} \\ \delta_{3k} \\ 0 \end{Bmatrix} \delta(t-t')\delta(x-x') \quad (k=1,2,3) \quad \text{(D. 6)}$$

where $D_i=\partial/\partial x_i$ (i=1,2,3). This equation can be written in a more condensed form:

$$\left[L_{ij}\right]\left\{u^*_{jk}\right\} = \left\{\delta_{ik}\delta(x-x')\delta(t-t')\right\} (i,j=1,2,3,4;\ k=1,2,3) \quad \text{(D. 7)}$$

where $u^*_{4k}=P^*_k$. The determinant of the matrix $[L_{ij}]$ by the formal calculation is given by:

$$L = \det\left[L_{ij}\right] = -\left(\Delta - \mathrm{Re}\frac{\partial}{\partial t}\right)^2 \Delta = \left(\Delta - \mathrm{Re}\frac{\partial}{\partial t}\right) L' \quad \text{(D. 8)}$$

in which $L'=(\mathrm{Re}\partial/\partial t-\Delta)\Delta$, Δ is a three dimensional Laplace operator. The adjugate matrix of $[L_{ij}]$, whose component is the cofactor of the entity L_{ij}, is denoted by $[M_{ij}]$. The matrix is given by:

$$\left[M_{ij}\right] = \left(\Delta - \mathrm{Re}\frac{\partial}{\partial t}\right)\left[M'_{ij}\right] \quad \text{(D. 9)}$$

where the matrix $[M'_{ij}]$ is represented by:

$$\left[M'_{ij}\right] = \begin{bmatrix} D_2^2 + D_3^2 & -D_1D_2 & -D_1D_3 & \left(\Delta - \mathrm{Re}\frac{\partial}{\partial t}\right)D_1 \\ -D_1D_2 & D_1^2 + D_3^2 & -D_2D_3 & \left(\Delta - \mathrm{Re}\frac{\partial}{\partial t}\right)D_2 \\ -D_1D_3 & -D_2D_3 & D_1^2 + D_2^2 & \left(\Delta - \mathrm{Re}\frac{\partial}{\partial t}\right)D_3 \\ \frac{D_1}{\mathrm{Re}}\left(\mathrm{Re}\frac{\partial}{\partial t} - \Delta\right) & \frac{D_2}{\mathrm{Re}}\left(\mathrm{Re}\frac{\partial}{\partial t} - \Delta\right) & \frac{D_3}{\mathrm{Re}}\left(\mathrm{Re}\frac{\partial}{\partial t} - \Delta\right) & \left(\Delta - \mathrm{Re}\frac{\partial}{\partial t}\right)^2 \frac{1}{\mathrm{Re}} \end{bmatrix} \quad \text{(D. 10)}$$

The following two relations can be established for L_{ij}, M_{jk} and M'_{jk}:

$$[L_{ij}][M_{jk}]=L\delta_{ik} \qquad (i,j=1,2,3,4;\ k=1,2,3) \qquad \text{(D. 11)}$$

and

$$[L_{ij}][M'_{jk}] = L'\,\delta_{ik} = \delta_{ik}(\mathrm{Re}\frac{\partial}{\partial t} - \Delta)\Delta \qquad \text{(D. 12)}$$

therefore

$$\left[L_{ij}\right]\left\{U_{jk}\right\} = \left[L_{ij}\right]\left[M'_{jk}\right]\Phi = \delta_{ik}(\mathrm{Re}\frac{\partial}{\partial t} - \Delta)\Delta\Phi = \delta_{ik}\delta(x - x')\delta(t - t') \qquad \text{(D. 13)}$$

Cancelling δ_{ik} in both sides of the last equality, following equation is finally obtained

$$\left(\mathrm{Re}\frac{\partial}{\partial t} - \Delta\right)\Delta\Phi = \delta(x - x')\delta(t - t') \qquad \text{(D. 14)}$$

Accordingly the explicit forms of the solution for the velocity and stress components can be produced:

$$u^*_{ik} = M'_{ik}\,\Phi = \delta_{ik}\Phi_{,jj} - \Phi_{,ik} \qquad \text{(D. 15)}$$

$$\sigma^*_{ikj} = (\delta_{ik}D_j + \delta_{jk}D_i + \delta_{ij}D_k)\Delta\Phi - 2\Phi_{,ikj} - \mathrm{Re}\,\delta_{ij}\frac{\partial}{\partial t}\Phi_{,k} \qquad \text{(D. 16)}$$

It is convenient to assume the following expression for solving equation (D.14):

$$\Psi = \mathrm{Re}\Delta\Phi \qquad \text{(D. 17)}$$

Then the equation becomes:

$$\left(\frac{\partial}{\partial t} - \frac{1}{\mathrm{Re}}\Delta\right)\Psi = \delta(x - x')\delta(t - t') \qquad \text{(D. 18)}$$

whose fundamental solution is known:

$$\Psi = \frac{ReH(t,t')}{[4\pi(t-t')]^{d/2}} \exp\left(\frac{-Rer^2}{4(t-t')}\right) \qquad (D.19)$$

where r is the absolute distance between the source point x' and the observation point x, d is the number of dimensions of the space, and H(t,t') is Heaviside function.

Substituting this solution into equation (D.17) yields

$$\Delta\Phi = \frac{1}{r}\frac{d}{dr}\left(r\frac{d\Phi}{dr}\right) = \frac{H(t,t')}{[4\pi(t-t')]^{d/2}} \exp\left(\frac{-Rer^2}{4(t-t')}\right) \qquad (D.20)$$

For two dimensional problems (d=2), it is not necessary to work out the solution of Φ according to equations (D.15) and (D.16) because of the following relations:

$$\frac{\partial\Phi}{\partial x} = \frac{d\Phi}{dr}\frac{\partial r}{\partial x}, \qquad \frac{\partial\Phi}{\partial y} = \frac{d\Phi}{dr}\frac{\partial r}{\partial y}$$

where

$$\frac{d\Phi}{dr} = \frac{H(t,t')}{2Re\pi r}\left[C - \exp\left(\frac{-Rer^2}{4(t-t')}\right)\right] \qquad (D.21)$$

Here C should be an arbitrary constant. This constant can be chosen by approaching t' to t in equation (D.20). According to one of the properties of the fundamental solution (D.19)

$$\lim_{t'\to t} \frac{Re}{4\pi(t-t')} \exp\left(\frac{-Rer^2}{4(t-t')}\right) = \delta(x-x') \qquad (D.22)$$

Replacing the right hand side of equation (D.20) by $H(t,t')\delta(x - x')$, C is 1.

Substituting those relations into equations (D.15) and (D.16), the fundamental solutions of u^*_{ik} and σ^*_{ikj} can be finally obtained

$$u^*_{ik} = \delta_{ik}(\Delta\Phi - S_1(r)) - \frac{x_i x_k}{r^2}(\Delta\Phi - 2S_1(r)) \qquad (D.23)$$

The stresses in two-dimensional case are:

$$\sigma^{*}_{ikj} = -\left(\delta_{ik}x_j + \delta_{ij}x_k + \delta_{jk}x_i\right)\left[\frac{Re\,\Delta\Phi}{2(t-t')} + \frac{2}{r^2}\left(\Delta\Phi - 2S_1(r)\right)\right]$$

$$+ \frac{4x_i x_k x_j}{r^4}\left[2\left(\Delta\Phi - 2S_1(r)\right) + \frac{Re\,r^2\Delta\Phi}{2(t-t')}\right]$$

$$- \delta_{ij}\,Re\,x_k\left\{\frac{\delta(t-t')}{2\pi\,Re\,r^2}\left[1 - \exp\left(\frac{-Re\,r^2}{4(t-t')}\right)\right] + \frac{\Delta\Phi}{2(t-t')}\right\} \qquad \text{(D. 24)}$$

Appendix E

Analytical Integrations over the Linear Collocation Elements For $S_0(s)$, and $\Phi(r)$

$$S_o(s) = \frac{1}{s}[1 - \exp(-s)]; \quad s = \frac{Rer^2}{4\Delta t}; \quad S = \frac{ReR^2}{4\Delta t}$$

$$\frac{dr}{r} = \frac{dr^2}{2r^2} = \frac{4\Delta t}{2\,Re\,r^2}ds = \frac{ds}{2s}$$

$$I_1 = \int_0^R \Phi_{,k} n_i dr = \frac{x_k n_i}{4\pi R}\int_0^R \frac{1}{r^2}\left[1 - \exp\left(\frac{-Rer^2}{4\Delta t}\right)\right]dr^2$$

$$= \frac{x_k n_i}{4\pi R}\int_0^S \frac{1-e^{-t}}{t}dt = \frac{x_k n_i}{4\pi R}\left[E_1(S) + \ln S + \gamma\right] \qquad \text{(E. 1)}$$

$$I_2 = \int_0^R \Phi_{,k} n_i \frac{r}{R}dr = \frac{x_k n_i}{4\pi R\sqrt{S}}\int_0^S \frac{1-e^{-t}}{\sqrt{t}}dt$$

$$= \frac{x_k n_i}{4\pi R\sqrt{S}}\left(2\sqrt{S} - \int_0^S \frac{e^{-t}}{\sqrt{t}}dt\right) = \frac{x_k n_i}{4\pi R}\left[2 - \sqrt{\frac{\pi}{S}}\,\mathrm{erf}(\sqrt{S})\right] \qquad \text{(E. 2)}$$

$$I_3 = \int_0^R S_o(s)dr = \sqrt{\frac{\Delta t}{Re}}\int_0^S \frac{1}{t\sqrt{t}}(1 - e^{-t})dt =$$

$$= \sqrt{\frac{\Delta t}{Re}}\left[\frac{2}{\sqrt{S}}(e^{-S} - 1) + 2\int_0^S \frac{e^{-t}}{\sqrt{t}}dt\right]$$

$$= \sqrt{\frac{\Delta t}{Re}}\left[\frac{2}{\sqrt{S}}(e^{-S} - 1) + 2\sqrt{\pi}\,\mathrm{erf}(\sqrt{S})\right] \qquad \text{(E. 3)}$$

$$I_4 = \int_0^R \frac{r}{R}S_o(s)dr = \frac{2\Delta t}{ReR}\int_0^S S_o(t)dt = \frac{2\Delta t}{ReR}\left[E_1(S) + \ln S + \gamma\right] \qquad \text{(E. 4)}$$

$$I_5 = \int_0^R \frac{r^2}{R^2}S_o(s)dr = \frac{4}{R^2}\left(\frac{\Delta t}{Re}\right)^{1.5}\int_0^S \frac{1}{\sqrt{t}}(1 - e^{-t})dt =$$

$$= \frac{4}{R^2}\left(\frac{\Delta t}{Re}\right)^{1.5}\left(2\sqrt{S} - \sqrt{\pi}\,\mathrm{erf}(\sqrt{S})\right) \qquad \text{(E. 5)}$$

$$I_6 = \int_0^R \frac{1}{r}[S_o(s) - e^{-s}]dr = \frac{1}{2}\int_0^S \left[\frac{1}{t}(1-e^{-t})-e^{-t}\right]\frac{dt}{t} = \frac{e^{-S}-1}{2S} \qquad (E.6)$$

$$I_7 = \int_0^R \frac{1}{R}[S_o(s) - e^{-s}]dr = \frac{1}{2\sqrt{S}}\int_0^S \left[\frac{1}{t}(1-e^{-t}) - e^{-t}\right]\frac{dt}{\sqrt{t}}$$

$$= \frac{(e^{-S}-1)}{S} + \frac{1}{2\sqrt{S}}\int_0^S \frac{e^{-t}}{\sqrt{t}}dt = \frac{(e^{-S}-1)}{S} + \frac{\sqrt{\pi}}{2\sqrt{S}}\text{erf}(\sqrt{S}) \qquad (E.7)$$

$$I_8 = \int_0^R \frac{1}{r}[S_o(s) - 1]dr = \frac{1}{2}\int_0^S \left[\frac{1}{t}(1-e^{-t}) - 1\right]\frac{dt}{t}$$

$$= \frac{1}{2}\left[\frac{e^{-S}-1}{S} - E_1(S) - \ln S - \gamma\right] \qquad (E.8)$$

$$I_9 = \int_0^R \frac{1}{R}[S_o(s) - 1]dr = \frac{1}{2\sqrt{S}}\int_0^S \left[\frac{1}{t}(1-e^{-t}) - 1\right]\frac{dt}{\sqrt{t}}$$

$$= \frac{1}{2\sqrt{S}}\left[\frac{2(e^{-S}-1)}{\sqrt{S}} + 2\sqrt{\pi}\,\text{erf}(\sqrt{S}) - 2\sqrt{S}\right] \qquad (E.9)$$

Appendix F

Error Function and Its Approximations

The definition of the error function is

$$\operatorname{erf}(x) = \frac{2}{\sqrt{\pi}} \int_0^x \exp(-t^2)\,dt \tag{F. 1}$$

Its series expansion is

$$\operatorname{erf}(x) = \frac{2}{\sqrt{\pi}} \sum_{n=0}^{\infty} \frac{(-1)^n x^{2n+1}}{n!(2n+1)} \tag{F. 2}$$

The rational approximation of the error function is given as follow:

$$\left.\begin{aligned} &\operatorname{erf}(x) = 1 - (a_1 t + a_2 t^2 + a_3 t^3 + a_4 t^4 + a_5 t^5)\exp(-x^2) + \varepsilon(x); \\ &t = \frac{1}{1+px};\ |\varepsilon(x)| \le 1.5 \times 10^{-7}; \\ &p = .3275911;\ a_1 = .254829592,\ a_2 = -.284496736, \\ &a_3 = 1.421413741,\ a_4 = -1.453152027,\ a_5 = 1.061405429 \end{aligned}\right\} \tag{F. 3}$$